

学校代码： 10491

研究生学号： 2201510192

中国地质大学
博士学位论文

地下水模型控制过程识别的多模型
全局敏感性分析方法及应用

姓名： 杨 静

学科专业： 水利工程

指导教师： 唐仲华 教授

合作导师： 叶 明 教授

培养单位： 环境学院

二〇二一年十一月

A Dissertation Submitted to China University of Geosciences
For the Doctor of Philosophy

**Methods and applications of multi-model
global sensitivity analysis for identifying
controlling processes in subsurface
hydrological modeling**

Ph.D. Candidate: Jing Yang
Major: Hydraulic Engineering
Supervisor: Prof. Zhonghua Tang
Collaborative Supervisor: Prof. Ming Ye
Department: School of Environmental Studies

China University of Geosciences
Wuhan 430074 P. R. China

中国地质大学（武汉）研究生学位论文原创性声明

本人郑重声明：本人所呈交的博士学位论文《地下水模型控制过程识别的多模型全局敏感性分析方法及应用》，是本人在导师的指导下，在中国地质大学（武汉）攻读博士学位期间独立进行研究工作所取得的成果。论文中除已注明部分外不包含他人已发表或撰写过的研究成果，对论文的完成提供过帮助的有关人员已在文中说明并致以谢意。

本人所呈交的博士学位论文没有违反学术道德和学术规范，没有侵权行为，并愿意承担由此而产生的法律责任和法律后果。

学位论文作者签名：

日期：2021年11月 日

中国地质大学（武汉）研究生学位论文导师承诺书

本人郑重承诺：本人所指导的博士学位论文《地下水模型控制过程识别的多模型全局敏感性分析方法及应用》，是在本人的指导下，研究生在中国地质大学（武汉）攻读博士学位期间独立进行研究工作所取得的成果，论文由研究生独立完成。

研究生所呈交的博士学位论文没有违反学术道德和学术规范，没有侵权行为，并愿意承担由此而产生的与导师相关的责任和后果。

指导教师（签字）：

日期：2021年11月 日

中国地质大学（武汉）学位论文使用授权书

本人授权中国地质大学（武汉）可采用影印、缩印、数字化或其它复制手段保存本学位论文；学校可向国家有关部门或机构送交本学位论文的电子版全文，编入有关数据库进行检索、下载及文献传递服务；同意在校园网内提供全文浏览和下载服务。

涉密论文解密后适用于本授权书。

学位论文作者签名：

日期：2021年11月 日

作者简历

一、基本情况

杨静，男，汉族，中共党员。1992年1月出生于河南省邓州市，2009年9月进入长江大学地球化学系（现资源与环境学院）学习，2013年6月获得水文与水资源工程专业学士学位，2013年9月进入中国地质大学（武汉）攻读水利工程专业硕士学位，同年10月被推荐为硕博连读研究生，师从唐仲华教授，主要研究方向为区域地下水化学特征时空演化与成因、地表水-地下水相互作用数值模拟与不确定性分析研究。于2018年2月到2018年8月期间，在中国地质大学（武汉）和导师唐仲华教授的共同资助下，在美国佛罗里达州立大学（Florida State University）科学计算系（Department of Scientific Computing）访问学习，师从叶明教授。另外，于2019年3月到2020年11月，在叶明教授的资助和邀请下，在佛罗里达州立大学地球、海洋与大气科学系（Department of Earth, Ocean, and Atmospheric Science）访问学习。

攻读博士学位期间，顺利完成了相关学位课程和选修课程的学习，共修读课程24门，合计53.5学分，平均成绩87.5。作为核心成员参加了3项导师唐仲华教授主持或合作的科研项目，并在美国参与叶明教授2项科研项目。以第一作者/通讯作者身份公开发表SCI论文4篇，EI论文2篇，在修/在审SCI论文3篇；与他人合作发表SCI论文1篇，在修SCI论文1篇。

二、学术论文（*通讯作者）

已发表论文

1. Honghua Liu, **Jing Yang***, Ming Ye*, Zhonghua Tang, Jie Dong, Tongju Xing. Using one-way and co-clustering methods to reveal spatio-temporal patterns and controlling factors of groundwater geochemistry. *Journal of Hydrology*, 2021, 603: 127085. (T1)
2. Honghua Liu, **Jing Yang***, Ming Ye*, Zhonghua Tang, Jie Dong, Tongju Xing, Using t-distributed Stochastic Neighbor Embedding (*t*-SNE) for cluster analysis and spatial zone delineation of groundwater geochemistry data. *Journal of Hydrology*, 2021, 597: 126146. (T1)
3. **Jing Yang**, Ming Ye*, Zhonghua Tang*, Tian Jiao, Xiaoyu Song, Yongzhen Pei,

Honghua Liu. Using cluster analysis for understanding spatial and temporal patterns and controlling factors of groundwater geochemistry in a regional aquifer. *Journal of Hydrology*, 2020, 583: 124594. (T1)

4. **Jing Yang**, Zhonghua Tang*, Tian Jiao, Malik M. Akhtar. Combining AHP and genetic algorithms approaches to modify DRASTIC model to assess groundwater vulnerability: a case study from Jianghan Plain, China. *Environmental Earth Sciences*, 2017, 76(12): 426. (T3)

5. **Jing Yang**, Zhonghua Tang*. Parameter identification in groundwater flow modeling using support vector machine. *Proceedings of the 4th International Conference of Geology Resource Management and Sustainable Development*, Beijing, 2016. (会议论文集, EI 检索)

6. 杨静, 肖天昀, 李海波, 王全荣*. 江汉平原地下水中硝酸盐的分布及影响因素 [J]. *中国环境科学*, 2018, 38(2): 710-718. (中文 EI)

7. Tian Jiao, Ming Ye*, Menggui Jin*, **Jing Yang**. A finite particle method (FPM) for Lagrangian simulation of conservative solute transport in heterogeneous porous media. *Advances in Water Resources*, 2021, 156: 104043. (T2)

8. 陈燕飞, 张翔*, 杨静. 基于可变模糊识别模型的水环境系统恢复力评价[J]. 武汉大学学报(工学版), 2014, 47(3): 341-349. (中文核心)

审稿中/返修中论文

1. **Jing Yang**, Ming Ye*, Xingyuan Chen, Heng Dai, Anthony P. Walker. Process interactions can change process ranking in a coupled complex system under process model and parametric uncertainty. *Water Resources Research*, 2021. (Revision submitted, T1)

2. **Jing Yang**, Ming Ye*. A new multi-model absolute difference-based sensitivity (MMADS) method to screen non-influential process under process model and parametric uncertainty. *Journal of Hydrology*, 2021. (Major revision, T1)

3. **Jing Yang**, Honghua Liu, Zhonghua Tang, Luk Peeters, Ming Ye*. Visualization of water geochemistry data using Python and WQChartPy. *Groundwater*, 2021. (Under review, T2)

4. Tian Jiao, Ming Ye*, Menggui Jin*, **Jing Yang**. An interactively corrected smoothed particle hydrodynamics (IC-SPH) for simulating solute transport in heterogeneous porous media. *Water Resources Research*, 2021. (Major revision, T1)

三、学术会议

1. **Jing Yang**, Honghua Liu, Ming Ye, Zhonghua Tang, Scott C. James. Using a machine learning method (t-SNE) to delineate spatial zones of groundwater geochemistry in regional aquifers, AGU annual meeting, Virtual, 2020.
 2. **Jing Yang**, Ming Ye, Zhonghua Tang, Tian Jiao, Xiaoyu Song, Yongzhen Pei, Honghua Liu. A cluster-based method for understanding spatial and temporal patterns and controlling factors of groundwater geochemistry in a regional aquifer, GSA annual meeting, Indianapolis, Indiana, USA, 2018.
 3. **Jing Yang**, Zhonghua Tang. Parameter identification in groundwater flow modeling using support vector machine. Proceedings of the 4th International Conference of Geology Resource Management and Sustainable Development, Beijing, China, 2016.
 4. Tian Jiao, Ming Ye, Menggui Jin, **Jing Yang**. An interactively corrected smoothed media particle hydrodynamics (IC-SPH) for simulating solute transport in heterogeneous porous media, AGU annual meeting, Virtual, 2021.
 5. Ming Ye, **Jing Yang**. A new multi-model difference-based sensitivity analysis method with consideration of process Model and parametric uncertainty, AGU annual meeting, Virtual, 2020.
 6. Tian Jiao, Ming Ye, Menggui Jin, **Jing Yang**. A Finite particle method for simulating solute transport in heterogenous porous media, AGU annual meeting, Virtual, 2020.
 7. Ahmed Elshall, Sally Gorrie, Julie Harrington, Sven Kranz, Emily Lizotte, Yongshan Wang, **Jing Yang**, Xiaojuan Yang, Ming Ye. Understanding and managing harmful algal bloom in west Florida shelf using E3SM Earth system model, AGU annual meeting, Virtual, 2020.
- #### 四、参与科研项目
1. 美国佛罗里达州立大学 FSU Research Foundation “Water Resources and Environmental Sustainability of Coastal Cities under Population Growth, Economic Development, and Climate Change”, 2020/3 - 2020/11;
 2. 美国能源部“Multi-model and Multi-scale Global Sensitivity Analysis for Identifying Controlling Processes of Complex Systems”, 2019/03 - 2020/03;
 3. 中国地质调查局“生态功能区地质环境脆弱性调查评价”, 2016/04–2017/05;
 4. 中国地质调查局“江汉-洞庭平原地下水及其环境问题调查评价”, 2013/09 – 2017/10;
 5. 中国地质调查局“长江中游江汉-洞庭平原国土资源综合监测示范”,

2013/09–2016/05.

摘要

地下水文过程是指水文循环中描述地下水运动的一系列水文要素在时间或者空间上持续变化或周期变化的动态过程。利用数学物理方程对相关的地下水文过程进行抽象和概化并建立的地下水系统模型（system model，或简称地下水模型）是认识和研究地下水循环演化规律的重要理论基础和技术手段。地下水系统模型通常包含多个相互作用的地下水文过程模型（process model），其中每一个水文过程模型都可以被看作是对一个现实水文过程的抽象和概化。由于地下水文过程的复杂性，现有的地下水系统模型很难做到准确地表述全部的地下水文过程。识别地下水系统模型的控制过程对于理解地下水模型结构，提高模型预测能力，简化复杂地下水系统模型，以及指导野外水文地质工作具有十分重要的意义。本文以不确定性分析方法理论为基础，首先阐述了地下水系统模型控制过程的内在含义和数学定义。从地下水系统模型建模过程中三个主要的不确定性来源（即数据的不确定性，参数的不确定性和模型的不确定性）出发，分析了当前利用全局敏感性分析方法识别地下水系统模型控制过程的局限性——仅考虑模型参数的不确定性，缺乏考虑模型的不确定性，例如同一个地下水文过程可以采用不同的地下水文过程模型描述。在地下水系统模型建立过程中，组合这些不同的水文过程模型往往会导致多个不同的地下水系统模型（多模型），不同的地下水系统的控制过程很可能会不同。针对多模型条件下地下水系统模型建模过程中同时涉及地下水文过程模型和模型参数的不确定性问题，本文扩展了传统的单模型全局敏感性分析方法，推导了两种新的方法，用于识别多模型情况下地下水系统模型的控制过程。本文主要内容主要可以分为方法推导、方法应用和软件集成三大部分。

(1) 第一部分是方法推导，包括第二章和第三章。本文推导了两种新方法用于识别多模型情况下地下水系统模型的控制过程，可以同时考虑地下水系统模型中过程模型和模型参数的不确定性。

第一种方法是基于方差的过程敏感性分析方法，在第二章。这种方法以方差分解法为基础，耦合了模型平均法和传统的 Sobol 全局敏感性分析方法，通过计算两类过程敏感性指标，用于衡量某一地下水文过程对地下水系统模型输出的重要性和影响程度。第一类过程敏感性指标基于 Dai et al. (2017b) 提出的一阶过程敏感性指标（first-order process sensitivity index），该指标可以定量分析地下水文过

程对系统模型的主要影响（main effect），用来识别地下水模型中的重要过程，即该地下水文过程一经确定，系统模型输出的不确定性（方差）减少最多。因此在实际的水文地质工作中需要投入更多的精力研究重要过程，提高对该过程的认识。第二类指标是本文提出的总效应过程敏感性指标（total-effect process sensitivity index），可以定量分析某一地下水文过程对模型的总影响（total effect）。该指标区别于 Dai et al. (2017b) 提出的一阶过程敏感性指标是因为其不仅考虑了地下水文过程对地下水模型的主要影响，还考虑了不同地下水文过程之间的相互作用（process interaction）。总效应过程敏感性指标可以用来识别地下水模型中的影响过程，即该地下水文过程若无法确定，系统模型输出的不确定性（方差）保留最多。如果某一地下水文过程对系统模型输出的总效应过程敏感性指标很小，实际的水文地质工作中可以忽略对该地下水文过程的研究，节省人力物力和时间成本。计算这两类指标依赖于蒙特卡洛运算，通常需要巨大的计算量。本文提出了一个新的高效计算方法，可以将计算复杂度从 $O(n^2)$ 降低到 $O(n)$ ，并利用一个假想的一维河间地块模型验证了该方法的可靠性。在一维河间地块模型中，概化了三个水文过程即降雨入渗过程、地质过程和融雪过程，每一个过程都可以用两个过程模型描述，如考虑降雨线性入渗和非线性入渗补给过程模型，均质渗透系数和非均质渗透系数地质过程模型，以及仅考虑温度的度一日融雪过程模型和同时考虑温度和太阳辐射的度一日融雪过程模型，组合这三个过程的过程模型可以得到八个不同的地下水系统模型。

第二种方法是基于绝对差值的多模型过程敏感性分析方法，在第三章。这种方法耦合了模型平均法和传统的 Morris 参数筛选法。该方法扩展了传统的 Morris 参数筛选法，其基本思想是首先评估由地下水过程模型的变化和过程模型中嵌入的参数值的变化引起的系统模型输出的差异（绝对值），然后计算系统模型输出差异的均值和方差，用于评估该过程的影响程度。系统模型输出差异的均值和方差越小，其对应的地下水文过程对系统模型的影响越小，反之，系统模型输出差异的均值和方差越大，其对应的地下水文过程对系统模型的影响越大。这种方法优于第二章提出的基于方差的过程敏感性分析方法在于其作为一种定性方法，可以利用较少的计算量，筛选出对地下水系统模型输出结果影响较小的地下水文过程。另外本文提出了一种高效计算方法 binning 方法用于进一步降低计算量，并利用第二章所使用的一维河间地块模型验证了该方法的有效性。

(2) 第二部分是方法应用，包括第四章和第五章。这一部分主要介绍了这两种新推导的方法在识别地下水模型控制过程中的应用，本文利用两个地下水模型评估了这两种方法的有效性。

第一个模型基于 Duan et al. (2020) 的砷 (As) 吸附和反应传输室内试验。本文利用 PFLOTRAN 构建了一个二维 As 吸附反应模型，用于模拟实验沙箱中 As 的浓度。在模型的构建过程中概化了三个地下水文过程，即物理过程（Physical process）、化学过程（Chemical process）和吸附过程（Sorption process），总共考虑了 $12 = 2 \times 2 \times 3$ 个不同的地下水系统模型，分别对应 2 个物理过程模型（即非均质或均质渗透率场模型）、2 个化学过程模型（即非均质或均质的吸附系数场模型），以及 3 种吸附过程模型（即线性平衡吸附模型、双室一阶动力学吸附模型和耦合线性平衡吸附模型和 Fe(II) 粘土矿物氧化的动力学模型）。这 12 个模型同时包含不同个数的模型参数，如渗透率，吸附系数和粘土矿物氧化速率。假定模型参数的真值也同样不确定，采用第二章提出的基于方差的过程敏感性分析方法，利用佛罗里达州立大学超算平台，在考虑不同模型配置和输入参数情况下，基于 $216,000 = 12 \times (3 + 2) \times 3,600$ 次模拟实验，本文量化了三个地下水文过程对单个地下水系统模型和多系统模型条件下抽水井中砷浓度的重要性和影响程度。结果表明，这三个地下水文过程对井中 As 的浓度的控制程度随时间发生变化，物理过程对抽水井中 As 的浓度在前期影响较大，吸附过程在后期影响较大，而化学过程则在中期对抽水井中 As 的浓度影响较大。

第二个模型基于 Song et al. (2018) 建立的美国华盛顿州 Hanford 场地 300 区域地表水-地下水相互作用下的生物地球化学反应模型。在这个模型中，本文考虑了四个水文过程，即气候（climate process）、水流（flow process）、热量（heat process）和反应（reaction process）过程，采用第二章提出的基于方差的多模型过程敏感性分析方法以及第三章提出的基于绝对差值的多模型过程敏感性分析方法，利用美国国家能源研究科学计算中心（NERSC）Hopper 超算平台，基于 $12,000 = 6 \times 5 \times 2 \times 2 \times 100$ 次 PFLOTRAN 模拟实验，分别对应 6 种气候情景、5 种冲积层厚度、非均质/均质地层、考虑/不考虑热传输过程，以及 100 组反应速率和渗透系数参数值组合，识别了这四个过程对有机碳消耗速率时空分布的影响，并验证了这两种方法的有效性和一致性。这两种方法都表明温度对该区域有机碳的消耗速率影响很小。因此，在建立该区域生物地球化学模型过程中，可以不考虑热量传输过程，实际水文地质工作可以考虑忽略对该区域热传输过程（即温度场）的监测。

（3）第三部分是软件集成，在第六章。

这部分主要介绍了本文新开发的开源 Python 软件包 SAMMPy，可以用于多模型条件下地下水文过程敏感性分析并识别地下水模型的控制过程。该软件包实现了上述两种敏感性分析方法，可以同时考虑地下水系统模型中过程模型和模型

参数不确定性，能够生成一系列过程敏感性指数，并搭载简单的可视化模块，用于识别地下水系统模型的控制过程。该软件包中也包含了两个数值算例，即一维河间地块模型数值算例和 Sobol-G*函数数值算例，用户可以通过开源代码托管平台 GitHub (<https://github.com/jyangfsu/SAMMPy>) 下载安装使用。

关键词：地下水模型；重要过程；影响过程；模型不确定；不确定性分析

ABSTRACT

Subsurface hydrologic processes include a series of water/energy/solute movements in water/energy/mass cycles below the surface of the Earth. In subsurface hydrological modeling the needs to identify controlling processes for model development and improvement have been long recognized, prompting the development of many identification methods. A subsurface hydrological model may consist of multiple process-level sub-models, and each sub-model represents a process that is key to the operation of the simulated system. Global sensitivity analysis methods have been widely used to identify important or influential processes for system model development and improvement. A variety of types of uncertainties sources exist in subsurface hydrologic modeling, including the data uncertainty, parameter uncertainty, and model uncertainty. Many existing methods of global sensitivity analysis only consider parametric uncertainty and are not capable of handling model uncertainty caused by multiple process models that arise from competing hypotheses about one or more processes. To address this problem, this dissertation focuses on addressing uncertainty in process models and parameters, and on identifying the controlling processes. The dissertation research includes the following three parts: proposal of new process sensitivity analysis methods, application of the new methods to subsurface hydrological models, and development of a new Python package for performing the proposed methods.

The first part of the dissertation is mainly concentrated on developing two new methods to probe model output sensitivity to competing process models:

The first new method is called variance-based process sensitivity analysis method and it is presented in Chapter 2. This method integrates the model averaging methods with traditional Sobol's variance-based global sensitivity analysis method to address uncertainty in process models and parameters. It yields two process sensitivity indices. The first one is called first-order process sensitivity index, which was derived by Dai et al. (2017b) as a single summary measure of relative process importance. The second one is called total-effect process sensitivity index, which is derived as a single summary measure of relative process influence. The total-effect process sensitivity index includes

the first-order process sensitivity index and high-order indices that address process interactions. Evaluating the two indices is computationally expensive, because it relies on a Monte Carlo scheme that requires tens of thousands and even millions of model executions. To reduce computational cost, this dissertation develops a computationally efficient design and estimator to reduce the computational cost. This is demonstrated by a hypothetical one-dimensional (1-D) groundwater flow modeling that considers recharge process, geological process, and snowmelt process. Each of the three processes has two alternative process models, i.e., the recharge process can be simulated by either linear or non-linear recharge models, the hydraulic conductivity field can be either homogenous or heterogeneous, and the snowmelt process can be either simulated by the degree-day method and the restricted degree-day radiation balance method, resulting in a total of eight system models by integrating the process models.

In addition to the two process-sensitivity indices, this dissertation research develops another new method called multi-model absolute difference-based process sensitivity analysis method, and it is presented in Chapter 3. This method integrates the model averaging methods with traditional Morris screening method to address uncertainty in process models and parameters. The basic ideas of this method are to first evaluate the differences of a system model output caused by varying process models and/or parameter values embedded in the process models, and then to calculate the mean and variance of the differences for investigating process influence as in the Morris screening method. The results of this method can be used to screen non-influential system processes and parameters from further investigation. A binning method is also developed to reduce computational cost. The efficiency of this method is also demonstrated using the 1-D groundwater flow model.

The second part of the dissertation is mainly focused on application of the two new methods for identifying the controlling processes in hydrologic modeling. We evaluated the performance of the two methods by using two hydrologic models:

The first one is a two-dimensional (2-D) arsenic (As) sorption and reactive transport model based a laboratory experiment by Duan et al. (2020). Three processes, namely, the physical process, the chemical process, and the sorption process were conceptualized. A total of $12 = 2 \times 2 \times 3$ individual system models were considered, corresponding to the two physical process models (i.e., heterogeneous and homogenous permeability field), two chemical process models (i.e., heterogeneous and homogenous distribution coefficient

filed), and three sorption process models (i.e., simple linear equilibrium model, dual first-order kinetic sorption model, and coupled linear equilibrium sorption model with a kinetic model for describing the oxidation of Fe(II)-bearing clay minerals). Each of the twelve models contains different number of uncertainty parameters. Using the variance-based process sensitivity analysis method with the computationally efficient schemes presented in Chapter 2, a total number of $216,000 = 12 \times (3 + 2) \times 3,600$ PFLOTRAN simulations were conducted on the supercomputer of the Florida State University to consider all possible combinations of model configurations and input parameters. We quantify the relative importance and influence of three processes to arsenic concentrations at the pumping wells under individual system models as well as multiple system models. Results show that the most important and influential process on the As concentration in the pumping well could change over time. At the very beginning of the simulation period after pumping started, the physical process significantly influences the As concentration in the pumping well. At the middle stage, the chemical process significantly influences the As concentration in the pumping well. At the final stage, the three different sorption models significantly influence the arsenic concentration in groundwater.

The second application is a biogeochemical model at the groundwater-surface water interface within the Hanford Site's 300 Area. Multiple uncertainty sources across climate, flow, heat, and reaction processes were considered based on our understanding of the complex system. Variance-based process sensitivity analysis presented in Chapter 2 as well as the multi-model absolute difference-based process sensitivity analysis methods presented in Chapter 3 were used to identify the controlling processes with respect to the spatio-temporal distribution of the organic carbon (OC) consumption rate in the aquifer at the Hanford Site. The total number of PFLOTRAN simulations considering all possible combinations of model inputs and model configurations is $12,000 = 6 \times 5 \times 2 \times 2 \times 100$ for representing six scenarios, five thicknesses of alluvium layer, heterogeneous/homogeneous formations, with/without heat transport process, and 100 reaction rates and permeability fields. Hopper supercomputer at the National Energy Research Scientific Computing Center (NERSC) is employed to perform the simulations. Both the variance-based process sensitivity analysis method and multi-model difference-based process sensitivity analysis method suggests the heat process is non-influential. Thus the biogeochemical model may be simplified without considering the heat process. In other words, the temperature-independent reaction rates may be sufficient to capture

the OC consumption rate.

The third part of the dissertation presents a new open-source Python package, SAMMPy, for performing process sensitivity analysis under multiple system models. Within this framework, an environmental system is conceptualized as an integration of multiple system processes, each of which is represented by one or more process models with uncertain process model parameters. SAMMPy implements the two new sensitivity analysis methods that enables simultaneous generation of a range of process sensitivity indices with considering both parametric uncertainty and process model uncertainty. This package is publicly available on GitHub via <https://github.com/jyangfsu/SAMMPy>. Example workflows of a mathematical test function (Sobol-G* function) and a 1-D groundwater flow model documented in Jupyter Notebooks are also available in the repository.

Keywords: Subsurface hydrological modeling; Important process; Influential process; Model uncertainty; Uncertainty analysis

CONTENTS

Chapter 1 Introduction.....	1
§1.1 Research Background.....	1
§1.2 Literature Review and Problems	5
1.2.1 Uncertainty in Subsurface Hydrologic Modeling.....	5
1.2.2 Sensitivity Analysis for Uncertainty Apportionment	10
1.2.3 Identifying the Controlling Processes via Sensitivity Analysis.....	16
1.2.4 Unresolved Problems.....	21
§1.3 Research Objectives, Procedure, and Innovations.....	21
1.3.1 Research Objectives	21
1.3.2 Research Procedure	22
1.3.3 Research Innovations.....	23
Chapter 2 A New Variance-based Process Sensitivity Analysis Method.....	22
§2.1 Introduction	22
§2.2 Background and Derivation of the New Method	28
2.2.1 Traditional Sobol's Parameter Sensitivity Indices for Single-Model	28
2.2.2 New Variance-based Process Sensitivity Indices for Multi-model	30
§2.3 Numerical Implementation	36
2.3.1 Model-averaging and Monte Carlo Integration	36
2.3.2 Efficient Design and Estimator to Reduce Computational Cost	38
§2.4 A Hypothetical Example.....	43
2.4.1 Model Settings.....	43
2.4.2 Identifying the Controlling Process for Single-Model	46
2.4.3 Identifying the Controlling Process for Multi-Model	48
2.4.4 Process Interactions	51
2.4.5 Relation between Parameter and Process Sensitivity Indices	54
2.4.6 Convergence and Computational Cost Analysis	59
§2.5 Summary.....	62
Chapter 3 A New Multi-Model Absolute Difference-based Process Sensitivity Analysis Method.....	64
§3.1 Introduction	65
§3.2 Background, Conceptualization, and Derivation	66
3.2.1 Traditional Morris Screening Method for a Single Model	66

3.2.2 Basic Ideas of MMADS for Multi-model	69
3.2.3 Derivation of MMADS Indices	71
§3.3 Numerical Implementation	76
3.3.1 Model-averaging and Monte Carlo Integration	76
3.3.2 Reduce the Computational Cost by Using Binning Method	78
§3.4 A Hypothetical Example.....	80
3.4.1 Identifying the Controlling Process for Single-Model	81
3.4.2 Identifying the Controlling Process for Multi-model	83
3.4.3 Computational Cost Analysis	84
§3.5 Summary.....	86
Chapter 4 Application to an Arsenic Sorption and Reactive Transport Model Based on a Laboratory Experiment.....	88
§4.1 Introduction	88
§4.2 Arsenic Sorption and Reactive Transport Model	91
4.2.1 Physical Model Based on a Laboratory Experiment	91
4.2.2 Mathematic Model	94
4.2.3 Numerical Model Setup	95
4.2.4 Uncertainty Sources	96
§4.3 Identifying the Controlling Processes to As Concentration in the Pumping Well	100
4.3.1 Simulated Results	100
4.3.2 Parameter Sensitivity Indices for Single-Model	103
4.3.3 Process Sensitivity Indices for Multi-Model	105
4.3.4 Implications and Limitations.....	107
§4.4 Summary	108
Chapter 5 Application to a Complex Biogeochemical Model at Hanford 300 Area	109
§5.1 Introduction	109
§5.2 The Complex Biogeochemical Model	112
5.2.1 Study Site	112
5.2.2 Model Setup	113
5.2.3 Uncertainty Sources	115
§5.3 Identifying the Controlling Processes to OC Consumption Rate	119
5.3.1 Simulation Results	119

5.3.2 First-order Process Sensitivity Indices for Identifying Important Process...	121
5.3.3 Total-effect Process Sensitivity Indices for Identifying Influential Process	126
5.3.4 Second-order and Third-order Process Interactions	129
5.3.5 MMADS Method for Identifying Non-Influential Processes	137
5.3.6 Comparison of the Two Methods	144
§5.4 Summary	146
Chapter 6 SAMMPy: An Open-source Python Package for Process Sensitivity Analysis under Multi-Model	148
§6.1 Introduction	148
§6.2 Structure of SAMMPy.....	150
§6.3 Software Available and Maintenance	154
6.3.1 Software Available	154
6.3.2 Software Maintenance	154
§6.4 Summary	155
Chapter 7 Summary, Contributions, and Future Work	156
§7.1 Summary.....	156
§7.2 Contributions	158
§7.3 Future Work	159
Acknowledgments	161
References	163

Chapter 1 Introduction

§1.1 Research Background

“For many phenomena 80% of the output or consequences are produced by 20% of the input or causes.”

—The Pareto Principle

Process-based hydrological modeling has been widely used for understanding and predicting behaviors of hydrological systems (Clark et al. 2015c, d, Fatichi et al. 2016, Gorelick and Zheng 2015, Montanari and Koutsoyiannis 2012, Singh 2018). These systems are often open, very complex, and have a large number of system processes and process interactions (Brenner et al. 2018, Clark et al. 2015a). When developing and improving process-based hydrologic models, it is practically difficult and theoretically unnecessary to incorporate all processes of a complex system into a model (conceptual, mathematical, or numerical). Pareto Principle (also known as the 80/20 Rule) states that for many phenomena, 80% of the output or consequences are produced by 20% of the input or causes. As a rule of thumb, this rule can be applied to many fields of physical science including subsurface hydrologic modeling where 80% of modeling performance can be effectively managed by prioritizing the implementation of 20% of the possible hydrologic processes (Callaham et al. 2021). For example, the well-known dimensionless quantity, Peclet Number, reflects relative importance of advection versus diffusion. How to represent physical, chemical, and biological processes and their interactions is thus a fundamental decision in model development, evaluation, and improvement (Chang et al. 2017, Clark et al. 2015b, Clark et al. 2015d, Gupta et al. 2012, Janetti et al. 2019, Mai et al. 2020, Markstrom et al. 2016, Mendoza et al. 2015). Clark et al. (2015b) stated that “*this [the decision] involves making choices on (1) model complexity, i.e., which physical processes should be represented explicitly, and, correspondingly, which processes can be ignored or greatly simplified; and (2) process representation, i.e., what modeling approaches should be used to represent the dominant biophysical and hydrologic processes*”. In many situations, the two choices depend on each other, and making the

choices requires identifying dominant, important, or controlling processes; conversely, it requires determining the processes that may be safely neglected so that they are not neither included in the models at the stage of model development nor further investigated at the stage of model improvement (e.g., Singh (2018) ; Cricic et al. (2012); Zeng et al. (2018); Ketema and Langergraber (2015), Markstrom et al. (2016)).

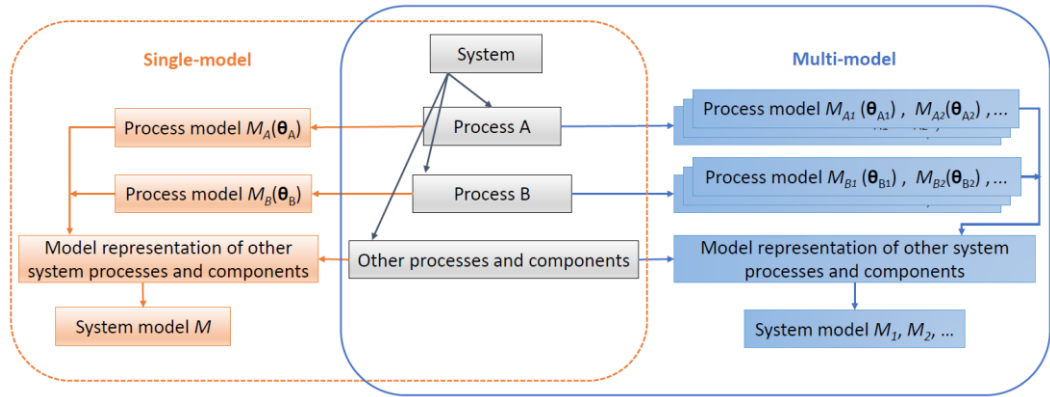


图 1-1 系统与过程之间的关系和过程模型与系统模型之间的关系。左侧虚线框表示传统的单模型系统框架，其中每个水文过程只包含一个过程模型。右侧实线框表示多模型系统框架，其中每个水文过程存在多个过程模型。

Figure 1-1 Relation between system and its processes as well as relation between process models and system models. The dashed box represents the conventional single system model framework, of which each process is characterized by only one process model and the solid box represents the multiple system model framework, of which each process can be simulated by multiple process models.

Research on identifying the controlling hydrologic processes has gained increasing attention since the last two decades (Sivakumar 2004b, Sivakumar 2007). Grayson and Bloschl (2000) proposed the “dominant processes concept” in catchment hydrology, which is quite different from the “controlling processes concept” used in this study. Beven (2002) stated as: “*The development of more and more complex models that incorporate more and more detail about processes, but which introduce more and more parameters that must be calibrated, does not appear to be the future.... The future of (environmental) modeling will have to place more emphasis on the value of data, carefully collected for specific purposes, and on parametrically simple robust models, carefully designed for specific purposes.*” Sivapalan (2003) reported that predictions of water quantity and quality at the watershed outlet are not substantially improved by using complex models instead of simple ones. Sivakumar (2007) summarized the dominant processes concept in catchment hydrology and discussed the concept of dominant processes in model

simplification and the utility of integration of concepts for modeling improvement. He augured that “... *it (the dominant processes concept) requires only less data collection, but more important and reliable data... (the dominant processes concept) would also provide a framework for the development and application of techniques especially designed to deal with those (dominant hydrologic) controls and help to avoid some of the overparameterization problems...*”.

The dominant processes concept discussed above suggests the following: (1) developing methods to identify dominant processes that control hydrologic response in different environments (landscapes and climates) and at different scales; and (2) developing models to focus on these dominant processes (Sivakumar 2004a). An examination of the current hydrologic literature reveals that most of the studies are model-driven (e.g., Markstrom et al. (2016)), starting from developing a system model for the hydrological system (referred to **system model** hereinafter). Since hydrological system usually involves various hydrologic, geochemical, and biogeochemical processes, the system model is composed of multiple process level sub-models (referred to **process model** hereinafter). Each sub-model represents a system process key to the operation of the simulated system. The relations between a system and its processes and between a system model and its process models are shown in Figure 1-1. In the conventional procedure of system model development as shown in the left dotted box of Figure 1-1, a system process (referred to the process involved in the system) is usually represented by a single process model, e.g., process model M_A for process A , which may contain its own parameters, e.g., Θ_A for process model M_A — the process model is denoted as $M_A(\Theta_A)$ in such case. Note that due to the incomplete knowledge, the true parameter values may be not known, i.e., the parametric uncertainty exists. Integrating these process models results in a single system model M . This concept of single-model representation of a system and its processes (and process interactions) has become questionable when process model uncertainty arises, i.e., available data and knowledge support multiple process models to represent a process, e.g., process model $M_{A_1}(\Theta_{A_1})$ and $M_{A_2}(\Theta_{A_2})$ for process A as shown in the right dashed box in Figure 1-1. Process model uncertainty leads to system model uncertainty, i.e., multiple alternative system models M_1, M_2, \dots are available when a system model is formed by integrating process models in a modular modeling framework (Chang et al. 2017, Lu et al. 2015, Ye et al. 2010a, Ye et al. 2010b, 夏强, 2011). With

process model uncertainty, the system model behaviors depend on the particular choice of the process models. For example, Ye et al. (2010b) showed that, for the Death Valley regional flow system, its recharge process can be simulated by five different models, and its hydrogeology can be described by five hydrostratigraphic frameworks, yielding a total of 25 plausible groundwater flow models. In such a case, a model developer is not only faced with the uncertainty in parameters but also the uncertainty in process models.

表 1-1 一个假想例子用来说明在不考虑模型不确定性的情况下控制过程的识别可能存在偏差。 $S_A - S_D$ 代表系统过程 $A - D$ 控制程度的虚拟值, M_1 和 M_2 表示两个可能的地下水模型。

Table 1-1 A hypothetical example to illustrate that biased identification of controlling processes resulted without considering model uncertainty. $S_A - S_D$ denote fictitious values of “controlling index” for processes $A - D$ of a system, and M_1 and M_2 denotes two system models based on two different representations of the processes.

	S_A	S_B	S_C	S_D
Model M_1	50%	20%	20%	10%
Model M_2	10%	20%	20%	50%

The consequence of ignoring model uncertainty for the identification of controlling processes is demonstrated using a synthetic case. Assuming that a system has four processes (denoted as processes A, B, C , and D) and that a system model (denoted as M_1) is developed based on a certain representation of the processes, Table 1 lists fictitious values of “controlling index” (denoted as S) evaluated for the four processes. This set of controlling index indicates process A is the controlling process. However, if another model, M_2 , is developed based on another representation of the process, the corresponding controlling index values listed in Table 1-1 may suggest that process D is the controlling process. This raises the following questions: which process is the controlling one? How can we identify the controlling processes in this situation of model uncertainty? The impacts of model uncertainty on identification of controlling processes should be addressed at the beginning of a modeling project for a complex system, before limited resources is used up.

This study aims at developing new methods for identifying controlling processes of complex systems such as groundwater-surface water transition zones, in which intricate hydrologic, microbiologic, and geochemical processes occur and interact to affect the hydrobiogeochemical behaviors under multiple system models (Harvey and Gooseff 2015).

§1.2 Literature Review and Problems

1.2.1 Uncertainty in Subsurface Hydrologic Modeling

Uncertainty is not an accident in subsurface hydrologic modeling, but rather its substance. It serves as the cornerstone that why and how the hydrology community needs to identify the controlling processes. Imaging that we totally know everything about the hydrology and no uncertainty exists in modeling the hydrological system, there is then no bother to identify the controlling processes because we know exactly which processes should be devoted, which processes can be ignored, what are the true parameter values, and the hydrological model accurately reflects the behaviors of the hydrological system and eventually, simulation results would perfectly match the observations. In such case, all processes involved in modeling are of same importance to the hydrological system, or in other words, all processes are of unimportance or non-controlling at all. However, this is something that will never happen since “*all models are wrong*” (Box and Draper 1987).

A hydrological model is an abstraction, simplification, and interpretation of real-world hydrological system. It uses simple mathematical equations to conceptualize and aggregate the complex, spatially distributed, and highly interconnected water, energy, and vegetation processes (Vrugt et al. 2005). These equations commonly include parameters whose exact values are not known precisely but may vary within some ranges that reflect our incomplete knowledge or uncertainty regarding them. Furthermore, the numerical equations needed to solve the various equations introduce themselves numerical errors. While technological and methodological advances have undoubtedly improved our understanding for a more accurate and complete pathway to deal with the workings of hydrologic systems and predictions of hydrologic phenomena, it is unfortunately to recognize that our recognition, knowledge, and experience are always limited, and the model may never accurately represent the real behavior. Because we simply do not know enough about hydrological systems and their inputs and outputs, the incompleteness of a hydrological model and the mismatch between the real causal structure of a system and the assumed causal structure as represented in a model always result in uncertainty about model predictions. Past analysis has distinguished a variety of types of uncertainties sources in the environmental sciences (Dubus et al. 2003b, Højberg and Refsgaard 2005,

Renard et al. 2010, Yen et al. 2014, 刘佩贵和束龙仓, 2008, 束龙仓和朱元生, 2000, 吴吉春和陆乐, 2011). For example, Walker et al. (2003) distinguished the uncertainty in three dimensions: location, level, and nature of uncertainty. The classification based on the location is mainly identified by the logic of model formulation, including context uncertainty, model uncertainty, input uncertainty, parameter uncertainty and model outcome uncertainty. The classification based on the level includes scenario uncertainty, recognized ignorance and statistical uncertainty. The classification based on the nature includes epistemic uncertainty and variability uncertainty. Yen et al. (2014) classified the uncertainties in hydrology and hydraulics into four aspects: (1) the input data uncertainty, (2) model structure uncertainty, (3) model parameter uncertainty, and (4) measurement uncertainty in calibration/validation data. For the sake of simplicity and clarity, we assumed the applied numerical code is error free and mainly focused the following three uncertainty sources: data uncertainty, parametric uncertainty, and structural uncertainty. This classification has also been widely accepted by the hydrology community (Ajami et al. 2007, Song et al. 2015). Table 1-2 lists one such classification relevant to the application of hydrological models.

表 1-2 地下水模型不确定性来源分类

Table 1-2 A classification of different types of uncertainty in subsurface hydrologic modeling

Type of uncertainty	Description
Data uncertainty	Uncertainty associated with the description of hydrological events and the external variables such as rainfall, temperature, soils, and land use/cover that driving the hydrological system (forcing data) as well as measurement data such as flowrate at the river outlets and hydraulic head in the observation wells that used to calibrate the model (conditioning data).
Parameter uncertainty	Uncertainty resulting from various physically or empirically based model parameters such as spatially distributed hydraulic conductivity which often cannot be measured directly or be known with certainty.
Model uncertainty (Model structure uncertainty)	Uncertainty contributed by the inability of the model structure to perfectly mimic hydrologic processes. Different models have different degrees of complexity and different algorithms to mimic natural processes. Even within a given modeling system, alternative methods may be offered. For example, three methods are available in SWAT to estimate the potential evapotranspiration (Neitsch et al. 2011).

1.2.1.1 Data Uncertainty

Data uncertainty refers to the uncertainty of input data (also known as forcing data) such as rainfall, temperature, soils, and land use/cover which are critical drivers for

hydrologic simulation as well as the calibration data (also known as conditioning data) such as flow rate at the river outlets and hydraulic head in the observation wells. For example, adequate characterization of rainfall inputs is critical to success in rainfall-runoff modelling and the impact of rainfall errors on predicted flow has been highlighted by many authors, including Bárdossy and Das (2008), Kavetski et al. (2006a, 2006b), Liu et al. (2020), Moulin et al. (2009), Sun et al. (2000).

There are three major sources of data uncertainty. The first source is uncertainty caused by measurement error. When we make any measurement, we can never be certain what the result exactly is. There is always an uncertainty associated with the measurement. The measurement uncertainty can be caused by a number of factors including the measuring instrument, operator skill, measurement process, and the environment such as temperature, air pressure, humidity and many other conditions can affect the measuring instrument, or the item being measured (Bell 2001). The second source results from hydrometric uncertainty in measured hydrological data. For the velocity area method, examples of uncertainty may be identified as: instantaneous uncertainty at one point, uncertainty of vertical average velocity calculated using restrict points along the vertical, depth and velocity sampling error, uncertainty at depth and width measuring and equipment uncertainties etc. (Steinbock et al. 2016). For the areal precipitation method, the uncertainty may arise from the number of rain gauges used to derive the areal precipitation by the method of Thiessen polygons (Kobold and Brilly 2006). The last source of uncertainty is stochastic uncertainty, e.g., uncertainty caused by inherent randomness of natural process such as climate change (Bonan et al. 2019) or uncertainty resulting from limited sample size during simulation.

To deal with the data uncertainty, Ajami et al. (2007) introduced the integrated Bayesian uncertainty estimator (IBUNE) to account for uncertainty contributed by rainfall data through an input error model, which assumed a random Gaussian error as a multiplier for every input observation. Raleigh et al. (2015) discussed the effects of different error types (i.e., bias and random errors), different error probability distributions, and different error magnitudes on physically based simulations of four snow variables (snow water equivalent, ablation rates, snow disappearance, and sublimation) simulated by Utah Energy Balance model. Their results suggested the model outputs were consistently more sensitive to forcing biases than random errors, generally less sensitive to forcing error distributions, and critically sensitive to different forcings depending on

the relative magnitude of errors. Shi et al. (2014) evaluated the validity of using Gaussian assumptions for model residuals in uncertainty quantification of a groundwater reactive transport model. Their work showed that the residuals of the reactive transport model are non-Gaussian, heteroscedastic, and correlated in time. 杨乐等 (2016) combined the DREAM (Differential Evolution Adaptive Metropolis) algorithm with MODFLOW to quantitatively analyze the uncertainty of the numerical simulation results of groundwater. The observation errors were assumed to follow normal distribution with standard deviations increasing from 0 to 1.0. The results suggested that the standard deviations of the posterior distribution of parameters obtained from DREAM increased with that of the observation errors.

1.2.1.2 Parameter Uncertainty

Currently, parameter uncertainty is a hot topic in the field of uncertainty research (Song et al., 2015, 宋晓猛等, 2015). Parameter uncertainty arises from various physically or empirically (conceptually) based model parameters which are not known with certainty or are difficult to obtain. Physically based parameters such as hydraulic conductivity and dispersion coefficient can be measured or estimated, if possible, when extensive data collection is possible. The empirically parameters such as CN₂ in the SCS curve method are defined as the conceptualization of a non-quantifiable process and determined by the process of model calibration (Shen et al. 2012).

During the past two decades, much work has been done to understand and to improve hydrologic model calibration techniques. Various uncertainty analysis techniques have been introduced in hydrologic literature, including Generalized Likelihood Uncertainty Estimation (GLUE, Beven and Binley (1992), 黄国如和解河海(2007)), Model-Independent Parameter Estimation and Uncertainty Analysis (PEST, Doherty et al. (2010)), Shuffled Complex Evolution Metropolis (SCEM, Vrugt et al (2003)), DREAM (Vrugt 2016, 杨运等, 2016), etc. These methods can be roughly classified into two groups: sophisticated methods and the global optimization strategies (Thiemann et al. 2001). In typical sophisticated methods, the goodness-of-fit between the simulated and observed outputs is measured and only one set (the optimal) of calibrated parameters is accepted with best goodness-of-fit statistic measures. However, the global optimization strategies aim to search the parameter space (the prior distributions) and return the posterior distributions of the parameters. These parameters are described in terms of probabilities associated with the simulated and observed outputs.

1.2.1.3 Model Uncertainty

Model uncertainty (also known as the model structure uncertainty) mainly derives from the simplifications of reality in models' principles. In most cases, the model structure is determined a priori, in keeping with the previous knowledge of the modeler. However, there is an ongoing debate in hydrology whether a "one model fits all" approach should be pursued, based on the assumption that the fundamental hydrological processes are the same everywhere (Knoben et al. 2020). In practice there are many different models available that all represent a certain view of which hydrologic processes are important and how these should be mathematically represented. Different models have different degrees of complexity and different algorithms to mimic natural processes. Even within a given modeling system, alternative methods may be offered. Uncertainty due to model structure can significantly impact the accuracy of model outputs and it has been recognized often to be the most important source of uncertainty (Dubus et al. 2003a, Neuman and Wierenga 2003, Poulin et al. 2011, 夏强, 2011). The sources of uncertainties in the model structure are manifold, e.g., choice of processes included in the model, the mathematical formulations, boundary conditions, initial conditions, and the hydrogeological interpretation. Recently, multi-model approaches to explicitly address conceptual uncertainty have gained renewed interest Gupta et al. (2012) and researchers have developed a set of multi-model frameworks to explicitly consider the model uncertainty such as FUSE, SUPERFLEX, and SUMMA which has been widely applied in many studies (Clark et al. 2011, Clark et al. 2015b, Fenicia et al. 2011, Kavetski and Fenicia 2011, van Esse et al. 2013). Multi-modeling means to postulate several alternative hydrologic models for a site and use model selection criteria (also known as model discrimination or information) to (1) rank these models, (2) eliminate some of them, and/or (3) weight and average predictions and statistics generated by multiple models. These models may differ in their conceptuality (e.g., being physics-based or data-driven), or in their level of detail (e.g., scale or resolution), but they all yield the same desired quantity as model output.

Working with a set of competing models (hypotheses), we can follow two intuitively distinct modeling approaches: the "winner-take all" perspective of model selection or the "team-of-rivals" perspective of model averaging (Höge et al. 2019). In the case of "winner-take all" perspective, the goal is typically to identify the "true model" (or the best model) in the available set of models, and as a result, to reduce the considered model

space in order to keep the computational effort for prediction low. In the case of model averaging, it avoids having to choose one model and allows to combine the best properties of different models, with the hope to obtain a combined estimate that is more skillful and reliable than any of the individual models.

The core idea behind the model averaging method is to obtain average predictions from a set of plausible models by linearly combining individual model predictions. Denote Δ as the quantity of interest predicated by a set of K alternative models $M = [M_1, M_2, \dots, M_K]$, then $p(\Delta|M_K)$ represents the distribution of Δ which is the quantity to be predicated under model M_K . The distribution of the model averaging prediction, Δ , is thus given by:

$$p(\Delta) = \sum p(\Delta|M_K) \times p(M_K) \quad (1.1)$$

where $p(M_K)$ is the model weight of M_K . This term is also known as the likelihood of M_K being the corrected model. The weights to aggregate multiple model outputs can be equal (model average) in the simplest case or can be determined through Bayesian model averaging (BMA) (Rojas et al. 2008, 董磊华等 2011, 薛亮和夏强 2016, 王慧亮等 2011, Zeng et al. 2016). Ye et al. (2008a) reviewed several commonly used model selection criteria such as the Akaike, Bayesian, or Kashyap Information Criteria. Höge et al. (2019) wrote an excellent review for Bayesian model selection (BMS) and BMA as a rigorous statistical framework for model choice under uncertainty.

1.2.2 Sensitivity Analysis for Uncertainty Apportionment

1.2.2.1 Sensitivity Analysis and Uncertainty Analysis

As mentioned above, a logical way to identify the controlling processes governing a system is to first deal with the uncertainty in hydrologic modeling. Sensitivity analysis (SA) thus emerges to address such a concern. A former definition of SA, according to Saltelli (2002), is “*the study of how uncertainty in the output of a model (numerical or otherwise) can be apportioned to different sources of uncertainty in the model input*”. In this context, it is important to note that SA is much related to – but distinct from – uncertainty analysis (UA) as modelers often tend to conflate the two terms (Saltelli et al. 2019). The goal of UA is to quantify the uncertainties of a model’s output that result from the uncertainties in the model inputs, which allows modelers to answer the question “How uncertain is my model output?”. SA is complementary to UA and aims to apportion

uncertainty in model output to different uncertain factors regarding their contribution to model output variability. SA allows us to infer that, for example, “this factor alone is responsible for 80% of the uncertainty in the output”. Generally, UA comes before SA and SA should precede UA (Kleijnen 1994): uncertainty needs to be first estimated and before it can be apportioned. However, this is not necessarily the case, and applications involving model calibration/optimization may not require the quantification of uncertainty (Saltelli et al. 2019).

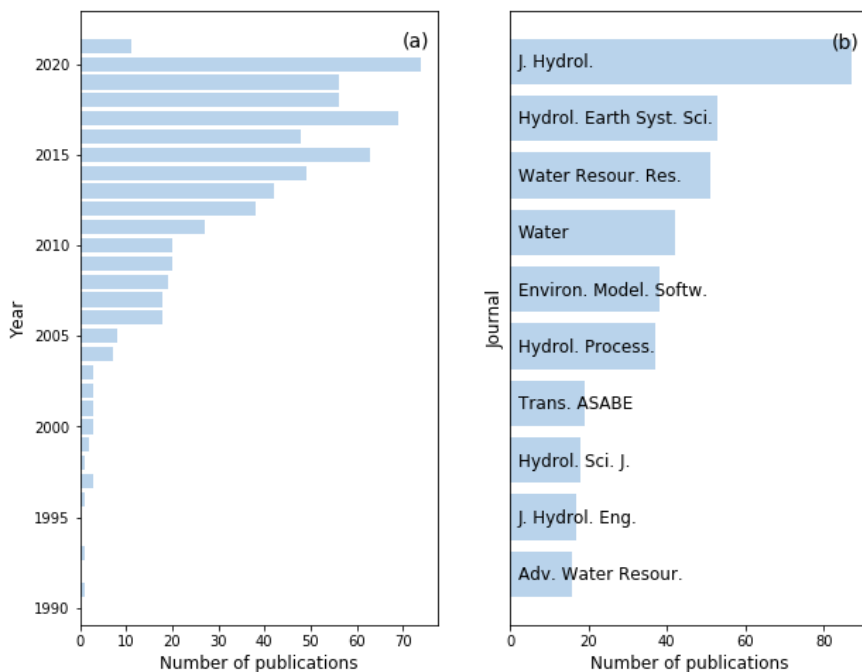


图 1-2 (a) Web of Science 核心集关于水文模拟领域敏感性分析研究发表期刊论文(即发表类型为 J)的年发表量; (b) 发表量累计排名前 10 的期刊。根据 2021 年 5 月 26 日的搜索结果, 搜索条件为: “sensitivity analysis” AND (“hydrologic” OR “hydrological”) AND (“model” OR “modeling”) AND “uncertainty”, 总记录数为 666 条。

Figure 1-2 (a) Yearly publications of peer-reviewed journal articles (i.e., the publication type should be “J”) on sensitivity analysis in the field of hydrologic modeling from the Web of Science Core Collection and (b) the top 10 publishing journals. The total number of records is 666 based on the search terms: “sensitivity analysis” AND (“hydrologic” OR “hydrological”) AND (“model” OR “modeling”) AND “uncertainty” on May 26, 2021.

1.2.2.2 Local Sensitivity Analysis and Global Sensitivity Analysis

Mainly focused on parameter uncertainty, SA techniques have been widely used in hydrologic modeling (Figure 1-2). SA techniques can be classified based on their scope, applicability, and characteristics (Song et al. 2015). The simplest and most common classifications are local SA (LSA) and global SA (GSA) (Borgonovo and Plischke 2016,

Song et al. 2015, Tian 2013, van Griensven et al. 2006). Table 1-3 lists these two typical categories and their descriptions, characteristics, and typical methods.

表 1-3 敏感性分析方法基本分类：局部敏感性分析(LSA) 和全局敏感性分析(GSA)

Table 1-3 Summary of basic classification for SA methods: Local sensitivity analysis (LSA) and Global sensitivity analysis (GSA)

Classifications	LSA	GSA
Descriptions	Compute local response of model output based on the gradients (derivatives) of the model output with respect to parameter values evaluated at a single location in the parameter space	Evaluate the effect in the entire ranges of uncertain parameters
Characteristics	Easy of operation and interpret, relatively low computational cost, no self-verification, local effect of individual parameters	Estimating the effect of all the inputs or their combined effect on the variation of output based on numerous model runs
Typical methods	Finite difference method; First-order second moment (FOSM) (Dettinger and Wilson 1981, Glasgow et al. 2003).	Regression method; Morris' method (Morris 1991); Sobol's method (Sobol' 2001); PAWN index (Pianosi and Wagener 2015); AMA indices (Dell et al. 2017); Delta moment-independent measure (Borgonovo 2007).
Software	C++ based PSUADE software (Gan et al. 2014a); Sensitivity package for R;	
Implementation	SAFE toolbox for MATLAB (Pianosi et al. 2015); SALib package for Python (Herman and Usher 2017).	

LSA focuses on the effects of uncertain inputs around a point (the base point or the reference point or the nominal point) of interest in the model input space, for example, the derivative-based approach. Sensitivity (typically resting on the derivative concept) is evaluated in the neighborhood of a given combination of parameters of a model (Cacuci 2003). LSA has the attraction of being very computational efficient. However, it only provides information at the base point and does not provide for an exploration of the rest space of the input factors. This would matter relatively little for linear systems, in which the property at a point away from the baseline can be computed quickly by linear extrapolation, but it would matter greatly for nonlinear ones. GSA approaches rest on the evaluation of sensitivity (usually quantified through metrics entailing the variability of

the model response) across the entire support within which model system parameters vary. Considering the inherent nonlinear nature of hydrological systems, the focus of this thesis is on GSA. In practice, GSA methods are usually recommended in hydrological modeling applications because they have certain advantages compared with LSA methods (Baroni and Tarantola 2014, Rosolem et al. 2012, Song et al. 2012). A wide range of GSA techniques is available (Song et al. 2015) and up-to-date reviews of GSA developments are given in Iooss and Lemaître (2015).

1.2.2.3 Uncertainty Apportionment: Factors Prioritization and Factors Fixing

An open question in SA is how the uncertainty of the model output can be apportioned. Within the framework of GSA, Saltelli et al. (2004) argued that this must be linked to the nature of the question(s) the SA is intended to address. They introduced four “settings”, i.e., (1) Factors Prioritization Setting, (2) Factors Fixing Setting, (3) Variance Cutting Setting, and (4) Factors Mapping Setting for SA. A setting is a way of framing the sensitivity quest in such a way that the answer can be confidently entrusted to a well-identified measure. The first two settings are discussed in this thesis as they are most frequently used in literature and closely related to the “controlling processes” defined in this thesis:

- (1) **Factors Prioritization Setting:** The objective of this setting is to identify the most important factor, which is defined as the one that, if determined (i.e., fixed to its true, albeit unknown, value), would result in the greatest reduction in the uncertainty of the system model output. Similarly, the second most important factor can be defined, and so on till all the factors are ranked in order of importance. If such a factor is identified, we can devote resources to study the factors for achieving the greatest reduction in predictive uncertainty to improve model predictions.
- (2) **Factors Fixing Setting:** The objective of this setting, which could also be labelled “screening”, is to identify the factor or the subset of input factors that we can fix at any given value within their range of uncertainty without significantly reducing the uncertainty in output. If such a factor or subset of factors are identified, we can avoid spending resources to study the factors (i.e., exclude them from further investigation) that have non-influential contribution to predictive uncertainty.

To better understand the above two settings, we assume that the model output y is simulated by a generic mathematical function f with k unknown input factors x_i ($i = 1, 2, \dots$,

k),

$$y = f(\mathbf{x}) = f(x_1, x_2, \dots, x_k). \quad (1.2)$$

Assuming that we already have some idea about the uncertainty range of these factors. This knowledge might originate from a variety of sources: measurements, expert opinion, physical bounds or an analogy with factors for similar species/compounds. Let us further assume that all the factors x_i are left free to vary over their entire range and we are able to compute the model output as much as we want, possibly sampling from the best joint probability distribution of input that we can come up with. Let \mathbf{X} denote the random model input vector and X_i denotes the random input factor of x_i . The model output then becomes a random variable Y , related to \mathbf{X} through Equation (1.2), i.e., $Y=f(\mathbf{X})$. As is standard in sensitivity analysis, we denote the joint cumulative distribution function (CDF) of the model parameters by $F_{\mathbf{x}}(\mathbf{x})$, their joint probability density function (PDF) by $f_{\mathbf{x}}(\mathbf{x})$, and the marginal cumulative distribution function and probability density function of X_i as $F_{X_i}(x_i)$ and $f_{X_i}(x_i)$. The CDF and PDF of the model output are denoted by $F_Y(y)$, and $f_Y(y)$, respectively.

Factors Prioritization

In Factors Prioritization Setting, the analyst's goal is to identify the input factor that, once fixed to its true value x_i^* , would lead to the greatest reduction in the uncertainty of the model output (Saltelli et al. 2004). One way is to consider the statistical dependence between Y and x_i^* , i.e., an operator between $\zeta(P_Y, P_{Y|x_i^*})$, where P_Y and $P_{Y|x_i^*}$ are unconditional and conditional (density) distributions (PDF or CDF) of the model output. An example of operators used in literature is

$$\zeta^V(P_Y, P_{Y|x_i^*}) = \frac{V(Y) - V(Y | X_i = x_i^*)}{V(Y)} \quad (1.3)$$

for Sobol's variance-based sensitivity measures (Homma and Saltelli 1996). The larger the statistical dependence $\zeta^V(P_Y, P_{Y|x_i^*})$, the more important factor x_i is. In general, we can consider any operator $\zeta(P_Y, P_{Y|x_i})$ as long as it satisfies $\zeta(P, P) = 0$, i.e., the operator $\zeta(,)$ is required to be null when the two distributions are identical, (Borgonovo et al. 2017). Examples of other operators are the L^1 -norm on PDFs

$$\zeta^{L1} \left(P_Y, P_{Y|x_i^*} \right) = \frac{1}{2} \int_y |f_Y(y) - f_{Y|x_i^*}(y)| dy \quad (1.4)$$

for the Delta moment-independent measure (Borgonovo 2007), or the Kolmogorov-Smirnov distance between CDFs

$$\zeta^{KS} \left(P_Y, P_{Y|x_i^*} \right) = \sup_y |F_Y(y) - F_{Y|x_i^*}(y)| \quad (1.5)$$

in the PAWN (named after the authors' names) method (Pianosi and Wagener 2015).

The issue is that we do not know what x_i^* is for each x_i . It appears sensible to take the average of the above measure over all possible values for each x_i . Taking the expectation of Equation (1.3) leads to the well-known first-order sensitivity index of Sobol's variance-based sensitivity method,

$$S_i = E_{X_i} \left(\frac{V(Y) - V_{X_{-i}}(Y | X_i = x_i)}{V(Y)} \right) = \frac{V(Y) - E_{X_i} (V_{X_{-i}}[Y | X_i = x])}{V(Y)} \quad (1.6)$$

Similarly, taking the expectation of equations (1.3) and (1.4), we obtain the well known

$$\delta_i = \frac{1}{2} E_{X_i} \int_y |f_Y(y) - f_{Y|X_i}(y)| dy \quad (1.7)$$

for Delta moment-independent measure (Borgonovo 2007), and

$$\zeta^{KS} \left(P_Y, P_{Y|X_i} \right) = \sup_y |F_Y(y) - F_{Y|X_i}(y)| \quad (1.8)$$

in PAWN method (Pianosi and Wagener 2015).

Factors Fixing

In Factors Fixing Setting, the analyst's goal is to identify factors in the model which, left free to vary over their range of uncertainty, make no significant contribution to the uncertainty of the model output. This can be turned into a setting: "which is the factor that, being left undetermined while all others are fixed to their true values, would leave the largest uncertainty (the uncertainty left) in the output?" Similarly, we can consider another operator between $\xi(P_Y, P_{Y|X_{-i}})$, where P_Y and $P_{Y|X_{-i}}$ are unconditional and conditional distributions (PDF or CDF) of the model output. An example of operators used in the literature is

$$\xi^V \left(P_Y, P_{Y|X_{-i}} \right) = \frac{V_{X_i}(Y | X_{-i}^*)}{V(Y)} \quad (1.9)$$

for Sobol's variance-based sensitivity measures. The educated guess (because even here we do not know where the other factors are fixed) is to look at the average of the above

measure over all possible values for all other factors except for x_i . Taking the expectation of Equation (1.9) leads to the well-known total-effect sensitivity index of Sobol's variance-based sensitivity method,

$$S_{Ti} = E_{X_{-i}} \left(\frac{V_{X_i}(Y | X_{-i})}{V(Y)} \right) = \frac{E_{X_{-i}} V_{X_i}(Y | X_{-i})}{V(Y)}. \quad (1.10)$$

1.2.3 Identifying the Controlling Processes via Sensitivity Analysis

1.2.3.1 Controlling Processes Concept

Controlling is not a mathematical concept. Besides, there is no formal definition of “controlling process” in hydrologic modeling. A similar phrase found in Wikipedia is the “controlling interest”. According to Wikipedia, “*a controlling interest is an ownership interest in a corporation with enough voting stock shares to prevail in any stockholders' motion*”. What is the meaning of controlling processes? Is it possible to quantify the degree of the “controlling” for a given process? In this thesis, the answer to these questions is that “controlling” must be defined rigorously, to the greatest extent possible, at the stage of framing the analysis to lay the groundwork for the subsequent discussion.

Extending the line of thought by Saltelli et al. (2004), the factors discussed in the two settings above can be replaced by processes without affecting the discussion. Processes are broader than factors, as a process may include multiple factors, their interactions, and various physical, chemical, and biological mechanisms involved in the process. A hydrologic process, qualitatively speaking, includes a series of water/energy/solute movements in water/energy/mass cycles. For example, a recharge process of an unconfined aquifer is referred to as water movements from land surface to the aquifer, a geological process of an aquifer is referred to as water movements in the aquifer, and a discharge process is referred to as water movements from an aquifer to a surface waterbody. A process may be divided into sub-processes, and two processes may be combined into a new process, depending on objectives of a study. For example, Dai et al. (2019) divide a groundwater flow process into a geological sub-process (to consider different configurations of an alluvial layer) and permeability sub-process (to consider different parameterizations of permeability). Using processes rather than factors can yield more hydrologically meaningful results to advance our understanding of a complex hydrologic system.

In this context, we distinguish the concept of controlling processes into twofold but closely connected aspects in this thesis:

- (1) In Factors Prioritization Setting, we want to make a rational bet on what is the process that one should fix to achieve the greatest reduction in the uncertainty of the output. In line with this, controlling processes are those control reductions of predictive uncertainty. We refer to these processes as **important processes** in hydrologic modeling.
- (2) In Factors Fixing Setting, we try to screen the input processes by identifying process or sets of processes that non-influential. In this sense, controlling processes are those control how much uncertainty caused by themselves and their interactions with other processes. We refer to these processes as **influential processes** in hydrologic modeling.

A summary conclusion is that any statistical measure that quantifies the difference between the unconditional variability of the model output and the conditional variability of the model output conditioning on a given process falls into the Factors Prioritization Setting and the controlling processes is referred to importance processes. Any statistical measure that quantifies the difference between the unconditional variability of the model output and the conditional variability of the model output conditioning on a given process falls into the Factors Fixing Setting and the controlling process is the influence process. Figure 1-3 shows the big picture linking the uncertainties in hydrologic modeling, uncertainty analysis, sensitivity analysis, and identifying the controlling process via sensitivity analysis.

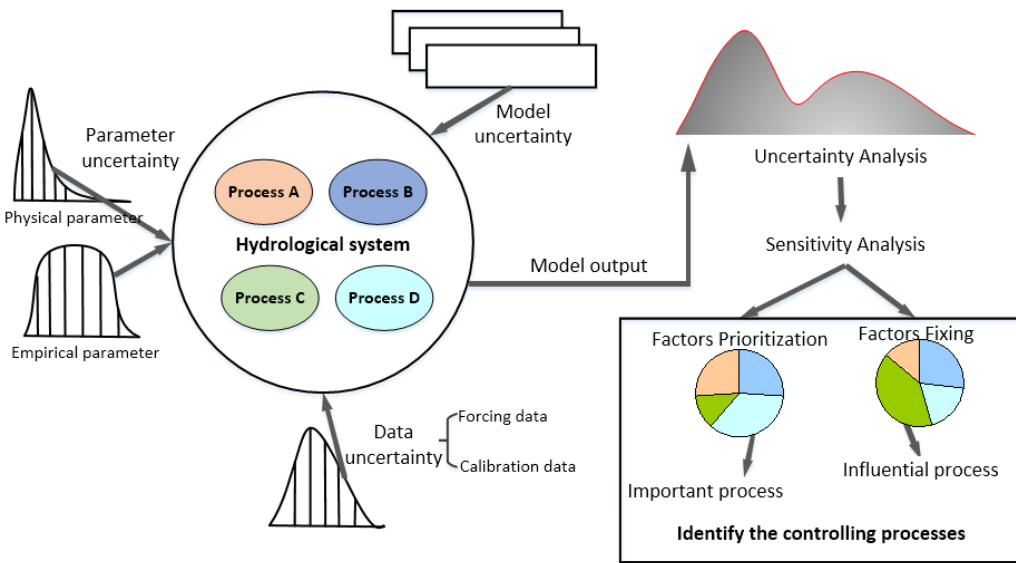


图 1-3 地下水模型不确定性来源、不确定性分析、敏感性分析，以及通过敏感性分析识别控制过程之间的联系。由于地下水模型中存在各种来源的不确定性，模型输出通常可以刻画为一定的概率分布函数（红色曲线）。将模型输出中的不确定性（例如可以利用方差来代表模型输出的不确定性）进行分解后划分和分配到输入中的不确定性来源，此过程称之为敏感性分析。重要过程可以通过因子排序识别，即寻找某一过程，该过程一旦确定，系统模型输出不确定减少最多。影响过程可以通过因子固定识别，即寻找某一过程，若该过程无法确定，系统模型输出的不确定性保留最多。

Figure 1-3 A picture depicting the uncertainties in subsurface hydrologic modeling, uncertainty analysis, sensitivity analysis, and identifying the controlling process via sensitivity analysis. Uncertainty coming from a variety of sources is propagated through the model, resulting in an empirical distribution of the desired output (red curve). The uncertainty in the model output, e.g., captured by its variance, is then decomposed according to source, thus producing a sensitivity analysis. The controlling process is then identified by looking for the important process that reduces the most variance for Factors Prioritization Setting and the influential process that leaves the maximum variance left for Factors Fixing Setting.

1.2.3.2 A Pedagogical Example

Before plunging into any details, we here consider a very simple problem. Imagine a system model consists of two processes A and B . Each of the two processes has only one process model (mathematical representation) described as follows:

$$M_A : a = 4x_1, \quad (1.11)$$

$$M_B : b = x_2^2. \quad (1.12)$$

Denoting model output as Δ , it equals the summation of two process model outputs, $\Delta = a + b$. Parameter x_1 of process A and parameter x_2 of process B are assumed to follow

the normal distribution $N(0,1^2)$. The two parameters are independent and uncorrelated.

Since there are only two processes in the system model, our research goal is to explore which process between A and B is the controlling process for the model output Δ . In this simple example, each process model only contains one uncertainty parameter, i.e., parameter x_1 for process A and parameter x_2 for process B . The uncertainty of this process can be represented by the parameter uncertainty associated with the corresponding process. The identification of the controlling process between A and B is then equivalent to identification of the controlling parameter between x_1 and x_2 . If parameter x_1 is identified as the controlling parameter, we can conclude that process A is the controlling process and vice versa.

The important process, according to the controlling processes concept, refers to the process that should be fixed to achieve the greatest uncertainty reduction in the uncertainty of the output. Using variance as an uncertainty measure and according to Equation (1.5), the uncertainty reduction by fixing process A is easily calculated as

$$V(\Delta) - E_{X_1} (V_{X_2}[\Delta | X_1 = x_1]) = 18 - 2 = 16. \quad (1.13)$$

Similarly, the uncertainty reduction achieved by fixing process B is easily calculated as

$$V(\Delta) - E_{X_2} (V_{X_1}[\Delta | X_2 = x_2]) = 18 - 16 = 2. \quad (1.14)$$

The results indicate that if process A is fixed to its true process, i.e., the true parameter value of x_1 can be learned, the uncertainty (in terms of variance) of the model output can be reduced by 16, which is significantly greater than the uncertainty of 2 if process B is fixed to its true process. In this case, we can say that process A is more important than process B .

In order to identify the influential process, we continue to use variance as an uncertainty measure and according to Equation (1.10), the uncertainty left if process B is fixed but process A cannot be determined is

$$E_{X_{\sim 1}} V_{X_1}(Y | X_{\sim 1}) = E_{X_2} V_{X_1}(Y | X_2) = 16. \quad (1.15)$$

Similarly, the uncertainty left if process A is fixed but process B cannot be determined is

$$E_{X_{\sim 2}} V_{X_2}(Y | X_{\sim 2}) = E_{X_1} V_{X_2}(Y | X_1) = 2. \quad (1.16)$$

The results indicate that if process A cannot be determined, the uncertainty left in the model output is 16, which is significantly greater than the uncertainty left of 2 if process B is ignored or cannot be determined. Thus, we can say that process A is more influential

than process B , and consequently, parameter x_2 of process B may be set at any value within its range without significantly affecting the model outputs.

This is a very simple example, but it demonstrates the fundamental concept of using sensitivity analysis to identify the controlling processes. There are only two processes in this example, and each process model only has one process model. In this case, the traditional sensitivity analysis methods can fulfill the goal for identifying the controlling processes in hydrologic modeling. Let us now extend this example by still considering two processes but this time process A is represented by two alternative process models as shown below:

$$M_{A_1} : a = 4x_1 \quad M_{A_2} : a = x_1 \quad (1.17)$$

Combining the process models for process A and the process models for process B leads to two alternative system models, A_1B and A_2B .

表 1-4 利用基于方差的不确定性分析方法识别控制过程的算例分析。黑体数字表示 A 过程和 B 过程 S_i 和 S_{Ti} 的较高值。

Table 1-4 Results for identifying the controlling process for the proof-of-concept example by using variance as an uncertainty measure. The higher value for S_i and S_{Ti} between the two processes is indicated by bold numbers.

System model		A_1B		A_2B	
Process		A	B	A	B
Uncertainty reduction		16	2	1	2
S_i (%)		88.89	11.11	33.33	66.67
Process		A	B	A	B
Uncertainty left		16	2	1	2
S_{Ti} (%)		88.89	11.11	33.33	66.67

Table 1-4 illustrates the results of identifying the controlling process for each system model, following the same produces as shown above. It should be noted that the S_i and S_{Ti} are calculated by normalizing the uncertainty reduction and uncertainty left to the total uncertainty for each system model based on Equations (1.5) and (1.0), respectively. The results suggest that process A is the most important/influential process for system model A_1B while process B is the most important/influential process for system model A_2B . The conflicting results support our hypothesis that we mentioned at the start of this chapter. Model uncertainty imposes challenges to the identification of controlling processes. It is also worth noting that the important process and influential process are the same in this case, and the variance reduction and variance left are the same for both processes. This is

due to the fact that there are only two processes in this sample example and there is no interaction between the two processes, as demonstrated later. There could be many processes and process models under consideration in practice.

1.2.4 Unresolved Problems

Based on the discussion above, a comprehensive review of current research in identifying the controlling process indicate the following unresolved problems:

(1) The existing methods ignore the inherent uncertainty in conceptualizing and modeling individual processes. Many studies have shown that using a single process model is questionable when available data and knowledge support use of multiple process models (e.g., Ye et al. (2010b), Lu et al. (2015)). Data will fit more than one conceptual model equally well, and consequently, a good calibration of a model does not ensure a correct conceptual model. To our knowledge, the issue of process model uncertainty has been largely ignored in the existing methods for identifying controlling processes.

(2) The existing methods are lack of a summary measure that explicitly quantifies the relative importance of individual processes because the existing methods measure process importance through parameter importance. Although the existing methods explicitly consider interactions between parameters, they do not explicitly consider the interactions between processes.

(3) The existing methods cannot be directly used for large-scale problems in practice because the methods are computationally expensive due to their relying on Monte Carlo implementations. This is a barrier to comprehensive identification of controlling processes for computationally expensive models, because only a small number of model executions are practically affordable to a small number of processes.

§1.3 Research Objectives, Procedure, and Innovations

1.3.1 Research Objectives

The overarching scientific question to be answered in this project is as follows: If we are not certain about the choice of process models and model parameters, can we correctly identify the controlling processes of a complex system? The answer to this question is important at the stage of model development, when we need to decide which process model(s) will be incorporated in the system model. The answer is also important

at the stage of model improvement, because we need to decide which processes deserve more research efforts. The goal of this project is therefore to develop approaches of multi-model global sensitivity analysis for identifying controlling processes for development and improvement of mechanically based hydrologic models. The specific objectives of this dissertation for achieving the research goal and for addressing the three theoretical and computational challenges described above are as follows:

- (1) Develop a set of new process sensitivity indices as summary measures to explicitly quantify relative importance and influence of individual processes. The new indices should take into account of not only the inherent uncertainty of process models but also the interactions between individual processes. Efficient methods for reducing computational costs should also be developed.
- (2) Introduce the concept of multiple working hypotheses, i.e., the multiple system models, into the identification of controlling processes of a complex system. Apply the new developed methods to real-word hydrologic models for identifying the controlling processes to improve the understanding complex hydrological systems.
- (3) Create new software or a package to put the ethos into action. The new software should allow for practical identification of controlling processes for any complex hydrological models using the newly developed methods.

1.3.2 Research Procedure

As shown in Figure 1-4, this dissertation will develop two different methods for identifying the controlling process in subsurface hydrologic modeling under multiple system models and apply the methods to two real-word subsurface hydrologic models. The first two chapters (Chapter 2 and Chapter 3) present the new developed methods, and the following two chapters (Chapter 4 and Chapter 5) are for the applications. Finally, Chapter 6 presents SAMMPy, a new open-source Python package for identifying the controlling process under multiple system models. The summary of this dissertation is presented in Chapter 7.

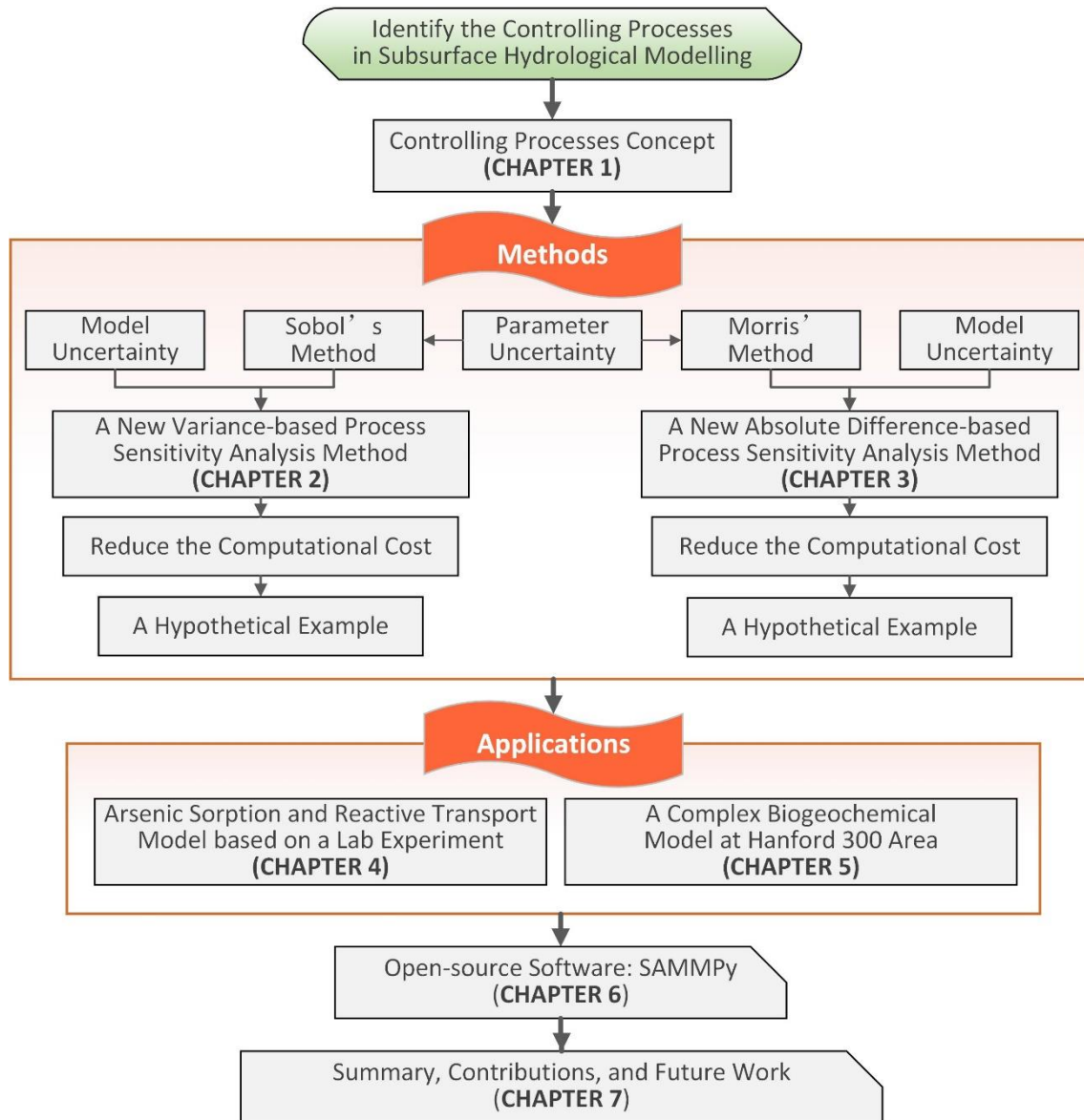


图 1-4 技术路线图

Figure 1-4 Research procedures

1.3.3 Innovations

The main innovations of this research are to develop a set of new process sensitivity indices as summary measures to explicitly quantify relative importance or influence of individual processes considering both parametric and model uncertainty, to apply the new methods to complex hydrologic models to improve our understanding, and to create a new software for the new methods, which are listed as follows:

- (1) In Chapter 2 and Chapter 3, this dissertation developed a set of new variance-

based process sensitivity indices are defined for identifying the controlling processes in hydrologic modeling. In Chapter 2, this dissertation extended the traditional Sobol's method to allow multiple plausible process models to represent a single process by using model averaging approach. An efficient estimator was proposed to reduce the computational cost. In Chapter 3, two absolute difference-based process sensitivity indices are defined for identifying the influential processes in hydrologic modeling. This method is rooted in Morris' screening method and is computational cheaper than the variance-based process sensitivity indices proposed in Chapter 2.

(2) In Chapter 4 and Chapter 5, the two new methods were applied to identify the controlling processes of two real-world subsurface hydrological modeling examples. In Chapter 4, a 2-D arsenic sorption and reactive transport numerical model is built based on a laboratory experiment, and the variance-based process sensitivity analysis method developed in Chapter 2 was applied to investigate the influence of physic-chemical aquifer heterogeneity as well as different sorption models on arsenic sorption and reactive transport in the flume system. In Chapter 5, the two newly developed methods presented in Chapter 2 and Chapter 3 are applied to a real-world biogeochemical model at the groundwater-surface water interface within the Hanford Site's 300 Area to identify the controlling processes governing the spatio-temporal distribution of the organic carbon (OC) consumption rate in the aquifer.

(3) In Chapter 6, this dissertation presents SAMMPy, an open-source python package for performing process sensitivity analysis across multiple system models. It provides visualization tools as well as workflows to assist users for performing process sensitivity analysis to identify the controlling process in subsurface hydrological modeling across multiple system models.

Chapter 2 A New Variance-based Process Sensitivity Analysis

Method

The purpose of this chapter is to develop a new variance-based process sensitivity analysis method for identifying the controlling processes in hydrologic modeling. This chapter extends the traditional Sobol's variance-based sensitivity analysis method to allow for multiple plausible process models to represent a single process by using model averaging approaches. Because of the integration, the new method allows for identifying the important process for Factors Prioritization Setting and for identifying the influential process for Factors Fixing Setting with consideration of uncertainty in process models and process model parameters. Besides, this chapter proposes an efficient design and estimator for estimating the process sensitivity indices to reduce the computational cost. The numerical evaluation is examined by a hypothetical one-dimensional (1-D) groundwater flow modeling, of which a total of eight system models are developed by considering three processes (recharge, geology, and snowmelt) and two alternative process models for each process. This modular modeling structure has been widely used in surface water and groundwater modeling (Dai et al. 2017b, Lu et al. 2015, Ye et al. 2010b). The numerical experiment of groundwater modeling is used to demonstrate the following: (1) how the first-order process sensitivity index is used to identify important processes, (2) how the total-effect process sensitivity index is used to identify influential and non-influential processes, and (3) why bother to distinguish the important process and influential process in the controlling processes concept (i.e., first-order and total-effect process sensitivity indices give different ranking orders due to process interactions).

§2.1 Introduction

Statistical methods have been developed recently to identify important or influential system processes under process model uncertainty by implicitly or explicitly address process model uncertainty (Mai et al. 2020). In an implicit approach, multiple models are developed, sensitivity analysis is conducted for parameters of each model, and importance

or influence of the parameters is examined across the models (Bianchi Janetti et al. 2019, Günther et al. 2019, Herman et al. 2013b, van Werkhoven et al. 2008). Taking the study of Bianchi Janetti et al. (2019) as an example, they considered three conceptual geological models with uncertain parameters, applied three different methods of global sensitivity analysis to each model, and evaluated intra-model and inter-model differences of the results of sensitivity analysis. They found that the choice of the conceptual model characterizing aquifer lithology affects parameter influence on model outputs. The study of Van Hoey et al. (2014) appears to be the first to explicitly consider model uncertainty in a qualitative model component sensitivity analysis, where a model component is defined as “a conceptual description of a subprocess of the entire model”. The model component sensitivity analysis method varies model components one at a time to evaluate how model outputs change accordingly, which is similar to the one-factor-at-a-time method for parameter sensitivity analysis. Francke et al. (2018) also used the one-at-a-time approaches and global sensitivity analysis to examine the impacts of model enhancements on improving system model performance. The model enhancements include not only enhancing process formulations but also collecting more monitoring data and improving calibration data. With calibration data, the variation between models (process models, model components, or system models) can be optimized in a framework used by Spieler et al. (2020) for automatic model structure identification.

In the context of explicitly addressing process model uncertainty, Dai et al. (2017b) are the first to use the variance-based global sensitivity analysis methods for identifying important processes. They developed the first-order process sensitivity index to answer the following question: *how can we identify important processes for the explicitly proposed process models and the probabilistically defined random parameters?* Instead of using a single process model, the first-order process sensitivity index considers multiple models that are plausible for representing a system process, and the identified important processes are thus unconditional given all plausible process models. This is made possible by integrating Sobol' variance-based global sensitivity analysis with model averaging approaches. The general procedure of model averaging is as follows (Burnham and Anderson 2002, Draper 1995, Hoeting et al. 1999, Poeter and Hill 2007, Ye et al. 2008a, Ye et al. 2004): (1) postulate multiple models and use the models to simulate the quantities of interest and their uncertainty, (2) evaluate model averaging weights (also known as model probabilities) as a measure of relative plausibility of the models, and (3)

calculate weighted average of the simulated quantities and their associated uncertainties given by the multiple models. The model averaging methods are used for deriving a multi-model parameter sensitivity index in Dai and Ye (2015) and the first-order process sensitivity index in Dai et al. (2017b), because they provide a general-purpose statistical tool to quantify model output variance caused by parametric uncertainty within each model together with the model output variance caused by the competing models. The first-order process sensitivity index has been used not only in hydrologic research but also in ecological studies (e.g., Walker et al. (2021), Walker et al. (2018)), and the R code to evaluate the index is available in the Multi-Assumption Architecture and Testbed (MATT v1.0). Dell'Oca et al. (2020) also integrated model averaging and global sensitivity analysis, and they further extended model averaging to multiple statistical moments (including mean, variance, skewness, and kurtosis). The process sensitivity indices of Dell'Oca et al. (2020), to our knowledge, are the most comprehensive set in the literature to consider model choice, parameter choice, and the model and parameter contributions to the statistical moments of a quantity of interest.

There still exists an open question, i.e., how to identify influential processes (or similarly non-influential processes) under process model uncertainty, which requires considering process interactions. A process is influential if it not only is important but also interacts with other processes to determine system behaviors. Following the definition of factor interactions discussed in Saltelli et al. (2004), two processes are said to interact when their joint effects on the model output cannot be expressed as a sum of their single effects. A process is said to be important if fixing it can substantially reduce model output uncertainty. If a process itself is not important and does not interact with other processes, this process is considered to be non-influential, and its representation can be fixed to any process model during model development and improvement. Under process model uncertainty, when a process representation is changed from one process model to another process model, the simulated interaction between this process and other processes may change accordingly. An influential process in one combination of process models may become non-influential in another combination. Identifying influential processes under process model uncertainty cannot be achieved by using the first-order process sensitivity index of Dai et al. (2017b), because it does not quantify process interactions under process model uncertainty. This motivates the development of total-effect process sensitivity index in this dissertation.

§2.2 Background and Derivation of the New Method

2.2.1 Traditional Sobol's Parameter Sensitivity Indices for a Single-Model

This section first briefly revisits the Sobol's method (Sobol' 2001) that is traditionally used to derive parameter sensitivity indices for identifying the important and influential parameters. Sobol's method implicitly assumes that variance is sufficient to describe output uncertainty and uses variance as a sensitivity measure to quantify the uncertainty in the model output hence it is also known as the Sobol's variance-based sensitivity analysis method. Following Saltelli et al. (2004), model output is denoted as y , and the model input-output is mapped by a generic multivariate function with k input parameters:

$$y = f(\mathbf{x}) = f(x_1, x_2, \dots, x_k), \quad (2.1)$$

Note that we here use \mathbf{x} to denote a set of deterministic parameter values, i.e., $\mathbf{x} = (x_1, x_2, \dots, x_k)$. Sobol' then considers an expansion of the model function f into terms of increasing dimensions (Saltelli et al. 2004):

$$f = f_0 + \sum_i f_i + \sum_i \sum_{j>i} f_{ij} + \dots + f_{12\dots k}, \quad (2.2)$$

where each term is a function only of the parameter in its index, e.g., $f_i = f_i(x_i)$, $f_{ij} = f_{ij}(x_i, x_j)$, and so on. With the presence of parameter uncertainty, each parameter becomes a random variable varying within its uncertainty range. Let X denote the input random variable vector and X_i denotes the set of random input values for x_i (x_i can be viewed as a realization of X_i). The model output then becomes a random variable Y , related to X through Equation (2.1), i.e., $Y = f(X)$. Then the attribution of total output variance to individual model parameters and their interactions can be written as follow (Saltelli et al. 2004):

$$V(Y) = \sum_i V_i + \sum_i \sum_{j>i} V_{i,j} + \dots + V_{12\dots k}, \quad (2.3)$$

where $V(Y)$ represents the total variance of the model output Y ; $V_i = V_{X_i}[E_{X_{\sim i}}(Y | X_i)]$ represents the first-order variance for parameter X_i ; $V_{i,j} = V_{X_{ij}}[E_{X_{\sim ij}}(Y | X_i, X_j)] - V_i - V_j$

to $V_{1,2,3,\dots,k}$ denote the variance of the (second-order to k -order) interaction among k parameters. The first-order variance, sometimes called the main effect, is used to indicate the importance of X_i on the variance of model output Y ,

$$S_i = \frac{V_{X_i}[E_{X_{\sim i}}(Y | X_i)]}{V(Y)}, \quad (2.4)$$

where S_i is the so-called first-order sensitivity index. In this paper, to distinguish it from the first-order process sensitivity index introduced latter, the S_i is referred to first-order parameter sensitivity index. The total-order variance defined as

$$V_{T_i} = V_i + V_{ij} + \dots + V_{12\dots k}, \quad (2.5)$$

measures the main effect of X_i as well as the interaction effects between X_i and the other parameters and is used to indicate the influence of X_i on the variance of Y ,

$$S_{T_i} = \frac{V_i + V_{ij} + \dots + V_{12\dots k}}{V(Y)}, \quad (2.6)$$

where S_{T_i} is the so-called total-effect sensitivity index. Also, to distinguish it from the total-effects process sensitivity index introduced latter, the S_{T_i} is referred to total-effect parameter sensitivity index. The total-effect parameter sensitivity index could be calculated in principle by computing all the terms in the decomposition of Equation (2.5), but there are as many as $2^k - 1$ terms. Taking a three-parameter (i.e., $y = f(\mathbf{x}) = f(x_1, x_2, x_3)$) model as an example, the total-order variance of X_1 equals the sum of four terms

$$V_{T_1} = V_1 + V_{12} + V_{13} + V_{123}. \quad (2.7)$$

There are techniques that enable us to estimate total indices at the same cost of first-order indices, thus circumventing the so-called “curse of dimensionality”. According to the law of total variance, the variance can be decomposed into

$$V(Y) = V_{X_{\sim i}}(E_{X_i}(Y | X_{\sim i})) + E_{X_{\sim i}}(V_{X_i}(Y | X_{\sim i})). \quad (2.8)$$

The measure $E_{X_{\sim i}}(V_{X_i}(Y | X_{\sim i})) = V(Y) - V_{X_{\sim i}}(E_{X_i}(Y | X_{\sim i}))$ is the remaining variance of Y that would be left, on average, if we could determine the true values of $X_{\sim i}$. The average is calculated over all possible combinations of $X_{\sim i}$, since $X_{\sim i}$ are uncertain parameters

and their “true values” are unknown. Then dividing by $V(Y)$, one can obtain the total-effect parameter sensitivity index of X_i

$$S_{T_i} = \frac{E_{X_{\sim i}} [V_{X_i}(Y | X_{\sim i})]}{V(Y)} = 1 - \frac{V_{X_{\sim i}} [E_{X_i}(Y | X_{\sim i})]}{V(Y)}. \quad (2.9)$$

Without considering process model uncertainty, i.e., each process involved in the system is represented by a single process model, the importance or influence of this process can be represented by the importance or influence of the model parameters embedded in this process. If a process model contains only one parameter, the first-order parameter sensitivity index and total-effect parameter sensitivity index can be directly used to identify the important processes and influential processes, respectively. When the process model contains more than one parameter, Mai et al. (2020) has extended the first-order parameter sensitivity index to the group parameters as:

$$S_{iG} = \frac{V_{X_{\sim iG}} [E_{X_{iG}}(Y | X_{\sim iG})]}{V(Y)}, \quad (2.10)$$

where $V_{X_{\sim iG}} [E_{X_{iG}}(Y | X_{\sim iG})]$ represent the variance reduction when the set of model parameters of i -th group X_{iG} is fixed. Equation (2.10) reduces to Equation (2.4) in case the group X_{iG} only contains one parameter X_i . Similarly, the total-effect parameter sensitivity index can be generalized to

$$S_{T_{iG}} = \frac{E_{X_{\sim iG}} [V_{X_{iG}}(Y | X_{\sim iG})]}{V(Y)} = 1 - \frac{V_{X_{\sim iG}} [E_{X_{iG}}(Y | X_{\sim iG})]}{V(Y)}, \quad (2.11)$$

where $E_{X_{\sim iG}} [V_{X_{iG}}(Y | X_{\sim iG})]$ is the expected variance left of model output when all model parameters except the ones of group X_{iG} is fixed. Equation (2.11) is simplified to Equation (2.9) when group X_{iG} contains only parameter X_i . Note that the groups are not assumed to be mutually exclusive, which means that parameters can appear in multiple groups (Mai et al. 2020).

2.2.2 New Variance-based Process Sensitivity Indices for Multi-Model

Denote a quantity of interest as Δ and assume that it is a model output. Without process model uncertainty, Δ is simulated by a single system model, M , i.e., $\Delta = M(\theta) = M(\theta_1, \dots, \theta_d)$, where $\theta = \{\theta_1, \dots, \theta_d\}$ is a vector of system model parameters.

Note that we here use θ to denote one realization of a set of parameter values and reserve Θ to denote an ensemble of θ . If the system of interest consists of multiple processes (denoted as A, B, \dots) and each process has its own process models (denoted as M_A, M_B, \dots) and associated parameters (denoted as $\theta_A, \theta_B, \dots$), the system model, $M(\theta)$, may be viewed as an integration of the process models, i.e., $M(\theta) = \bigcup(M_A(\theta_A), M_B(\theta_B), \dots)$, together with other system model components common to the processes (e.g., domain discretization, system initial conditions, and driving forces). The process model integration (denoted by the union symbol above) may need to consider nonlinear interactions between the process models. An example of such integration is the development of a system model of groundwater reactive transport, as it integrates processes of groundwater flow, thermal transport, solute transport, and biogeochemical reactions. In addition, a process may have its sub-processes. For example, a groundwater flow process may consist of sub-processes such as recharge, geology, and evapotranspiration. More discussions on process-based modular modeling are referred to Clark et al. (2015b), Clark et al. (2015d), Clark et al. (2008).

With the presence of process model uncertainty, a system process may be represented by several alternative process models. Taking process A as an example, it may be represented by multiple process models that form a set $\mathbf{M}_A(\theta_A) = \{M_{A_1}(\theta_{A_1}), M_{A_2}(\theta_{A_2}), \dots\}$; each process model may have its own parameters or have parameters in common with other process models. The integration of the alternative process models leads to alternative system models, i.e., $M(\theta) = \bigcup(\mathbf{M}_A(\theta_A), \mathbf{M}_B(\theta_B), \dots)$. If the process model parameters are random, they are denoted as Θ to be differentiated from θ , which is a realization of Θ . In this case, $M(\theta) = \bigcup(\mathbf{M}_A(\theta_A), \mathbf{M}_B(\theta_B), \dots)$ becomes $\mathbf{M}(\Theta) = \bigcup(\mathbf{M}_A(\Theta_A), \mathbf{M}_B(\Theta_B), \dots)$.

With the above formulation of process models and system models, we derive the total-effect process sensitivity index within the framework of variance-based global sensitivity analysis. The uncertainty of model output, Δ , is measured by its variance $V(\Delta)$, and decomposing the variance in two different ways leads to the first-order process sensitivity index defined by Dai et al. (2017b) and the total-effect process sensitivity index of this study. The two indices are discussed here to better understand the derivation of the

total-effect process sensitivity index.

The first-order process sensitivity index is defined by examining how much the variance, $V(\Delta)$, can be reduced if the process model of process K can be fixed to the true model M_K^* , i.e., $V(\Delta)$ becomes $V_{M_{-K}}[\Delta | M_K^*]$, where subscription \mathbf{M}_{-K} indicates that the variance of Δ is over the process models of all processes but process K , and $\Delta | M_K^*$ means that Δ is simulated conditioning on M_K^* . The variance reduction due to fixing the process model is $V(\Delta) - V_{M_{-K}}[\Delta | M_K^*]$. Since the true process model, M_K^* , is unknown, it is practically sensible to examine the average reduction over all possible process models, i.e., over the set, \mathbf{M}_K , of the process models for process K . Therefore, the average reduction of variance is $V(\Delta) - E_{M_K}(V_{M_{-K}}[\Delta | M_K])$, where M_K is one plausible process model in the process model set, \mathbf{M}_K . Considering the law of total variance with respect to the models of process K , i.e.,

$$V(\Delta) = E_{M_K}(V_{M_{-K}}[\Delta | M_K]) + V_{M_K}(E_{M_{-K}}[\Delta | M_K]), \quad (2.12)$$

we have $V(\Delta) - E_{M_K}(V_{M_{-K}}[\Delta | M_K]) = V_{M_K}(E_{M_{-K}}[\Delta | M_K])$. Normalizing it by $V(\Delta)$ gives the first-order process sensitivity index (Dai et al. 2017b),

$$PS_K = \frac{V_{M_K}(E_{M_{-K}}[\Delta | M_K])}{V(\Delta)}, \quad (2.13)$$

which measures the importance of process K in terms of variance reduction by fixing this process. A process with larger value of PS_K is more important in the sense of larger variance reduction. Derivation of $V_{M_K}(E_{M_{-K}}[\Delta | M_K])$ in Equation (2.13) has been given by Dai et al. (2017b) as:

$$\begin{aligned} V_{M_K}(E_{M_{-K}}[\Delta | M_K]) &= E_{M_K} E_{\theta_K | M_K} (E_{M_{-K}} E_{\theta_{-K} | M_{-K}} [\Delta | M_{-K}, \theta_{-K}, \theta_K, M_K])^2 \\ &\quad - (E_{M_K} E_{\theta_K | M_K} E_{M_{-K}} E_{\theta_{-K} | M_{-K}} [\Delta | M_{-K}, \theta_{-K}, \theta_K, M_K])^2. \end{aligned} \quad (2.14)$$

The total-effect process sensitivity index is defined by examining how much the variance, $V(\Delta)$, is left if the models of all processes but process K are fixed to the true

model $M_{\sim K}^*$, i.e., $V(\Delta)$ becomes $V_{M_K}(\Delta | M_{\sim K}^*)$ with the subscription \mathbf{M}_K indicating that the variance of Δ is over the process models of process K . Since the true process model, $M_{\sim K}^*$, is unknown, it is practically sensible to examine the average variance, $E_{M_{\sim K}}(V_{M_K}[\Delta | M_{\sim K}])$, over the process models, $\mathbf{M}_{\sim K}$, of all processes but process K . The average variance answers the following question: Which process would leave the largest variance of Δ , if the process is left unfixed but all other processes are fixed? This average variance, $E_{M_{\sim K}}(V_{M_K}[\Delta | M_{\sim K}])$, can be evaluated as $V(\Delta) - V_{M_{\sim K}}(E_{M_K}[\Delta | M_{\sim K}])$ based on the following expression of the law of total variance with respect to the process models of all the processes but K , i.e.,

$$V(\Delta) = E_{M_{\sim K}}(V_{M_K}[\Delta | M_{\sim K}]) + V_{M_{\sim K}}(E_{M_K}[\Delta | M_{\sim K}]). \quad (2.15)$$

Normalizing either $E_{M_{\sim K}}(V_{M_K}[\Delta | M_{\sim K}])$ or $V(\Delta) - V_{M_{\sim K}}(E_{M_K}[\Delta | M_{\sim K}])$ by $V(\Delta)$ gives two equivalent expressions of the total-effect process sensitivity index for process K , i.e.,

$$PS_{TK} = \frac{E_{M_{\sim K}}(V_{M_K}[\Delta | M_{\sim K}])}{V(\Delta)} = 1 - \frac{V_{M_{\sim K}}(E_{M_K}[\Delta | M_{\sim K}])}{V(\Delta)}. \quad (2.16)$$

A process with larger value of PS_{TK} is more influential to system model output Δ ; influence of a process is discussed in the paragraph below. The total-effect process sensitivity index is symbolically similar to the Sobol's total-effect parameter sensitivity index for a single model, M_K ,

$$S_{Ti} = \frac{E_{\theta_{\sim i}}(V_{\theta_i}[\Delta | \theta_{\sim i}])}{V_{M_K}(\Delta)} = 1 - \frac{V_{\theta_{\sim i}}(E_{\theta_i}[\Delta | \theta_{\sim i}])}{V_{M_K}(\Delta)}, \quad (2.17)$$

where $\boldsymbol{\theta}_i$ and $\boldsymbol{\theta}_{\sim i}$ denote the parameter sets of the i -th parameter and the other parameters, respectively, $\theta_{\sim i}$ denotes a realization of $\boldsymbol{\theta}_{\sim i}$, and $V_{M_K}(\Delta)$ denotes variance of Δ for model M_K due to parametric uncertainty. We explained in Section 5 that the total-effect process sensitivity index is not simply weighted average of the total-effect parameter sensitivity index. This is also true for the first-order parameter and process sensitivity indices.

One purpose of defining the total-effect process sensitivity index is to screen a non-influential process (or several processes) that can be set at any of its process models. Following Saltelli et al. (2004), a process is said to be influential to system model output

Δ if the process itself affects Δ and its interactions with other processes also affect Δ . Process interactions may imply that extreme values of Δ are obtained by particular combinations of model processes, not by a single process. In other words, two processes are said to interact when their joint effects on Δ cannot be expressed as a sum of their single effects on Δ . We can imagine an extreme case that a process has no interactions with other processes. In this case, $E_{M_{\sim K}}(V_{M_K}[\Delta | M_{\sim K}])$ becomes $V_{M_K}[\Delta | M_{\sim K}]$, and it measures the effects of process K only. We explain in Section 4 that the total-effect process sensitivity index includes the first-order process sensitivity index of a single process and high-order indices for interactions between multiple processes (e.g., second-order for two processes and third-order for three processes). Using the total-effect process sensitivity index avoids calculating the higher-order indices, because they are all included in the total-effect index.

Equation (2.16) considers only process model uncertainty, and it is necessary to extend the definition to consider uncertainty in the parameters of each process model. The extension can be done in two ways for the $E_{M_{\sim K}}(V_{M_K}[\Delta | M_{\sim K}])$ and $V(\Delta) - V_{M_{\sim K}}(E_{M_K}[\Delta | M_{\sim K}])$ terms used to define the total-effect process sensitivity index in Equation (2.16). When working with $E_{M_{\sim K}}(V_{M_K}[\Delta | M_{\sim K}])$, using the definition of variance gives

$$\begin{aligned} E_{M_{\sim K}}(V_{M_K}[\Delta | M_{\sim K}]) &= E_{M_{\sim K}} \left(E_{M_K} ([\Delta | M_{\sim K}])^2 - (E_{M_K} [\Delta | M_{\sim K}])^2 \right) \\ &= E_{M_{\sim K}} E_{M_K} ([\Delta | M_{\sim K}])^2 - E_{M_{\sim K}} (E_{M_K} [\Delta | M_{\sim K}])^2. \end{aligned} \quad (2.18)$$

Subsequently, applying the law of total expectation to the two expectations with respect to process model $M_{\sim K}$ at the right-hand side of Equation (2.18) leads to

$$\begin{aligned} E_{M_{\sim K}}(V_{M_K}[\Delta | M_{\sim K}]) &= E_{M_{\sim K}} E_{\theta_{\sim K} | M_{\sim K}} E_{M_K} ([\Delta | \theta_{\sim K}, M_{\sim K}])^2 \\ &\quad - E_{M_{\sim K}} E_{\theta_{\sim K} | M_{\sim K}} (E_{M_K} [\Delta | \theta_{\sim K}, M_{\sim K}])^2, \end{aligned} \quad (2.19)$$

where subscript $\theta_{\sim K} | M_{\sim K}$ of $E_{\theta_{\sim K} | M_{\sim K}}$ indicates that the expectation is with respect to random parameter $\theta_{\sim K}$ specific to process model combination, $M_{\sim K}$, and the $\Delta | \theta_{\sim K}, M_{\sim K}$ term indicates that the system model output, Δ , is for the a single

combination $M_{\sim K}$ of $\mathbf{M}_{\sim K}$ and for a single realization $\theta_{\sim K}$ of $\boldsymbol{\theta}_{\sim K}$. Applying the law of

total expectation again to process model M_K gives

$$\begin{aligned} E_{\mathbf{M}_{\sim K}}(V_{\mathbf{M}_K}[\Delta | M_{\sim K}]) &= E_{\mathbf{M}_{\sim K}} E_{\theta_{\sim K} | M_{\sim K}} E_{\mathbf{M}_K} E_{\theta_K | M_K} ([\Delta | \theta_K, M_K, \theta_{\sim K}, M_{\sim K}])^2 \\ &\quad - E_{\mathbf{M}_{\sim K}} E_{\theta_{\sim K} | M_{\sim K}} (E_{\mathbf{M}_K} E_{\theta_K | M_K} [\Delta | \theta_K, M_K, \theta_{\sim K}, M_{\sim K}])^2. \end{aligned} \quad (2.20)$$

If process model uncertainty does not exist, the two expectation terms, $E_{\mathbf{M}_{\sim K}}$ and $E_{\mathbf{M}_K}$, disappear, and $E_{\mathbf{M}_{\sim K}}(V_{\mathbf{M}_K}[\Delta | M_{\sim K}])$ becomes $E_{\theta_{\sim K}}(V_{\theta_K}[\Delta | \theta_{\sim K}])$. Accordingly, the total-effect process sensitivity index defined in Equation (2.16) becomes the total-effect parameter sensitivity index defined in equation (2.9).

When working with $V_{\mathbf{M}_{\sim K}}(E_{\mathbf{M}_K}[\Delta | M_{\sim K}])$ in Equation (2.16), using the definition of variance, $V_{\mathbf{M}_{\sim K}}(E_{\mathbf{M}_K}[\Delta | M_{\sim K}])$ can be evaluated via

$$V_{\mathbf{M}_{\sim K}}(E_{\mathbf{M}_K}[\Delta | M_{\sim K}]) = E_{\mathbf{M}_{\sim K}}(E_{\mathbf{M}_K}[\Delta | M_{\sim K}])^2 - (E_{\mathbf{M}_{\sim K}} E_{\mathbf{M}_K}[\Delta | M_{\sim K}])^2. \quad (2.21)$$

Similar to the derivation of Equations (2.19) and (2.20), applying the law of total expectation twice to M_K and $M_{\sim K}$, Equation (2.21) becomes

$$\begin{aligned} V_{\mathbf{M}_{\sim K}}(E_{\mathbf{M}_K}[\Delta | M_{\sim K}]) &= E_{\mathbf{M}_{\sim K}} E_{\theta_{\sim K} | M_{\sim K}} (E_{\mathbf{M}_K} E_{\theta_K | M_K} [\Delta | M_{\sim K}, \theta_K, \theta_{\sim K}, M_K])^2 \\ &\quad - (E_{\mathbf{M}_{\sim K}} E_{\theta_{\sim K} | M_{\sim K}} E_{\mathbf{M}_K} E_{\theta_K | M_K} [\Delta | M_{\sim K}, \theta_K, \theta_{\sim K}, M_K])^2. \end{aligned} \quad (2.22)$$

If process model uncertainty does not exist, the two expectation terms, $E_{\mathbf{M}_{\sim K}}$ and $E_{\mathbf{M}_K}$, disappear, and $V_{\mathbf{M}_{\sim K}}(E_{\mathbf{M}_K}[\Delta | M_{\sim K}])$ becomes $V_{\theta_{\sim K}}(E_{\theta_K}[\Delta | \theta_{\sim K}])$. Accordingly, the total-effect process sensitivity index defined in Equation (2.16) becomes the total-effect parameter sensitivity index defined in Equation (2.17). Adding Equations (2.20) and (2.22) together leads to

$$\begin{aligned} E_{\mathbf{M}_{\sim K}}(V_{\mathbf{M}_K}[\Delta | M_{\sim K}]) + V_{\mathbf{M}_{\sim K}}(E_{\mathbf{M}_K}[\Delta | M_{\sim K}]) &= V(\Delta) \\ &= E_{\mathbf{M}_{\sim K}} E_{\theta_{\sim K} | M_{\sim K}} E_{\mathbf{M}_K} E_{\theta_K | M_K} ([\Delta | \theta_K, M_K, \theta_{\sim K}, M_{\sim K}])^2 \\ &\quad - (E_{\sim M_K} E_{\sim \theta_K | \sim M_K} E_{M_K} E_{\theta_K | M_K} [\Delta | \sim M_K, \sim \theta_K, \theta_K, M_K])^2 \end{aligned} \quad (2.23)$$

This is another way of evaluating $V(\Delta)$ based on the definition of variance, i.e., $V(\Delta) = E(\Delta^2) - (E\Delta)^2$, confirming that the deviation of Equations (2.20) and (2.22) is

correct.

§2.3 Numerical Implementation

2.3.1 Model-averaging and Monte Carlo Integration

Although Equations (2.20) and (2.22) are theoretically equivalent, Equation (2.20) is used in this study to numerically evaluate the total-effect process sensitivity index, because this equation is symbolically the same as Equation (6) of Dai et al. (2017b) used to evaluate the first-order process sensitivity index. This enables us to use the similar algorithm structure to evaluate the two process sensitivity indices with minor code revisions. For the two expectation terms, $E_{\theta_{-K}|M_{-K}}$ and $E_{\theta_K|M_{-K}}$, with respect to model parameters, they are evaluated using Monte Carlo methods. For the two expectation terms, $E_{M_{-K}}$ and E_{M_K} , with respect to process models, they are evaluated using the model averaging approach (Höge et al. 2019, Ye et al. 2010b). Taking the $E_{M_{-K}} E_{\theta_{-K}|M_{-K}}$ term as an example, $E_{M_{-K}}$ is evaluated using the model averaging approach via

$$E_{M_{-K}} E_{\theta_{-K}|M_{-K}}(\bullet) = \sum_{M_{-K}} E_{\theta_{-K}|M_{-K}}(\bullet) P(M_{-K}), \quad (2.24)$$

where the dot (\bullet) denotes the two terms $(E_{M_K} E_{\theta_K|M_K}[\Delta| \sim M_K, \sim \theta_K, \theta_K, M_K])^2$ or $E_{M_K} E_{\theta_K|M_K}[\Delta| \sim M_K, \sim \theta_K, \theta_K, M_K]$, and $P(M_{-K})$ is the process model weight of a process model combination M_{-K} . For the process model weights, it is required that, for process K, the weights, $P(M_K)$, of its process models satisfy $\sum P(M_K) = 1$. To evaluate $P(M_{-K})$ for a combination of process models, it is assumed that selecting one process model of a process is independent to selecting one process model of another process. With this assumption, $P(M_{-K})$ can be evaluated as $P(M_{-K}) = \prod_{i=1}^{N_{-K}} P(M_{-K,i})$, where N_{-K} is the number of processes minus one (i.e., number of all processes but process K) and $P(M_{-K,i})$ is the model weight of a process model. Thinking a system with three processes A, B, and

C , each process has two alterative models (i.e., A_1, A_2, B_1, B_2, C_1 , and C_2), and the process models have the following weights, i.e., $P(A_1) = P(A_2) = 0.5$, $P(B_1) = 0.7$, $P(B_2) = 0.3$, $P(C_1) = 0.6$, and $P(C_2) = 0.4$. The combination, B_1C_1 , of process models B_1 and C_1 has the probability of $P(B_1C_1) = P(B_1) \times P(C_1) = 0.7 \times 0.6 = 0.42$. The model weights can be evaluated in more sophisticated ways, e.g., using Bayesian network as shown in Dai et al. (2019). The process model weights can be prior probability determined based on prior information or posterior probability determined by using both prior information and observations used for model calibration and uncertainty quantification. Prior weights are used in this study, and using posterior weights is discussed in Dai et al. (2017b).

Figure 2-1 is the pseudo code for evaluating the total-effect process sensitivity index based on Equation (2.20). The implementation is computationally straightforward, and four loops are needed, i.e., two loops for the process models $\mathbf{M}_{\sim K}$ and \mathbf{M}_K , and two loops for the process model parameters $\boldsymbol{\theta}_{\sim K} | M_{\sim K}$ and $\boldsymbol{\theta}_K | M_K$ associated with model $M_{\sim K}$ and M_K , respectively. The total number of model executions is $(N_{\sim K} \times m_{\sim K}) \times (N_K \times m_K)$, where $N_{\sim K}$ is the number of process model combinations for the processes $\sim K$, $m_{\sim K}$ is the number of realizations for parameters $\boldsymbol{\theta}_{\sim K} | M_{\sim K}$, N_K is the number of process models for process K , and m_K is the number of realizations for parameter $\boldsymbol{\theta}_K | M_K$.

```

Loop [1] over model combinations  $M_{\sim K}$  for process  $\sim K$  in  $\mathbf{M}_{\sim K}$ 
    Loop [2] over parameter realizations  $\theta_{\sim K}$  of model  $M_{\sim K}$  in  $\boldsymbol{\theta}_{\sim K}$ 
        Loop [3] over process models  $M_K$  for process  $K$  in  $\mathbf{M}_K$ 
            Loop [4] over parameter realizations  $\theta_K$  of model  $M_K$  in  $\boldsymbol{\theta}_K$ 
                Compute  $\Delta | M_{\sim K}, \theta_{\sim K}, M_K, \theta_K$ 
            End Loop [4]
            Compute  $E_{\boldsymbol{\theta}_K | M_K} [\Delta | \sim M_K, \sim \theta_K, \theta_K, M_K]$ 
        End Loop [3]
        Compute  $E_{M_K} E_{\boldsymbol{\theta}_K | M_K} [\Delta | \sim M_K, \sim \theta_K, \theta_K, M_K]$  and
         $(E_{M_K} E_{\boldsymbol{\theta}_K | M_K} [\Delta | \sim M_K, \sim \theta_K, \theta_K, M_K])^2$  using model averaging
    End Loop [2]
    Compute  $E_{\sim \boldsymbol{\theta}_K | \sim M_K} E_{M_K} E_{\boldsymbol{\theta}_K | M_K} [\Delta | \sim M_K, \sim \theta_K, \theta_K, M_K]$  and
     $(E_{\sim \boldsymbol{\theta}_K | \sim M_K} (E_{M_K} E_{\boldsymbol{\theta}_K | M_K} [\Delta | \sim M_K, \sim \theta_K, \theta_K, M_K]))^2$ 
End Loop [1]
Compute  $(E_{\sim M_K} E_{\sim \boldsymbol{\theta}_K | \sim M_K} E_{M_K} E_{\boldsymbol{\theta}_K | M_K} [\Delta | \sim M_K, \sim \theta_K, \theta_K, M_K])^2$  and
 $E_{\sim M_K} E_{\sim \boldsymbol{\theta}_K | \sim M_K} (E_{M_K} E_{\boldsymbol{\theta}_K | M_K} [\Delta | \sim M_K, \sim \theta_K, \theta_K, M_K])^2$  using model averaging

```

图 2-1 基于蒙特卡罗方法和模型平均法计算总效应过程敏感性指标的伪代码

Figure 2-1 Pseudo codes to compute the total-effect process sensitivity index using the Monte Carlo method and the model averaging method

2.3.2 Efficient Design and Estimator to Reduce the Computational Cost

As discussed in Section 2.3 and shown in Figure 2-1, to evaluate the total-effect process sensitivity index (as well as the first-order process sensitivity index proposed by Dai et al. (2017b)) for each process needs four loops, the corresponding total number of model executions is $(N_{\sim K} \times m_{\sim K}) \times (N_K \times m_K)$. The $m_{\sim K} \times m_K$ would be computationally demanding since it relies on Monte Carlo simulations, which renders the evaluation of process sensitivity index practically unaffordable for models with moderate computational cost. This section discusses a efficient design and estimator to substantially reduce the computational cost.

To provide a better understanding of how the estimator is designed, we assume a system has three processes, denoted as R , G , and S , respectively. The model response Δ (a scalar variable), as a function of the three processes, is defined by

$$\Delta = f(R, G, S). \quad (2.25)$$

Each of the three processes is assumed to have two plausible process models to interpret the corresponding process, denoted as R_1 and R_2 for process R , G_1 and G_2 for process G ,

and S_1 and S_2 for process S , respectively:

$$R_1 = M_{R1}(\theta_{R1}), \quad (2.26)$$

$$R_2 = M_{R2}(\theta_{R2}), \quad (2.27)$$

$$G_1 = M_{G1}(\theta_{G1}), \quad (2.28)$$

$$G_2 = M_{G2}(\theta_{G2}^1, \theta_{G2}^2), \quad (2.29)$$

$$S_1 = M_{S1}(\theta_{S1}), \quad (2.30)$$

$$S_2 = M_{S2}(\theta_{S2}^1, \theta_{S2}^2). \quad (2.31)$$

As indicated by Equations (2.26) ~ (2.31), we further assume that all the process models have only one parameter (e.g., θ_{R1} for process model R_1), except that process models G_2 and S_2 have two parameters (e.g., θ_{G2}^1 and θ_{G2}^2 for process model G_2). These parameters are assumed to be independent, and each parameter has its own distribution due to the parametric uncertainty. Integration of the process models allows for a total of $8 = 2 \times 2 \times 2$ system models, i.e., $R_1G_1S_1$, $R_1G_1S_2$, $R_1G_2S_1$, $R_1G_2S_2$, $R_2G_1S_1$, $R_2G_1S_2$, $R_2G_2S_1$, and $R_2G_2S_2$. The number of the parameters for the eight system models ranges from three (e.g., θ_{R1} , θ_{G1} , and θ_{S1} of $R_1G_1S_1$) to five (e.g., θ_{R2} , θ_{G2}^1 , θ_{G2}^2 , θ_{S2}^1 , and θ_{S2}^2 of $R_2G_2S_2$).

Inspired by the algorithm proposed by Saltelli et al. (2010) to compute Sobol's parameter sensitivity indices, a computationally efficient estimator to evaluate the two process sensitivity indices is implemented in the following procedure:

- (1) For each system model, generate two sample matrices A and B , each of which is an $n \times k$ matrix containing n sets of k -dimensional parameter vectors using quasi-random sampling such as the Sobol sequence. Note the values of k may be varied among the system models since the parameter dimensions embedded in the system models may be different. Taking the two system models $R_1G_1S_1$ and $R_1G_1S_2$ as an example, k equals to three for the former one while four for the latter one. It is also important to note that the parameter vectors of a same process model must be same among the system models for matrices A and B , respectively. For example, the parameter vectors of θ_{R1} of process model R_1 and θ_{G1} of process model G_1 in

the matrix \mathbf{A} (or \mathbf{B}) of system model $R_1G_1S_1$ is the same as that of \mathbf{A} (or \mathbf{B}) in system model $R_1G_1S_2$. Below is an example of matrices \mathbf{A} and \mathbf{B} for system model $R_1G_1S_2$.

$$\mathbf{A} = \begin{bmatrix} \theta_{R1}^{(1)} & \theta_{G1}^{(1)} & \theta_{S2}^{1(1)} & \theta_{S2}^{2(1)} \\ \theta_{R1}^{(2)} & \theta_{G1}^{(2)} & \theta_{S2}^{1(2)} & \theta_{S2}^{2(2)} \\ \dots & \dots & \dots & \dots \\ \theta_{R1}^{(n)} & \theta_{G1}^{(n)} & \theta_{S2}^{1(n)} & \theta_{S2}^{2(n)} \end{bmatrix}, \quad (2.32)$$

$$\mathbf{B} = \begin{bmatrix} \theta_{R1}^{(1)} & \theta_{G1}^{(1)} & \theta_{S2}^{1(1)} & \theta_{S2}^{2(1)} \\ \theta_{R1}^{(2)} & \theta_{G1}^{(2)} & \theta_{S2}^{1(2)} & \theta_{S2}^{2(2)} \\ \dots & \dots & \dots & \dots \\ \theta_{R1}^{(n)} & \theta_{G1}^{(n)} & \theta_{S2}^{1(n)} & \theta_{S2}^{2(n)} \end{bmatrix}. \quad (2.33)$$

- (2) For each system model, create matrices \mathbf{C}_i ($i=1, 2, \dots, n_K$, where n_K is the number of processes) formed by all columns of \mathbf{A} except the parameter vector(s) of the i -th process which is taken from \mathbf{B} . Taking the two matrices \mathbf{A} and \mathbf{B} generated in Step (1) as an example, the three matrices \mathbf{C}_1 , \mathbf{C}_2 , and \mathbf{C}_3 corresponding to the three processes R , G , and S for system model $R_1G_1S_2$ are:

$$\mathbf{C}_1 = \begin{bmatrix} \theta_{R1}^{(1)} & \theta_{G1}^{(1)} & \theta_{S2}^{1(1)} & \theta_{S2}^{2(1)} \\ \theta_{R1}^{(2)} & \theta_{G1}^{(2)} & \theta_{S2}^{1(2)} & \theta_{S2}^{2(2)} \\ \dots & \dots & \dots & \dots \\ \theta_{R1}^{(n)} & \theta_{G1}^{(n)} & \theta_{S2}^{1(n)} & \theta_{S2}^{2(n)} \end{bmatrix}, \quad (2.34)$$

$$\mathbf{C}_2 = \begin{bmatrix} \theta_{R1}^{(1)} & \theta_{G1}^{(1)} & \theta_{S2}^{1(1)} & \theta_{S2}^{2(1)} \\ \theta_{R1}^{(2)} & \theta_{G1}^{(2)} & \theta_{S2}^{1(2)} & \theta_{S2}^{2(2)} \\ \dots & \dots & \dots & \dots \\ \theta_{R1}^{(n)} & \theta_{G1}^{(n)} & \theta_{S2}^{1(n)} & \theta_{S2}^{2(n)} \end{bmatrix}, \quad (2.35)$$

$$\mathbf{C}_3 = \begin{bmatrix} \theta_{R1}^{(1)} & \theta_{G1}^{(1)} & \theta_{S2}^{1(1)} & \theta_{S2}^{2(1)} \\ \theta_{R1}^{(2)} & \theta_{G1}^{(2)} & \theta_{S2}^{1(2)} & \theta_{S2}^{2(2)} \\ \dots & \dots & \dots & \dots \\ \theta_{R1}^{(n)} & \theta_{G1}^{(n)} & \theta_{S2}^{1(n)} & \theta_{S2}^{2(n)} \end{bmatrix}. \quad (2.36)$$

- (3) For each system model, compute the model outputs for all the parameter value combinations in the sample matrices \mathbf{A} , \mathbf{B} , and \mathbf{C}_i , respectively, resulting in multiple vectors of model outputs of dimension $n \times 1$, denoted as

$$\Delta_A = f(\mathbf{A}) = \left(\Delta_A^{(1)}, \Delta_A^{(2)}, \dots, \Delta_A^{(n)} \right)^T, \quad \Delta_B = f(\mathbf{B}) = \left(\Delta_B^{(1)}, \Delta_B^{(2)}, \dots, \Delta_B^{(n)} \right)^T, \quad \text{and}$$

$$\Delta_{C_i} = f(\mathbf{C}_i) = \left(\Delta_{C_i}^{(1)}, \Delta_{C_i}^{(2)}, \dots, \Delta_{C_i}^{(n)} \right)^T.$$

We anticipate that these output vectors are all we need to compute Sobol's parameter sensitivity indices S_i and S_{Ti} as well as the first-order and total-effect process indices PS_K and PS_{TK} of all processes. Because there are n_K processes, the cost is $n + n$ runs of the system model for matrices \mathbf{A} and \mathbf{B} , plus n_K times n to estimate the output vectors corresponding to matrix \mathbf{C}_i . Hence the computational cost is $(n_K + 2) \times n$ for each system model. The total cost of this estimator hence is $(m_K \times m_{\sim K}) \times (n_K + 2) \times n$, where $(m_K \times m_{\sim K})$ corresponding to the number of the system models. In such case, the evaluation of the two sensitivity indices becomes a problem of order $O(n)$, which is much smaller than that of the brute force method of $O(n_K \times n_{\sim K})$.

According to Saltelli et al. (2007), the first-order and total-effect parameter sensitivity indices under each individual system model can be evaluated as:

$$S_i = \frac{V_{\theta_i}(E_{\theta_{\sim i}}[\Delta | \theta_i])}{V(\Delta)} = 1 - \frac{(1/2n) \sum_{j=1}^n (\Delta_B^{(j)} - \Delta_{C_i}^{(j)})^2}{(1/n) \sum_{j=1}^n (\Delta_A^{(j)})^2 - \overline{\Delta_A}^2}, \quad (2.37)$$

$$S_{Ti} = \frac{E_{\theta_{\sim i}}(V_{\theta_i}[\Delta | \theta_{\sim i}])}{V(\Delta)} = \frac{(1/2n) \sum_{j=1}^n (\Delta_A^{(j)} - \Delta_{C_i}^{(j)})^2}{(1/n) \sum_{j=1}^n (\Delta_A^{(j)})^2 - \overline{\Delta_A}^2}, \quad (2.38)$$

where $\overline{\Delta_A} = (1/n) \sum_{j=1}^n \Delta_A^{(j)}$ denotes the mean of model output for this system model; the

superscript (j) of $\Delta_A^{(j)}$, $\Delta_B^{(j)}$ and $\Delta_{C_i}^{(j)}$ denotes j -th model output in vectors Δ_A , Δ_B , and

Δ_C , respectively. For example, the first-order parameter sensitivity of θ_{S2}^1 together with

θ_{S2}^1 under system model $R_1G_1S_2$ (we use the sensitivity of these two parameters to

represent the sensitivity of process S under individual system model), is computed as

$$1 - \left(\frac{(1/2n) \sum_{j=1}^n (\Delta_B^{(j)} - \Delta_{C_3}^{(j)})^2}{(1/n) \sum_{j=1}^n (\Delta_A^{(j)})^2 - \overline{\Delta_A}^2} \right), \quad \text{where } \mathbf{A}, \mathbf{B}, \text{ and } \mathbf{C}_3 \text{ are the three}$$

matrices in Equations (2.32), (2.33) and (2.36). Note that output variance $V(\Delta)$ is only

estimated using the output vector Δ_A here, i.e., the denominator $(1/n)\sum_{j=1}^n (\Delta_A^{(j)})^2 - \overline{\Delta_A}^2$ in

Equations (2.37) and (2.38) but the accuracy of which may be improved by using both Δ_A and Δ_B while the vectors Δ_{C_i} should be excluded from the computation as they are not independent from Δ_A and Δ_B .

As for the two process sensitivity indices PS_K and PS_{TK} , we decompose Equations (2.14) and (2.20) into several items to facilitate the evaluation by using these output vectors. To compute the first-order process sensitivity index of i -th process, namely process K , the first item $E_{M_K} E_{\theta_K|M_K} (E_{M_{\sim K}} E_{\theta_{\sim K}|M_{\sim K}} [\Delta | \Delta | \theta_K, M_K, \theta_{\sim K}, M_{\sim K}])^2$ in the right-hand side of Equation (2.14) can be estimated as:

$$\begin{aligned} & E_{M_K} E_{\theta_K|M_K} (E_{M_{\sim K}} E_{\theta_{\sim K}|M_{\sim K}} [\Delta | \Delta | \theta_K, M_K, \theta_{\sim K}, M_{\sim K}])^2 \\ &= \sum_{p=1}^{m_k} \sum_{q=1}^{m_{\sim k}} \frac{1}{n} \sum_{j=1}^n [\Delta_B^{(j)} | M_{K_p}, M_{\sim K_q}] [\Delta_{C_i}^{(j)} | M_{K_p}, M_{\sim K_q}] P(M_{\sim K_q})^2 P(M_{K_p}) \\ &+ \sum_{p=1}^{m_k} \sum_{q=1}^{m_{\sim k}} \sum_{r=1 \atop r \neq q}^{m_{\sim k}} \frac{1}{n} \sum_{j=1}^n [\Delta_B^{(j)} | M_{K_p}, M_{\sim K_q}] [\Delta_{C_i}^{(j)} | M_{K_p}, M_{\sim K_r}] P(M_{\sim K_r}) P(M_{\sim K_q}) P(M_{K_p}) \end{aligned} \quad . \quad (2.39)$$

where the condition of $M_{K_p}, M_{\sim K_q}$ of $\Delta_B | M_{K_p}, M_{\sim K_q}$ and $\Delta_{C_i} | M_{K_p}, M_{\sim K_q}$ indicate that

output vectors Δ_B and Δ_{C_i} are respected to the system model integrated by process

models M_{K_p} and $M_{\sim K_q}$; $P(M_{K_p})$ and $P(M_{\sim K_q})$ are the model weights used to

evaluate by process models M_{K_p} and $M_{\sim K_q}$, respectively. As for the total-effect process

sensitivity index, the first item $E_{M_{\sim K}} E_{\theta_{\sim K}|M_{\sim K}} (E_{M_K} E_{\theta_K|M_K} [\Delta | M_{\sim K}, \theta_{\sim K}, \theta_K, M_K])^2$ in the

right-hand side of Equation (2.20) can be estimated as:

$$\begin{aligned} & E_{M_{\sim K}} E_{\theta_{\sim K}|M_{\sim K}} (E_{M_K} E_{\theta_K|M_K} [\Delta | \theta_K, M_K, \theta_{\sim K}, M_{\sim K}])^2 \\ &= \sum_{q=1}^{m_{\sim K}} \sum_{p=1}^{m_K} \frac{1}{n} \sum_{j=1}^n [\Delta_A^{(j)} | M_{K_p}, M_{\sim K_q}] [\Delta_{C_i}^{(j)} | M_{K_p}, M_{\sim K_q}] P(M_{K_p})^2 P(M_{\sim K_q}) \\ &+ \sum_{q=1}^{m_{\sim K}} \sum_{p=1}^{m_K} \sum_{r=1 \atop r \neq p}^{m_K} \frac{1}{n} \sum_{j=1}^n [\Delta_A^{(j)} | M_{K_p}, M_{\sim K_q}] [\Delta_{C_i}^{(j)} | M_{K_r}, M_{\sim K_q}] P(M_{K_r}) P(M_{K_p}) P(M_{\sim K_q}) \end{aligned} \quad . \quad (2.40)$$

The second item $(E_{\mathbf{M}_K} E_{\theta_K | M_K} E_{\mathbf{M}_{\sim K}} E_{\theta_{\sim K} | M_{\sim K}} [\Delta | \theta_K, M_K, M_{\sim K}, \theta_{\sim K}])^2$ in the right-hand side of Equation (2.14) equals to the second item $(E_{\mathbf{M}_{\sim K}} E_{\theta_{\sim K} | M_{\sim K}} E_{\mathbf{M}_K} E_{\theta_K | M_K} [\Delta | M_{\sim K}, \theta_{\sim K}, \theta_K, M_K])^2$ in the right-hand side of Equation (2.20), which equals to the total mean of all system models, $E(\Delta)^2$:

$$E(\Delta)^2 = \left(\sum_{p=1}^{m_k} \sum_{q=1}^{m_{\sim k}} \frac{1}{n} \sum_{j=1}^n \left[\Delta_A^{(j)} | M_{K_p}, M_{\sim K_q} \right] P(M_{\sim K_q}) P(M_{K_p}) \right)^2. \quad (2.41)$$

Substituting Equations (2.39) and (2.41) to Equation (2.14) yields $V_{\mathbf{M}_K}(E_{\mathbf{M}_{\sim K}}[\Delta | M_K])$ and substituting Equations (2.40) and (2.41) to Equation (2.20) yields $V_{\mathbf{M}_{\sim K}}(E_{\mathbf{M}_{\sim K}}[\Delta | M_K])$. To evaluate the two process sensitivity indices, the only unknown item $V(\Delta)$ in Equations (2.13) and (2.16) can be evaluated by using the definition of variance:

$$\begin{aligned} V(\Delta) &= E(\Delta^2) - E(\Delta)^2 \\ &= \left(\sum_{p=1}^{m_k} \sum_{q=1}^{m_{\sim k}} \frac{1}{n} \sum_{j=1}^n \left[\Delta_A^{(j)} | M_{K_p}, M_{\sim K_q} \right]^2 P(M_{\sim K_q}) P(M_{K_p}) \right) - E(\Delta)^2. \end{aligned} \quad (2.42)$$

Note that the accuracy of vectors $E(\Delta)$ and $V(\Delta)$ can be improved by using both matrixes Δ_A and Δ_B rather than just Δ_A in Equations (2.41) and (2.42). This will improve the estimation of the process sensitivity indices, although the processes' ranking should be remaining unchanged. Error estimates for the two process sensitivity indices can be obtained by bootstrapping data points from vectors Δ_A , Δ_B , and Δ_{C_i} .

§2.4 A Hypothetical Example

2.4.1 Model Settings

A hypothetical 1-D groundwater flow model is performed to evaluate the first-order and total-effect process sensitivity indices proposed above. This experiment is revised after Dai et al. (2017b). As shown in Figure 2-2, the unconfined aquifer has a length of $L=10,000$ m and is under a steady state condition. The aquifer is bounded by two constant-head boundaries, and subject to a uniform precipitation. Process model uncertainty exists

in the following three system processes: (1) recharge process that converts precipitation to aquifer recharge, (2) geology process that characterizes hydraulic conductivity of the aquifer, and (3) snow-melt process that estimates snow-melt rate to determine hydraulic head at the east boundary of the domain. The process models are described below.

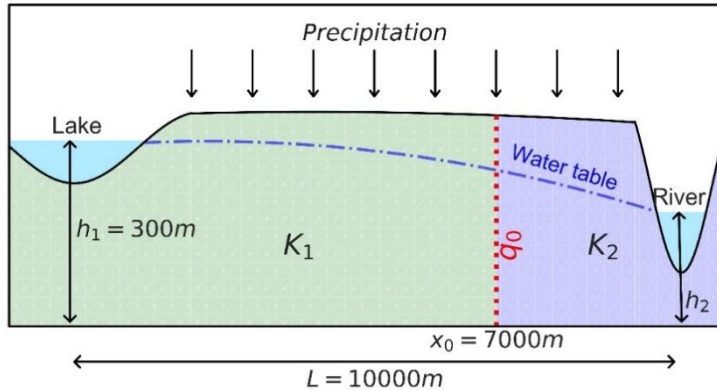


图 2-2 一维河间地块地下水水流模型示意图。模型两侧为定水头边界，假定左侧边界水头 $h_1 = 300 \text{ m}$ ，右侧边界为河流，河流水位无观测数据。在非均质渗透系数假设下，含水层在 $x_0 = 7000 \text{ m}$ 处划分为两个渗透系数分区，此处单宽流量(q_0)是模型输出变量。

Figure 2-2 Sketch of the one-dimensional groundwater flow model. The aquifer is bounded with constant head boundary conditions. The left boundary is adjacent to a lake with a constant head of $h_1=300 \text{ m}$. The right boundary is adjacent to a river while no measuring data is available for the river stage. The divide of the two zones for the hydraulic conductivity at $x_0=7000 \text{ m}$ is marked with dashed line and the groundwater discharge per unit width at this location (q_0) is our quantity of interest.

Following Dai et al. (2017b), two recharge models (R_1 and R_2) are used to simulate the recharge process that converts precipitation [inch/yr] to groundwater recharge [m/d], and they are

$$\begin{aligned} R_1 : w &= a(P-14)^{0.5} \times 0.0254 / 365 \\ R_2 : w &= b(P-15.7) \times 0.0254 / 365 \end{aligned} \quad (2.43)$$

where a and b are scaling parameters which are assumed to follow the normal distribution, $N(2.0, 0.4^2)$, and the uniform distribution, $U[0.2, 0.5]$, respectively, P is an annual precipitation which is set as 60 inch/yr. Hydraulic conductivity (K) [m/d] over the domain is parameterized by two geology process models (G_1 and G_2) as follows,

$$\begin{aligned} G_1 : K &\text{ for any } x \\ G_2 : K &= \begin{cases} K_1 & \text{for } x < 7000 \\ K_2 & \text{for } x \geq 7000 \end{cases} \end{aligned} \quad (2.44)$$

In model G_1 , the aquifer is assumed to be homogeneous, and the hydraulic conductivity follows the lognormal distribution, $LN(2.9, 0.5^2)$. Model G_2 has two zones of hydraulic conductivity separated at the location of $x_0 = 7,000$ m (Figure 2-2). The hydraulic conductivities K_1 of zone 1 ($x < 7000$ m) and K_2 of zone 2 ($x \geq 7000$ m) are assumed to follow the lognormal distributions, $LN(2.6, 0.3^2)$ and $LN(3.2, 0.3^2)$, respectively.

For the lake boundary, its hydraulic head is set to constant as $h_1 = 300$ m (Figure 2-2). For the river boundary, the river stage, h_2 , is determined by the empirical rating curve function below to convert a river discharge into the river stage

$$h_2 = 0.3Q^{0.6} + 289, \quad (2.45)$$

where Q is a river discharge [m^3/s], and the coefficients 0.3, 0.6, and 289 are chosen arbitrarily. The river discharge depends on snowmelt runoff via

$$Q = C_{sn} \times M \times SVC \times A \times \frac{0.001}{86400}, \quad (2.46)$$

where C_{sn} is a runoff coefficient, M is the snow-melt rate [mm/d], SVC is the ratio of snow-covered area to watershed area, A [m^2], and 0.001/86400 is the conversion factor from mm/d to m^3/s . We set $C_{sn} = 0.8$, $SVC = 0.7$ and $A = 2,000 \text{ km}^2$, and use two models to estimate the daily snow-melt rate based on the degree-day method and the restricted degree-day radiation balance method (Hock 2003, Kustas et al. 1994, Martinec et al. 1998). The two models are

$$\begin{aligned} M_1 : M &= f_1(T_a - T_m) \\ M_2 : M &= f_2(T_a - T_m) + rR_n, \end{aligned} \quad (2.47)$$

where f_1 and f_2 [$\text{mm} \cdot ^\circ\text{C}^{-1} \cdot \text{d}^{-1}$] are snowmelt factors that are assumed to follow a normal distribution, $N(3.5, 0.75^2)$, and a normal distribution, $N(2.5, 0.3^2)$, respectively, T_a [$^\circ\text{C}$] is the average temperature for a given day, and T_m [$^\circ\text{C}$] is the temperature threshold (typically set to be 0) when snow melt occurs. The second model considers the effects of surface radiation budget, R_n [W/m^{-2}], and uses a conversion factor r [$(\text{mm/d})/(\text{W/m}^2)$] to convert the energy flux to snowmelt rate. T_a and R_n are set as 7 $^\circ\text{C}$ and 80 W/m^{-2} , respectively, and r was assumed to follow a normal distribution, $N(0.3, 0.05^2)$.

A combination of the two recharge process models, two geology process models, and two snowmelt process models leads to a total of eight system models, and they are denoted as $R_1G_1M_1$, $R_1G_1M_2$, $R_1G_2M_1$, $R_1G_2M_2$, $R_2G_1M_1$, $R_2G_1M_2$, $R_2G_2M_1$, and $R_2G_2M_2$. All

process models have equal weights, i.e., $P(R_1) = P(R_2) = 0.5$, $P(G_1) = P(G_2) = 0.5$, and $P(M_1) = P(M_2) = 0.5$. The groundwater discharge per unit width at the location $x_0 = 7,000$ m is the quantity of interest for the sensitivity analysis, and it is labeled as q_0 in Figure 2. The analytical solution of the discharge, $q(x)$, at any location x , was derived as

$$q(x) = K_1 \frac{h_1^2 - h_2^2}{2(x_0 - \lambda x_0 + \lambda L)} - \frac{1}{2} w \frac{x_0^2 - \lambda x_0^2 + \lambda L^2}{x_0 - \lambda x_0 + \lambda L} + wx, \quad (2.48)$$

where $\lambda = K_1/K_2$. For the geology model (G_1) with homogenous hydraulic conductivity, i.e., $K = K_1 = K_2$, Equation (2.48) reduces to

$$q(x) = K \frac{h_1^2 - h_2^2}{2L} - \frac{1}{2} wL + wx, \quad (2.49)$$

which is the well-known solution available in hydrogeology textbooks. The analytical solutions help us understand the process interactions. For example, Equation (2.49) indicates that the recharge process (w) does not interact with the geology (K) and snowmelt (h_2) processes. More discussion on process interactions in the sensitivity analysis is given in Section 2.5.4. Using the analytical solutions of $q(x)$, the first-order and total-effect sensitivity indices for parameters and processes are evaluated using Monte Carlo simulations based on the pseudo code shown in Figure 2-1.

2.4.2 Identifying the Controlling Process for Single-Model

Table 2-1 lists the numerical results for the parameter sensitivity (S_{iG} and S_{TG}) of individual system models and the process sensitivity (PS_K and PS_{TK}) considering model uncertainty and parametric uncertainty. Without considering the model uncertainty, the sensitivity of the parameters represents the sensitivity of the process in which the parameters embedded. Taking system model $R_2G_2M_2$ as an example, the system model is governed by five parameters: parameter b corresponding to the recharge process (Equation (2.43)), parameters K_1 and K_2 corresponding to geology process (Equation (2.44)) and parameters f_2 and r corresponding to the snowmelt process (Equation (2.47)). The parameter sensitivity values of $K_1\&K_2$ and $f_2\&r$ list in Table 2-1 are for parameters $K_1\&K_2$ and $f_2\&r$ together, respectively. Specifically speaking, the $X_{\sim iG}$ term in the $E_{X_{\sim iG}}[V_{X_{iG}}(Y | X_{\sim iG})]$ of Equation (2.10) includes all the parameter combinations except for K_1 and K_2 when calculating the total parameter sensitivity for geology process and all

the parameter combinations except for f_2 and r when calculating the total-effect parameter sensitivity for snowmelt process, respectively.

表 2-1 单模型条件下一维河间地块模型一阶(S_i)和总效应(S_{Ti})参数敏感性指标, 以及考虑多模型条件的一阶(PS_K)和总效应(PS_{TK})过程敏感性指标的数值解。该一维河间地块模型考虑了三个水文过程: 降雨入渗过程(R), 地质过程(G)和融雪过程(M)。模型总运行次数为 $216,000,000 = 2 \times 300 \times 2 \times 300 \times 2 \times 300$ 次, 分别对应 2 个降雨入渗过程模型 \times 每个模型 300 个可能参数取值 \times 2 个地质过程模型 \times 每个模型 300 个可能参数取值 \times 2 个融雪过程模型 \times 每个模型 300 个可能参数取值。

Table 2-1 Numerical solutions of first-order (S_i) and total-effect (S_{Ti}) parameter sensitivity indices for each system model and of first-order (PS_K) and total-effect (PS_{TK}) process sensitivity indices of multiple system models of groundwater flow model. Each system model has three processes: recharge (R), geology (G), and snowmelt (M). The results were obtained by using a total number of $216,000,000 = 2 \times 300 \times 2 \times 300 \times 2 \times 300$ Monte Carlo simulation runs, corresponding to 2 recharge process models \times 300 parameters \times 2 geology process models \times 300 parameters \times 2 snowmelt process models \times 300 parameters.

Considering parametric uncertainty but not process model uncertainty												
Model	$R_1G_1M_1$			$R_1G_1M_2$			$R_1G_2M_1$			$R_1G_2M_2$		
Parameter	a	K	f_1	a	K	$f_2 \& r$	a	$K_1 \& K_2$	f_1	a	$K_1 \& K_2$	$f_2 \& r$
S_i (%)	12	22	51	15	47	30	33	11	51	35	36	26
Rank	3	2	1	3	1	2	2	3	1	2	1	3
S_{Ti} (%)	12	37	66	15	56	38	34	16	55	36	39	28
Rank	3	2	1	3	1	2	2	3	1	2	1	3
Model	$R_2G_1M_1$			$R_2G_1M_2$			$R_2G_2M_1$			$R_2G_2M_2$		
Parameter	b	K	f_1	b	K	f_1	b	$K_1 \& K_2$	f_1	b	$K_1 \& K_2$	$f_2 \& r$
S_i (%)	22	20	45	26	41	26	49	11	37	49	30	19
Rank	2	3	1	2	1	3	1	3	2	1	2	3
S_{Ti} (%)	22	33	59	26	48	33	50	14	40	50	32	20
Rank	3	2	1	3	1	2	1	3	2	1	2	3
Considering parametric uncertainty and process model uncertainty												
Process	R (Recharge)				G (Geology)				M (Snowmelt)			
PS_K (%)	14.32				6.79				63.99			
Rank	2				3				1			
PS_{TK} (%)	14.67				21.68				78.54			
Rank	3				2				1			

Table 2-1 shows that both the first-order and total-effect parameter sensitivity indices change dramatically among the individual system models. Any of the three processes can be the most important/influential or least important/influential process. For example, the recharge process is identified to be the least important/influential process

and the snowmelt process is the most important/influential process for system model $R_1G_1M_1$ while the opposite observations are drawn for system model $R_2G_2M_2$. However, Table 2-1 illustrates some new findings: (1) The rankings of the first-order and total parameter sensitivity could be different under a single system model and (2) the rankings of the first-order process sensitivity and total process sensitivity under the multi-system model configuration are also different. We will explore the reasons in the next section.

2.4.3 Identifying the Controlling Process for Multi-Model

Within the multi-system model context, the PS_K values suggest that the snowmelt process is the most important process followed by recharge process and geology process. The relative importance of the three processes is physically meaningful by examining Figure 2-3. The $E_{\theta_K|M_K}(V_{M_K}[\Delta|\theta_K, M_K])$ term is the average variance of the system output after fixing a process model. Taking Figure 3f as an example, M_K denotes process model G_2 , $E_{\theta_K|M_K}$ denotes the expectation with respect to all parameter realizations of K_1 and K_2 associated with process model G_2 , $V_{M_K}[\Delta|\theta_K, M_K]$ represents the output variance considering all other process model combinations (i.e., R_1M_1 , R_1M_2 , R_2M_1 , and R_2M_2) and the corresponding parameter combinations under a single parameter realization of K_1 and K_2 . The PDF in black is for q_0 values simulated by using all the system models and their random parameters; this PDF thus presents the original uncertainty measured by $V(\Delta)$.

Recall that the first-order process sensitivity is proposed to identify the most important process, that is when fixe or learned, would lead to the greatest variance reduction. In other words, the variance of the system output would be smallest after fixing this process. As show in Figure 2-3, no matter we fix the snowmelt process to either of the process model M_1 (Figure 2-3a) or M_2 (Figure 2-3b), the PDFs are most concentrated compared with Figures 2-3c ~ 2-3f thus the variance reduction is largest, resulting in the smallest variance of the system output 0.59 or 0.86. As for the recharge process and geology process, Figure 2-3f shows that by fixing the geology process to G_2 , the (average) variance of the system output becomes 1.41. It seems that geology process is important than recharge process. However, since we have equally weighted process models, i.e., the problem that we are not for sure the true geology process model, an average variance of $0.5 \times 2.36 + 0.5 \times 1.41 = 1.885$ is computed thus using the model averaging method and

it is larger than that of $0.5 \times 1.71 + 0.5 \times 1.75 = 1.73$ of recharge process. Therefore, the variance reduction is smaller for geology process which means that the recharge process is more important than geology process. One may note that if the process model weights for geology process are changed, e.g., $P(G_1) = 0.2$ and $P(G_2) = 0.8$, the variance of the system output by fixing geology process becomes $0.2 \times 2.36 + 0.8 \times 1.41 = 1.60$, which is smaller than that of recharge process. In this case, the geology process is more important than recharge process.

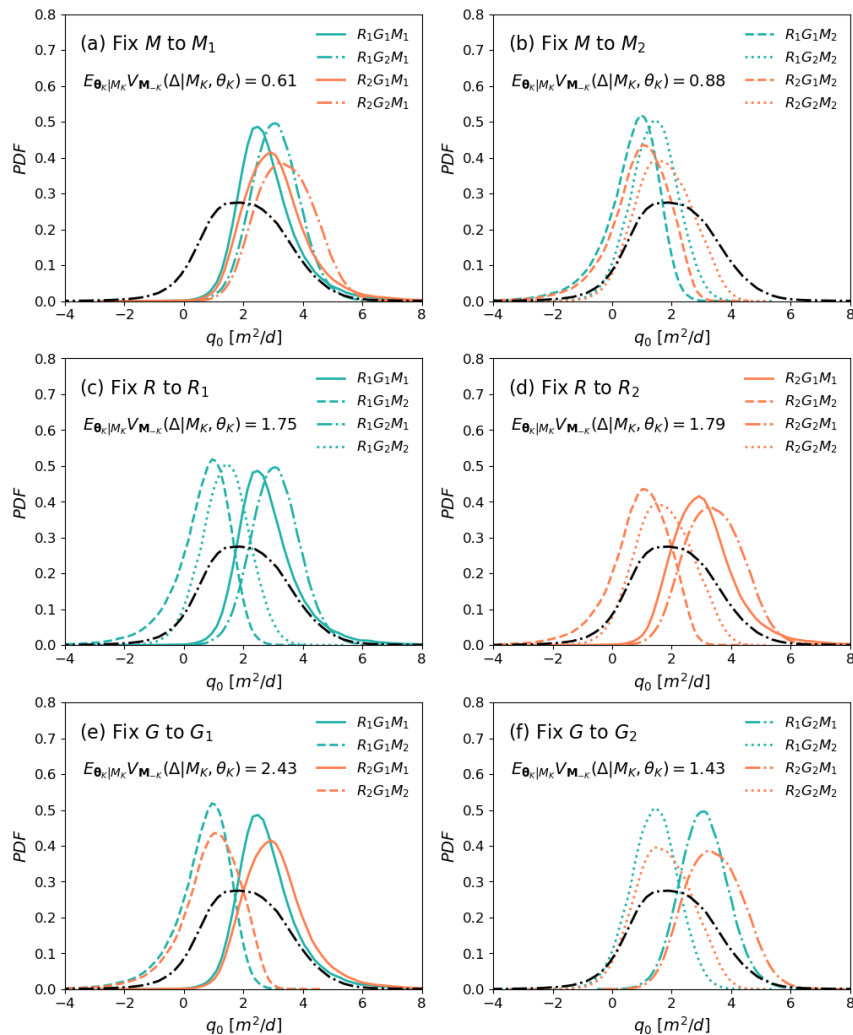


图 2-3.一维河间地块模型 $x_0 = 7,000$ m 处单宽流量概率分布函数曲线: (a) 假定真实融雪过程模型为 M_1 ; (b) 假定真实融雪过程模型为 M_2 ; (c) 假定真实降雨入渗过程模型为 R_1 ; (d) 假定真实降雨入渗过程模型为 R_2 ; (e) 假定真实地质过程模型为 G_1 ; (f) 假定真实地质过程模型为 G_2 。

Figure 2-3 PDFs of the groundwater discharge per unit width at $x_0 = 7,000$ m simulated by individual system models when fixing (a) snowmelt process M to M_1 , (b) snowmelt process M to M_2 , (c) recharge process R to R_1 , (d) recharge process R to R_2 , (e) geology process G to G_1 , and (f) geology process G to G_2 .

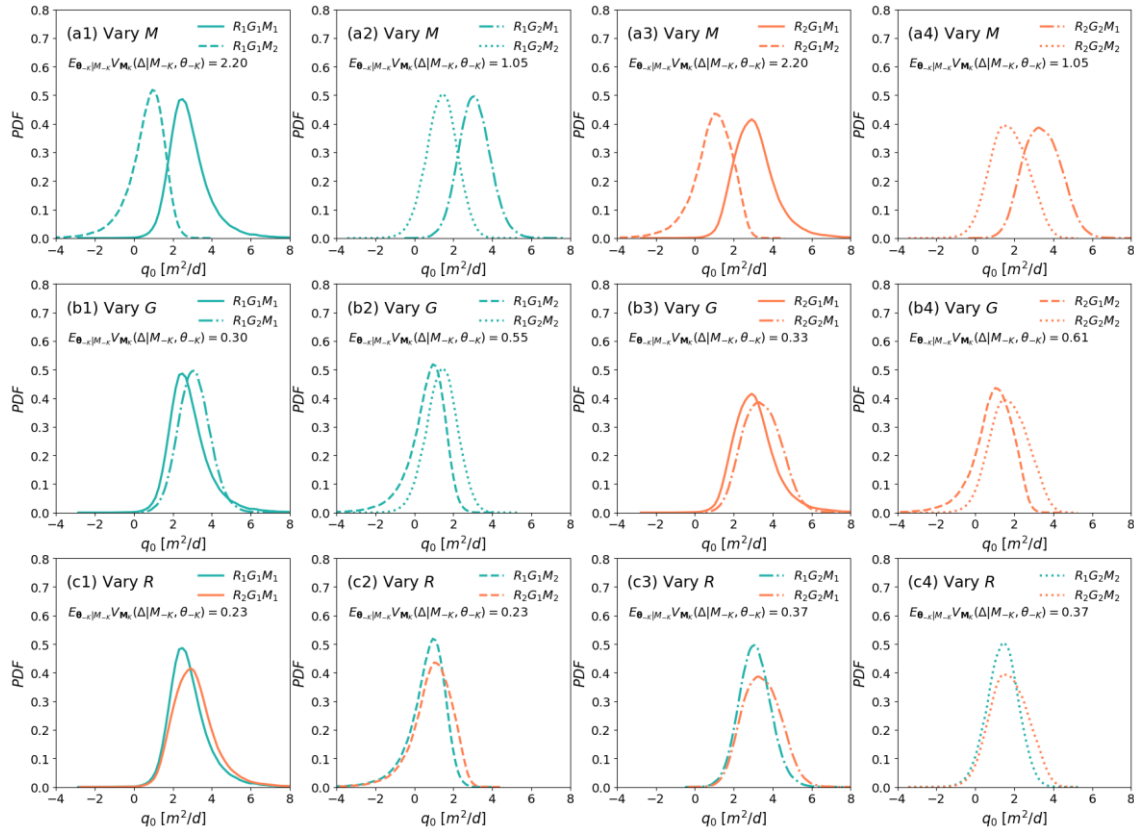


图 2-4 一维河间地块模型 $x_0 = 7,000$ m 处单宽流量概率分布曲线: (a1 – a4) 融雪过程模型从 M_1 变化为 M_2 ; (b1 – b4) 地质过程模型从 M_1 变化为 M_2 ; (c1 – c4) 降雨入渗过程模型从 R_1 变化为 R_2 。

Figure 2-4 PDFs of the groundwater discharge per unit width (q_0) at $x_0 = 7,000$ m simulated by individual system models when varying (a1 – a4) snowmelt process model from M_1 to M_2 , (b1 – b4) geology process model from G_1 to G_2 , and (c1 – c4) recharge process model from R_1 to R_2 .

The PS_{TK} values suggest that the snowmelt process is the most influential process, and the recharge process is the most non-influential process. The relative influence of the three process is physically meaningful as supported by Figure 2-4. The $E_{\theta_{-K}|M_{-K}}(V_{M_K}[\Delta | \theta_{-K}, M_{-K}])$ term is the average variance of q_0 after fixing the other two process models. Taking Figure 2-4(c4) as an example, M_{-K} denotes the process model combination G_2M_2 , $E_{\theta_{-K}|M_{-K}}$ is the expectation of all realizations of parameters K_1, K_2, f_2 and r associated with G_2M_2 , $V_{M_K}[\Delta | \theta_{-K}, M_{-K}]$ is the output variance of q_0 considering the uncertainty of process model R and the corresponding parameter realizations under a single parameter combination of K, f_2 and r .

Recall that the total-effect process sensitivity is proposed to screen the non-influential process, that is if all other processes are fixed, the unknown (variation) of this

process would cause the smallest variance of the model response. In Figures 2-4a1 ~ 2-4a4, when the recharge and geology models are fixed, the unknown of the snowmelt process obviously cause the largest variance of the output. As for the recharge process and geology process, Figures 2-4c1 ~ 2-4c2 indicate that the average variance left because of the variation of recharge process is smaller than that of geology process. Thus, the geology process is the most non-influential process.

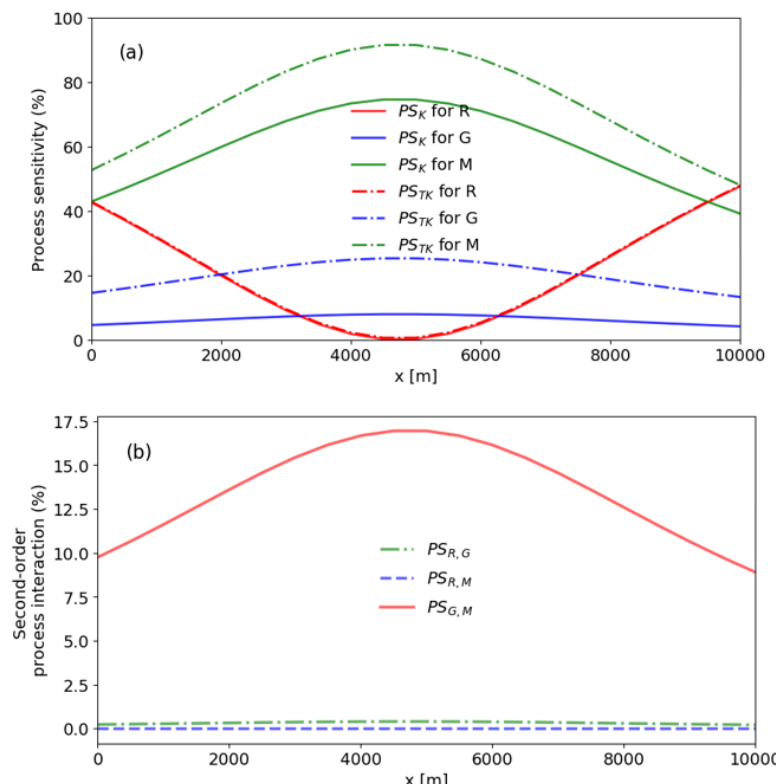


图 2-5 一维河间地块模型 $x_0 = 7,000$ m 处单宽流量的：(a) 一阶过程敏感性指标和总效应过程敏感性指标；(b) 二阶过程敏感性指标。

Figure 2-5 (a) First-order and total-effect process sensitivity indices and (b) second-order process sensitivity indices for the groundwater discharge per unit width throughout the entire domain.

2.4.4 Process Interactions

The inconsistence rankings between the first-order and total-effect process sensitivity of the multi-system model is due to the process interaction. From the variance decomposition point, the total process sensitivity measures the total effects, i.e., the first and higher order effects (interactions) of this process and can be written as the sum of the first-order process sensitivity, the second-order and higher-order process interaction

effects that include process K :

$$PS_{TK} = PS_K + \sum_K \sum_V PS_{K,V} + \sum_K \sum_V \sum_W PS_{K,V,W} + \dots, \quad (2.50)$$

where PS_{KV} is second-order process interaction effect between processes K and V , PS_{KVV} is the third-order process interaction effect between processes K , V and W . The second-order process interaction effect can be defined as:

$$PS_{K,V} = \frac{V_{K,V}(E_{\sim(K,V)}[\Delta | K, V])}{V(\Delta)} - \frac{V_K(E_{\sim K}[\Delta | K])}{V(\Delta)} - \frac{V_V(E_{\sim V}[\Delta | V])}{V(\Delta)}. \quad (2.51)$$

The first item in the right-hand side of equation (33) enables us to consider the joint effect of variance reduction by simultaneously fixing processes K and V on the variance of Δ and the remain two items at the right-hand side of equation (33) are the first-order process sensitivity index for process K and process V , respectively. Extension of $V_{K,V}(E_{\sim(K,V)}[\Delta | K, V])$ in the first item to consider model uncertainty and perimetric uncertainty is straightforward, leading to:

$$\begin{aligned} & V_{K,V}(E_{\sim(K,V)}[\Delta | K, V]) \\ &= V_{M_{K,V}}(E_{M_{\sim(K,V)}}[\Delta | M_{K,V}]) \\ &= E_{M_{K,V}} E_{\theta_{K,V}|M_{K,V}} (E_{M_{\sim(K,V)}} E_{\theta_{\sim(K,V)}|M_{\sim(K,V)}} [\Delta | M_{K,V}, \theta_{K,V}, M_{\sim(K,V)}, \theta_{\sim(K,V)}])^2 \\ &\quad - (E_{M_{K,V}} E_{\theta_{K,V}|M_{K,V}} E_{M_{\sim(K,V)}} E_{\theta_{\sim(K,V)}|M_{\sim(K,V)}} [\Delta | M_{K,V}, \theta_{K,V}, M_{\sim(K,V)}, \theta_{\sim(K,V)}])^2 \end{aligned}, \quad (2.52)$$

where $M_{K,V}$ is a set of alternative process model combinations used to simulate processes K and V , $M_{K,V}$ is a single model in the set $M_{K,V}$, $\theta_{K,V} | M_{K,V}$ denotes the set of parameter combinations with respect to $M_{K,V}$ and $\theta_{K,V}$ is a single combination realization in the set $\theta_{K,V} | M_{K,V}$. Similarly, $M_{\sim(K,V)}$, $M_{\sim(K,V)}$, $\theta_{\sim(K,V)} | M_{\sim(K,V)}$, and $\theta_{\sim(K,V)}$ denote the same except they are for processes other than K and V . Equation (2.52) can be numerically evaluated using the Monte Carlo method and model averaging method as described in Section 2.3. The third-order and higher-order process interaction effects can be defined and derived analogously thus they are not given here.

表 2-2 同时考虑模型不确定性和参数不确定性的—维河间地块模型 $x_0 = 7,000$ m 处单宽流量的方差分解

Table 2-2 Variance decomposition of groundwater discharge per unit width at $x_0 = 7000$ m considering both model uncertainty and parametric uncertainty

First-order effect			Second-order effect			Third-order effect		
	V_K	$PS_K(\%)$	Pair	$V_{K,V}$	$PS_{K,V}(\%)$	Pair	$V_{K,V,W}$	$PS_{K,V,W}(\%)$
R	0.2966	14.32	G,R	0.0071	0.34	M,R,G	0.00	0.00
G	0.1406	6.79	M,R	0.00	0.00			
M	1.3252	63.99	M,G	0.3013	14.55			

Total effects								
	V_{TK}^*	$PS_{TK}(\%)$	V_{TK}^{**}					
R	0.3038	14.67	$V_{TR}=V_R+V_{G,R}+V_{M,R}+V_{M,R,G}=V_R+V_{G,R}=0.3037$					
G	0.4490	21.68	$V_{TG}=V_G+V_{G,R}+V_{M,G}+V_{M,R,G}=V_G+V_{G,R}+V_{M,G}=0.4490$					
M	1.6265	78.54	$V_{TM}=V_M+V_{M,R}+V_{M,G}+V_{M,R,G}=V_M+V_{M,G}=1.6265$					

Variance $V = V_R + V_G + V_M + V_{G,R} + V_{M,R} + V_{G,M} + V_{M,R,G} = 2.0708^{**}$
--

* : Calculated based on Equation (2.20)

** : Calculated based on variance decomposition

Table 2-2 lists the variance decomposition of groundwater discharge per unit width at $x_0 = 7000$ m considering both model uncertainty and parametric uncertainty. Note that since there are only three processes, the third-order process interaction effect is calculated using the difference between one and the sum of first-order and second order interaction effects. Note that since there is always no interaction between the recharge process and the snowmelt process, the theoretical third-order process interaction effect should be zero. The negative near-zero value (-0.17%) of the third-order effect is caused by the Monte Carlo approximation. One may note that recharge process and geology process have a small interaction (0.35%) as indicated by the second-order process interaction effect between the two processes. The non-zero interaction effect can be explained by examining equation (20). Recall that for geology process model G_1 , $K = K_1 = K_2$, there is no interaction between w and the other two factors h_2 and K . However, when the geology process model changes from G_1 to G_2 , there is interaction between w and λ which is K_1/K_2 (Table 3). One may also note that second-order process interaction effect between recharge process and snowmelt process is zero. This is because whatever the process model changes, there is no interaction between the w and h_2 for all of the eight system

models. Besides, due to the relatively large process interaction effect between geology process and snowmelt process, the total process sensitivity index of geology process is larger than that of recharge process, thus changing the ranking orders of the process sensitivity.

Figure 2-5b illustrates the spatial variation of second-order process interaction effects of groundwater discharge per unit width for the entire domain. Note that in the hydrological case there is no fourth-order or higher-order process interaction effects since there are only three processes and the third-order process interaction effects should be theoretically all zeros thus they are not shown here. As mentioned above, there is no interaction between recharge and snowmelt processes and variation of the location x would not change the independent relationship between w and h_2 as indicated by equation (2.48). The second-order process interaction effects are zeros between recharge and snowmelt processes for the entire domain. The second-order process interaction effects between geology and snowmelt process are generally very large causing the total process sensitivity values of the geology process at some locations are larger than that of the recharge process.

2.4.5 Relation between Parameter and Process Sensitivity Indices

This section shows that the process sensitivity indices of multiple system models are not simply a weighted average of parameter sensitivity indices of individual system models for two reasons. The first reason is that the total variance, $V(\Delta)$ (the denominator in Equations (2.13) and (2.16)) of multiple system models is more than a weighted average of the variance of the individual models. Following Equations (4) and (5) of Ye et al. (2004), the variance term $V(\Delta)$ in the denominator is evaluated as

$$\begin{aligned} E(\Delta) &= \sum_{k=1}^K E(\Delta|M_k)P(M_k) \\ V(\Delta) &= \sum_{k=1}^K V(\Delta|M_k)P(M_k) + \sum_{k=1}^K (E(\Delta|M_k) - E(\Delta))^2 P(M_k) \end{aligned}, \quad (2.53)$$

where $E(\Delta)$ is model averaged mean, M_k is a system model. Separating a system model M_k into a combination of process models M_K and $M_{\sim K}$, and then applying the law of total expectation to the parameter level, Equation (2.53) becomes

$$\begin{aligned}
E(\Delta) &= \sum_{N_K} \sum_{N_{\sim K}} E_{\theta_K | M_K} E_{\theta_{\sim K} | M_{\sim K}} [\Delta | \theta_K, M_K, \theta_{\sim K}, M_{\sim K}] P(M_{\sim K}) P(M_K) \\
V(\Delta) &= \underbrace{\sum_{N_K} \sum_{N_{\sim K}} V_{\theta_K | M_K, \theta_{\sim K} | M_{\sim K}} [\Delta | \theta_K, M_K, \theta_{\sim K}, M_{\sim K}] P(M_{\sim K}) P(M_K)}_{\text{within-model variance}} \\
&\quad + \underbrace{\sum_{N_K} \sum_{N_{\sim K}} \left(E_{\theta_K | M_K} E_{\theta_{\sim K} | M_{\sim K}} [\Delta | \theta_K, M_K, \theta_{\sim K}, M_{\sim K}] - E(\Delta) \right)^2 P(M_{\sim K}) P(M_K)}_{\text{between-model variance}}
\end{aligned} \tag{2.54}$$

where $E(\Delta)$ and $V(\Delta)$ are also called posterior mean and variance, respectively, in the context of model averaging for multiple system models, and $E_{\theta_K | M_K} E_{\theta_{\sim K} | M_{\sim K}} [\Delta | \theta_K, M_K, \theta_{\sim K}, M_{\sim K}] V_{\theta_K | M_K, \theta_{\sim K} | M_{\sim K}} [\Delta | \theta_K, M_K, \theta_{\sim K}, M_{\sim K}]$ are the mean and variance, respectively, of a single system model consisting of process models M_K and $M_{\sim K}$. The expression of $V(\Delta)$ include not only the weighted average of the variance of individual models (the within-model variance term) but also the variance between the means of individual models (the between-model variance term).

Between-model terms also exist for the variance-reduction term $V_{M_K} (E_{M_{\sim K}} [\Delta | M_K])$ used to define the first-order process sensitivity index in Equation (2.13) and for the variance-left term $E_{M_{\sim K}} (V_{M_K} [\Delta | M_{\sim K}])$ used to define the total-effect process sensitivity index in Equation (2.16). This is the other reason that the process sensitivity indices of multiple system models are not simply a weighted average of parameter sensitivity indices of individual system models. For the numerator term $V_{M_K} (E_{M_{\sim K}} [\Delta | M_K])$ in the definition of the first-order process sensitivity index, according to the law of total variance, it can be expressed as

$$V_{M_K} (E_{M_{\sim K}} [\Delta | M_K]) = V(\Delta) - E_{M_K} (V_{M_{\sim K}} [\Delta | M_K]). \tag{2.55}$$

Applying the law of total expectation to the second term at the right-hand side of Equation (2.53) gives

$$E_{M_K} (V_{M_{\sim K}} [\Delta | M_K]) = E_{M_K} E_{\theta_K | M_K} (V_{M_{\sim K}} [\Delta | M_K]). \tag{2.56}$$

which considers parametric uncertainty. For the $V_{M_{\sim K}} [\Delta | M_K]$ term of Equation (2.53), it is for multiple models, $M_{\sim K}$, and using the expression of model-averaged variance (Equation 5 of Ye et al. (2004)) gives

$$\begin{aligned}
& E_{M_K}(V_{M_{\sim K}}[\Delta | M_K]) \\
&= E_{M_K} E_{\theta_K | M_K}(V_{M_{\sim K}}[\Delta | M_K]) \\
&= E_{M_K} E_{\theta_K | M_K} \left(\begin{array}{l} E_{M_{\sim K}} V_{\theta_{\sim K} | M_{\sim K}}[\Delta | \theta_K, M_K, \theta_{\sim K}, M_{\sim K}] + \\ E_{M_{\sim K}} \left(\begin{array}{l} E_{\theta_{\sim K} | M_{\sim K}}[\Delta | \theta_K, M_K, \theta_{\sim K}, M_{\sim K}] \\ - E_{M_{\sim K}} E_{\theta_{\sim K} | M_{\sim K}}[\Delta | \theta_K, M_K, \theta_{\sim K}, M_{\sim K}] \end{array} \right)^2 \end{array} \right) . \quad (2.57) \\
&= E_{M_K} E_{\theta_K | M_K} E_{M_{\sim K}} V_{\theta_{\sim K} | M_{\sim K}}[\Delta | \theta_K, M_K, \theta_{\sim K}, M_{\sim K}] \\
&\quad + E_{M_K} E_{\theta_K | M_K} E_{M_{\sim K}} \left(\begin{array}{l} E_{\theta_{\sim K} | M_{\sim K}}[\Delta | \theta_K, M_K, \theta_{\sim K}, M_{\sim K}] \\ - E_{M_{\sim K}} E_{\theta_{\sim K} | M_{\sim K}}[\Delta | \theta_K, M_K, \theta_{\sim K}, M_{\sim K}] \end{array} \right)^2
\end{aligned}$$

Assuming independent processes and parameters, Equation (2.57) can be rearranged as:

$$\begin{aligned}
& E_{M_K}(V_{M_{\sim K}}[\Delta | M_K]) \\
&= E_{M_K} E_{M_{\sim K}} E_{\theta_K | M_K} V_{\theta_{\sim K} | M_{\sim K}}[\Delta | \theta_K, M_K, \theta_{\sim K}, M_{\sim K}] \\
&\quad + E_{M_K} E_{M_{\sim K}} E_{\theta_K | M_K} \left(\begin{array}{l} E_{\theta_{\sim K} | M_{\sim K}}[\Delta | \theta_K, M_K, \theta_{\sim K}, M_{\sim K}] \\ - E_{M_{\sim K}} E_{\theta_{\sim K} | M_{\sim K}}[\Delta | \theta_K, M_K, \theta_{\sim K}, M_{\sim K}] \end{array} \right)^2 . \quad (2.58) \\
&= \sum_{N_K} \sum_{N_{\sim K}} E_{\theta_K | M_K} V_{\theta_{\sim K} | M_{\sim K}}[\Delta | \theta_K, M_K, \theta_{\sim K}, M_{\sim K}] P(M_{\sim K}) P(M_K) \\
&\quad + \sum_{N_K} \sum_{N_{\sim K}} E_{\theta_K | M_K} \left(\begin{array}{l} E_{\theta_{\sim K} | M_{\sim K}}[\Delta | \theta_K, M_K, \theta_{\sim K}, M_{\sim K}] \\ - E_{M_{\sim K}} E_{\theta_{\sim K} | M_{\sim K}}[\Delta | \theta_K, M_K, \theta_{\sim K}, M_{\sim K}] \end{array} \right)^2 P(M_{\sim K}) P(M_K)
\end{aligned}$$

Substituting equations (2.54) and (2.58) into equation (2.55) leads to

$$\begin{aligned}
& V_{M_K}(E_{M_{\sim K}}[\Delta | M_K]) \\
&= \sum_{N_K} \sum_{N_{\sim K}} \left(\begin{array}{l} V_{\theta_K | M_K, \theta_{\sim K} | M_{\sim K}}[\Delta | \theta_K, M_K, \theta_{\sim K}, M_{\sim K}] P(M_{\sim K}) P(M_K) \\ - E_{\theta_K | M_K} V_{\theta_{\sim K} | M_{\sim K}}[\Delta | \theta_K, M_K, \theta_{\sim K}, M_{\sim K}] P(M_{\sim K}) P(M_K) \end{array} \right) P(M_{\sim K}) P(M_K) \\
&\quad + \sum_{N_K} \sum_{N_{\sim K}} \left(\begin{array}{l} \left(E_{\theta_K | M_K} E_{\theta_{\sim K} | M_{\sim K}}[\Delta | \theta_K, M_K, \theta_{\sim K}, M_{\sim K}] - E(\Delta) \right)^2 \\ - E_{\theta_K | M_K} \left(\begin{array}{l} E_{\theta_{\sim K} | M_{\sim K}}[\Delta | \theta_K, M_K, \theta_{\sim K}, M_{\sim K}] \\ - E_{M_{\sim K}} E_{\theta_{\sim K} | M_{\sim K}}[\Delta | \theta_K, M_K, \theta_{\sim K}, M_{\sim K}] \end{array} \right)^2 \end{array} \right) P(M_{\sim K}) P(M_K) . \quad (2.59)
\end{aligned}$$

Applying the law of total variance to the term in the first parenthesis at the right-hand side of (2.58) gives

$$\begin{aligned}
V_{M_K}(E_{M_K}[\Delta | M_K]) &= \\
&= \sum_{N_K} \sum_{N_{\sim K}} \underbrace{V_{\theta_K|M_K} E_{\theta_{\sim K}|M_{\sim K}}[\Delta | \theta_K, M_K, \theta_{\sim K}, M_{\sim K}] P(M_{\sim K}) P(M_K)}_{\text{within-model variance reduction}} \\
&\quad + \sum_{N_K} \sum_{N_{\sim K}} \underbrace{\left(E_{\theta_K|M_K} E_{\theta_{\sim K}|M_{\sim K}}[\Delta | \theta_K, M_K, \theta_{\sim K}, M_{\sim K}] - E(\Delta) \right)^2}_{-E_{\theta_K|M_K} \left(\frac{E_{\theta_{\sim K}|M_{\sim K}}[\Delta | \theta_K, M_K, \theta_{\sim K}, M_{\sim K}]}{-E_{M_K} E_{\theta_{\sim K}|M_{\sim K}}[\Delta | \theta_K, M_K, \theta_{\sim K}, M_{\sim K}]} \right)^2} P(M_{\sim K}) P(M_K) . \quad (2.60)
\end{aligned}$$

The $V_{\theta_K|M_K} E_{\theta_{\sim K}|M_{\sim K}}[\Delta | \theta_K, M_K, \theta_{\sim K}, M_{\sim K}]$ term at the right-hand side term of Equation (2.60) is the variance-reduction term of a single system model (consisting of M_K and $M_{\sim K}$) when its parameters, $\theta_K | M_K$, of process model M_K are fixed. Therefore, the first item (called *within-model variance reduction*) at the right-hand side of Equation (2.60) is a weighted average of the variance reduction for all the system models. The second term at the right-hand side of Equation (2.60) is called *between-model variance reduction*, and it measures the variance of the variance-reduction between multiple system models. Note that the between-model variance reduction could be negative. For the variance-left term $E_{M_{\sim K}}(V_{M_K}[\Delta | M_{\sim K}])$, instead of using the equations in Section 2.2.2, is derived in a similar manner as, i.e.,

$$\begin{aligned}
&E_{M_{\sim K}}(V_{M_K}[\Delta | M_{\sim K}]) \\
&= E_{M_{\sim K}} E_{\theta_K|M_K}(V_{M_K}[\Delta | M_{\sim K}]) \\
&= \sum_{N_K} \sum_{N_K} \underbrace{E_{\theta_K|M_K} V_{\theta_K|M_K}[\Delta | \theta_K, M_K, \theta_{\sim K}, M_{\sim K}] P(M_K) P(M_{\sim K})}_{\text{within-model variance left}} \\
&\quad + \sum_{N_K} \sum_{N_K} \underbrace{E_{\theta_K|M_K} \left(\frac{E_{\theta_K|M_K}[\Delta | \theta_K, M_K, \theta_{\sim K}, M_{\sim K}]}{-E_{M_K} E_{\theta_K|M_K}[\Delta | \theta_K, M_K, \theta_{\sim K}, M_{\sim K}]} \right)^2}_{-E_{\theta_K|M_K} \left(\frac{E_{\theta_K|M_K}[\Delta | \theta_K, M_K, \theta_{\sim K}, M_{\sim K}]}{-E_{M_K} E_{\theta_K|M_K}[\Delta | \theta_K, M_K, \theta_{\sim K}, M_{\sim K}]} \right)^2} P(M_K) P(M_{\sim K}) . \quad (2.61)
\end{aligned}$$

The $E_{\theta_K|M_K} V_{\theta_K|M_K}[\Delta | \theta_K, M_K, \theta_{\sim K}, M_{\sim K}]$ term is the variance-left term of a single system model (consisting of M_K and $M_{\sim K}$) when its parameters, $\theta_{\sim K} | M_{\sim K}$, for all process model but those of process K are fixed. Therefore, the first item (called *within-model variance left*) at the right-hand side of Equation (2.61) is a weighted average of the variance left

for all the system models. The second term is called *between-model variance left*, and it measures the variance of the variance-left between multiple system models. Because the three between-model terms for $V(\Delta)$, $V_{M_K}(\Delta | M_K)$, and $E_{M_{\sim K}}(V_{M_K}(\Delta | M_{\sim K}))$ in Equations (2.13) and (2.16), the first-order and total-effect process sensitivity indices for all the system models are not simply the weighted average of first-order and total-effect parameter sensitivity indices of individual system models.

Equation (2.60) for the first-order process sensitivity index is useful for understanding whether the variance reduction (after a process model is fixed) is from the within-model or the between-model variance reduction. This is further useful for understanding whether process ranking of a single system model is the same as process ranking of multiple system models, in that the two sets of ranking are not likely to be the same when the between-model variance reduction is substantially larger than the within-model variance reduction. In an extreme case that the between-model variance reduction is zero, the two sets of ranking may still be different, depending on process model weights. This is also true for the ranking given by the total-effect parameter and process sensitivity indices, according to equation (2.61).

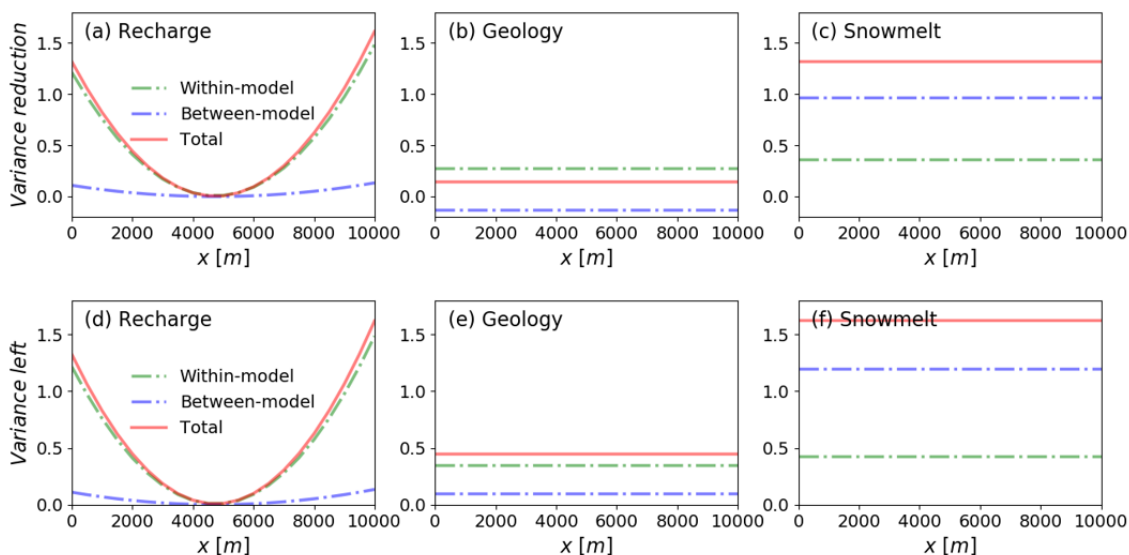


图2-6 (a) 降雨入渗过程, (b) 地质过程, 和 (c) 融雪过程组内和组间方差减少量; (d) 降雨入渗过程, (e) 地质过程, 和 (f) 融雪过程组内和组间方差保留量

Figure 2-6 Within- and between-model variance reduction for (a) recharge process (b) geology process, and (c) snowmelt process, and within- and between-model variance left for (d) recharge process (e) geology process, and (f) snowmelt process over the entire domain.

Figures 2-6a – 2-6c plot the total variance reduction and its within-model and between-model terms (calculated using Equation (2.60)) for the entire domain when recharge, geology, and snowmelt process models are fixed. Figures 2-6d – 2-6f do the same for the variance left when recharge, geology, and snowmelt process models are left unfixed. The variance reduction/left terms are a constant for the geology and snowmelt processes but vary in space for the recharge process. This is not surprising, because Equations (2.48) and (2.49) show that the recharge variable w is multiplied with x to determine groundwater discharge q , but geology variable K and snowmelt variable h_2 are not. For the recharge process, Figures 2-6a and 2-6d show that the within-model terms are larger than the between-model terms over the entire domain except at the center of the domain and its vicinity, where the two terms equal zero. The reason that the between-model terms are small can be explained by examining the PDFs shown in Figures 2-3 and 2-4 for the location of $x = 7,000$ m. Taking Figure 2-4 as an example, Figures 2-4c1 – 2-4c4 show that, in each figure, the two PDFs are close, indicating that the between-model variance left is small for each M_K . Figures 2-6c and 2-6f show that the between-model terms are larger than the within-model terms for the snowmelt process, and this can also be explained by examining Figures 2-3 and 2-4. Taking Figure 2-4 as an example again, the two PDFs in each plot of Figures 2-4a1 – 2-4a4 are separated, and this explains why the between-model term is larger than the within-model term for the snowmelt process. It also should be noted that Figure 2-6b shows the between-model variance reduction of geology process is negative, resulting in the total variance reduction is smaller than the within-model variance reduction. These analyses suggest that identifying important or influential processes under model and parametric uncertainty is complicated, as it depends on multiple factors discussed at the beginning of the section.

2.4.6 Convergence and Computational Cost Analysis

The first-order and total-effect process sensitivity index of the three processes were evaluated by using the brute force method as shown in Figure 2-1 and the proposed estimator to reduce the computational cost in Section 2.4. Since the analytical values of the sensitivity indices are not available, the sensitivity indices obtained from the brute force method by using 8×10^9 model simulations, which was calculated as 2 recharge process models \times 1000 parameters \times 2 geology process models \times 1000 parameters \times 2 snowmelt process models \times 1000 parameters, were used as reference values. Figure 2-7

illustrates the convergence of the sensitivity indices of the three processes for brute force method. The figure shows that the brute force method is stabilized to the after about 1,000,000 model simulations. The large number of 8×10^9 Monte Carlo simulation runs should provide reliable results for the reference values.

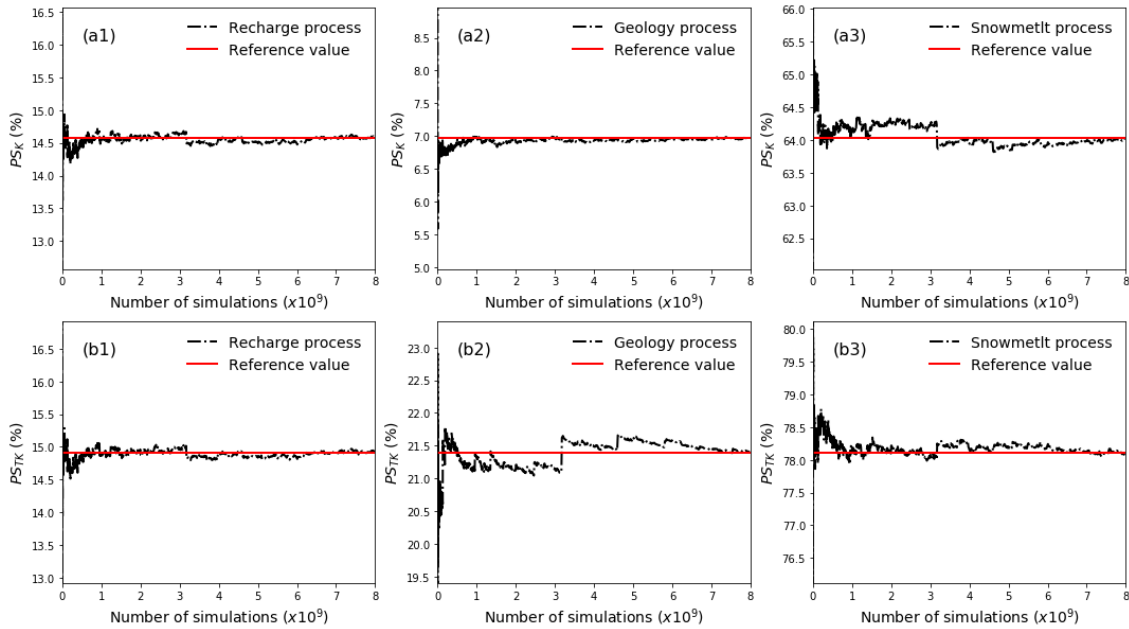


图 2-7 (a1 – a3) 降雨入渗过程, 地质过程, 和融雪过程的一阶过程敏感性指标收敛过程;
(b1 – b3) 降雨入渗过程, 地质过程和融雪过程的总效应过程敏感性指标收敛过程。

Figure 2-7 Convergence plots of (a1-a3) first-order process sensitivity index PS_K and (b1-b3) total-effect process sensitivity index PS_{TK} for the three processes. The reference values are obtained by using 8×10^9 model simulations.

Using the process sensitivity index of brute force method as the reference values, the absolute relative errors (%) were calculated for the two methods. Figure 2-8 plots variation of the absolute relative errors with the number of model simulations for the process sensitivity index of the three processes. It shows that, for example, for the first-order process sensitivity index of recharge process, the brute force method is stabilized to the reference value after about 5×10^8 model simulations with the absolute relative error less than 1% while for the proposed estimator, its absolute relative error becomes less than 1% after about 5×10^5 model simulations.

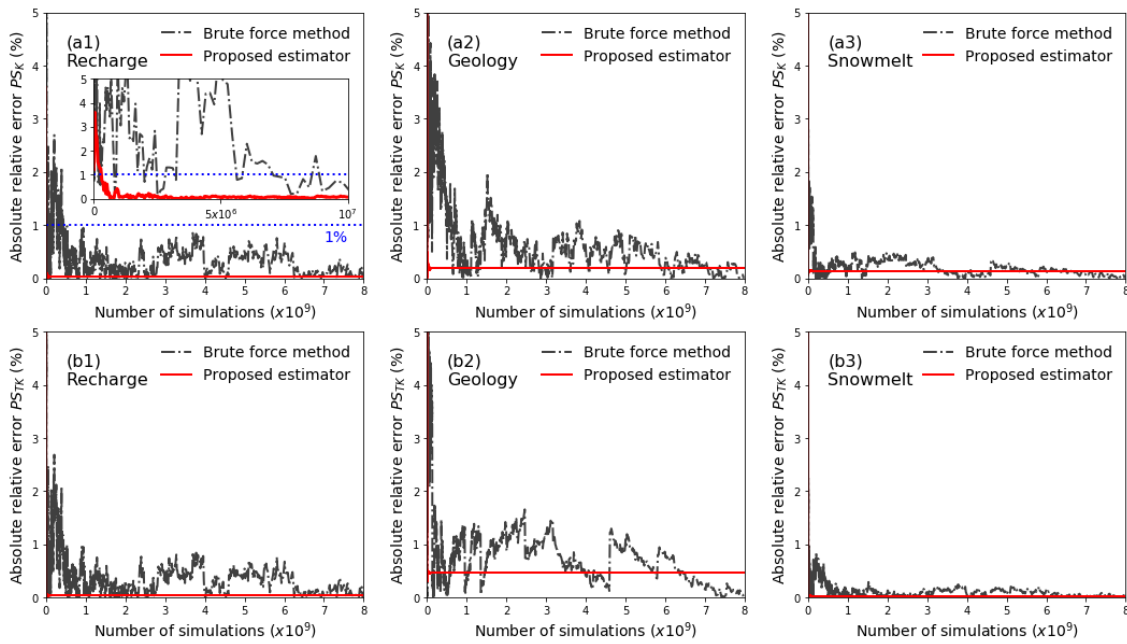


图 2-8 (a1-a3) 降雨入渗过程, 地质过程, 和融雪过程的绝对相对误差收敛过程; (b1-b3) 降雨入渗过程, 地质过程, 和融雪过程的总效应过程敏感性指标收的绝对相对误差收敛过程。

Figure 2-8 Absolute relative error of process sensitivity index for (a1-a3) first-order process sensitivity index PS_K and (b1-b3) total-effect process sensitivity index PS_{TK} for the three processes.

The process sensitivity index values obtained by brute force method with 216,000,000 model simulations is used as the reference value calculating the absolute relative error.

To assess the effect of sampling uncertainty and evaluate the robustness of the estimator to sampling variability, the 95% confidence intervals of the 100 realizations of each experiment are presented. The 95% bootstrap confidence intervals are also estimated for the groundwater flow modeling. Figure 2-9 illustrates the results of the brute force method and the proposed estimator for estimating the of the first-order and total-effect process sensitivity indices of recharge process. The proposed estimator converges faster than the brute force method. Besides, the confidence intervals of the proposed estimator are much smaller than that of the brute force method. Therefore, the proposed estimator outperforms the brute force method.

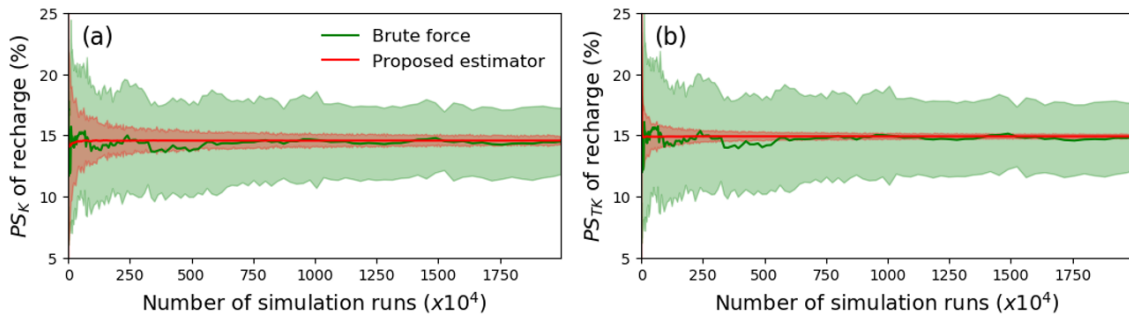


图 2-9 一维河间地块模型降雨入渗补给过程的 (a) 一阶过程敏感性指标 PS_K 和 (b) 总效过程敏感性指标 PS_{TK} 收敛过程。绿色和红色区域分别表示使用 bootstrap 抽样估计的穷举法和本文新提出的高效算法的 95% 置信区间。

Figure 2-9 Convergence plots of (a) first-order process sensitivity index PS_K and (b) total-effect process sensitivity index PS_{TK} of recharge process in the groundwater flow modeling. The green and red areas denote the 95% confidence intervals estimated using bootstrap sampling for the brute force method and proposed efficient estimator, respectively.

§2.5 Summary

Within the framework of variance-based global sensitivity analysis method, this chapter derives the total-effect process sensitivity index by integrating Sobol's total-effect parameter sensitivity index and the model averaging method to consider uncertainty in both process models and process model parameters. Different from the first-order process sensitivity index defined by Dai et al. (2017b) that identifies important processes in terms of variance reduction, the total-effect process sensitivity index identifies influential processes in terms of not only process importance but also process interactions that jointly influence a system model output. Because of the process interactions, the process ranking given by the total-effect process sensitivity index may differ from that given by the first-order process sensitivity index. This is not unreasonable, because the former index is for processes fixing and the latter index is for process prioritization. In other words, the two indices serve different purposes, and this is why it is necessary to develop the total-effect process sensitivity index in this study.

The numerical experiment using the groundwater modeling demonstrate that process importance or influence may change across system models, indicating the needs of using the process sensitivity indices to explicitly consider uncertainty in process models and process model parameters. The numerical experiment of groundwater modeling further demonstrates that the first-order and total-effect process sensitivity indices give different

process ranking due to process interactions. For a complex hydrologic system that deriving analytical solution of a model output is not feasible, the two process sensitivity indices should be useful took for understanding process interactions by evaluating differences between the ranking of important processes and influential processes.

The first-order and total-effect process sensitivity indices of multiple system models are not simply weighted averages of the first-order and total-effect parameter sensitivity indices of individual system models. This is evidenced by breaking up the variance reduction/left into two terms: the within-model variance reduction/left term and between-model variance reduction/left term. Although the total-effect process sensitivity index addresses process interactions, it should be noted that the model averaging method used in this study for deriving the index assumes that the process models are independent. This is a drawback because it neglects process interactions when determining process model weights. A related issue is the hierarchical relation between a process and its subprocesses brought up by Martyn Clark in a personal communication. For example, a vadose zone flow process may be represented by gravity drainage and Richards' equation at a coarse level; at a fine level, there may be multiple soil retention curves associated with the Richards' equation. The fine-level uncertainty depends on the coarse-level uncertainty, in that the probability of choosing a soil retention curve depends on the probability of choosing the Richards' equation. One possible solution to this problem may be using the Bayesian network to incorporate known process interactions, as shown in Dai et al. (2019). If new process interactions are found by using the first-order and total-effect process sensitivity indices, the new interactions may be incorporated into the Bayesian network in an iterative manner. Resolving these problems also depends on progress on developing a more comprehensive modular modeling framework for process-based modeling.

This chapter develop a new computationally efficient estimator to evaluate the variance-based sensitivity indices under both process model and parametric uncertainty. The estimator allows simultaneously estimating the Sobol's parameter sensitivities and the process sensitivities. With the synthetic groundwater flow example, this chapter demonstrate that the estimator dramatically reduces the computational cost.

Chapter 3 A New Multi-model Absolute Difference-based Process Sensitivity Analysis Method

This chapter presents a new method, called multi-model absolute difference-based sensitivity (MMADS) analysis, which expands the design ideas of Morris screening method (Morris 1991) from parameter space to parameter-process-model space. The method evaluates not only the absolute differences of a model output when model parameters change from one set of values to another set of values but also the differences of a model output when a process representation changes from one process model to another process model. After the absolute differences are evaluated for each process, their mean and variance are calculated and used to identify non-influential processes. The calculation in the model space is based on model averaging method that has been used in the hydrologic community for several decades (Beven 2002, Neuman 2003, Poeter and Anderson 2005, Ye et al. 2004). A process with small mean and variance is considered to be non-influential. A small mean indicates small differences of the model output when process models and process model parameter values are changed. A small variance is resulted from a lack of nonlinear effects and/or interactions between process models and/or process model parameter values. In other words, the MMADS method identifies non-influential processes with consideration of uncertainty in both process models and process model parameters. The numerical evaluation is examined by the same hypothetical groundwater flow modeling used in Chapter 2. The biggest difference between the MMADS method and variance-based process sensitivity analysis method proposed in Chapter 2 is that MMADS is born as a qualitative method, and it requires much fewer model evaluations. The numerical experiment of groundwater modeling demonstrates that with a limited number of model executions, the ranking of the influential processes from MMADS is the same as that of variance-based process sensitivity method.

§3.1 Introduction

The method of Morris (1991) yields measures of global sensitivity from a set of local derivatives, or elementary effects, sampled on a grid throughout the parameter space. Rooted on one-at-a-time (OAT) methods, efficiency of the Morris method has been proved by a rich body of studies in hydrologic modeling (Braddock and Schreider 2006, Herman et al. 2013a, King and Perera 2013). However, the conventional Morris method cannot be directly used to identify non-influential processes, because the method only addresses parametric uncertainty and cannot be applied to multiple system models. To resolve this problem, based on Morris' one-factor-at-a-time concept, Van Hoey et al. (2014) developed a new method to vary model components one at a time. A model component was defined by Van Hoey et al. (2014) as “a conceptual description of a subprocess of the entire model”, which appears to be a system process of interest to this study. The method of Van Hoey et al. (2014) applies the Morris method to each alternative models of a process for evaluating the mean of absolute elementary effects, denoted as μ^* , an important term of the Morris screening method as discussed in Section 3.2.1. The μ^* values of any two alternative process models are plotted in a so-called “evaluation chart”, and the chart is used to evaluate impacts of process models on model outputs or model evaluation metrics. While this method is conceptually straightforward and easy to implement, it performs sensitivity analysis on individual system models and does not explicitly consider impacts of process models on model outputs, because it does not evaluate variation of model outputs caused by changing a process representation from one process model to another process model. In other words, Van Hoey et al. (2014) applied the Morris method only in a parameter space, but not in a parameter-process-model space.

This chapter presents a new method, called multi-model absolute difference-based sensitivity (MMADS) analysis, which expands the design ideas of Morris screening method from parameter space to parameter-process-model space. The MMADS method is conceptually different from other methods that have been recently developed to identify important or influential processes such as the variance-based methods (Dai et al. 2017a, Dai and Ye 2015, Dai et al. 2017b, Mai et al. 2020). The variance-based methods evaluate how variance of a model output is reduced (or remains), when a process model is fixed (or left unfixed). For example, the first-order process sensitivity index developed by (Dai

et al. 2017b) identifies an important process by examining the average variance reduction caused by fixing a process representation to each of its alternative process models. The total-effect process sensitivity index developed in Chapter 2 identifies an influential process by examining the averaging variance remaining if the process is left unfixed but all other processes are fixed to their process models. The extended Sobol' sensitivity analysis (xSSA) developed by Mai et al. (2020) uses weighted process models of a process to represent the process involved in the system model and extends Sobol' sensitivity analysis to simultaneously determining global sensitivities of model parameters and model structure. The method of model sensitivity analysis developed by (Dell'Oca et al. 2020b) is more general to consider not only variance but also other statistical moments (e.g., skewness and kurtosis). While these methods are more theoretically rigorous than MMADS is, they are computationally expensive, because their implementation using Monte Carlo simulations to approximate variance (or other statistical moments) which may require millions of model executions. Although various approaches can be used to reduce computational cost (see the review article of (Razavi et al. 2012)), a large number of model executions are still needed, which may be a barrier to use the variance-based process sensitivity analysis methods in practice. Similar to the Morris screening method, the MMADS method is computationally efficient. This study shows that reasonable results can be obtained by only 800 model executions, which makes MMADS appealing to real-world applications for identifying non-influential processes.

§3.2 Background, Conceptualization, and Derivation

3.2.1 Traditional Morris Screening Method for Single-Model

To better understand the rational of developing the MMADS method, we start with introducing the Morris screening method of parameter sensitivity analysis for a single system model. Following Saltelli et al. (2004), we use $y(\mathbf{x})$ to denote a model output evaluated with k parameters, $\mathbf{x} = (x_1, x_2, \dots, x_k)$. The range of each parameter is scaled to the unit interval $[0, 1]$ (e.g., by using its cumulative distribution), and the unit interval is then partitioned into $(p-1)$ equally sized intervals, where p is the number of levels. The Morris screening method evaluates the elementary effect (EE) defined as

$$EE_i = \frac{[y(x_1, \dots, x_{i-1}, x_i + \delta, x_{i+1}, \dots, x_k) - y(\mathbf{x})]}{\delta} \quad (3.1)$$

where EE_i is the elementary effect of the i -th parameter x_i , and δ is a predetermined multiple of the interval (note we use δ here and reserve Δ to denote the system model output later) with the size of $1/(p-1)$. $\mathbf{x} = (x_1, \dots, x_{i-1}, x_i, x_{i+1}, \dots, x_k)$ is the vector of the reference parameter values, and each value is selected randomly from the set $\{0, 1/(p-1), 2/(p-1), \dots, 1\}$ except that x_i is selected randomly from the set $\{0, 1/(p-1), 1/(p-1), \dots, 1-\delta\}$ so that $(x_i + \delta)$ is still in range of $[0, 1]$. Randomly sampling x_i gives a number of EE_i , and three statistics of EE_i are computed as follows: the mean (μ_i) of EE_i , the mean (μ_i^*) of absolute EE_i , and the standard deviation (σ_i) of EE_i . As noted by Saltelli et al. (2004) and Campolongo et al. (2007), μ^* is a better choice than μ for detecting parameters that have important overall influence on the output, because EE values with opposite signs may cancel each other out when the model function is non-monotonic. The standard deviation, σ_i , is used to detect parameters that either have nonlinear effects on the output or interact with other parameters to affect the output. A parameter with both small μ^* and σ values is identified as a non-influential parameter. Since the Morris screening method is qualitative in nature in comparison with other global sensitivity analysis methods such as variance-based methods using Sobol' first-order or total-effect sensitivity indices, it is commonly used for screening non-influential parameters, rather than ranking importance or influence of model parameters.

Figure 3-1a is an illustration of evaluating the EE values based on a figure of Saltelli et al. (2004). Assume that a system model has two processes, denoted as A and B , for sensitivity analysis, and that each process is represented by one process model, i.e., M_A for process A and M_B for process B . For the sake of illustration, we further assume that each model has only one parameter for sensitivity analysis, i.e., x_A for M_A and x_B for M_B . The system model is thus formed as $M_A(x_A) \cup M_B(x_B)$ by integrating process models M_A and M_B . With the number of levels $p = 5$ for each parameter, a total of 20 EE values can be obtained for each parameter. If all the 20 values are small and the variation of the 20 values is also small, the corresponding μ^* and σ values are small. This indicates that the model output changes slightly when parameter values change, and the parameter is thus identified to be non-influential. If process model uncertainty does not exist and a process is represented by a single process model, a process is identified to be non-influential if its model parameters are identified to be non-influential by the Morris screening method. If a process model contains more than one parameter, the Morris screening method is

applied to a group of parameters associated with this process. More details are referred to Saltelli et al. (2004).

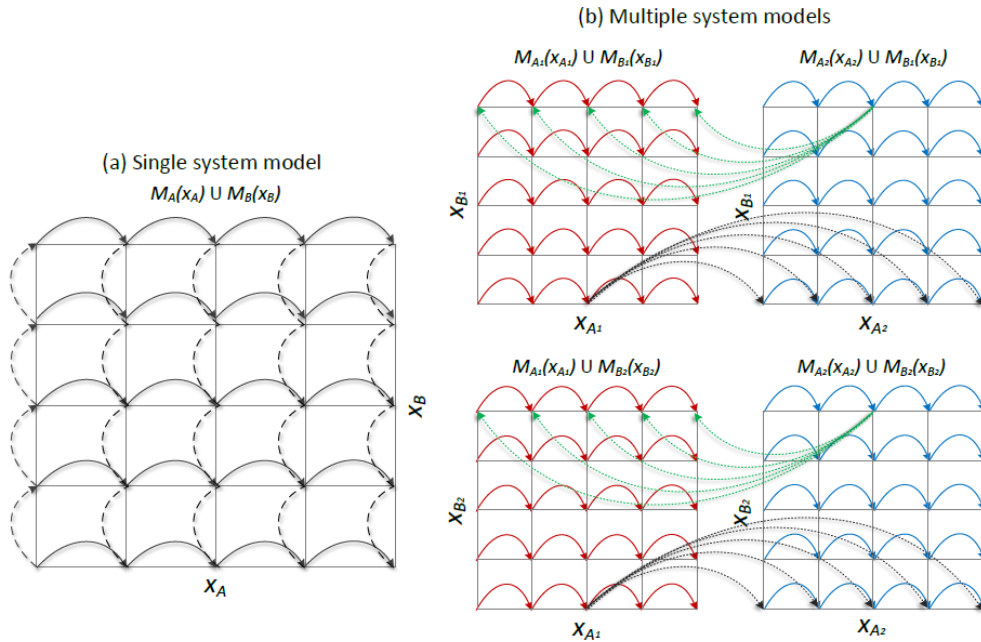


图 3-1. 基于五层网格的 (a) 单系统模型和 (b) 多系统模型参数空间示意图。假设系统模型由 A 和 B 两个过程组成。单模型系统条件下，过程 A 和 B 分别由过程模型 M_A 和 M_B 表示，每个过程模型有各自参数 x_A 和 x_B 。水平实线箭头表示参数 x_A 的 20 个基效应，垂直虚线箭头表示 x_B 的 20 个基效应。多模型系统条件下，假设过程 A 有两个可能的过程模型 M_{A1} 和 M_{A2} ，每个模型都有各自的参数 x_{A1} 和 x_{A2} ；过程 B 有两个可能的过程模型 M_{B1} 和 M_{B2} ，每个模型都有各自的参数 x_{B1} 和 x_{B2} 。红色和蓝色虚线箭头表示参数在同一个过程模型中变化，而绿色和黑色虚线箭头表示参数可以在不同的过程模型间变化。

Figure 3-1 Representation of the five-level grid of (a) single system model behaved by two processes A and B, each of which are conceptualized by process model M_A and M_B , respectively. Each process model (denoted as M_A and M_B) is functioned by its own parameter x_A and x_B , respectively. The horizontal dashed arrows identify the 20 elementary effects relative to x_A , while the vertical dotted arrows identify the 20 elementary effects relative to x_B . (b) multi-model functioned by two processes A and B. Process A has two alternative process models M_{A1} and M_{A2} , each of which has its own parameter x_{A1} and x_{A2} , respectively. Process B has two alternative process models M_{B1} and M_{B2} , each of which has its own parameter x_{B1} and x_{B2} , respectively. The red and blue dashed arrows indicate that the parameters vary within their process models while the green and black dotted arrows indicate that the parameter can be changed across the process models.

Without considering process model uncertainty, i.e., a process is represented by a single process model, the influence of this process can be represented by the influence of the model parameters embedded in this process. If a process model contains only one parameter, the two sensitivity measures (μ^* and σ_i) can be directly used to identify the influential processes. When the process model contains more than one parameter, Campolongo et al. (2007) adjusted the Morris screening method to work with group of

factors, i.e., to produce an overall sensitivity measure relative to a group by using the mean (μ_i^*) of absolute EE_i . For a process model contains two parameters $\mathbf{u}=(x_{i1}, x_{i2})$, the absolute EE of this process in point \mathbf{x} is:

$$|EE_u| = \frac{|y(\tilde{\mathbf{x}}) - y(\mathbf{x})|}{\delta}, \quad (3.2)$$

where \mathbf{x} is any selected value in the unit parameter space such that the transformed point $\tilde{\mathbf{x}}$ is still in the unit parameter space, and each of the components \tilde{x}_{i1} and \tilde{x}_{i2} have been either increased or decreased by δ with respect to x_{i1} and x_{i2} . Note that this as two factors may have been changed in opposite directions, i.e., one increased and one decreased by δ , the definition of standard deviation, σ_u , of the EE_u would be meaningless thus usually not be calculated for grouped parameters.

3.2.2 Basic Ideas of MMADS for Multi-Model

Figure 3-1b illustrates the design idea of MMADS to consider both process model uncertainty and process model parameter uncertainty. For the sake of illustration, we assume that process A is represented by two alternative process models, M_{A_1} and M_{A_2} . M_{A_1} has one parameter, \mathbf{x}_{A_1} , and M_{A_2} has one parameter \mathbf{x}_{A_2} , where the bold \mathbf{x} denotes a random variable with multiple parameter values. Similarly, process B also has two alternative process models, i.e., process model M_{B_1} with parameter \mathbf{x}_{B_1} and process model M_{B_2} with parameter \mathbf{x}_{B_2} . As a result, we have four system models denoted as $M_{A_1} \cup M_{B_1}$, $M_{A_2} \cup M_{B_1}$, $M_{A_1} \cup M_{B_2}$, and $M_{A_2} \cup M_{B_2}$. The basic ideas of MMADS are to evaluate the absolute difference, $d\Delta$, of the system model output, Δ , in the following two situations under process model uncertainty (assuming that parametric uncertainty does not exist at this stage):

- (1) Transition between the two models of process A , conditioning on model, M_{B_1} , of process B . There are four transitions between the two models of process A as follows: $T_{M_A} = \{M_{A_1} \rightarrow M_{A_1}, M_{A_1} \rightarrow M_{A_2}, M_{A_2} \rightarrow M_{A_1}, M_{A_2} \rightarrow M_{A_2}\}$, where $\mathbf{M}_A = \{M_{A_1}, M_{A_2}\}$. The difference, $d\Delta$, of model output for each transition is evaluated, and then averaged over all the transitions to yield $E_{T_{M_A}}(d\Delta | M_{B_1})$ (the way of calculating the average will be discussed in Section 2.3). The $E_{T_{M_A}}(d\Delta | M_{B_1})$ term is conditioned on M_{B_1} , and measures how the changes between and within the two

process models, $\mathbf{M}_A = \{M_{A_1}, M_{A_2}\}$ affect model output given M_{B_1} . When there is no parametric uncertainty, $d\Delta = 0$ for $M_{A_1} \rightarrow M_{A_1}$ and $M_{A_2} \rightarrow M_{A_2}$, and $d\Delta$ for $M_{A_1} \rightarrow M_{A_2}$ equals $d\Delta$ for $M_{A_2} \rightarrow M_{A_1}$. These however are not the case when parametric uncertainty exists for the process models, and more discussion on this is given later.

(2) Transition between the two models of process A, conditioning on model, M_{B_2} , of process B. Repeat the calculation above for M_{B_1} , we have $E_{T_{M_A}}(d\Delta | M_{B_2})$ that is conditioned on M_{B_2} , and measures how the changes between and within the two process models, $\mathbf{M}_A = \{M_{A_1}, M_{A_2}\}$, affect model output given M_{B_2} .

For $E_{T_{M_A}}(d\Delta | M_{B_1})$ and $E_{T_{M_A}}(d\Delta | M_{B_2})$, calculate the average to yield $E_{M_B} E_{T_{M_A}}(d\Delta | M_B) = E_A(d\Delta)$ for process A, which measures how the changes between and within the two models of process A affect model output. Similarly, we can also have $E_{M_A} E_{T_{M_B}}(d\Delta | M_B) = E_B(d\Delta)$ for process B, which measures how the changes between and within the two models of process B affect model output. If process A is more influential than process B to the model output, then $E_A(d\Delta)$ is larger than $E_B(d\Delta)$. This calculation for the average of $d\Delta$ can be extended to a calculation for the variance, $V(d\Delta)$, of $d\Delta$, and its corresponding equation is given in Section 2.3.

Now further consider parametric uncertainty of each process model, and discretize each random parameter as in the Morris screening method shown in Figure 3-1b. The transition $T_{M_A} = \{M_{A_1} \rightarrow M_{A_1}, M_{A_1} \rightarrow M_{A_2}, M_{A_2} \rightarrow M_{A_1}, M_{A_2} \rightarrow M_{A_2}\}$ used above is not just between the two process models, but from a parameter value of one process model to a parameter value of the other process model. Specifically speaking, $M_{A_1} \rightarrow M_{A_1}$ means from one point of \mathbf{x}_{A_1} to another point of \mathbf{x}_{A_1} . This parameter transition is denoted as $x_{A_1} \rightarrow x'_{A_1}$, where x_{A_1} and x'_{A_1} are two points of \mathbf{x}_{A_1} . Therefore, $d\Delta$ for $M_{A_1} \rightarrow M_{A_1}$ is not zero anymore, depending on influence of \mathbf{x}_{A_1} on Δ . Such a $d\Delta$ may be denoted as $d\Delta|(x_B, M_B, M_{A_1} \rightarrow M_{A_1}, x_{A_1} \rightarrow x'_{A_1})$. Note that M_B denotes a model (M_{B_1} or M_{B_2}) of process B, and x_B denotes a point in the parameter space of M_B . Similarly, for transition $M_{A_2} \rightarrow M_{A_2}$, we have $d\Delta|(x_B, M_B, M_{A_2} \rightarrow M_{A_2}, x_{A_2} \rightarrow x'_{A_2})$. For the transitions $M_{A_1} \rightarrow M_{A_2}$ and $M_{A_2} \rightarrow M_{A_1}$, their corresponding $d\Delta$ terms are denoted as $d\Delta|(x_B, M_B, M_{A_1} \rightarrow M_{A_2}, x_{A_1} \rightarrow x'_{A_2})$ and $d\Delta|(x_B, M_B, M_{A_2} \rightarrow M_{A_1}, x_{A_2} \rightarrow x'_{A_1})$, respectively. Note that because the parameter transition $x_{A_1} \rightarrow x'_{A_2}$ for $M_{A_1} \rightarrow M_{A_2}$ may not be the same as the parameter transition $x_{A_2} \rightarrow x'_{A_1}$ for $M_{A_2} \rightarrow M_{A_1}$,

$d\Delta|(x_B, M_B, M_{A_1} \rightarrow M_{A_2}, x_{A_1} \rightarrow x_{A_2})$ and $d\Delta|(x_B, M_B, M_{A_2} \rightarrow M_{A_1}, x_{A_2} \rightarrow x_{A_1})$ may be different. For each of the four $d\Delta$ terms, there are multiple parameter transitions for a process model transition. Calculating the average of $d\Delta$ first over the parameter transitions and then over the model transitions gives $E_{T_{M_A}}(d\Delta|x_B, M_B) = E_{T_{M_A}}E_{T_{x_A}|T_{M_A}}(d\Delta|x_B, M_B, T_{x_A}, T_{M_A})$, where T_{x_A} is a parameter transition of x_A for the process model transition T_{M_A} of process A. Note that $E_{T_{M_A}}(d\Delta|x_B, M_B)$ is for one model of process B and one point of its parameter. Taking average of $E_{T_{M_A}}(d\Delta|x_B, M_B)$ first over all parameter points (x_B) and then over all process models gives $E_A(d\Delta) = E_{M_B}E_{T_{M_A}}(d\Delta|M_B) = E_{M_B}E_{x_B|M_B}E_{T_{M_A}}E_{T_{x_A}|T_{M_K}}(d\Delta|x_B, M_B, T_{x_A}, T_{M_A})$ for process A. $E_B(d\Delta)$ can be evaluated in a similar manner. The variance, $V(d\Delta)$, of $d\Delta$ for process A can be evaluated in a similar way, and a general equation is given in Section 2.3. $E_A(d\Delta)$, $E_B(d\Delta)$, $V_A(d\Delta)$, and $V_B(d\Delta)$ are the most critical quantities of MMADS, and they consider both process model uncertainty and model parameter uncertainty.

Figure 3-1b illustrates the transitions between model parameters and between process models. The top row of the figure shows the transitions for a given parameter of x_{B_1} specific to process model M_{B_1} . The red arrows represent possible parameter transitions $x_{A_1} \rightarrow x_{A_1}'$ for process model transition $M_{A_1} \rightarrow M_{A_2}$, and similarly the blue arrows represent possible parameter transitions $x_{A_2} \rightarrow x_{A_2}'$ for process model transition $M_{A_2} \rightarrow M_{A_1}$. The black arrows illustrate possible parameter transition $x_{A_1} \rightarrow x_{A_2}'$ for process model transition $M_{A_1} \rightarrow M_{A_2}$, and similarly the green arrows illustrate possible parameter transitions $x_{A_2} \rightarrow x_{A_1}'$ for process model transition $M_{A_2} \rightarrow M_{A_1}$. The bottom row of Figure 3-1b shows the transitions for a given parameter of x_{B_2} specific to process model M_{B_2} , and the arrows show the same transitions as those in the top row of Figure 3-1b. Because different process models may have different number of parameter and the parameters may have different physical meaning and ranges, we do not use partial-based EE of the Morris method, but only use the difference, $d\Delta$, of model output Δ in MMADS.

3.2.3 Derivation of MMADS Indices

The basic ideas explained above for two system processes and two process models of each process are generalized in this section for any number of system processes and any number of process models of each process. Without process model uncertainty, Δ is

simulated by a single system model, M , i.e., $\Delta = M(\boldsymbol{\Theta}) = M(\theta_1, \theta_2, \dots, \theta_k)$, where

$\boldsymbol{\Theta} = \{\theta_1, \theta_2, \dots, \theta_k\}$ is a vector of system model parameters. Note that we here use θ to denote a set of deterministic parameter values and reserve $\boldsymbol{\Theta}$ to denote a set of random parameter values (θ can be viewed as a realization of $\boldsymbol{\Theta}$). If the system of interest consists of multiple processes (denoted as A, B, \dots) and each process has its own process model (denoted as M_A, M_B, \dots) and associated parameters (denoted as $\theta_A, \theta_B, \dots$), the system model, $M(\theta)$, may be viewed as an integration of the process models, i.e., $M(\theta) = \bigcup(M_A(\theta_A), M_B(\theta_B), \dots)$, together with other system model components common to the processes (e.g., domain discretization, system initial conditions, and driving forces). The process model integration (denoted by the union symbol above) may need to consider nonlinear interactions between the process models. An example of such integration is the development of a system model of groundwater reactive transport, as it integrates processes of groundwater flow, thermal transport, solute transport, and biogeochemical reactions (Dai et al., 2019). In addition, a process may have its sub-processes. For example, a groundwater flow process may consist of sub-processes such as recharge, geology, and evapotranspiration. More discussions on process-based modular modeling are referred to Clark et al. (2015a), Clark et al. (2015b), Clark et al. (2015d).

With the presence of process model uncertainty, a system process may be represented by several alternative process models. Taking process A as an example, it may be represented by multiple process models that form a set, $\mathbf{M}_A(\theta_A) = \{M_{A_1}(\theta_{A_1}), M_{A_2}(\theta_{A_2}), \dots\}$; each process model may have its own parameters or have parameters in common with other process models. Integration of the alternative process models leads to alternative system models, i.e., $\mathbf{M}(\theta) = \bigcup(\mathbf{M}_A(\theta_A), \mathbf{M}_B(\theta_B), \dots)$. If the process model parameters are random, they are denoted as $\boldsymbol{\Theta}$ to be differentiated from θ , which is viewed as a realization of $\boldsymbol{\Theta}$. In this case, $\mathbf{M}(\theta) = \bigcup(\mathbf{M}_A(\theta_A), \mathbf{M}_B(\theta_B), \dots)$ becomes $\mathbf{M}(\boldsymbol{\Theta}) = \bigcup(\mathbf{M}_A(\boldsymbol{\Theta}_A), \mathbf{M}_B(\boldsymbol{\Theta}_B), \dots)$.

We first give the definitions of mean and variance of $d\Delta$ for process K (e.g., process A in Section 3.2.2) with a consideration of process model uncertainty only. Following the definition of posterior mean and variance of Bayesian model averaging (e.g., Equations (4) and (5) in Ye et al. (2004)), the mean and variance of $d\Delta$ for process K are defined as

$$E_K(d\Delta) = E_{M_{\sim K}} E_{T_{M_K}}(d\Delta | M_{\sim K}), \quad (3.3)$$

$$V_K(d\Delta) = E_{M_{\sim K}} V_{T_{M_K}}(d\Delta | M_{\sim K}) + V_{M_{\sim K}} E_{T_{M_K}}(d\Delta | M_{\sim K}), \quad (3.4)$$

where $\mathbf{M}_{\sim K}$ is the set of multiple process model combinations that represent all processes but K , i.e., $\sim K$ (e.g., process B in Section 3.2.2), \mathbf{M}_K is the set of multiple process models that represent process K , and T_{M_K} is the set of process model transitions within process K , i.e., $T_{M_K} = \{M_{K_i} \rightarrow M_{K_j}\}$ where $i, j=1, 2, \dots, N_{M_K}$ with N_{M_K} being the number of process models that represent process K . A process with small mean and small variance is considered to be a non-influential process.

The rationale behind Equation (3.2) is that if the model output changes substantially when a process's representation changes from M_{K_i} to M_{K_j} , then this process is considered to have significant influence on the model output. Since there are multiple transitions within process K , it is practically sensible to use the average $E_{T_{M_K}}(d\Delta | M_{\sim K})$ of $d\Delta$ over all possible transitions. Since the average is for a combination, $M_{\sim K}$, of the process models for all the processes but process K , it is necessary to evaluate the average, $E_{M_{\sim K}} E_{T_{M_K}}(d\Delta | M_{\sim K})$, over all the combinations. The mean, $E_K(d\Delta)$, of the output difference for process K measures the overall influence of process K through transitions between any two of the process models.

The variance, $V_K(d\Delta)$, of the output difference defined in Equation (3.4) measures to what extent the output difference spreads out due to nonlinear effect of the process models and/or interaction effect between process K and other processes. The nonlinear effect is reflected by the $V_{T_{M_K}}(d\Delta | M_{\sim K})$ term, in that $d\Delta$ is large under a transition between one process model to another process model, if the process models are nonlinear. The $E_{M_{\sim K}} V_{T_{M_K}}(d\Delta | M_{\sim K})$ term measures the average nonlinear effect over model set $\mathbf{M}_{\sim K}$. The interaction effect is reflected in the $V_{M_{\sim K}} E_{T_{M_K}}(d\Delta | M_{\sim K})$ term, in that the variance $V_{M_{\sim K}}$ is large when $E_{T_{M_K}}(d\Delta | M_{\sim K})$ is evaluated for two models in model set $\mathbf{M}_{\sim K}$, i.e., M_K of process K interacts with $M_{\sim K}$ of all process but K .

Now extend Equations (3.3) and (3.4) to consider random parameters of the process models. Applying the law of total expectation to the two expectations $E_{M_{\sim K}}$ and $E_{T_{M_K}}$ in Equation (3.3) gives

$$\begin{aligned} E_K(d\Delta) &= E_{M_{\sim K}} E_{T_{M_K}}(d\Delta | M_{\sim K}) \\ &= E_{M_{\sim K}} E_{\theta_{\sim K} | M_{\sim K}} E_{T_{M_K}} E_{T_{\theta_{\sim K}} | T_{M_K}}(d\Delta | \theta_{\sim K}, M_{\sim K}, T_{\theta_{\sim K}}, T_{M_K}), \end{aligned} \quad (3.5)$$

where subscript $\theta_{\sim K} | M_{\sim K}$ of $E_{\theta_{\sim K} | M_{\sim K}}$ indicates that the expectation is with respect to random parameter $\theta_{\sim K}$ specific to model $M_{\sim K}$, subscript $T_{\theta_K} | T_{M_K}$ of $E_{T_{\theta_K} | T_{M_K}}$ indicates that the expectation is with respect to the random parameters involved in the parameter transitions, T_{θ_K} , associated with the process model transitions T_{M_K} ; $\theta_{\sim K}$ and T_{θ_K} are a single realization of $\theta_{\sim K}$ and T_{θ_K} , respectively. Taking the process model transition $T_{M_K} = \{M_{A_1} \rightarrow M_{A_2}\}$ as an example, the set of parameter transitions with respect to $M_{A_1} \rightarrow M_{A_2}$ is $T_{\theta_A} = \{\theta_{A_1}^m \rightarrow \theta_{A_2}^n\}$, where $\theta_{A_1}^m$ and $\theta_{A_2}^n$ are two randomly selected parameter realizations in θ_{A_1} and θ_{A_2} . T_{θ_A} includes all possible parameter transitions from parameters of M_{A_1} to parameters of M_{A_2} .

For the variance of $d\Delta$ in Equation (3.3), by first applying the law of the total expectation to $E_{M_{\sim K}}$ and $E_{T_{M_K}}$, we have

$$\begin{aligned} V_K(d\Delta) &= E_{M_{\sim K}} E_{\theta_{\sim K} | M_{\sim K}} V_{T_{M_K}}(d\Delta | \theta_{\sim K}, M_{\sim K}) \\ &\quad + V_{M_{\sim K}} E_{T_{M_K}} E_{T_{\theta_K} | T_{M_K}}(d\Delta | M_{\sim K}, T_{\theta_K}, T_{M_K}). \end{aligned} \quad (3.6)$$

According to the definition of the variance, the first term at the right-hand side of Equation (3.5) can be rewritten as

$$\begin{aligned} &E_{M_{\sim K}} E_{\theta_{\sim K} | M_{\sim K}} V_{T_{M_K}}(d\Delta | \theta_{\sim K}, M_{\sim K}) \\ &= E_{M_{\sim K}} E_{\theta_{\sim K} | M_{\sim K}} \left(E_{T_{M_K}}(d\Delta | \theta_{\sim K}, M_{\sim K})^2 - \left(E_{T_{M_K}}(d\Delta | \theta_{\sim K}, M_{\sim K}) \right)^2 \right) . \quad (3.7) \\ &= E_{M_{\sim K}} E_{\theta_{\sim K} | M_{\sim K}} E_{T_{M_K}}(d\Delta | \theta_{\sim K}, M_{\sim K})^2 - E_{M_{\sim K}} E_{\theta_{\sim K} | M_{\sim K}} \left(E_{T_{M_K}}(d\Delta | \theta_{\sim K}, M_{\sim K}) \right)^2 \end{aligned}$$

Subsequently, applying the law of total expectation to $E_{T_{M_K}}$, Equation (3.6) becomes

$$\begin{aligned} &E_{M_{\sim K}} E_{\theta_{\sim K} | M_{\sim K}} V_{T_{M_K}}(d\Delta | \theta_{\sim K}, M_{\sim K}) \\ &= E_{M_{\sim K}} E_{\theta_{\sim K} | M_{\sim K}} E_{T_{M_K}} E_{T_{\theta_K} | T_{M_K}}(d\Delta | \theta_{\sim K}, M_{\sim K}, T_{\theta_K}, T_{M_K})^2 . \quad (3.8) \\ &\quad - E_{M_{\sim K}} E_{\theta_{\sim K} | M_{\sim K}} \left(E_{T_{M_K}} E_{T_{\theta_K} | T_{M_K}}(d\Delta | \theta_{\sim K}, M_{\sim K}, T_{\theta_K}, T_{M_K}) \right)^2 \end{aligned}$$

Similarly, the second term at the right-hand side of Equation (3.5) can be rewritten as

$$\begin{aligned}
& V_{M_{\sim K}} E_{T_{M_K}} E_{T_{\theta_K} | T_{M_K}} (d\Delta | M_{\sim K}, T_{\theta_K}, T_{M_K}) \\
&= E_{M_{\sim K}} \left(E_{T_{M_K}} E_{T_{\theta_K} | T_{M_K}} (d\Delta | M_{\sim K}, T_{\theta_K}, T_{M_K}) \right)^2 \\
&\quad - \left(E_{M_{\sim K}} E_{T_{M_K}} E_{T_{\theta_K} | T_{M_K}} (d\Delta | M_{\sim K}, T_{\theta_K}, T_{M_K}) \right)^2 . \\
&= E_{M_{\sim K}} E_{\theta_{\sim K} | M_{\sim K}} \left(E_{T_{M_K}} E_{T_{\theta_K} | T_{M_K}} (d\Delta | \theta_{\sim K}, M_{\sim K}, T_{\theta_K}, T_{M_K}) \right)^2 \\
&\quad - \left(E_{M_{\sim K}} E_{\theta_{\sim K} | M_{\sim K}} E_{T_{M_K}} E_{T_{\theta_K} | T_{M_K}} (d\Delta | \theta_{\sim K}, M_{\sim K}, T_{\theta_K}, T_{M_K}) \right)^2
\end{aligned} \tag{3.9}$$

Substituting Equations (3.8) and (3.9) into Equation (3.5) leads to

$$\begin{aligned}
V_K(d\Delta | K) &= E_{M_{\sim K}} E_{\theta_{\sim K} | M_{\sim K}} E_{T_{M_K}} E_{T_{\theta_K} | T_{M_K}} (d\Delta | \theta_{\sim K}, M_{\sim K}, T_{\theta_K}, T_{M_K})^2 \\
&\quad - \left(E_{M_{\sim K}} E_{\theta_{\sim K} | M_{\sim K}} E_{T_{M_K}} E_{T_{\theta_K} | T_{M_K}} (d\Delta | \theta_{\sim K}, M_{\sim K}, T_{\theta_K}, T_{M_K}) \right)^2 .
\end{aligned} \tag{3.10}$$

When process model uncertainty does not exist (i.e., each process is represented by only one process model), Equations (3.5) and (3.6) becomes

$$E_K(d\Delta) = E_{\theta_{\sim K}} E_{T_{\theta_K}} (d\Delta | \theta_{\sim K}, T_{\theta_K}), \tag{3.11}$$

$$V_K(d\Delta) = E_{\theta_{\sim K}} E_{T_{\theta_K}} (d\Delta | \theta_{\sim K}, T_{\theta_K})^2 - \left(E_{\theta_{\sim K}} E_{T_{\theta_K}} (d\Delta | \theta_{\sim K}, T_{\theta_K}) \right)^2. \tag{3.12}$$

These are the similar as the calculation of mean and variance of the elementary effects in the Morris screening method, and can be used to screen non-influential parameters for a single system model.

For either a single system model or multiple system models, $E_K(d\Delta)$ and $V_K(d\Delta)$ are used in the same way as that the mean and standard deviation (μ^* and σ) of EE are used. The $E_K(d\Delta)$ and $V_K(d\Delta)$ of all processes under consideration are plotted in one figure, and a process is more influential than other processes if its $E(d\Delta)$ and $V(d\Delta)$ values are larger than those of other processes. However, we do not suggest using MMADS to rank processes or identify influential processes, but to screen non-influential processes, because the MMADS method is qualitative in nature for process identification. A quantitative process ranking can be done by using more rigorous (but more computationally expensive) approaches, one of which is the total-effective process sensitivity index developed by in Chapter 2.

§3.3 Numerical Implementation

3.3.1 Model-averaging and Monte Carlo Integration

The expectations with respect to the process models ($E_{M_{\sim K}}$) and with respect to process model transitions ($E_{T_{M_K}}$) in Equation (3.5) and (3.10) can be evaluated using the model averaging method via

$$E_{M_{\sim K}} E_{\theta_{\sim K}|M_{\sim K}} (\bullet) = \sum E_{\theta_{\sim K}|M_{\sim K}} (\bullet) P(M_{\sim K}), \quad (3.13)$$

$$E_{T_{M_K}} E_{T_{\theta_K}|T_{M_K}} (\bullet) = \sum E_{T_{\theta_K}|T_{M_K}} (\bullet) P(T_{M_K}), \quad (3.14)$$

where the dot (\bullet) denotes the quantities in Equations. (3.5) and (3.10) (e.g., $E_{T_{M_K}} E_{T_{\theta_K}|T_{M_K}} (d\Delta | \theta_{\sim K}, M_{\sim K}, T_{\theta_K}, T_{M_K})$ in Equation (3.5)), $P(M_{\sim K})$ is the model weight of a combination of the models for all the processes but process K , $P(T_{M_K})$ is the probability of the transition from one process model to another process model.

Evaluating $P(M_{\sim K})$ and $P(T_{M_K})$ requires that the weights, $P(M_K)$, of process models for process K satisfying $\sum P(M_K) = 1$. To evaluate $P(M_{\sim K})$ for a combination of process models, it is assumed that selecting one process model of a process is independent to selecting one process model of another process. With this assumption, $P(M_{\sim K})$ can be evaluated as $P(M_{\sim K}) = \prod_{i=1}^{N_{\sim K}} P(M_{\sim K,i})$, where $N_{\sim K}$ is the number of processes minus one (i.e., the number of all processes but process K) and $P(M_{\sim K,i})$ is the model weight of a process model. Thinking a system with three processes A , B , and C , each process has two alternative models (i.e., A_1, A_2, B_1, B_2, C_1 , and C_2), and the process models have the following weights, i.e., $P(A_1) = P(A_2) = 0.5$, $P(B_1) = 0.7$, $P(B_2) = 0.3$, $P(C_1) = 0.6$, and $P(C_2) = 0.4$. The combination, B_1C_1 , of process models B_1 and C_1 has the probability of $P(B_1C_1) = P(B_1) \times P(C_1) = 0.7 \times 0.6 = 0.42$. $P(T_{M_K})$ of the process model transition $M_{K_i} \rightarrow M_{K_j}$ can be evaluated as $P(T_{M_K}) = P(M_{K_i}) \times P(M_{K_j})$, where $P(M_{K_i})$ and $P(M_{K_j})$ are the process model weights of M_{K_i} and M_{K_j} , respectively. This calculation implies that each process model transitions has its own probability, depending on probability of each process model. Using process B and its process model probabilities in the example above, the probability for transition $M_{B_1} \rightarrow M_{B_1}$ is $0.7 \times 0.7 = 0.49$, and the probability for the transition $M_{B_1} \rightarrow M_{B_2}$ is $0.7 \times 0.3 = 0.21$. The process model weights can be either prior probability determined based on prior information or posterior

probability determined by using both prior information and observations used for model calibration and uncertainty quantification. Prior weights are used in this study, and using posterior weights is discussed in Dai et al. (2017a).

The expectations ($E_{\theta_{\sim K} | M_{\sim K}}(\bullet)$ and $E_{T_{\theta_K} | T_{M_K}}(\bullet)$) with respect to the process model parameters and parameter transitions can be evaluated using Monte Carlo methods. For the convenience of discussion, we use the same number, n , of parameter realizations for each process model combination $M_{\sim K}$ and process model M_K . To evaluate the mean and variance of $d\Delta$ using Eqs. (4) and (9), a total $(N_{M_{\sim K}} \times n) \times (N_{M_K}^2 \times n^2)$ numbers of $d\Delta$ are needed, where N_{M_K} and $N_{M_{\sim K}}$ are the number of models of process K and the number of combinations of the models for all process but K , respectively; the square terms are for the parameter transitions and process model transitions. To obtain $(N_{M_{\sim K}} \times n) \times (N_{M_K}^2 \times n^2)$ numbers of $d\Delta$ requires a total $(N_{M_{\sim K}} \times n) \times (N_{M_K} \times n)$ numbers of model executions. To reduce computational cost, the n parameter realizations can be generated using the Latin Hypercube Sampling (LHS) method so that a small number of realizations can cover the entire parameter space. The procedure of generating the realizations of $\theta_{\sim K} | M_{\sim K}$ and $\theta_K | M_K$ and the procedure of computing $d\Delta | (\theta_K, M_K, \theta_{\sim K}, M_{\sim K})$ and $d\Delta | (\theta_{\sim K}, M_{\sim K}, T_{\theta_K}, T_{M_K})$ are as follows:

Steps 1: Equally divide the cumulative distribution of each parameter into n strata, and sample n parameter values from the n strata using the LHS scheme. This results in a sample matrix with the dimension of $n \times n_p$, where n_p is the number of parameters involved in the multi-models.

Step 2: For each process model combination $M_{\sim K}$, combine the columns of parameter values (from the parameter matrix generated in Step 1) for parameters associated with $M_{\sim K}$ to yield the parameter set $\theta_{\sim K} | M_{\sim K}$.

Step 3: For each process model M_K , combine the columns of parameter values (from the parameter matrix generated in Step 1) for parameters associated with M_K to yield the parameter set $\theta_K | M_K$.

Step 4: Loop over the parameter sets $\theta_{\sim K} | M_{\sim K}$ and $\theta_K | M_K$, compute $d\Delta | (\theta_K, M_K, \theta_{\sim K}, M_{\sim K})$.

Step 5: Loop over the process model transitions and parameter transitions to compute $d\Delta | (\theta_{\sim K}, M_{\sim K}, T_{\theta_K}, T_{M_K})$.

Figure 3-2 shows the pseudo code to compute the mean and variance of $d\Delta$ based on Equations (3.5) and (3.10) and the parameter sampling procedure described above.

```

Use LHS method to generate the sampling matrix of all parameters
Loop [1] over model combinations  $M_{\sim K}$  for process  $\sim K$  in  $\mathbf{M}_{\sim K}$ 
    Combine parameter values for parameters associate with  $M_{\sim K}$  to yield  $\boldsymbol{\theta}_{\sim K} | M_{\sim K}$ 
    Loop [2] over parameter realizations  $\boldsymbol{\theta}_{\sim K} | M_{\sim K}$ 
        Loop [3] over process model  $M_K$  for process  $K$  in  $\mathbf{M}_K$ 
            Combine parameter values for parameters associated with  $M_K$  to yield  $\boldsymbol{\theta}_K | M_K$ 
            Loop [4] over parameter realizations  $\boldsymbol{\theta}_K | M_K$ 
                Compute  $\Delta | \boldsymbol{\theta}_{\sim K}, M_{\sim K}, \boldsymbol{\theta}_K, M_K$ 
            End loop [4]
        End loop [3]
        Loop [5] over process model transitions in  $T_{M_K}$ 
            Loop [6] over parameter realizations  $T_{\boldsymbol{\theta}_K | T_{M_K}}$  associated with  $T_{M_K}$ 
                Compute  $d\Delta | \boldsymbol{\theta}_{\sim K}, M_{\sim K}, T_{\boldsymbol{\theta}_{\sim K}}, T_{M_K}$  and  $(d\Delta | \boldsymbol{\theta}_{\sim K}, M_{\sim K}, T_{\boldsymbol{\theta}_{\sim K}}, T_{M_K})^2$ 
            End Loop [6]
            Compute  $E_{T_{\boldsymbol{\theta}_K | T_{M_K}}} (d\Delta | \boldsymbol{\theta}_{\sim K}, M_{\sim K}, T_{\boldsymbol{\theta}_{\sim K}}, T_{M_K})$  and  $E_{T_{\boldsymbol{\theta}_K | T_{M_K}}} (d\Delta | \boldsymbol{\theta}_{\sim K}, M_{\sim K}, T_{\boldsymbol{\theta}_{\sim K}}, T_{M_K})^2$ 
        End Loop [5]
        Compute  $E_{T_{M_K}} E_{T_{\boldsymbol{\theta}_K | T_{M_K}}} (d\Delta | \boldsymbol{\theta}_{\sim K}, M_{\sim K}, T_{\boldsymbol{\theta}_{\sim K}}, T_{M_K})$  and
         $E_{T_{M_K}} E_{T_{\boldsymbol{\theta}_K | T_{M_K}}} (d\Delta | \boldsymbol{\theta}_{\sim K}, M_{\sim K}, T_{\boldsymbol{\theta}_{\sim K}}, T_{M_K})^2$  using model averaging
    End Loop [2]
    Compute  $E_{\boldsymbol{\theta}_{\sim K} | M_{\sim K}} E_{T_{M_K}} E_{T_{\boldsymbol{\theta}_K | T_{M_K}}} (d\Delta | \boldsymbol{\theta}_{\sim K}, M_{\sim K}, T_{\boldsymbol{\theta}_{\sim K}}, T_{M_K})$  and
     $E_{\boldsymbol{\theta}_{\sim K} | M_{\sim K}} E_{T_{M_K}} E_{T_{\boldsymbol{\theta}_K | T_{M_K}}} (d\Delta | \boldsymbol{\theta}_{\sim K}, M_{\sim K}, T_{\boldsymbol{\theta}_{\sim K}}, T_{M_K})^2$ 
End Loop [1]
Compute  $E_{\mathbf{M}_{\sim K}} E_{\boldsymbol{\theta}_{\sim K} | M_{\sim K}} E_{T_{M_K}} E_{T_{\boldsymbol{\theta}_K | T_{M_K}}} (d\Delta | \boldsymbol{\theta}_{\sim K}, M_{\sim K}, T_{\boldsymbol{\theta}_{\sim K}}, T_{M_K})$  and
 $E_{\mathbf{M}_{\sim K}} E_{\boldsymbol{\theta}_{\sim K} | M_{\sim K}} E_{T_{M_K}} E_{T_{\boldsymbol{\theta}_K | T_{M_K}}} (d\Delta | \boldsymbol{\theta}_{\sim K}, M_{\sim K}, T_{\boldsymbol{\theta}_{\sim K}}, T_{M_K})^2$  using model averaging

```

图 3-2 基于拉丁-超立方采样方法计算过程 K 的两个过程敏感性指标的伪代码
Figure 3-2 Pseudo codes for evaluating the two sensitivity measures for process K using LHS.

3.3.2 Reduce the Computational Cost by Using Binning Method

As discussed in Section 3.3, the number of model execution based on the pseudo code shown in Figure 3-2 is $(N_{M_{\sim K}} \times n) \times (N_{M_K} \times n)$, where the n^2 is caused by the nested loops [2] and [4] for parameters $\boldsymbol{\theta}_{\sim K} | M_{\sim K}$ and $\boldsymbol{\theta}_K | M_K$, respectively. One way to reduce the computational cost of MMADS is to break the two nested loops, and this can be done by using the binning method that has been used in our previous studies of (Dai et al. 2017b). Taking $E(d\Delta | K) = E_{\mathbf{M}_{\sim K}} E_{\boldsymbol{\theta}_{\sim K} | M_{\sim K}} E_{T_{M_K}} E_{T_{\boldsymbol{\theta}_K | T_{M_K}}} (d\Delta | \boldsymbol{\theta}_{\sim K}, M_{\sim K}, T_{\boldsymbol{\theta}_K}, T_{M_K})$ of Equation (3.5) as an example, since the $E_{\boldsymbol{\theta}_{\sim K} | M_{\sim K}}$ term can be computed as $E_{\boldsymbol{\theta}_{\sim K} | M_{\sim K}} = \sum_{bin} E_{\boldsymbol{\theta}_{\sim K}^{bin} | M_{\sim K}}$, for the binning method, replacing $E_{T_{\boldsymbol{\theta}_K | T_{M_K}}} (d\Delta | \boldsymbol{\theta}_{\sim K}, M_{\sim K}, T_{\boldsymbol{\theta}_K}, T_{M_K})$ with $E_{T_{\boldsymbol{\theta}_K | T_{M_K}}} (d\Delta | \boldsymbol{\theta}_{\sim K}^{bin}, M_{\sim K}, T_{\boldsymbol{\theta}_K}, T_{M_K})$ can theoretically

achieve the same accuracy as the original calculation of the pseudo code does. In other words, we have

$$\begin{aligned} E_K(d\Delta) &= E_{M_{\sim K}} E_{\theta_{\sim K}|M_{\sim K}} E_{T_{M_K}} E_{T_{\theta_K}|T_{M_K}}(d\Delta|\theta_{\sim K}, M_{\sim K}, T_{\theta_K}, T_{M_K}) \\ &= E_{M_{\sim K}} E_{\theta_{\sim K}^{bin}|M_{\sim K}} E_{T_{M_K}} E_{T_{\theta_K}|T_{M_K}}(d\Delta|\theta_{\sim K}^{bin}, M_{\sim K}, T_{\theta_K}, T_{M_K}), \end{aligned} \quad (3.15)$$

As a result, the nested two loops can be replaced by only one loop over the number of bins. The $E_{T_{\theta_K}|T_{M_K}}(d\Delta|\theta_{\sim K}, M_{\sim K}, T_{\theta_K}, T_{M_K})$ term can be evaluated in the following steps:

- (1) Generate m parameter realizations of $\theta_{\sim K}$ for all $M_{\sim K}$ in $\mathbf{M}_{\sim K}$ and θ_K for all M_K in \mathbf{M}_K , and evaluate $\Delta|(\theta_{\sim K}, M_{\sim K}, \theta_K, M_K)$ for the realizations;
- (2) Separate the $\theta_{\sim K}|M_{\sim K}$ realization into multiple bins $\theta_{\sim K}^{bin}|M_{\sim K}$ by a hyper-cubing method that is discussed below, and then loop over the bins;
- (3) For each bin, first count the system model outputs $\Delta|(\theta_{\sim K}, M_{\sim K}, \theta_K, M_K)$ in the bin, then use the outputs to computer the output differences between parameter transitions for each model transitions, and ultimately evaluate $E_{T_{\theta_K}|T_{M_K}}(d\Delta|\theta_{\sim K}^{bin}, M_{\sim K}, T_{\theta_K}, T_{M_K})$ over all parameter transitions.

Among many methods to form bins for step 2 above, we use the hyper-cubing method. The range of a parameter is divided into p equal intervals. If the parameter follows a uniform distribution, the p level intervals are obtained simply by dividing the parameter range into p equal intervals. Otherwise, the intervals are obtained by dividing the parameter's cumulative distribution function into p equal intervals. The total number of bins is thus D^p , where D is the number of parameters associated with $M_{\sim K}$. The pseudo code for evaluating $E(d\Delta)$ and $V(d\Delta)$ using the binning method is given in Fig. 5. The number of model executions needed by the binning method is $N_{M_{\sim K}} \times N_{M_K} \times m$ needed in step 1 above and implemented in loops [1] – [3] of the pseudo code, where m is the number of $\theta_{\sim K}$ and θ_K realizations. Loops [4] – [6] replace loops [1] – [4] in the pseudo code shown in Figure 3-3.

```

Loop [1] over model combinations  $M_{\sim K}$  for process  $\sim K$  in  $\mathbf{M}_{\sim K}$ 
    Loop [2] over process model  $M_K$  for process  $K$  in  $\mathbf{M}_K$ 
        Loop [3] over parameter realizations  $\boldsymbol{\theta}_{\sim K} | M_{\sim K}$  and  $\boldsymbol{\theta}_K | M_K$ 
            Compute  $\Delta | \boldsymbol{\theta}_{\sim K}, M_{\sim K}, \boldsymbol{\theta}_K, M_K$ 
        End loop [3]
    End Loop [2]
End loop [1]

Loop [4] over model combinations  $M_{\sim K}$  for process  $\sim K$  in  $\mathbf{M}_{\sim K}$ 
    Loop [5] over parameter combination bins  $\boldsymbol{\theta}_{\sim K}^{bin} | M_{\sim K}$ 
        Loop [6] over process model transition  $T_{M_K}$ 
            Compute  $E_{T_{\boldsymbol{\theta}_{\sim K}|M_K}}(d\Delta | T_{M_K}, T_{\boldsymbol{\theta}_{\sim K}}, M_{\sim K}, \boldsymbol{\theta}_{\sim K}^{bin})$  and
             $E_{T_{\boldsymbol{\theta}_{\sim K}|M_K}}(d\Delta | T_{M_K}, T_{\boldsymbol{\theta}_{\sim K}}, M_{\sim K}, \boldsymbol{\theta}_{\sim K}^{bin})^2$  for all  $T_{\boldsymbol{\theta}_{\sim K}}$  of each bin
        End loop [6]
        Compute  $E_{T_{M_K}} E_{T_{\boldsymbol{\theta}_{\sim K}|M_K}}(d\Delta | T_{M_K}, T_{\boldsymbol{\theta}_{\sim K}}, M_{\sim K}, \boldsymbol{\theta}_{\sim K}^{bin})$  and
         $E_{T_{M_K}} E_{T_{\boldsymbol{\theta}_{\sim K}|M_K}}(d\Delta | T_{M_K}, T_{\boldsymbol{\theta}_{\sim K}}, M_{\sim K}, \boldsymbol{\theta}_{\sim K}^{bin})^2$  using model averaging
    End Loop [5]
    Compute  $E_{\boldsymbol{\theta}_{\sim K}^{bin}|M_{\sim K}} E_{T_{M_K}} E_{T_{\boldsymbol{\theta}_{\sim K}|M_K}}(d\Delta | T_{M_K}, T_{\boldsymbol{\theta}_{\sim K}}, M_{\sim K}, \boldsymbol{\theta}_{\sim K}^{bin})$  and
     $E_{\boldsymbol{\theta}_{\sim K}^{bin}|M_{\sim K}} E_{T_{M_K}} E_{T_{\boldsymbol{\theta}_{\sim K}|M_K}}(d\Delta | T_{M_K}, T_{\boldsymbol{\theta}_{\sim K}}, M_{\sim K}, \boldsymbol{\theta}_{\sim K}^{bin})^2$ 
End Loop [4]
Compute  $E_{M_{\sim K}} E_{\boldsymbol{\theta}_{\sim K}^{bin}|M_{\sim K}} E_{T_{M_K}} E_{T_{\boldsymbol{\theta}_{\sim K}|M_K}}(d\Delta | T_{M_K}, T_{\boldsymbol{\theta}_{\sim K}}, M_{\sim K}, \boldsymbol{\theta}_{\sim K}^{bin})$  and
 $E_{M_{\sim K}} E_{\boldsymbol{\theta}_{\sim K}^{bin}|M_{\sim K}} E_{T_{M_K}} E_{T_{\boldsymbol{\theta}_{\sim K}|M_K}}(d\Delta | T_{M_K}, T_{\boldsymbol{\theta}_{\sim K}}, M_{\sim K}, \boldsymbol{\theta}_{\sim K}^{bin})^2$  using model averaging

```

图 3-3 采用高效算法 binning 方法计算过程 K 的两个过程敏感性指标的伪代码
Figure 3-3 Pseudo codes for evaluating the two sensitivity measures for process K using binning method.

§3.4 A Hypothetical Example

To evaluate the performance of MMADS proposed above, a hypothetical example is used. This groundwater flow modeling experiment uses the same model in Section 2.5.1. Three processes, namely, recharge, geology and snowmelt processes are considered, each of which has two alternative process models with associated uncertainty parameters. The goal of this model settings is to identify the controlling processes, specifically, the influential processes with the consideration of both model uncertainty and parametric uncertainty.

3.4.1 Identifying the Controlling Process for Single-Model

Table 3-1 lists the $E(d\Delta)$ and $V(d\Delta)$ values evaluated for the recharge, geology, and snowmelt processes of the individual system models with consideration of parametric uncertainty of the models. If a process model has more than one parameter (e.g., K_1 and K_2 associated with process model G_2 , and f_2 and r associate with process model M_2), the indices are evaluated for the grouped parameters. Specifically speaking, the θ_K term in Equations (3.5) and (3.10) includes two parameters. For each system model, since $E(d\Delta)$ and $V(d\Delta)$ are evaluated for all parameters of each process, $E(d\Delta)$ and $V(d\Delta)$ measure influence of each process. Taking system model $R_2G_2M_2$ as an example, the mean and variance of parameter b measure influence of the recharge process, those of parameters K_1 and K_2 measure influence of the geology process, and those of parameters f_2 and r measure influence of the snowmelt process. Table 3-1 also lists the total-effect parameter sensitivity S_{Ti} (%) that can be used to quantitatively rank the three processes in terms of their influence within each system model. The corresponding process rank is used as a reference to evaluate the results of MMADS.

Table 3-1 shows that, for each system model, the process rank of MMADS is the same as that given by S_{Ti} , indicating that the MMADS results are reliable. The process rank changes substantially between the system models, and any of the three processes can be ranked as the most influential (or the least influential) process. For example, in system model $R_1G_1M_1$, the recharge process is identified as the least influential process and the snowmelt process as the most influential process, whereas it is the opposite case for system model $R_2G_2M_2$. This is also observed in Figure 3-4 that plots the three processes in three colors (recharge in red, geology in green, and snowmelt in blue). The open symbols of the eight individual system models are mixed, and do not reveal a pattern to indicate process influence under process model uncertainty. It is therefore necessary to use MMADS for identifying non-influential processes for all the system models to address process model uncertainty.

表 3-1 单系统模型条件下一维河间地块模型由于参数取值变化引起模型输出差值的均值和方差和多系统模型条件下考虑模型不确定性的三个水文过程模型及参数取值变化引起模型输出差值的均值和方差。计算结果采用拉丁超立方采样方法获得，样本量 $n = 5000$ 。 S_{Ti} 表示采用 $10,000 \times (k + 2)$ 次模拟的 Sobol 的总效应参数敏感性指标，其中 k 为系统模型中的参数个数。该表也列出了采用 $n=20$ 的拉丁超立方采样方法计算结果和本文提出的 binning 法所获得的结果。

Table 3-1 Numerical mean and variance of the output difference of parameters under individual system model and those of the three processes considering model uncertainty of the groundwater flow model using LHS with parameter realization $n = 5000$. S_{Ti} denotes Sobol's total-effect sensitivity index calculated numerically by using $10,000 \times (k + 2)$ simulation runs, where k is the number of parameters in the system model. Note that the unit of mean is $\text{m}^2 \cdot \text{d}^{-1}$ while the unit of variance is $[\text{m}^2 \cdot \text{d}^{-1}]^2$. The results of the two sensitivity measures of the three processes using LHS with $n=20$ and binning method with $n=100$ are also listed.

Considering parametric uncertainty but not process model uncertainty												
Model	$R_1G_1M_1$			$R_1G_1M_2$			$R_1G_2M_1$			$R_1G_2M_2$		
Parameter	a	K	f_1	a	K	$f_2\&r$	a	$K_1\&K_2$	f_1	a	$K_1\&K_2$	$f_2\&r$
S_{Ti}	12	37	66	15	56	38	34	16	55	36	39	28
Rank	3	2	1	3	1	2	2	3	1	2	1	3
Mean	43	56	86	43	70	60	53	35	66	53	54	46
Variance	10	53	76	10	58	37	17	8	30	17	19	14
Model	$R_2G_1M_1$			$R_2G_1M_2$			$R_2G_2M_1$			$R_2G_2M_2$		
Parameter	b	K	f_1	b	K	f_1	b	$K_1\&K_2$	f_1	b	$K_1\&K_2$	$f_2\&r$
S_{Ti}	22	33	59	26	48	33	50	14	40	50	32	20
Rank	2	3	1	2	1	3	1	3	2	1	2	3
Mean	62	56	86	62	70	60	77	38	66	77	59	46
Variance	19	53	76	19	58	36	31	11	30	31	23	14
Considering parametric uncertainty and process model uncertainty												
Process	R (Recharge)				G (Geology)				M (Snowmelt)			
PS_{TK}	14.67				21.68				78.54			
Rank	3				2				1			
Mean	61.9	60.8 ^a	65.5 ^b		66.2	65.8 ^a	68.9 ^b		130.1	125.8 ^a	136.5 ^b	
Variance	22.0	21.1 ^a	33.6 ^b		43.3	37.9 ^a	40.9 ^b		146.9	129.7 ^a	164.8 ^b	

For the individual system models, the MMADS results can reflect process interactions. This is made clear by examining the $E(d\Delta)$ and $V(d\Delta)$ values of $R_1G_1M_1$ and $R_2G_1M_1$, which have different recharge models but the same geology and snowmelt models. For the two models with homogeneous hydraulic conductivity, based on Equation (2.49), the groundwater discharge per unit width at $x_0 = 7,000$ m (which equals to $0.7L$) is

$$q(x_0) = K \frac{h_1^2 - h_2^2}{2L} + 0.2wL, \quad (3.16)$$

This equation shows that w does not interact with K or h_2 , indicating that the recharge process does not interact with the geology or snowmelt process. As a result, between $R_1G_1M_1$ and $R_2G_1M_1$, the $E(d\Delta)$ and $V(d\Delta)$ values of a (the recharge model parameter) change, but those of K (the geology model parameter) and f_1 (the snowmelt model parameter) do not change. This is not surprising in the context of MMADS calculation. To evaluate the output difference ($d\Delta$) caused by the variation of parameter K of the geology process, parameter a or b of the recharge process (Equation (2.43)) and parameter f_1 of the snowmelt process (Equation (2.47)) are fixed. Since the recharge and geology processes do not interact, the second term, $0.2wL$, in Equation (3.15) does not affect $d\Delta$ due to change of K , which means that $d\Delta$ is not affected by parameter a or b . Therefore, the $d\Delta$ values for K are the same for $R_1G_1M_1$ and $R_2G_1M_1$. The process interaction is reflected in the $E(d\Delta)$ and $V(d\Delta)$ values of $R_1G_1M_1$ and $R_1G_1M_2$. These values of K and f_1 for $R_1G_1M_1$ are different from those of K and $f_2&r$ for $R_1G_1M_2$, because the interaction between K and f_1 is different from the interaction between K and $f_2&r$, as indicated by Equation (3.15).

3.4.2 Identifying the Controlling Process for Multi-Model

Table 3-1 lists the $E(d\Delta)$ and $V(d\Delta)$ values of the recharge, geology, and snowmelt processes for all the eight system models with consideration of both process model and parametric uncertainty. The MMADS method identifies the snowmelt process as the most influential one, followed by the geology process, and then the recharge process. This is shown clearly in Figure 3-4 that plots $E(d\Delta)$ and $V(d\Delta)$ for the three processes using filled symbols in three colors (recharge in red, geology in green, and snowmelt in blue). Filled symbols denote the sensitivity measures considering the process model uncertainty. Open symbols in each subplot denote the sensitivity measures of the eight individual system models only consider parametric uncertainty. Note some open symbols are overlapped as the mean and variance are the same (Table 3-1). The snowmelt process has the largest $E(d\Delta)$ and $V(d\Delta)$ values, substantially larger than those of the geology and recharge process. This may be due to the nonlinear effect of the snowmelt process and the interaction between the snowmelt and geology processes discussed above (reflected by the h_2^2 term in Equations (2.48) or (2.49)). Due to the qualitative nature of MMADS, using it to

explain the nonlinear effect and process interactions is not straightforward.

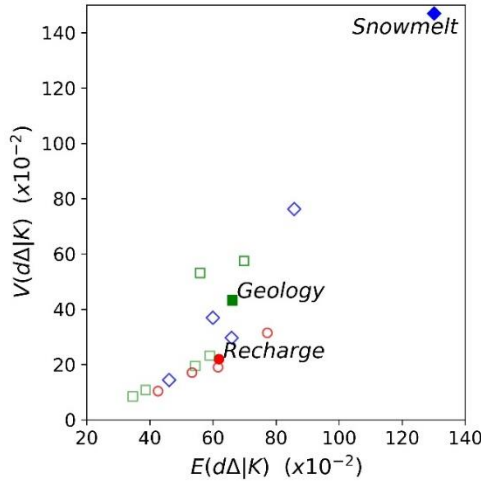


图 3-4 一维河间地块模型三个水文过程输出差值的均值与方差。不同的颜色和符号代表了不同的水文过程。

Figure 3-4 The mean vs. variance of the output difference of the three processes for the groundwater flow model. The three processes are marked with different colors and symbols.

The MMADS results shown in Table 3-1 are obtained by using $n = 5,000$ random samples for each parameter. The total number of model executions is $200,000,000 = 2 \times 2 \times 5,000 \times 2 \times 5,000$, which ensures that the Monte Carlo calculation of MMADS converges. The high computational cost is unnecessarily and can be substantially reduced. Table 3-1 shows that the MMADS results are still accurate enough when using $n = 20$, and the corresponding number of model executions is $3,200 = 2 \times 2 \times 20 \times 2 \times 20$, which is computationally affordable to moderate models with the current computational resources.

3.4.3 Computational Cost Analysis

The binning method is applied to the two numerical experiments of Section 3 for computing $E(d\Delta)$ and $V(d\Delta)$ for multiple system models. For the Sobol's G*-function, each of the three parameters, X_1 , X_2 and X_3 , is divided into 5 equal intervals, resulting in $25 = 5^2$ bins for any process model combinations, $M_{\sim K}$, of which the parameter dimension all equals to 2. For the groundwater flow modeling, each of the eight parameters, a , b , K , K_1 , K_2 , f_1 , f_2 , and r is divided into 3 intervals. The number of bins varies for different process model combinations. For example, when $E(d\Delta)$ and $V(d\Delta)$ are calculated for the recharge process, the combinations of the geology and snowmelt process models are G_1M_1 , G_1M_2 , G_2M_1 , and G_2M_2 , and the corresponding numbers of bins

are 3^2 , 3^3 , 3^3 , and 3^4 , respectively. For any system model of the two numerical experiments, we generate $m = 100$ random numbers for the system model parameters. Figure 3-5 shows the number of parameter realizations, which is also the number of system model outputs, falling into the bins for the process model combination $G_I M_I$ of the groundwater flow modeling. Note for the normal (parameter f_1) and lognormal (parameter K) distributions, the tails are cut at quantiles 0.1% and 99.9%. The marginal plots illustrate the probability distributions of the parameters and the histogram of the 100 samples.

Tables 3-1 list the $E(d\Delta)$ and $V(d\Delta)$ values evaluated for the multiple system models of the groundwater flow example by using the binning method. While the results of the binning method are different from those of analytical solutions (for the Sobol' G^* -function) and from those of the numerical solution with a large number (200 millions) of realizations (for the groundwater flow modeling), the results are good enough for ranking the processes and for identifying non-influential processes. The number of model executions of the binning method is $800 = 2 \times 2 \times 2 \times 100$, substantially smaller than the number of $3,200 = 2 \times 2 \times 20 \times 2 \times 20$ needed for the pseudo code shown in Figure 3-2. This reduction of computational cost is attributed to replacing the nested two loops shown in Figure 3-2 by one loop over the number of bins.

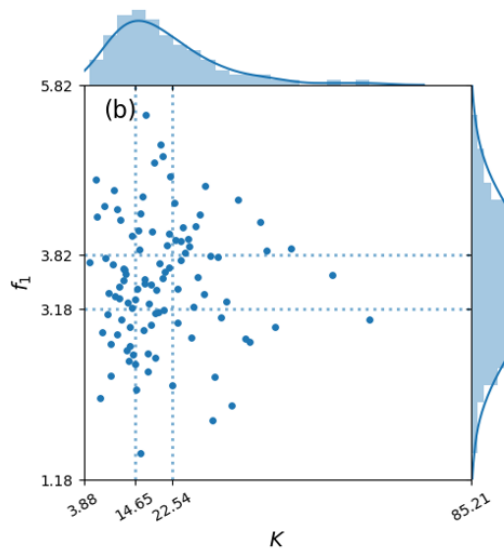


图 3-5 一维河间地块模型考虑均值渗透系数模型 (G_I) 和度-日模型 (M_I) 情况下 100 个参数取值分布图。

Figure 3-5 Parameter distributions falling into the bins of process model combination $G_I M_I$ of the one-dimensional groundwater flow modeling.

It is an open question to determine the number of bins, and the number is determined empirically in this study. For a model with a relatively large number of parameters (i.e.,

the number of bins, D^p , is relatively large), a small number of realizations may result in two problems, i.e., empty bins and thin bins. An empty bin is the one without any parameter samples and thus no model output, Δ . Therefore, the output difference $d\Delta$ cannot be evaluated. A thin bin has a small number of parameter samples and thus a small number of model outputs. While $d\Delta$ can be computed for a thin, its mean and variance may not be statistically meaningful. In an extreme case that there is only one sample in a bin (a very thin bin), the output difference would be zero, i.e., the variation of process K (either process model uncertainty or parameter uncertainty) cannot be captured within this bin. To be on the safe side, one may increase the number of parameter realizations to avoid empty bins and thin bins at the cost of increasing the number of model executions. If the MMADS method is used for process screening, it is acceptable to have empty or thin bins. In the numerical experiment of groundwater flow modeling, with the 100 parameter samples, both empty and thin bins occur, recalling that the number of bins is as large as $81 = 3^4$. Nonetheless, the results of the binning methods are still satisfactory to identify a non-influential process, as shown in Table 3-1. Determining the number of bins and parameter samples is warranted in a future study.

§3.5 Summary

This chapter develops a new multi-model difference-based sensitivity (MMADS) analysis method to identify non-influential system processes with consideration of uncertainty in both process model structures and process model parameters. MMADS is an expansion of the Morris method from the parameter space to the parameter-process-model space, in which a system process may be represented by multiple process models. Differences of a model output are evaluated for the following two situations: (1) within a process model, model parameters change from one set of values to another set of values, and (2) across two process models of the same system process, model parameters change from one set of values specific to one process model to another set of values specific to the other process models. The differences thus consider not only process model variation but also process model parameter variation. The variations are quantified by the mean and variance of the differences, which are evaluated using the model averaging approaches based on weights of process models. A process with small mean and variance is considered to be non-influential. To our knowledge, there does not exist a method like MMADS that explicitly considers uncertainty in process model structures and process

model parameters and integrates the expended Morris method with model averaging methods.

The hypothetical numerical experiment leads to the following conclusions:

(1) Process ranking changes between alternative system models, because different system models have different parameters and/or different process model structures. This manifests the needs of identifying non-influential system processes under process model uncertainty and process model parametric uncertainty. Considering only parametric uncertainty may lead to biased results of identifying non-influential processes.

(2) The MMADS method, similar to the Morris method, plots the mean and variance of the multi-model differences in a mean-variance figure, and the figure can be used to visually identify non-influential system processes.

(3) The hypothetical example of groundwater modeling with three interacting processes shows that the mean and variance of MMADS reflect interactions between geology and snowmelt processes and no interactions between the two processes and the recharge process.

(4) The hypothetical example demonstrates that the MMADS method is computationally efficient, in that the process ranking based on several thousand model executions. The binning method is computationally model efficient, because it only requires several hundred model executions to achieve the same model ranking.

When a small number of model executions are used for the MMADS method, the mean and variance of the multi-model differences may not be accurate, although they can give a meaningful process ranking. In this sense, the results of MMADS are less accurate than the results of the variance-based sensitivity index. The latter method is thus preferred when it is computationally affordable. Similar to the Morris method, MMADS may be used as a screening tool for identifying non-influential processes. One needs to choose appropriate methods of sensitivity analysis meet his/her own research needs, as there is no single sensitivity analysis method for all model types and project needs.

Chapter 4 Application to Arsenic Sorption and Reactive Transport Modeling Based on a Laboratory Experiment

Arsenic (As) sorption and reactive transport in a groundwater system are strongly influenced by various aquifer properties that affect flow paths, transport of chemical species, and spatial distribution of sorption complexes, which further affect overall As removal efficiency and As concentrations in groundwater. Based on a flume experiment conducted by Duan et al. (2020), this chapter develops a 2-D numerical model to simulate As sorption and reactive transport in a sand tank, where three processes, namely, the physical process, the chemical process, and the sorption process are conceptualized. Twelve different system models integrated by two physical process models (i.e., homogenous and heterogeneous permeability fields), two chemical process models (i.e., homogenous and heterogeneous distribution coefficient fields), and three sorption models (i.e., linear equilibrium model, dual first-order kinetic sorption model, and coupled linear equilibrium sorption model with a kinetic model for describing oxidation of Fe(II)-bearing clay minerals) are developed to account for the uncertainty of aquifer heterogeneity in physical and chemical properties and for uncertainty due to our incomplete knowledge of sorption process. Each of the twelve system models also contains different number of uncertainty parameters (i.e., permeability of heterogeneous and homogenous permeability fields). The variance-based process sensitivity analysis method presented in Chapter 2 is employed to investigate the influence of physicochemical aquifer heterogeneity as well as different sorption models on As concentrations at a pumping well, and to identify the most important and influential processes throughout the simulation time.

§4.1 Introduction

Elevated As concentration in groundwater ($\text{As} \geq 10 \mu\text{g/L}$; WHO (2011)) has been reported as a major environmental problem (Bhattacharya et al. 2007, Johannesson et al. 2019, Smedley and Kinniburgh 2002), especially in Asia such as Bangladesh (Huq et al.

2020), India(Shaji et al. 2021), Vietnam (Agusa et al. 2014, Postma et al. 2012), and China (Duan et al. 2015, Duan et al. 2017, Gan et al. 2014b), affecting the health of 94 to 220 million people worldwide (Fendorf et al. 2010a, Podgorski and Berg 2020, Zinke 2020). Since As can strongly absorb to sediment materials such as iron and aluminum oxides and hydroxides, clay minerals, and organic matters (Bissen and Frimmel 2003a, b, Fendorf et al. 2010b, Stollenwerk 2003), an outstanding question for mitigating groundwater arsenic exposure is to identify important hydro-biogeochemical processes that control arsenic sorption and reactive transport in groundwater systems.

In subsurface environments, there are various hydro-biogeochemical processes that strongly influence the arsenic sorption and reactive transport. For example, a heterogenous hydraulic conductivity field can cause a wide range of groundwater travel times and flow patterns which influence transport and distribution of As concentrations. Heterogeneous aquifer mineralogy affects local geochemical conditions and, therefore, the spatial distribution of sorption sites that contribute to the complexation reactions (Jang et al. 2017). Controlled field experiments may be performed to interrogate the mechanisms leading to the As spatial distributions and temporal variations (Nikolaidis et al. 2003, Pi et al. 2017, Voegelin and Hug 2003). Under field conditions, however, it is often difficult to unambiguously identify individual hydro-biogeochemical processes that control arsenic concentration distribution and mobility as such experiments are often costly and time consuming. Numerical simulations provide an alternative approach for cost-effective interrogation of major processes controlling arsenic distribution and variations especially in a strongly coupled hydrobiogeochemical systems. In the last two decades, a large variety of studies have used numerical tools such as MODFLOW with MT3DMS (Sathe and Mahanta 2019), MODFLOW with PHT3D (Jung et al. 2009, Wallis et al. 2010), PHREEQC (Charlet et al. 2007, Stolze et al. 2019, Yu et al. 2018), and PFLOTRAN (Huang et al. 2018) (see the review article of Steefel et al. (2014)). Despite a significant body of knowledge of the fate and transport of arsenic has been acquired by the aforementioned existing methods, one of the main challenges is the proper characterization of the subsurface because geological and sedimentological structure are usually heterogenous and their associated physical-chemical porosities are inherently uncertainty. Previous studies typically neglect these uncertainties and draw conclusions depending on a particular choice of a model conceptualization and model parameter realization thus fail to provide a comprehensive understanding of these factors on arsenic

mobility and migration in the groundwater system (Lu et al. 2015, Ye et al. 2008b).

Based on a laboratory experiment, Duan et al. (2020) built a 3-D reactive transport model to simulate As sorption and reactive transport in a flume under water extraction conditions. They considered nine different cases with either heterogenous or homogenous physio-chemical properties of the aquifer and three different sorption models to explore the effects of physico-chemical aquifer heterogeneity on As migration and retention. Their simulation results indicate that in the early breakthrough curve (0 – 30 d), physical heterogeneity significantly affects the As concentrations at the pumping well due to the preferential flow while after 30 d, both the simple linear equilibrium model and the dual first-order kinetic sorption model tends to overestimate the As concentration. After incorporating Fe(II) oxidation to Fe(III) and its effects on the increased As sorption, the simulation results match well with the laboratory measurements. The study of Duan et al. (2020) highlights the importance of coupled heterogeneity of physio-chemical properties and the oxidation of clay-associated Fe(II) to Fe(III) in the clay matrix domains to the As sorption and reactive transport. However, their study did not consider the parameter uncertainty such as the uncertainty of permeability values or distribution coefficients in the flume system. For example, the local permeability of the sand materials used to pack the tank was estimated using the Kozeny–Carman equation (Male et al. 2020) based on the sand particle size in their study while this method may give lower estimates than the measured permeability (Latief and Fauzi 2012). Besides, the sands cannot be perfectly sorted, and the particle diameters may vary in a small range (Illman et al. 2010). Moreover, it is still unknown to what extent the physico-chemical properties and the utilization of different sorption models would affect the As sorption and reactive transport.

This work extends the study of Duan et al. (2020) by explicitly considering not only the process model uncertainty (e.g., permeability field can be either heterogenous or homogenous) but also the process model parameter uncertainty (e.g., the permeability values under both heterogenous and homogenous permeability field can be also random) to identify the controlling processes to As sorption and reactive transport in the flume system. We conceptualized the three processes, namely, the physical process, the chemical process, and the sorption process in the models. A total of $12 = 2 \times 2 \times 3$ individual system models were considered, corresponding to the two physical process models (i.e., heterogenous and homogenous permeability field), two chemical process models (i.e., the heterogenous and homogenous distribution coefficient field), and three

sorption process models (i.e., the simple linear equilibrium model, the dual first-order kinetic sorption mode and the coupled linear equilibrium sorption model with a kinetic model for describing the oxidation of Fe(II)-bearing clay minerals), and each of the twelve models contains different number of uncertainty parameters. Using the variance-based process sensitivity analysis method with efficient design proposed in Chapter 2, we quantify the relative importance and influence of the three processes to arsenic concentrations at the pumping wells under individual system models as well as multiple system models.

§4.2 Arsenic Sorption and Reactive Transport Model

4.2.1 Physical Model Based on a Laboratory Experiment

Based on the observed hydrogeological conditions in a high As groundwater field site at Jianghan Plain (Gan et al. 2014c, Yang et al., 2020), a synthetic heterogeneous aquifer was constructed in a sand tank and a flume experiment was performed by Duan et al. (2020) to investigate the effect of physio-chemical heterogeneity with preferential flow paths on As sorption and reactive transport under water extraction in a layered system. The tank made with acrylic sheets is 50 cm in length, 40 cm in height, and 8cm in width (Figure 4-1). Thirty sampling ports, which were sealed with rubber plugs. 23 G needles with 8 cm long, was drilled at the front wall of the tank to allow collecting aqueous samples in the layered system. The flow system of the tank is driven by two hydraulic pressure (water head) controllers (Figure 4-1a, no.5), which were connected to the layered system using two perforated plates, one installed inside of the tank with 5 cm from each side of the tank. In the experiment, the perforated plates were sealed from the bottom to 25 cm upper, and the layered system was connected to the hydraulic pressure controllers only through upper part of the plates (Figure 4-1a).

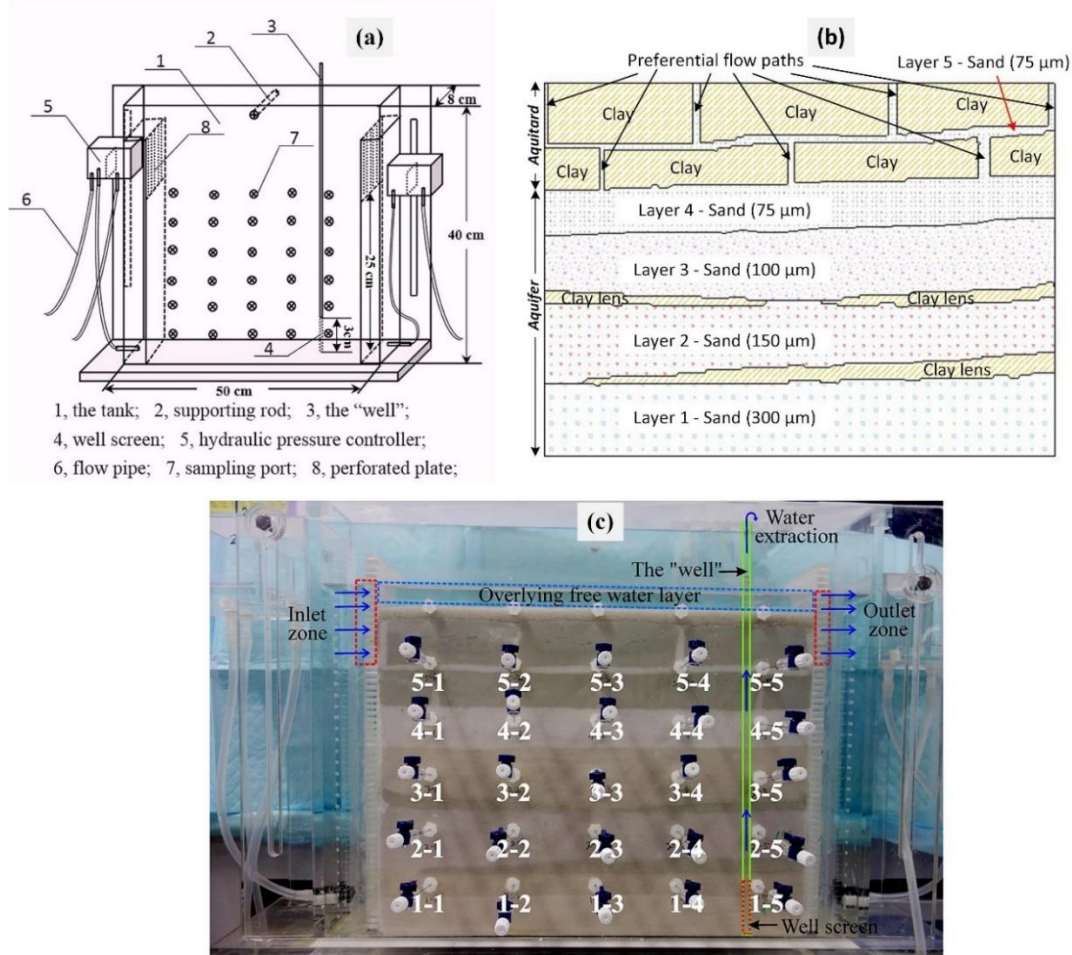


图 4-1 室内实验示意图: (a) 沙箱设计图; (b) 具有复杂优先流动路径的含水层分层示意
图; (c) 采样孔位置及编号 (改自 Duan et al. (2020))

Figure 4-1 Schematic diagram of the experimental setup: (a) experimental tank design; (b) schematic diagram of the layered system with complex preferential flow paths; (c) image of the packed flume showing the sampling ports with numeric labels (modified from Duan et al. (2020)).

Various sorted quartz sands of variable grain sizes and clay were wet-packed into the tank layer by layer to create the aquitard and aquifers based on the observed hydrogeological conditions (Figures 4-1b and 4-1c). The aquifers (0 – 21 cm) included four layers of packed sands with decreasing sizes of quartz sands from the bottom (layer 1) to the top layer (layer 4), with particle size decreasing from 300 to 75 μm in diameter. Three clay lens were “sandwiched” by the sand layers as illustrated in Figures 4-1b and 4-1c. The aquitard (21 – 29 cm) was packed with clay, which was made by mixing montmorillonite, illite, kaolinite, chlorite, and silty quartz sand to mimic the mineral composition of the clay sediment from field site observations. A thin silty sand layer (layer 5) was embedded in the clay layer. Seven preferential flow paths were penetrated

into the clay layer, and the paths were filled with silty sand. The surface of the clay layer was covered with a thin layer of coarse sand (0.8 – 2.0 mm in diameter) in order to prevent clay from flowing out of the system. A miniature water extraction “well” (a glass tubing, Figures 4-1a and 4-1c) was installed in the tank during the processes of sand/clay filling. The tubing has an inner diameter of 5 mm, and the screen has a 3 cm length located at the end of the well (Figure 4-1a, no. 4), and thus, only the water from the bottom layer can be extracted. In addition to the designed preferential paths, an unintended fracture was observed inside the clay lens along the well pipe and connected the sand layer 3 and layer 2.

To saturate the packed materials and remove the air captured in the tank during the processes of sand/clay filling, groundwater medium (10 mM PIPES, 2.7 mM KCl, 0.3 mM MgSO₄, 7.9 mM NaCl, and 0.4 mM CaCl₂·2H₂O with pH at 7.1) containing no Br and As was pumped into the tank through the well at injection rate of 2.0 mL/min. The water level in the tank was raised progressively and maintained to a designed height to form an overlying free water layer (~2 cm deep) throughout the experiment (Figure 4-1c). The water level of the inlet side (left) was 3 – 4 mm higher than that of the outlet side (right) to provide a 7.5×10^{-3} to 1.0×10^{-2} horizontal hydraulic gradient. The flume was left to stabilize for five days to achieve a local chemical equilibrium between clay minerals and injected water. The water flowed continuously through the flume during the stabilization period.

Groundwater medium containing 0.5 mM NaBr (C_{in} , Br) and 35 μ M Na₂HAsO₄·7H₂O (As(V), C_{in} , As) (related to the highest As concentration observed in the field site) was used for the As reactive transport experiment. The groundwater medium was supplied at 2 mL/min constant flow rate from the inlet side of the tank to the overlying free water layer on the top. The experiment was conducted in three periods: a period with no water extraction (0 – 7.75 d), a period with water extraction (7.75 – 99 d), and a period for tracer (dye) visualization test (99 – 104 d). In the period of no water extraction, the “well” was sealed, while during the period with water extraction, water from the bottom sand layer was extracted through the “well” at a rate of 1.0 mL/min, driving the downward flow of the overlying free oxic water across the heterogeneously layered system. The pumping ends at the period of tracer visualization test (red ink to visualize the flow direction and flow paths). No bubbles were observed in the extraction tube during the whole experiment, indicating that the pumping rate was slow enough to

avoid the exsolution of dissolved gas in the aqueous phase. The water supplying rate from the inlet was larger than the extraction rate at the “well”, and the excessive water flowed out directly through the overlying water layer to the outlet side instead of infiltrating into the layered system.

Water samples were taken from the 25 sampling ports (Figure 4-1c) at increasing time intervals from one day to five days. For each sampling event, a ~2.5 mL aliquot of solution was extracted for aqueous chemical analysis. Besides, water samples extracted from the “pumping well” were collected at increasing time intervals from 1 to 8 h using an automatic sample collector. The Br concentration and As concentration in these aqueous samples were then measured. Interested readers are referred to Duan et al. (2020) for details on the lab experiment such as sampling and analysis.

4.2.2 Mathematic Model

A 2-D reactive transport model adopted from Duan et al. (2020) was built to simulate the As sorption and transport in the flume system. Richards equation was used to compute the subsurface flow (Lichtner et al. 2015):

$$\frac{\partial}{\partial z}(\varphi s \rho) + \nabla \cdot (\rho \mathbf{q}) = Q_w, \quad (4.1)$$

with Darcy flux \mathbf{q} defined as

$$\mathbf{q} = -\frac{kk_r(s)}{\mu} \nabla(P - W_w pgz). \quad (4.2)$$

Here, Q_w denotes the source/sink term [$\text{kmol}\cdot\text{m}^{-3}\cdot\text{s}^{-1}$], φ the porosity [-], s saturation [$\text{m}^3\cdot\text{m}^{-3}$], ρ water density [$\text{kmol}\cdot\text{m}^{-3}$], \mathbf{q} Darcy flux [$\text{m}\cdot\text{s}^{-1}$], k intrinsic permeability [m^2], k_r reactive permeability [-], μ viscosity [$\text{Pa}\cdot\text{s}$], P pressure [Pa], W_w formula weight of water [$\text{kg}\cdot\text{kmol}^{-1}$], g gravity [$\text{m}\cdot\text{s}^{-2}$], and z the vertical component of the position vector [m]. Van Genuchten capillary properties are used for relative permeability in this study. The velocity of water moving through a flow field (the average pore velocity) is then calculated by $\mathbf{v} = \mathbf{q} / \varphi$.

The fate of and transport of the arsenic in the flume system was simulated based on the following equation (Zheng and Wang 1999):

$$\frac{\partial(\theta C^{As})}{\partial t} = \frac{\partial}{\partial x_i} \left(\theta D_{ij} \frac{\partial C_{As}}{\partial x_j} \right) - \frac{\partial}{\partial x_i} (\theta v_i C^{As}) - q_s C_s^{As} - \sum R_n, \quad (4.3)$$

where C^{As} is the aqueous arsenic concentration [$M \cdot L^{-3}$]; θ is the porosity of the subsurface medium; x_i is the distance along the respective Cartesian coordinate axis (L); D_{ij} is the hydrodynamic dispersion coefficient tensor [$L^2 \cdot T^{-1}$] which can be calculated based on the longitude (α_L) and transverse dispersivity values (α_T), v_i is the average pore velocities ($L \cdot T^{-1}$), q_s is the volumetric flow rate per unit volume of aquifer [L^{-1}] representing fluid sources (positive) and sinks (negative); C_s^{As} is the concentration of the source or sink flux for arsenic concentration [$M \cdot L^{-3}$]; $\sum R_n$ is the chemical reaction term [$M \cdot L^{-3} \cdot T^{-1}$] and only the sorption of the arsenic was considered in this study.

4.2.3 Numerical Model Setup

The numerical model was built using PFLOTRAN, an open source, state-of-the-art massively parallel reactive flow and transport model for describing subsurface processes (Hammond et al., 2014). The modeling domain is 40 cm in the x direction, 8 cm in the y direction, and 30 cm in the z direction, which was discretized into $200 \times 1 \times 150$ uniform grid cells. A constant hydraulic pressure head boundary was used on the upper part of the lateral boundaries from 25.0 to 30.0 cm, where the layered system was connected to two hydraulic pressure controllers. The hydraulic head in the left controller was set to be 32.3 mm, which is 3 mm higher than the head in the right controller, imposing a 7.5×10^{-3} horizontal hydraulic gradient from left to right. A Dirichlet concentration boundary was also applied to the upper part of the lateral boundaries and the top boundary, where groundwater medium containing constant concentrations of tracers (0.5 mM NaBr) and arsenic (35 μM Na₂HAsO₄·7H₂O) were supplied to capture the flow path and As sorption and transport under water extraction condition. A pumping well with an inner diameter of 5 mm and 3 cm screen length was placed at the bottom of the domain to force water flowing down toward the well once start pumping. The sampling at each sampling port was also treated as a water mass sink as it removed water. The model simulation was conducted for a length of 104 days and the pumping well started pumping at 1 mL/min at 7.75 d and the pumping ended at 99 d. The Richards' equation was used to compute the subsurface flow, and the initial hydraulic head field was set to be the hydraulic heads obtained from the steady flow between the two lateral boundaries without pumping.

The porosity θ was assumed to be a constant of 0.44 across the modeling domain and the longitude and transverse dispersivity values were set to be 10^{-3} and 10^{-4} m, respectively. It is worth noting that Duan et al. (2020) treated the flume system as a 3-D numerical model to consider the effects of an unintended fracture occurred inside the clay lens between layer 2 and layer 3 along the well pipe. In this study, the 3-D numerical model was simplified into 2D ignoring the effects of the unintended fracture to reduce the computational cost to facilitate the sensitivity analysis. The simplification is reasonable since in this study we only focus on the As concentration in the pumping well. The unintended fracture mainly affects the As concentration near the well pipe in layer 2 (e.g., ports 2-5) and has limited effects on the arsenic concentration in the pumping well as shown in Figure 4-2b.

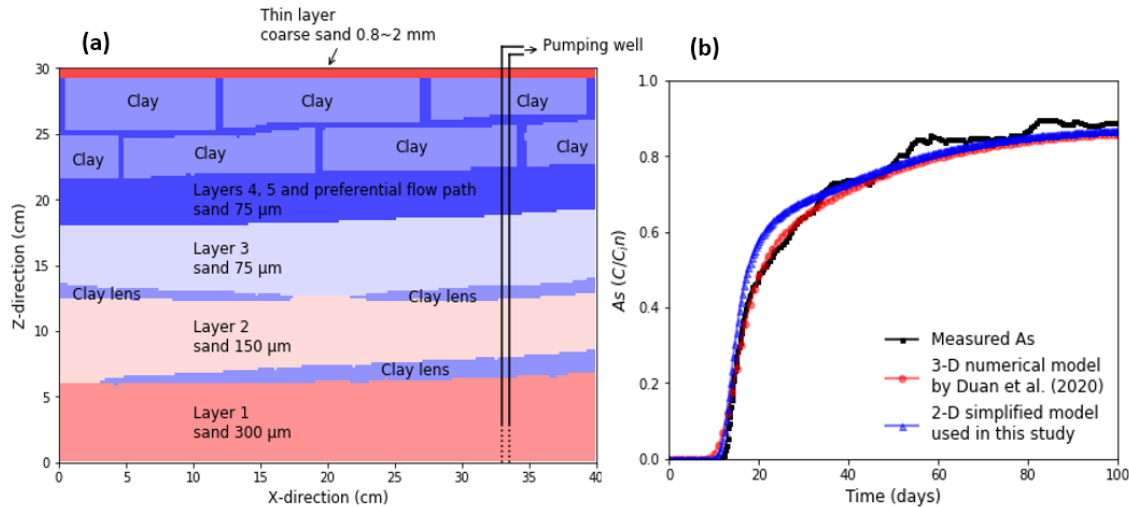


图 4-2 (a) 二维数值模型含水层概化示意图; (b) 抽水井中砷浓度的: 实测变化曲线, Duan et al. (2020)建立的三维数值模型模拟结果, 以及本论文中使用的二维简化模型模拟结果。

Figure 4-2 (a) Schematic diagram of the layered system with complex preferential flow paths and (b) time series of As concentration in the pumping well from the sampling measurements, the 3-D numerical model from Duan et al. (2020), and 2-D simplified model used in this study.

4.2.4 Uncertainty Sources

The characterization of subsurface heterogeneity is of importance for subsurface flow and solute transport simulations. In this experiment, heterogeneous distribution of the hydrogeological framework as shown in Figure 4-2a were well designed thus there is no uncertainty in conceptualization of aquifer structure in the tank. Yet in field work subsurface is like a “black box” and is inherently not fully accessible with existing

techniques, rendering them prone to multiple interpretations and conceptualizations (e.g., Ye et al. (2010b)). To investigate the impact of physio-chemical heterogeneity as well as other factors on As sorption and reactive transport, we conceptualized three processes, namely, the physical process, the chemical process, and the sorption process and postulated a total of $12 = 2 \times 2 \times 3$ individual system models, corresponding to the two physical process models (i.e., heterogenous and homogenous permeability field), two chemical process models (i.e., the heterogenous and homogenous distribution coefficient field), and three sorption process models (i.e., the simple linear equilibrium model, the dual first-order kinetic sorption model and the coupled linear equilibrium sorption model with a kinetic model for describing the oxidation of Fe(II)-bearing clay minerals). Figure 4-3 illustrates the twelve different model choices and the associated process model parameters.

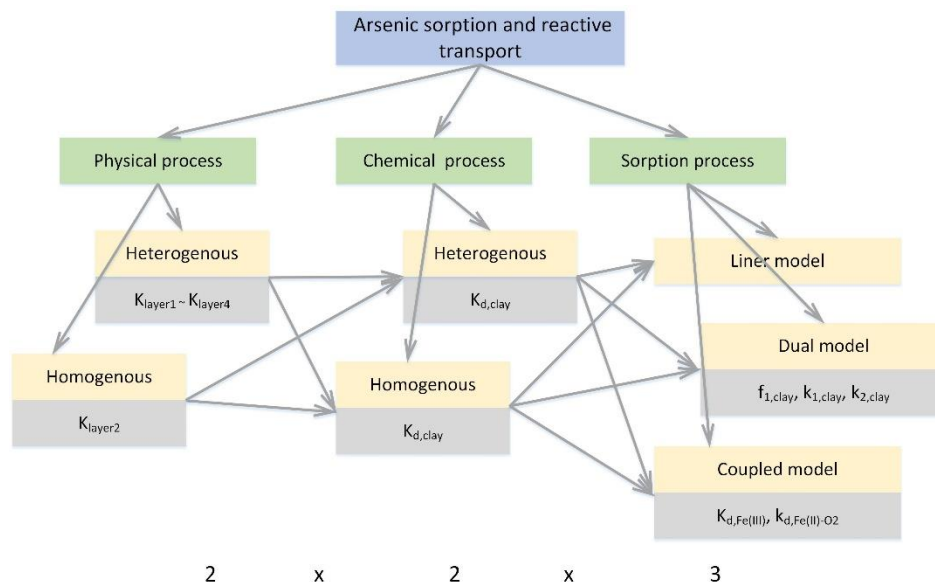


图 4-3 考虑 $12 = 2 \times 2 \times 3$ 个不同的模型用于模拟沙箱中砷的浓度，分别对应于 2 个非均质和均质渗透场(物理过程)模型、2 个非均质或均质分布系数(化学过程)场模型和三种吸附模型(吸附过程)。灰色矩形框表示与相应过程模型相关的不确定参数，其中线性吸附模型没有参数。

Figure 4-3 Overview of the $12 = 2 \times 2 \times 3$ alternative models, corresponding to the heterogenous or homogenous permeability field (physical process), heterogenous or homogenous distribution coefficient (chemical process), and three sorption models (sorption process). The gray boxes show the uncertainty parameters associated with the corresponding process models. Note there is no parameter involved in the linear sorption model

The permeability filed of the heterogenous physical process model was delineated into zones based on the heterogenous distributed materials as shown in Figure 4-2a. According to Duan et al. (2020), the local permeability of the sand materials was estimated using the Kozeny-Carman equation based on the sand particle size. Considering

the sands may not be perfectly sorted and consequentially, the particle diameters could vary in a certain range, the uncertainty of permeability values of layers 1, 2, 3, 45p (short for layers 4, 5 and preferential flow path, Figure4-2a) were considered. The permeability values of these layers were assumed to follow uniform distributions ranging from 0.5 to 1.5 times their nominal values (the nominal values refer to the results obtained by using the Kozeny-Carman equation), respectively. The permeability value of clay (the clay and clay lens are both referred as clay hereinafter) was set to be a constant of $5.17 \times 10^{-15} \text{ m}^2$. The uncertainty of the permeability of clay was negligible here as they were treated as aquitard and Duan et al. (2020) has already showed that the tracer concentration was not sensitivity to the permeability of clay. As for homogenous physical process model, we assume a homogenous permeability field, where the effective permeability was set to be the permeability of layer 2 following Duan et al. (2020). For this physical process model, the uncertainty of the permeability was also considered, and the permeability was also assumed to follow uniform distributions ranging from 0.5 to 1.5 times the nominal permeability.

表 4-1 本文考虑的不确定参数及其范围。参数标准值参考 Duan et al. (2020)，假定所有的参数服从均匀分布，在 0.5~1.5 倍的标准值内变化。注意双室一阶动力学吸附模型参数 $f_{l,clay}$ 的变化范围为 0.445 to 1.0。

Table 4-1 Uncertainty parameters. The nominal values were taken from Duan et al. (2020). All parameters are assumed to follow the uniform distribution ranging from the 0.5 to 1.5 times of their nominal values except for the $f_{l,clay}$ ranging from 0.445 to 1.0.

Parameter	Unit	Nominal value	Description
K_{layer1}	m^2	1.86×10^{-11}	Permeability of layer 1
K_{layer2}	m^2	4.66×10^{-12}	Permeability of layer 2
K_{layer3}	m^2	2.07×10^{-12}	Permeability of layer 3
K_{layer4}	m^2	1.16×10^{-12}	Permeability of layer 4
$K_{d,clay}$	mL/g	5.65	Sorption distribution coefficient of clay
$f_{l,clay}$	-	0.89	Site fraction of clay at sorption site 1
$k_{l,clay}$	h^{-1}	118.07	First-order rate constant of clay at site 1
$k_{2,clay}$	h^{-2}	0.23	First-order rate constant of clay at site 2
$K_{d,Fe(III)}$	mL/g	3.01×10^3	Sorption distribution coefficient of Fe(III)
$k_{Fe(II)-O_2}$	L/mol/s	0.5	Reaction rate constant

The distribution coefficient field of the heterogenous chemical process model was delineated into zones based on the heterogenous materials as shown in Figure 4-2a. The distribution coefficient values of the sands, clay was determined based on the kinetic batch experiments. In this chemical process model, only the uncertainty of distribution

coefficient of clay was considered. The distribution coefficients of the other materials were treated as constant values and not considered as they are much smaller compared with the distribution coefficient of clay and of low contribution to the As sorption. The distribution coefficient of clay was assumed to follow uniform distributions ranging from 0.5 to 1.5 times its nominal values. In the homogenous chemical process model, a homogenous distribution coefficient filed was assumed. Average solid composition for the homogeneous materials was obtained by mixing all the packed materials, which means that the mixing fraction of each material was constant over the domain. The effective distribution coefficient equals to the summation of the distribution coefficient of each mineral times the fraction. Thus, we still only consider the uncertainty of distribution coefficient of clay and treated the distribution coefficients of the other materials as constant values.

The three sorption models of the sorption process are described briefly below. The first one is the simple linear equilibrium model (referred to as linear sorption model hereinafter). This is the simplest model for describing the solute (sulfamethazine) partition in the solution and the surface of the sorbent (soil) in the evaluation of the sorption behavior (Mutavdzic Pavlovic et al. 2014):

$$q_{As} = K_d \times C_{As}, \quad (4.4)$$

where q_{As} is the amount of absorbed As; C_{As} is the aqueous As concentration; and K_d is distribution coefficient. For this model, there is no parametric uncertainty. The second one is the dual first-order kinetic sorption model (referred as dual sorption model) to describe the kinetic sorption of As to the grains:

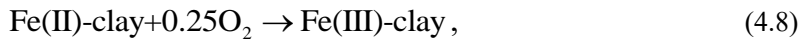
$$\frac{dq_{t,i}}{dt} = k_i(q_{e,i} - q_{t,i}) \quad (i=1,2), \quad (4.5)$$

$$q_{e,i} = K_d \times C_{As} \times f_i, \quad (4.6)$$

$$q_t = q_{t,1} + q_{t,2}, \quad (4.7)$$

where t is the contact time during the simulation (h), $k_i(\text{h}^{-1})$ is the first-order rate constant at sorption site i , f_i is the site fraction for site i , $K_d(\text{mL/g})$ is the linear equilibrium sorption constant, C_{As} is the aqueous As concentration, $q_{t,i}(\mu\text{g/g})$ is the actual absorbed amount of arsenic at time t on site i , $q_{e,i}(\mu\text{g/g})$ is the estimated absorbed amount of arsenic at site i in equilibrium with C_{As} at time t . For this sorption model, the uncertainty of three

parameters, i.e., f_1 , k_1 and k_2 of clay (lens) were considered. The fraction of site 2, f_2 , is not considered explicitly, because the summation of the two site fractions is one. The third sorption model is the linear equilibrium sorption model coupled with a kinetic model accounting for oxidation of Fe(II)-bearing clay minerals (referred to as coupled sorption model hereinafter):



The oxidation of the Fe(II)-bearing clay minerals was described using

$$R_{\text{Fe(III)}} = k_{\text{Fe(II)-O}_2} c(\text{Fe(II)})c(\text{DO}), \quad (4.9)$$

where $k_{\text{Fe(II)-O}_2}$ is the rate constant, $c(\text{Fe(II)})$ is the concentration of clay-associated Fe(II), and $c(\text{DO})$ is the concentration of dissolved oxygen (DO). In this model, the reactive transport of DO was also simulated in this model to calculate local DO concentrations. The increase of Fe(III) as a result of Fe(II) oxidation is expected to increase the arsenic sorption capacity for the clay materials. Consequently, the K_d value in the equilibrium sorption model for As was also assumed to increase. For this sorption model, the parameter uncertainty of $k_{\text{Fe(II)-O}_2}$ and the distribution coefficient of the clay was considered.

These twelve different models represent model uncertainty on As sorption and reactive transport processes due to our incomplete knowledge. The permeability filed represents the physical heterogeneity which influences the flow path and transport of the arsenic; the spatial distribution coefficient represents the chemical heterogeneity which influences the sorption efficiency of arsenic, and the three sorption models represent different sorption mechanisms. Table 4-1 list the uncertainty parameters and their ranges associated with the process models.

§4.3 Identifying the Controlling Processes to As Concentration in the Pumping Well

4.3.1 Simulation Results

Using the efficient design discussed in Chapter 2 for variance-based process sensitivity analysis method, PFLOTTRAN simulations were ran on a total of $2 \times 2 \times 3 \times (3 + 2) \times 3,600 = 216,000$ model simulations considering all possible combinations of

model configuration and input parameters, i.e., the two physical process models, two chemical process models, three sorption models, and five sample matrices **A**, **B**, and **C₁** ~ **C₃**, each of which contains 3,600 parameter realizations. The wall clock time for each simulation run was approximately 2 ~ 5 mins using 8 cores on the high-performance computer system at the Florida State University.

The simulated As breakthrough curves at the pumping well resulting from the (3 + 2) × 3,600 = 18,000 realizations for each of the twelve system model were first summarized and compared to the laboratory measurements to assess the overall uncertainty (Figures 4-4). Visually speaking, with the consideration of parameter uncertainty, six out of the twelve system models corresponding to Figures 4-4a, b, c, f, g, and j may be acceptable for simulating the arsenic sorption and reactive transport in the flume system due to the 18,000 realizations of simulated arsenic breakthrough encapsulated the observed arsenic behavior for the pumping well. This renders it necessary to include the model uncertainty when performing the sensitivity analysis and identifying the controlling processes for hydrologic models.

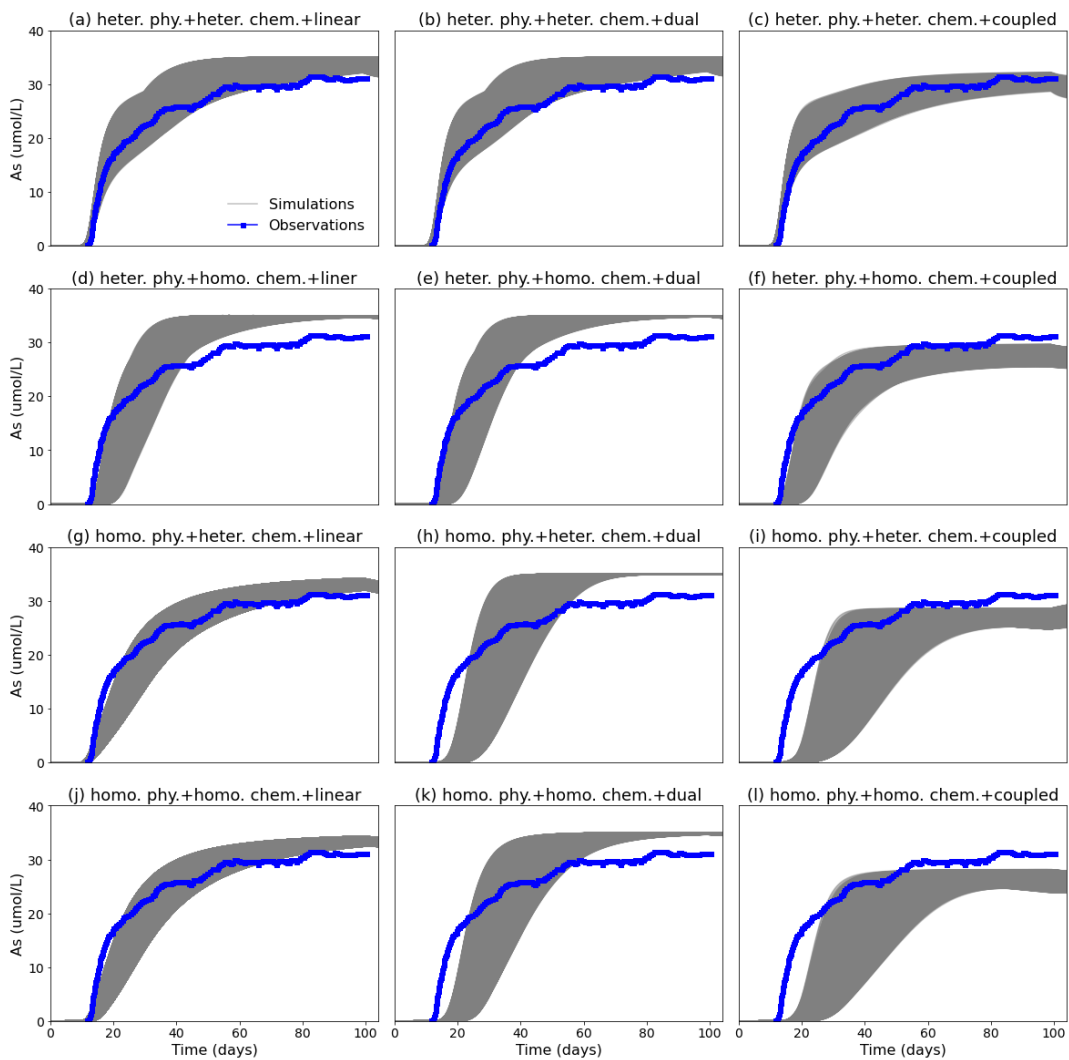


图4-4 PFLOTRAN 模拟的抽水井中砷浓度变化曲线和实测浓度曲线对比。考虑参数不确定情况下，12个模型每个模型有 $(3+2)\times 3,600 = 18,000$ 个模拟曲线。图中“homo. phy.”表示均值的渗透系数场，“heter. phy.”表示非均值的渗透系数场，“homo. chem.”表示均值的化学吸附系数场，“heter. chem.”表示非均值的化学吸附系数场，“linear”表示线性吸附模型，“dual”表示双室一阶动力学吸附模型，“coupled”表示耦合线性平衡吸附模型和 Fe(II) 粘土矿物氧化的动力学模型。

Figure 4-4 PFLOTRAN arsenic concentration simulation results of $(3+2)\times 3,600 = 18,000$ realizations at the pumping well compared to laboratory measurements for each of 12 individual system models. The “homo. phy.” denotes homogenous permeability filed and “heter. phy.” denotes the heterogenous permeability filed. The “homo. chem.” denotes homogenous sorption coefficient filed and “heter. chem.” denotes heterogenous sorption coefficient filed. The “linear”, “dual”, and “coupled” denote the three sorption models, i.e., the simple linear equilibrium model, the dual first-order kinetic sorption model, and the coupled linear equilibrium sorption model with a kinetic model for describing the oxidation of Fe(II)-bearing clay minerals.

4.3.2 Parameter Sensitivity Indices for Single-Model

Based on Equations (2.37) and (2.38) in Chapter 2, the traditional Sobol's parameter sensitivity indices of the three processes for each of the twelve system models are computed. Figure 4-5 is the convergence diagnosis for the parameter sensitivity indices (over Monte Carlo sample size in matrixes \mathbf{A} , \mathbf{B} , and \mathbf{C}_i) of arsenic concentrations at the pumping well for system model heterogenous permeability filed + heterogenous sorption coefficient filed + coupled sorption model. This system model was selected because it is the most complex model and contains the highest number of parameters among the twelve models. The figure shows that the sensitivity indices converge after 3,600 samples are used. The larger number of sample size should be enough to produce reliable sensitivity results showing below.

Figure 4-6 plots the temporal variation of parameter sensitivity indices of the three processes to arsenic concentrations at the pumping well of the three processes for each of the twelve system models. This figure illustrates the following four points:

(1) Within a single system model, the importance/influence corresponding to the first-order/total-effect parameter sensitivity indices of the three processes change dramatically along the simulation time. Taking the system model comprising heterogenous permeability filed, heterogenous distribution coefficient filed, and linear sorption model as an example (Figure 4-7a), the physical process (red lines) gradually becomes less important/influential, while the importance/influence of the chemical process (green lines) gradually increases. As for the chemical process (blue lines), the parameter sensitivity indices are almost zero over the simulation period, indicating this process is totally non-important or non-influential at all. This could also be observed for Figures 4-d, g, and j as the linear sorption model is used for all the three system models. This is not surprising since the simple linear sorption model does not contain any parameter thus there is no parameter uncertainty for this process.

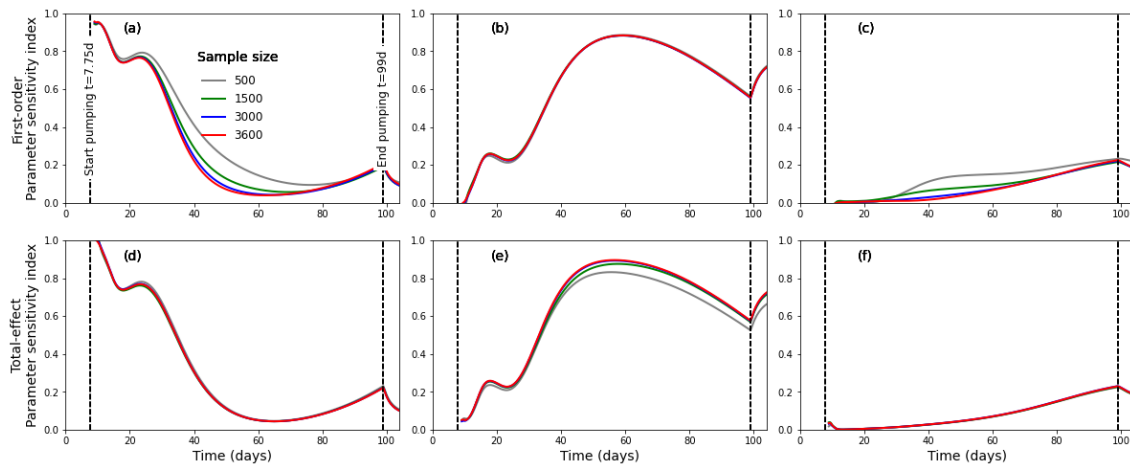


图4-5 考虑非均质渗透系数场，非均质吸附系数场和耦合线性平衡吸附模型和Fe(II)粘土矿物氧化的动力学模型条件下（a）物理过程，（b）化学过程，（c）吸附过程一阶参数敏感性指标收敛过程。图（d），（e），（f）分别对应三个过程的总效应参数敏感性指标收敛过程。

Figure 4-5 Convergence of the first-order parameter sensitivity indices of (a) physical process, (b) chemical process, (c) sorption process for the simulated arsenic concentrations at the pumping well with different Monte Carlo sample size in system model heterogenous permeability filed + heterogenous sorption coefficient filed + coupled sorption model. Subplots (d), (e), (f) show the convergence of the total-effect parameter sensitivity indices of the three processes.

(2) Within a single system model, the total-effect parameter sensitivity index is always higher than the first-order parameter sensitivity index. As noted in Section 2.2.1, this is due to the existence of parameter interactions. The slightly higher total-effect parameter sensitivity index showing in Figures 4a – 4l expect for Figures 4d, 4e, and 4l indicate the weak parameter interaction among these models.

(3) The relative importance/influence of the three process changes dramatically among the twelve models. Taking the two system models with both heterogenous permeability filed and coupled sorption model but one with heterogenous sorption distribution coefficient field (Figure 4-7c) and one with homogenous sorption distribution coefficient field (Figure 4-7f) as an example, the relative importance/influence of the chemical process gradually increases for the former while that decreases for the latter. This renders again it necessary to include the model uncertainty when performing the sensitivity analysis and identifying the controlling processes for hydrologic models.

(4) The physical process is only identified to be the controlling process at the beginning simulation period when heterogenous permeability filed and heterogenous sorption diffusion coefficient field are used. When the heterogenous sorption diffusion coefficient field is ignored (Figures 4-7e and 4-7l), the physical process seems to have

limited effects on the arsenic concentration. This observation is consistent with Duan et al. (2020).

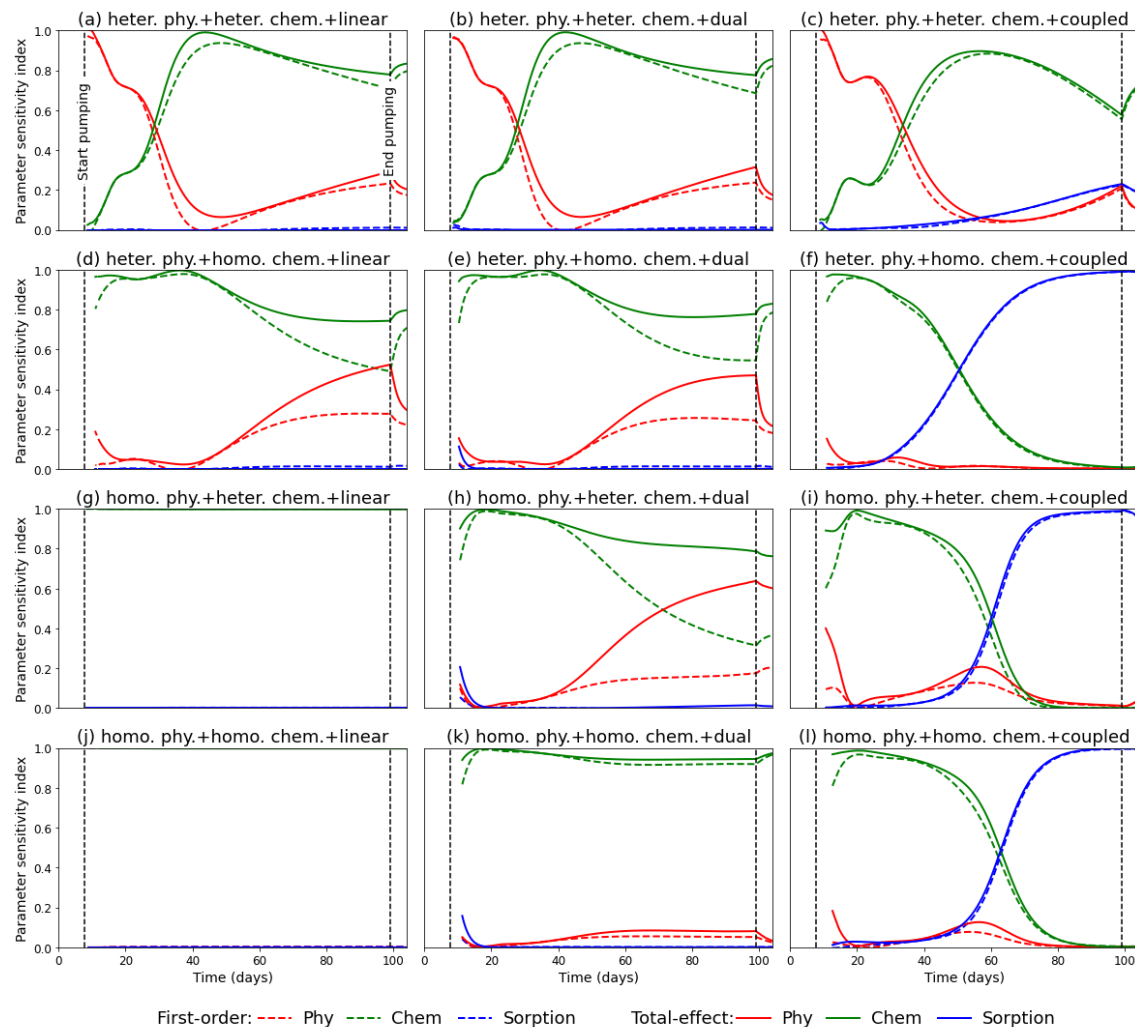


图 4-6 单模型系统条件下，三个过程对抽水井中砷浓度灵敏性随时间变化图

Figure 4-6 Temporal variation of parameter sensitivity indices of the three processes to arsenic concentration at the pumping well for each of the twelve system models.

4.3.3 Process Sensitivity Indices for Multi-Model

Figure 4-7a illustrates the temporal variation of the first-order process sensitivity of the arsenic concentration evaluated for at the pumping well. This figure shows that, at the very beginning of the simulation period, the chemical process is the most important process and the sorption process is not important at all. The chemical process gradually becomes less important, while the importance of the physical process gradually increases. After the simulation time of $t = 16$ d, the physical process becomes more important than

the chemical process and becomes the most important process. The first-order process sensitivity index of physical process reaches its maximum at $t = 25$ d, and correspondingly, that of the chemical process reaches its local minimum. After that, the importance of the physical process continues to decrease while that of the chemical process increases. The chemical process becomes the most important process once again after $t = 32$ d. The first-order process sensitivity index of the chemical process reaches to its maximum at $t = 37.5$ day and then continuously decreases. Different from the wobbling variation of the first-order process sensitivity indices of physical process or chemical process, the first-order process sensitivity index of sorption process continuously increases after the start of pumping. The first-order process sensitivity index of sorption process becomes the largest one among the three process after $t = 41$ d, indicating the importance of this process.

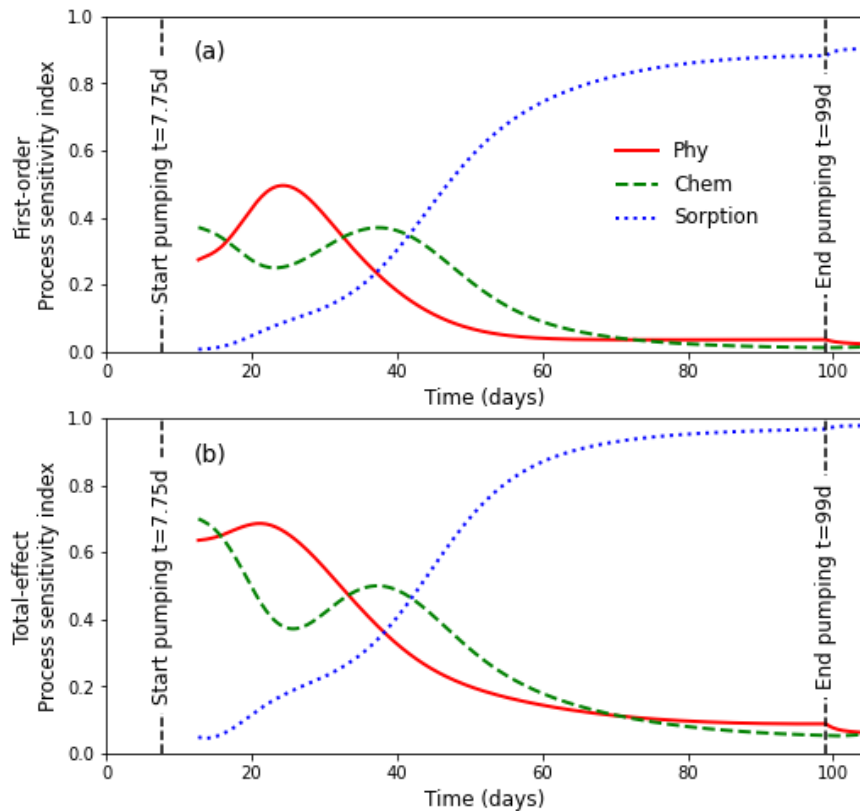


图 4-7 多模型条件下，三个过程对抽水井中砷浓度敏感性指标变化曲线图

Figure 4-7 (a) First-order and (b) total-effect process sensitivity indices for the arsenic concentrations in the pumping well.

Figure 4-7b illustrates the temporal variation of the total-effect process sensitivity of the arsenic concentration evaluated for at the pumping well. This figure shows the variations of the realative influence of the three processes are similar as variations of the realative importance of the three processes as shown in Figure 4-7a except for that the

total-effect process sensitivity indices of the three processes are generally higher than the first-order process sensitivity indices. As noted in Section 2.3.5, this can be explained by process interactions. However, the process interaction can not be computed by using this design. Extending this design to include the computation of the process interaction indices proposed in Section 2.3.5 are warranted in the future study.

4.3.4 Implications and Limitations

The importance and influence of the three processes revealed by the first-order process sensitivity index and total-effect process sensitivity index indicate that either physical or chemical heterogenous can be ignored. Generally speaking, the physical process plays the most important/influential role at the beginning of the simulation period due to the existence of preferential flow path, while the chemical process plays the most important/influential role at the middle simulation period. The sorption process reflects our understanding of sorption mechanism and determines how the arsenic is absorbed. The sorption process controls the arsenic sorption and reactive transport at the final simulation period. The results have important implications that if the As concentration data at the pumping wells are used to learn the physical process, the As concentration at the early stage should be collected and if the As concentration data at the pumping wells are used to learn the sorption process, the As concentration at the final stage should be collected and well measured.

The limitation of current study is that the observation data are not included in the sensitivity analysis when identifying the controlling processes. The process models are assumed to be equally weighted, and the process model parameters are assumed to be uniformly distributed. Such weights and parameter distributions are equivalent to prior model probability from the Bayesian perspective. When the observation data (denoted as \mathbf{D}) are available, the model weights used for model averaging method can be updated to posterior model probability via the Bayes' theorem via (Hoeting et al. 1999, Ye et al. 2010b):

$$p(M_K | \mathbf{D}) = \frac{p(\mathbf{D}|M_K)p(M_K)}{p(\mathbf{D})}, \quad (4.10)$$

where $p(M_K)$ is the prior model probability, $p(\mathbf{D}|M_K)$ is the marginal likelihood function to measure how well data, \mathbf{D} , is simulated by model M_K . Similarly, the posterior parameter distributions can be estimated by using the Markov Chain Monte Carlo techniques (陆乐

等, 2008). The data, \mathbf{D} , can significantly change not only model probability (from the prior to the posterior) but also the mean and variance values used for evaluating the process sensitivity index. This may lead to changes of the values of process sensitivity index, and thus to changes of controlling process identification.

§4.4 Summary

In this chapter, numerical modeling based on a laboratory experiment was used to investigate the importance and influence of physic-chemical aquifer heterogeneity as well as different sorption models on arsenic sorption and reactive transport processes. We employed variance-based process sensitivity analysis method to account for not only the uncertainty of model structures (e.g., either the permeability field is homogenous or heterogeneous) but also the uncertainty of model parameters (e.g., the permeability values for both homogenous and heterogeneous permeability fields) to identify the important and influential processes throughout the simulation time. Using the efficient design proposed in Chapter 2 for variance-based process sensitivity analysis method, PFLOTRAN simulations were run on a total of $2 \times 2 \times 3 \times (3 + 2) \times 3,600 = 216,000$ model simulations considering all possible combinations of model configuration and input parameters. Results show that the most important and influential process on the As concentration in the pumping well could change over time. At the very beginning of the simulation period after pumping started ($t < 16$ d), the chemical process significantly influences the As concentration in the pumping well. At the initial stage ($16 \text{ d} < t < 32$ d), the physical process significantly influences the As concentration in the pumping well since it enables the preferential transport of arsenic to the pumping well. Chemical aquifer heterogeneity and the sorption models play a comparatively minor role. At the middle stage ($32 \text{ d} < t < 41$ d), the chemical aquifer heterogeneity significantly influences the arsenic concentration in groundwater since it adsorbs the preferential transport of arsenic. At the final stage ($t > 41$ d), the three different sorption models significantly influence the arsenic concentration in groundwater since they can enhance the sorption capacity the aquifer.

Chapter 5 Application to a Complex Biogeochemical Model at Hanford 300 Area

This chapter presents a better understanding for identifying the controlling processes to a real-world biogeochemical model at the groundwater-surface water interface within the Hanford Site's 300 Area. Multiple uncertainty sources across four different processes, namely, the climate, flow, heat, and reaction processes were considered based on our understanding of the complex system. Variance-based process sensitivity analysis proposed in Chapter 2 as well as the MMADS analysis methods proposed in Chapter 3 were used to identify the controlling processes in terms of the spatio-temporal distribution of the organic carbon (OC) consumption rate in the aquifer. This chapter compared the two methods and demonstrated that: (1) the controlling processes could vary in space and time; (2) the influential processes identified by the total-effect process sensitivity index could be significantly different to the important processes identified by the first-order process sensitivity index due to process interactions; (3) multi-model absolute difference-based process sensitivity analysis evaluates the total effect of each process including its interaction with others, similar to the total-effect process sensitivity index from variance-based process sensitivity analysis.

§5.1 Introduction

Driven by increasing computing power and coupled with the abundance of available data, often hydrologic models of complex systems are designed such that they have increasing interdisciplinary and interacted processes to fulfill our notion of “trying to model everything”. However, when developing process-based hydrologic models, it occurs often that not all processes are necessary to be considered and only a few processes control the hydrologic response in a given site and/or at a given temporal/spatial scale (Sivakumar 2004a). Identifying the dominant, important or influential processes has long been recognized in the hydrologic science community (Grayson and Bloschl 2000). A fundamental question is how to characterize the uncertainty in the model simulation since

the processes are subject to various sources of uncertainty (Beven 2016).. Sensitivity analysis provides information on the relative importance or influence of model processes.

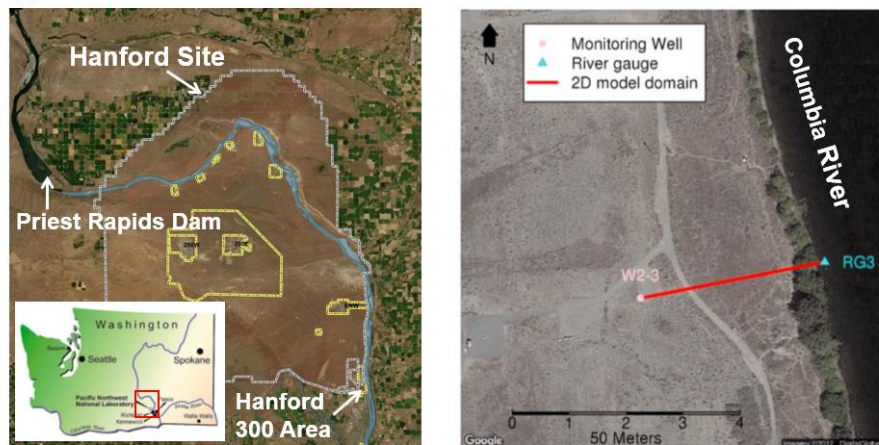
Starting from the parameter sensitivity analysis within a single system model, the process sensitivity analysis methods under multiple system models have been increasingly applied in recent years. A process may be historically amassed a wide range of models, which differ in many aspects of their conceptualization and implementation. In other words, a process may have multiple plausible model representations, and the availability of different conceptualization schemes leads to multiple system models by integrating the process models with the other model components. The uncertainty introduced by these process model representations is usually referred to as process model uncertainty or model structural uncertainty, which is often acknowledged to be the main source of uncertainty in model predictions (Refsgaard et al. 2007). There have been several attempts to identify important processes or influential processes to include the process model uncertainty. One notable attempt is introduced by Dai et al. (2017b) proposing the first-order process sensitivity index which is based on Sobol' variance-based sensitivities. Their method enables the derivation of a countable set of process options for each of the model processes and derive an overall sensitivity through model averaging. The first-order process sensitivity index is used to assign importance to the processes and allows considering both the parametric uncertainty and process model uncertainty. In Chapter 2, we further extended this method by proposing the total-effect process sensitivity index and the second-order process interaction sensitivity index. The total-effect process sensitivity index includes the first-order process sensitivity index and the second-order and higher-order process sensitivity indices and is used to assign the influence of the processes.

Variance-based process sensitivity analysis proposed in Chapter 2 allows quantitatively to rank the processes in order of importance (the first-order process sensitivity analysis index) or influence (the total-effect process sensitivity analysis index) but may not be directly used for large-scale problems in practice, because the methods are computationally expensive due to their relying on Monte Carlo implementations. To reduce the computational cost exacerbated by the variance-based process sensitivity analysis, Chapter 3 proposed a new multi-model difference-based process sensitivity analysis method to quantitatively measure the influence of the system processes. This method could be treated as an alternative approximation method to the total-effect process

sensitivity index as the scientific question they intend to answer is same: to identify the non-influential (correspondingly the influential) processes by both considering the parameter uncertainty and process model uncertainty. A key element distinguishing the two methods is the definition of the metric employed to measure sensitivity.

The objective of this chapter is to improve a better understanding of the sensitivity analysis under multiple system models through applying the two methodologies discussed above for a real-word groundwater biogeochemical model which involves broad range of biophysical and hydrologic processes. This chapter demonstrate the process interaction has strong influence on the total-effect process sensitivity index and the results of the multi-model difference-based process sensitivity analysis method are consistent to those of the total-effect process sensitivity analysis method.

(a) Sketch of river reach



(b) Spatial structural of the permeability field

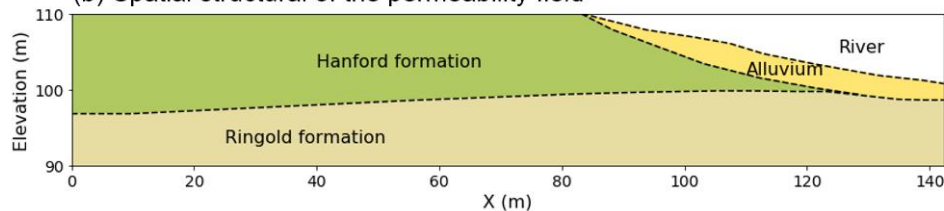


图 5-1 研究区地理位置示意图：(a) Hanford 河段示意图及二维剖面平面位置示意图（红线）。其中左边界为地下水长期观测孔 W2-3，右边界为河流水文监测点 RG3。地下水长观孔和河流水文监测点都具有连续的水位和温度数据；(b) Hanford、Ringold 和 Alluvium 的地质结构剖面示意图。

Figure 5-1 Location map and conceptual model. (a) Sketch of the river reach. The redline is the profile on the 2-D model between inland groundwater monitoring well W2-3 and the river gauge RG3 with continuous level and temperature data. (b) Geological structure of the Hanford formation, Ringold formation, and Alluvium layer beneath the Columbia River.

§5.2 The Complex Biogeochemical Model

5.2.1 Study Site

The study site is located on the western shore of the Columbia River's Hanford Reach in the 300 Area of the U.S. Department of Energy's Hanford Site (Figure 5-1). The Hanford Site, suited within the semiarid Pasco Basin in southeastern Washington State, was set aside in the early 1940s by the U.S. Government to perform a top-secret mission, the Manhattan Project, for production of plutonium for atomic weapons used to end World War II and later to support the Cold War with the Soviet Union. Starting in 1943–1945, thousands of workers were employed on the largest construction project in the world at that time. The workers built a series of nuclear reactors along with large monolithic concrete buildings used to reprocess wastes. Plutonium production continued at Hanford for over 40 years. During the late 1980s, in the aftermath of the Chernobyl accident, plutonium production was suspended at Hanford (Gee et al. 2007). Since then, the U.S. Department of Energy have made massive efforts at Hanford focusing on cleaning up the legacy of wastes stemming from years of nuclear-weapons production (Bjornstad et al. 2009, Chen et al. 2013, Chen et al. 2012, Fritz 2007, Gephart 2003, Ma et al. 2014, Williams et al. 2008).

The Columbia River is the second largest river in the contiguous United States in terms of total flow and is the dominant surface-water body on the Hanford Site (Cushing 1992). The Hanford Reach is an 80-km free-flowing section of the Columbia River with a hydroelectric dam (Priest Rapids Dam, Figure 5-1a) at its upstream boundary and impounded water (from McNary Dam) at its downstream boundary (Shuai et al. 2019). The climate is arid to semiarid with an average annual precipitation less than 180 mm. As a typical regulated river, the river stage at the study site is highly dynamic due to the upstream dam operations, fluctuating ~0.5 m daily and up to 2–3 m annually. The temperature of river water varies between 5 and 22 °C on an annual basis, while the temperature of groundwater remains relatively stable at ~17 °C (Song et al. 2018). The unconfined aquifer that exists within the river corridor and extends beneath the riverbed can be delineated into three distinct geologic formations as shown in Figure 5-1b: low-

permeability sandy alluvium of recent fluvial deposits; high-permeability Hanford formation, consisting of coarse gravelly sand and sandy gravel; and low permeability Ringold formation composed primarily of silt and fine sand. More descriptions about the site hydrogeology can be found in previous studies by Bjornstad et al. (2009), (2013), Chen et al. (2012), and Zachara et al. (2016), Zachara et al. (2013).

5.2.2 Model Setup

A 2-D groundwater biogeochemical reactive transport model has been recently built using site-specific data to study the coupled hydrologic, thermal, and biogeochemical processes in the hyporheic corridor of the Columbia River's Hanford Reach in the 300 Area (Song et al. 2018). The model domain extended from the Columbia River on the right to an inland well on the left as shown in Figure 5-1b, with a length of 143.2 m in the horizontal direction and 20 m in the vertical direction. Three distinct geologic formations, i.e., Hanford formation, Ringold formation and alluvium layer, form the unconfined aquifer and are delineated within the model domain as shown in Figure 5-1c. The numerical model was built using PFLOTRAN, a massively parallel three-dimensional flow and reactive transport code (Hammond et al. 2014). The model domain was discretized by 580×325 nonuniform grid cells, with finer grids used in the area closer to the river to better capture the exchange dynamics and the associated biogeochemical processes at the groundwater-surface water interface. A transient hydraulic pressure head boundary and a Dirichlet temperature boundary were used on both lateral boundaries using the monitoring data obtained from a piezometer RG3 in the river and a groundwater monitoring well W2-3 at the 300 Area as shown in Figure 5-1b. No-flow and no-heat transfer boundary conditions were used at the top and bottom boundaries. Non-reactive numerical tracers were placed at the right boundary to track the intrusion of river water in the model domain. The model was run for a 6-year time window (2010–2015) with the first year used for model spin-up and the other five years used for analysis. The details of the modeling are referred to Song et al. (2018), and we only describe in this chapter the modeling components related to sensitivity analysis.

The geologic framework for the 2-D bank storage model was informed by previous geological and geophysical surveys. Hydraulic and thermal properties were modified from earlier modeling studies performed at the same site (Chen et al. 2013, Ma et al. 2012). Heterogeneous permeability fields of the alluvium and Hanford formation were

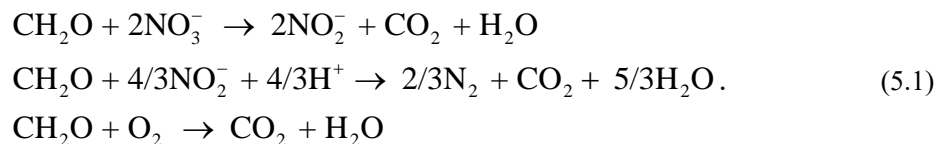
generated with unconditional geostatistical simulations via the R package “gstat” (Pebesma 2004) using the exponential variogram model with the parameters shown in Table 5-1. The least permeable Ringold Formation that serves as a local aquitard was assumed to be homogenous.

表 5-1 研究区 Hanford/Alluvium/Ringold 的水力学和热力学参数（改自 Song et al. 2018）

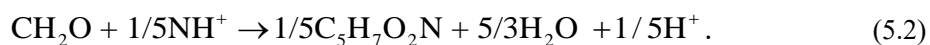
Table 5-1 Hydraulic and thermal properties of Hanford/Alluvium/Ringold formations (modified from Song et al. 2018)

	Hanford	Alluvium	Ringold
Geostatistical parameters of permeability field (exponential variogram)			
Mean (log, m ²)	-8.13	-13	-15
SD (log, m ²)	0.83	0.81	homogenous
Integral scale (m)	20	8	homogenous
Anisotropy ratio	0.1	0.1	homogenous
Anisotropy angle (deg)	-3	9	homogenous
Nugget	0	0	homogenous
Other hydraulic properties			
Porosity	0.2	0.43	0.43
Residual saturation	0.16	0.13	0.13
van Genuchten alpha parameter (Pa ⁻¹)	7.27e-4	1.43e-4	1.43e-4
van Genuchten <i>m</i> parameter	0.34	0.75	0.75
Thermal properties			
Soil particle density of material (kg/m ³)	2,760	2,650	2,650
Specific heat capacity of material (J/kg K)	715	920	920
Wet thermal conductivity of material (W/K m)	1.88	0.93	0.93
Dry thermal conductivity of material (W/K m)	0.93	0.68	0.68

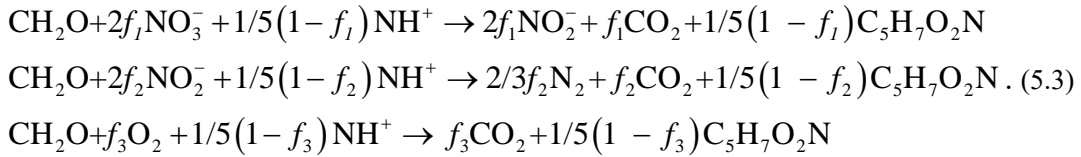
The biogeochemical reaction network and the reaction rates in the model were adopted from the work of Li et al. (2017b) and Song et al. (2017). A two-step denitrification for the dissolved organic carbon (CH₂O) and oxidative respiration were considered as follows:



Microbial biomass (MB, C₅H₇O₂N) synthesis was considered as



Depending on what electron acceptors are available in the environment, microbes obtain energy for growth and maintenance through aerobic or anaerobic respiration. To account for this coupling, each of the energy-producing reactions in Equation (5.1) was combined with BM synthesis reaction in Equation (5.2) as follows:



where f_1 , f_2 , and f_3 are parameters denoting the fractional contribution of energy-producing pathways in Equation (5.1). Parameter values of f_1 and f_2 are estimated from the batch denitrification data collected by (Li et al. 2017a) at 0.65 and 0.99, respectively. With the assumption that oxidative respiration is energetically more favorable than NO_3^- reduction, parameter value of f_3 is assumed to be $1/3f_1$. Temperature-dependent reaction rate, r_i , is defined using the Arrhenius equation as

$$r_i = r_{base,i} \exp\left[-\frac{E_a}{R}\left(\frac{1}{T} - \frac{1}{26+273.15}\right)\right], \quad i=1,2,3, \quad (5.4)$$

where r_i is the reaction rate for BM under temperature T (in Kelvin) with subscript i being the i -th generic reaction in Equation (6.3); E_a is the activation energy (0.65 ev in this study), R is the gas constant ($8.314 \text{ J}\cdot\text{mol}^{-1}\cdot\text{K}^{-1}$), and $r_{base,i}$ is the base rate derived from laboratory batch experiments under the room temperature of 26 °C. After incorporating the microbial regulation term into the Monod kinetics, the base rate $r_{base,I}$ is defined by

$$r_{base,i}^{kin} = e_i^{rel} k_i \frac{d_i}{K_{d,i} + d_i} \frac{a_i}{k_{a,i} + a_i}, \quad i=1,2,3, \quad (5.5)$$

where $e_i^{rel} = r_i^{kin} / \sum_{j=1}^3 r_j^{kin}$ denotes the relative enzyme levels, which regulates the rates of oxidative respiration and denitrification reactions, k_i ($\text{mol}\cdot\text{L}^{-1}\cdot\text{day}^{-1}$) is the maximum specific uptake rate of organic carbon (CH_2O), a_i (mol/L) is the electron acceptor concentration, d_i (mol/L) is the electron donor concentration, and $K_{a,i}$ (mol/L) and $K_{d,i}$ (mol/L) are the half-saturation constants for electron acceptors and electron donors, respectively.

5.2.3 Uncertainty Sources

Dai et al. (2019) considered the following six uncertainty sources as shown in Figure

5-2: (1) climate scenarios for river stage, inland well water level, and temperature; (2) thickness of a alluvial layer at the interface between the Columbia River and the Hanford formation beneath the river; (3) parameterization (homogeneous vs. heterogeneous) of permeability of Hanford Formation and the Alluvial layer; (4) random samples of permeability if it is homogeneous or random fields of permeability if it is heterogeneous; (5) reaction rates related to organic carbon consumption; and (6) whether reaction rates are affected by temperature. Dai et al. (2019) grouped these uncertainty sources into four categories, i.e., climate scenario, groundwater flow, heat transport, and reactive transport. They conducted a sensitivity analysis to quantify relative importance of the four categories to OC consumption rate at three simulation times of 8, 10, and 12 weeks, and concluded that groundwater flow is the most important process, and that heat transport is the least important one.

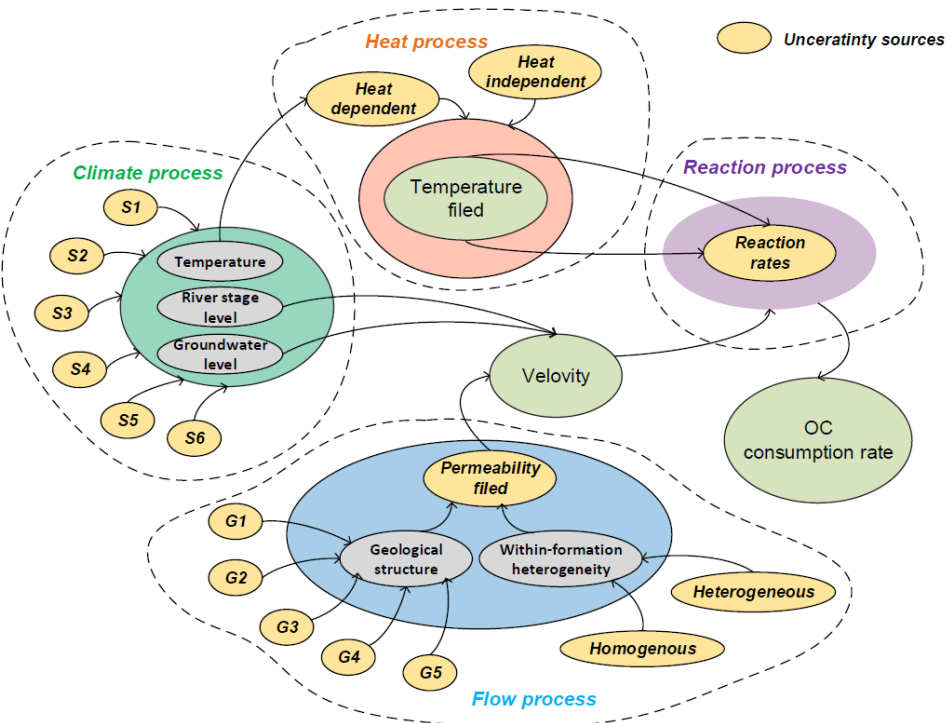


图 5-2 Hanford 场地 300 区域生物地球化学反应模型不确定性来源示意图

Figure 5-2 Uncertainty sources for the biogeochemical model.

The uncertainty sources considered are in consistent with Dai et al. (2019): there are six climate scenarios (denoted as $S_1 \sim S_6$), five thickness of alluvial layer ($G_1 \sim G_5$), heterogeneity or homogeneity formulations, 100 permeability fields in all the formations no matter being homogeneous or heterogeneous, whether the heat transport process is

modeled to enable temperature-dependent reaction rates, and the 100 reaction rates. Note that the 100 permeability fields are conject the 100 reaction rates. These uncertainty sources are conceptualized into four processes in this study: the climate process, flow process, heat process, reaction process.

The biogeochemical model and uncertainty sources of Dai et al. (2019) are used to perform sensitivity analysis in this study as it has both process model uncertainty and parameter uncertainty. We conceptualize the four categories of uncertainty sources in the context of process model and parameter uncertainty as follows:

- (1) Climate process (P_s). The future climate can be represented by six competing scenarios, and there is no parametric uncertainty for the scenarios (Figure 5-3).

The six climate scenarios, one from each year of 2010 – 2015 with a length a 12 weeks, were selected to start with similar river stage, inland groundwater table, and temperature at the beginning so that there is not significant uncertainty caused by the initial condition.

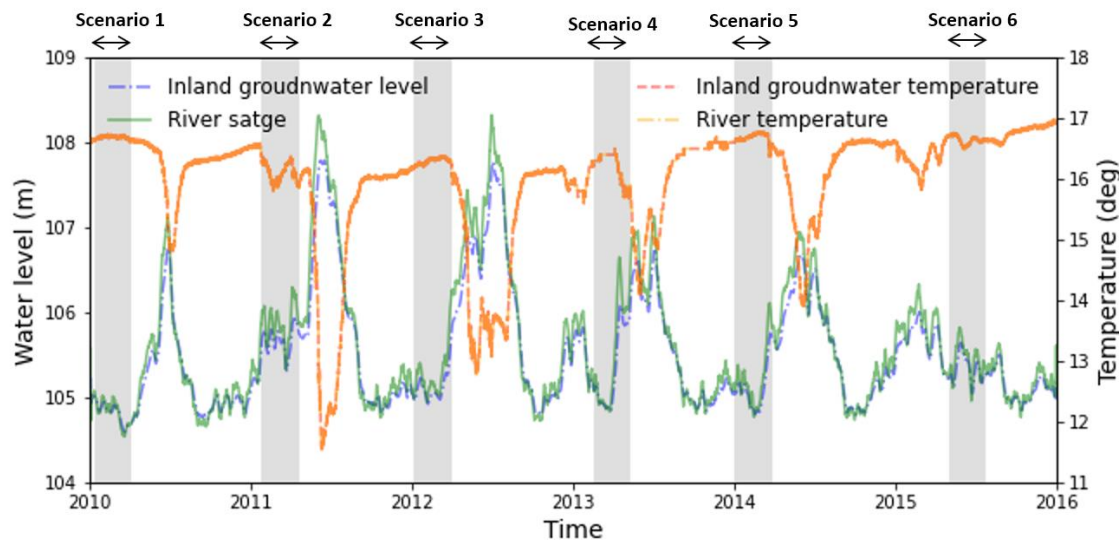


图 5-3 河流和地下水水位、水温 2010 年~2015 年时变化曲线图。灰色区域代表本文所考虑的 6 个气候场景，其中每个场景时长 12 周。

Figure 5-3 Time series of hourly river stage, groundwater elevation at the model inland boundary, temperature of the river water and groundwater at simulation times from 1 January 2010 to 31 December 2015. The grey areas demonstrate the six scenario periods under six different years, each of which has a length of 12 weeks.

- (2) Flow process (P_f). The permeability of Hanford formation can be parameterized as either homogeneous or heterogeneous. The permeability and the thickness of the alluvial layer are two random parameters. Dai et al. (2019) further separate the flow process into a geology sub-process (P_G) and a permeability sub-process (P_P).

The geology sub-process has five competing geological configurations of the alluvial layer thickness but does not have parametric uncertainty; the permeability sub-process does not have process model uncertainty but parametric uncertainty for permeability (Figure 5-4). For each of the five different thicknesses, 100 different realizations were generated for the reaction rates and permeability fields combination using the Latin Hypercube Sampling for both heterogeneous and homogeneous within-formation permeability cases.

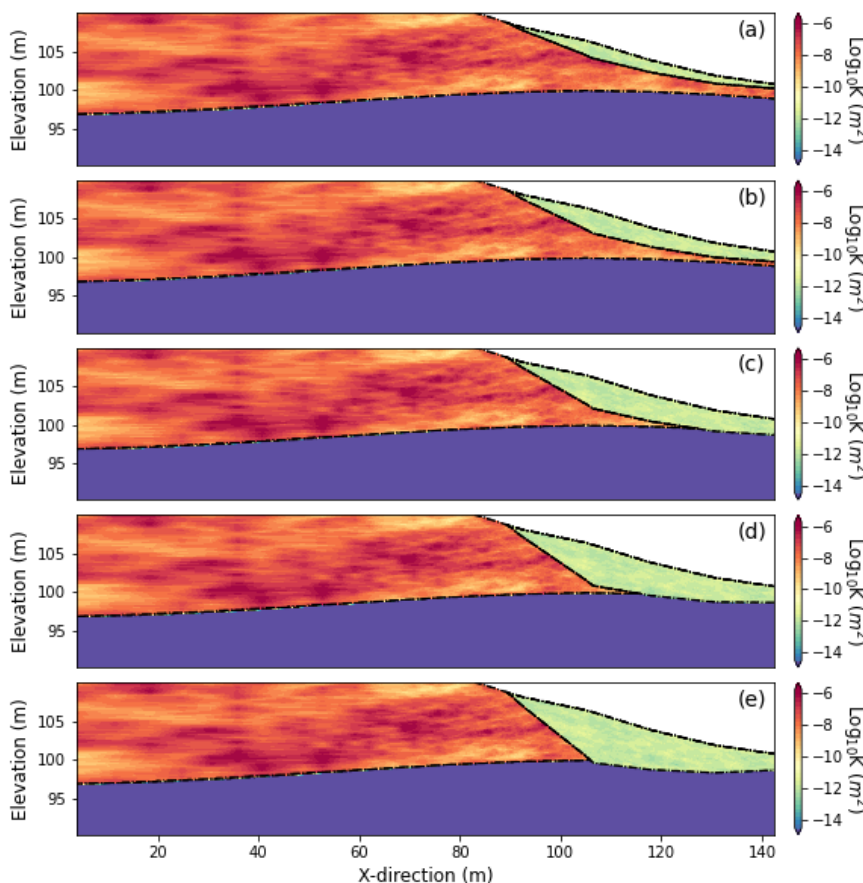


图 5-4 举例说明在冲积层厚度的五个相互竞争的地质结构下，每 100 个非均质分布渗透率场中就有一个。请注意，假设 Ringold 地层是均匀的(表 5-1)，5 个不同的冲积层厚度从(a)增加到(e)。这 5 个地质构造具有相同的渗透率地层地质统计学实现，即:我们首先为每个编队的整体建模域选择一个实现，然后为其他情况屏蔽掉编队外部的区域。

Figure 5-4 Example illustration of one out of 100 heterogenous distributed permeability fields under five competing geological configurations of the alluvial layer thickness. Note that the Ringold formation is assumed to be homogenous (Table 5-1) and the five distinct alluvial layer thickness increases from (a) to (e). The five geological configurations shared the same geostatistical realizations of permeability formation, that is, we first selected a realization for the whole modeling domain for each formation and then masked the areas that fall outside of the formation for the other case.

-
- (3) Heat process (P_H). There are two options to either consider or ignore heat transport. If heat transport is modeled, the reaction rates are temperature dependent; otherwise, reaction rates are temperature independent. There is no parametric uncertainty related to the heat process.
 - (4) Reaction process (P_R). There is no process model uncertainty to represent reactions related to organic carbon consumption, but the reaction rates are random. The reaction rates of r_1 , r_2 , and r_3 were assumed to follow uniform distributions ranging from 0 to twice of their mean values, i.e., 28.26, 23.28, and $84.78 \text{ mol} \cdot \text{L}^{-1} \cdot \text{day}^{-1}$, respectively.

The discussion above indicates complexity of the sensitivity analysis in the following senses: (1) the climate and heat processes have only process model uncertainty but not parametric uncertainty, (2) the reaction process does not have process model uncertainty but only parametric uncertainty, and (3) the flow process has both process model and parameter uncertainties.

§5.3 Identifying the Controlling Processes to OC Consumption Rate

5.3.1 Simulation Results

The total number of model simulations considering all possible combinations of model inputs and model configuration is $6 \times 5 \times 2 \times 2 \times 100 = 12,000$, which represents six scenarios, five thicknesses of alluvium layer, heterogeneous/homogeneous formations, with/without heat transport process, and 100 reaction rates and permeability fields. The concentration of river tracer and organic carbon consumption rate are the two primary outputs of our interest. The concentration of river tracer is the marker of the hydrologic exchange between the groundwater and river water, driven by the hydraulic gradient between the river and the underlying groundwater aquifer. The carbon consumption rate is the most important indicator for the biogeochemical processes because it is the energy source for all biogeochemical reactions in the reaction network of the underlying system. The wall clock time of model simulation for each realization was approximately 15 min using 128 cores on the Hopper supercomputer at the National Energy Research Scientific Computing Center (NERSC).

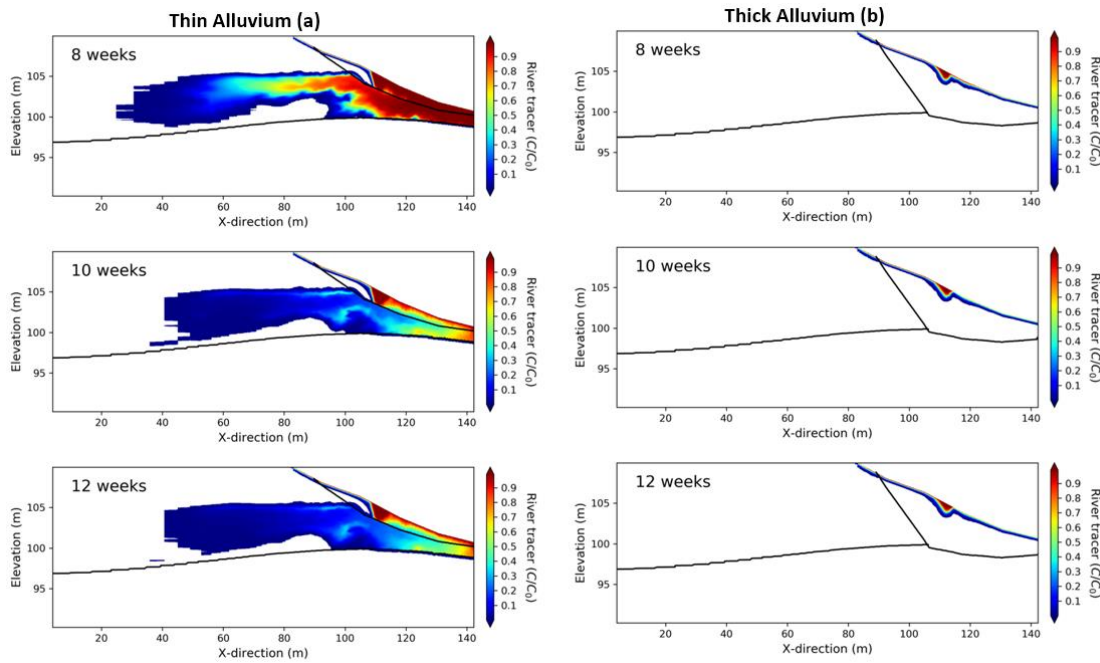


图 5-5 模拟时间为 8 周、10 周、12 周时，标准化河流示踪剂浓度的空间分布。左侧一列为最薄的 Alluvium 层厚，右侧一列为最厚的 Alluvium 层厚。考虑气候场景 1，均值渗透系数和热传输过程。

Figure 5-5 Snapshots of normalized river tracer concentration at the three different simulation times under scenario 1 using two distinct thicknesses of the alluvium layer. The homogeneous formation and heat transport process were used.

Figures 5-5 and 5-6 illustrate the snapshots of simulated normalized river tracer concentration (C/C_0) and simulated OC consumption rate in the aquifer at the end of the eighth, tenth, and twelfth weeks of simulation under scenario 1 for two distinct thicknesses of the alluvial layer, respectively. Figure 5-5 shows that the alluvial thickness plays a significant role in controlling the spatial extent of river water intrusion. The river tracer plume first spread from the alluvial layer to the Hanford formation then started to retreat from the aquifer. Thus, the low-permeability alluvial layer acts as a resistance layer to the river water intrusion. In case of a thick alluvium layer, the river water was constrained to intrude into the aquifer and consequently, the zone that is biogeochemically active appeared to be smaller considering the river provides the primary organic carbon source for all the biogeochemical reactions with oxygenated conditions on both ends of the domain. Besides, there was negligible river tracer and carbon consumption in the Ringold formation because its low permeability prevents river water infiltration. As each reaction consumed OC, the OC consumption rate was adopted as key criteria in the study of Song et al. (2018) to identify the biogeochemical reaction hot spots and hot monuments.

Thus this study also focused on OC consumption rate and tried to identifying the impacts of different processes on the biogeochemical activities in the next section.

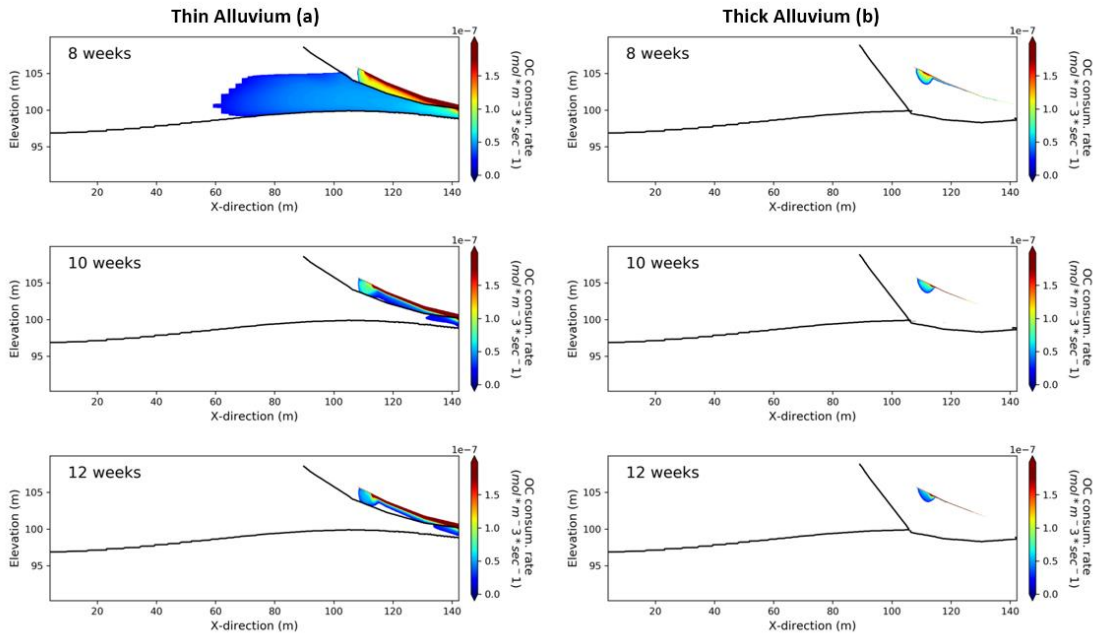


图 5-6 模拟时间为 8 周、10 周、12 周时，有机碳 OC 消耗速率的空间分布。左侧一列为最薄的 Alluvium 层厚，右侧一列为最厚的 Alluvium 层厚。考虑气候场景 1，均值渗透系数和热传
输过程。

Figure 5-6 OC consumption rate at the three different simulation times under scenario 1 using two distinct thicknesses of the alluvium layer. The homogeneous formation and heat transport process were used.

5.3.2 First-order Process Sensitivity Indices for Identifying the Important processes

According to Section 2.5.3, the first-order process sensitivity index measures the main effect of a process. It quantifies how much the variance of the model response is reduced if the corresponding process could be learned, according to which the importance of the process can be identified. In this case, the first-order process sensitivity indices of the four processes are defined as:

$$PS_{P_S} = \frac{V_{M_{P_S}}(E_{M_{P_S}}[\Delta | M_{P_S}])}{V(\Delta)} \text{ for climate process,} \quad (5.6)$$

$$PS_{P_F} = \frac{V_{M_{P_F}}(E_{M_{P_F}}[\Delta | M_{P_F}])}{V(\Delta)} \text{ for flow process,} \quad (5.7)$$

$$PS_{P_H} = \frac{V_{M_{P_H}}(E_{M_{\sim P_H}}[\Delta | M_{P_H}])}{V(\Delta)} \text{ for heat process,} \quad (5.8)$$

$$PS_{P_R} = \frac{V_{M_{P_R}}(E_{M_{\sim P_R}}[\Delta | M_{P_R}])}{V(\Delta)} \text{ for reaction process.} \quad (5.9)$$

Equations (5.6) ~ (5.9) can be further expanded to parameter level to include the parametric uncertainty of permeability fields and reaction rates. Taking PS_{P_S} as an example, the $V_{M_{P_S}}(E_{M_{\sim P_S}}[\Delta | M_{P_S}])$ term of Equation (5.4) can be rewritten as

$$V_{M_{P_S}}(E_{M_{\sim P_S}}[\Delta | M_{P_S}]) = E_{M_{P_S}} \left(E_{M_{\sim P_S}}[\Delta | M_{P_S}] \right)^2 - \left(E_{M_{P_S}}(E_{M_{\sim P_S}}[\Delta | M_{P_S}]) \right)^2. \quad (5.10)$$

where \mathbf{M}_{P_S} denotes the six climate scenarios of climate process and M_{P_S} is a single plausible climate scenario; $\mathbf{M}_{\sim P_S}$ denotes the set of process model combinations of the other three processes except for climate process. According to the law of total exception, Equation (5.6) can be expanded to the parameter level as

$$\begin{aligned} & V_{M_{P_S}}(E_{M_{\sim P_S}}[\Delta | M_{P_S}]) \\ &= E_{M_{P_S}} E_{\theta_{P_S} | M_{P_S}} (E_{M_{\sim P_S}} E_{\theta_{\sim P_S} | M_{\sim P_S}} [\Delta | \theta_{P_S}, M_{P_S}, \theta_{\sim P_S}, M_{\sim P_S}])^2 \\ &\quad - (E_{M_{P_S}} E_{\theta_{P_S} | M_{P_S}} E_{M_{\sim P_S}} E_{\theta_{\sim P_S} | M_{\sim P_S}} [\Delta | \theta_{P_S}, M_{P_S}, \theta_{\sim P_S}, M_{\sim P_S}])^2, \quad (5.11) \\ &= E_{M_{P_S}} E_{\theta_{P_S} | M_{P_S}} (E_{M_{P_F, P_H, P_R}} E_{\theta_{P_F, P_H, P_R} | M_{P_F, P_H, P_R}} [\Delta | \theta_{P_S}, M_{P_S}, \theta_{P_F, P_H, P_R}, M_{P_F, P_H, P_R}])^2 \\ &\quad - (E_{M_{P_S}} E_{\theta_{P_S} | M_{P_S}} E_{M_{P_F, P_H, P_R}} E_{\theta_{P_F, P_H, P_R} | M_{P_F, P_H, P_R}} [\Delta | \theta_{P_S}, M_{P_S}, \theta_{P_F, P_H, P_R}, M_{P_F, P_H, P_R}])^2 \end{aligned}$$

where the subscript of $\theta_{P_S} | M_{P_S}$ of $E_{\theta_{P_S} | M_{P_S}}$ indicates that the expectation is with respect to random parameter θ_{P_S} specific to climate scenario M_{P_S} ; the subscript of $\theta_{P_F, P_H, P_R} | M_{P_F, P_H, P_R}$ of $E_{\theta_{P_F, P_H, P_R} | M_{P_F, P_H, P_R}}$ indicates that the expectation is with respect to random parameter combination θ_{P_F, P_H, P_R} specific to process model combination M_{P_F, P_H, P_R} . We assume the selections of the process models are independent, e.g., employment of which of the six climate scenarios would not affect our selection of the flow models and section of the flow model would not affect whether the heat transport

process would be simulated or not. The parameters embedded in the process models are also assumed to be independent. Equation (5.11) can be rewritten as:

$$\begin{aligned} & V_{P_S}(E_{\sim P_S}[\Delta | M_{P_S}]) \\ &= E_{M_{P_S}} E_{\theta_{P_S} | M_{P_S}} \left(\frac{E_{M_{P_F}} E_{\theta_{P_F} | M_{P_F}} E_{M_{P_H}} E_{\theta_{P_H} | M_{P_H}} E_{M_{P_R}} E_{\theta_{P_R} | M_{P_R}}}{[\Delta | \theta_{P_S}, M_{P_S}, \theta_{P_F}, M_{P_F}, \theta_{P_H}, M_{P_H}, \theta_{P_R}, M_{P_R}]} \right)^2. \\ & - \left(\frac{E_{M_{P_S}} E_{\theta_{P_S} | M_{P_S}} E_{M_{P_F}} E_{\theta_{P_F} | M_{P_F}} E_{M_{P_H}} E_{\theta_{P_H} | M_{P_H}} E_{M_{P_R}} E_{\theta_{P_R} | M_{P_R}}}{[\Delta | \theta_{P_S}, M_{P_S}, \theta_{P_F}, M_{P_F}, \theta_{P_H}, M_{P_H}, \theta_{P_R}, M_{P_R}]} \right)^2 \end{aligned} \quad (5.12)$$

Since there is no parametric uncertainty in climate process (P_S) and heat process (P_H), the two items $E_{\theta_{P_S} | M_{P_S}}$, and $E_{\theta_{P_H} | M_{P_H}}$ disappear; and there is no model uncertainty in reaction process, item $E_{M_{P_R}}$ disappears. Equation (5.12) is simplified to

$$\begin{aligned} & V_{P_S}(E_{\sim P_S}[\Delta | M_{P_S}]) \\ &= E_{M_{P_S}} (E_{M_{P_F}} E_{\theta_{P_F} | M_{P_F}} E_{M_{P_H}} E_{\theta_{P_F}} [\Delta | M_{P_S}, \theta_{P_F}, M_{P_F}, M_{P_H}, \theta_{P_R}])^2. \\ & - (E_{M_{P_S}} E_{M_{P_F}} E_{\theta_{P_F} | M_{P_F}} E_{M_{P_H}} E_{\theta_{P_F}} [\Delta | M_{P_S}, \theta_{P_F}, M_{P_F}, M_{P_H}, \theta_{P_R}])^2 \end{aligned} \quad (5.13)$$

The flow process is further decomposed into geological module (P_G) and permeability module (P_P). According to the law of total exception, $E_{M_{P_F}} E_{\theta_{P_F} | M_{P_F}}$ can be rewritten as

$E_{M_{P_G}} E_{M_{P_P}} E_{\theta_{P_P} | M_{P_P}}$. Equation (5.12) becomes

$$\begin{aligned} & V_{P_S}(E_{\sim P_S}[\Delta | M_{P_S}]) \\ &= E_{M_{P_S}} \left(\frac{E_{M_{P_G}} E_{M_{P_P}} E_{\theta_{P_P} | M_{P_P}} E_{M_{P_H}} E_{\theta_{P_R}}}{[\Delta | M_{P_S}, \theta_{P_P}, M_{P_P}, M_{P_G}, M_{P_H}, \theta_{P_R}]} \right)^2. \\ & - \left(\frac{E_{M_{P_S}} E_{M_{P_G}} E_{M_{P_P}} E_{\theta_{P_P} | M_{P_P}} E_{M_{P_H}} E_{\theta_{P_R}}}{[\Delta | M_{P_S}, \theta_{P_P}, M_{P_P}, M_{P_G}, M_{P_H}, \theta_{P_R}]} \right)^2 \end{aligned} \quad (5.14)$$

Given the reaction rate and permeability values are generated using Latin Hypercube Sampling and paired with each other, equation (5.12) can be re-arranged as

$$V_{P_S}(E_{\sim P_S}[\Delta | M_{P_S}]) = E_{M_{P_S}} \left(\frac{E_{M_{P_G}} E_{M_{P_P}} E_{M_{P_H}} E_{\theta_{P_R}, \theta_{P_p}|M_{P_p}}}{[\Delta | M_{P_S}, \theta_{P_R, P_p}, M_{P_G}, M_{P_P}, M_{P_H}]} \right)^2, \quad (5.15)$$

$$- \left(\frac{E_{M_{P_S}} E_{M_{P_G}} E_{M_{P_P}} E_{\theta_{P_p}|M_{P_p}} E_{M_{P_H}} E_{\theta_{P_R}}}{[\Delta | M_{P_S}, \theta_{P_p}, M_{P_P}, M_{P_G}, M_{P_H}, \theta_{P_R}]} \right)^2,$$

Similarly, the $V_{P_F}(E_{\sim P_F}[\Delta | M_{P_F}])$ of Equation (5.7), $V_{P_H}(E_{\sim P_H}[\Delta | M_{P_H}])$ of Equation (5.8), and $V_{P_R}(E_{\sim P_R}[\Delta | M_{P_R}])$ of Equation (5.9) can be derived as

$$V_{M_{P_F}}(E_{M_{\sim P_F}}[\Delta | M_{P_F}])$$

$$= E_{M_{P_G}} E_{M_{P_P}} E_{\theta_{P_p}^{bin}|M_{P_p}} \left(E_{M_{P_S}} E_{M_{P_H}} E_{\theta_{P_R}} [\Delta | M_{P_G}, \theta_{P_p}^{bin}, M_{P_p}, M_{P_S}, M_{P_H}, \theta_{P_R}] \right)^2, \quad (5.16)$$

$$- \left(E_{M_{P_G}} E_{M_{P_P}} E_{\theta_{P_p}^{bin}|M_{P_p}} E_{M_{P_S}} E_{M_{P_H}} E_{\theta_{P_R}} [\Delta | M_{P_G}, \theta_{P_p}^{bin}, M_{P_p}, M_{P_S}, M_{P_H}, \theta_{P_R}] \right)^2$$

$$V_{M_{P_H}}(E_{M_{\sim P_H}}[\Delta | M_{P_H}])$$

$$= E_{M_{P_H}} \left(E_{M_{P_S}} E_{M_{P_G}} E_{M_{P_P}} E_{\theta_{P_R}, \theta_{P_p}|M_{P_p}} [\Delta | M_{P_H}, M_{P_S}, \theta_{P_R, P_p}, M_{P_G}, M_{P_P}] \right)^2, \quad (5.17)$$

$$- \left(E_{M_{P_H}} E_{M_{P_S}} E_{M_{P_G}} E_{M_{P_P}} E_{\theta_{P_R}, \theta_{P_p}|M_{P_p}} [\Delta | M_{P_H}, M_{P_S}, \theta_{P_R, P_p}, M_{P_G}, M_{P_P}] \right)^2$$

$$V_{M_{P_R}}(E_{M_{\sim P_R}}[\Delta | M_{P_R}])$$

$$= E_{\theta_{P_R}^{bin}} \left(E_{M_{P_S}} E_{M_{P_G}} E_{M_{P_P}} E_{\theta_{P_p}|M_{P_p}} E_{M_{P_H}} [\Delta | M_{P_S}, \theta_{P_R}^{bin}, \theta_{P_p}, M_{P_p}, M_{P_G}, M_{P_H}] \right)^2, \quad (5.18)$$

$$- \left(E_{\theta_{P_R}^{bin}} E_{M_{P_S}} E_{M_{P_G}} E_{M_{P_P}} E_{\theta_{P_p}|M_{P_p}} E_{M_{P_H}} [\Delta | M_{P_S}, \theta_{P_R}^{bin}, \theta_{P_p}, M_{P_p}, M_{P_G}, M_{P_H}] \right)^2$$

Because the permeability and reaction rates are paired with each other, the binning method is used when evaluating the first-order process sensitivity indices of flow process and reaction process. Details of the binning method are referred to Dai et al. (2017b).

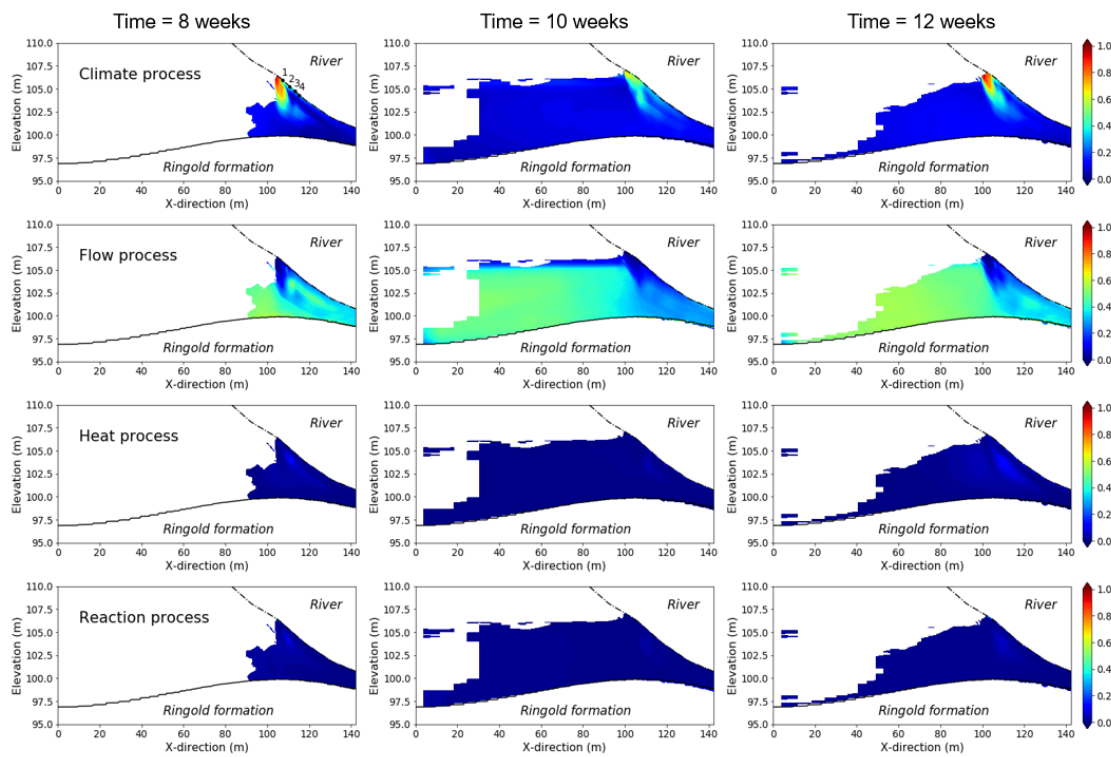


图5-8 模拟时间为8周、10周、12周时，气候情景(P_S)、地下水水流(P_F)、热运移(P_H)和反应运移过程(P_R)的一阶过程敏感性分析指标的空间分布。每一行对应四个相应的过程，每一列对应三个相应的模拟时间。

Figure 5-7 Spatial distribution of first-order process sensitivity analysis indices for climate, flow, heat, and reaction processes at the simulation times of 8, 10, and 12 weeks. The four rows and three columns are corresponding to the four processes and three simulation times, respectively.

The sensitivity indices corresponding to four primary model input uncertainty sources at the process level, that is, climate process, flow process, heat process, and reaction process, were calculated for the carbon-consumption rates at simulation times of 8, 10, and 12 weeks after the starting point based on Equations (2) ~ (5). The spatially distributed sensitivity indices are shown in Figure 5-7 at simulation times of 8, 10, and 12 weeks considered in Dai et al. (2019), including only the grid cells with carbon-consumption rate greater than of $1 \times 10^{-7} \text{ mol} \cdot \text{m}^{-3} \cdot \text{s}^{-1}$ for all 12,000 simulation runs to avoid numerical artifact.

Figure 5-7 shows that the flow process contributes significant uncertainties to the carbon-consumption rate at all simulation times in most of the biogeochemically active zones followed by the climate process. The four points of the first subplot in Figure 5-7 are located at the river-sediment interface, and their elevations are 105.97m, 105.23m, 104.76m, and 104.36m, which are the 90th, 50th, 10th, and 0th percentiles of the river stage

levels across the six climate scenarios, respectively. The climate process contributed the most uncertainty in small areas within the river stage fluctuation range above the 50th percentiles where the saturation-desaturation dynamics controlled the biogeochemical reactions. The heat transport process and reactive transport process seem to contribute little to the overall uncertainty, reflected by their small sensitivity indices across the model domain (< 0.1). This means that to improve the performance of simulation results of OC consumption rate, we need to improve our knowledge (i.e., the uncertainty) on flow process by figuring out the real geological structure and the permeability fields.

5.3.3 Total-effect Process Sensitivity Indices for Identifying Influential Processes

The total-effect process sensitivity index considers not only the main effect of a process but also the process interactions. According to Section 2.5.3, the total-effect process sensitivity indices of the four processes in this case are defined as:

$$PST_{P_S} = 1 - \frac{V_{M_{\sim P_S}}(E_{M_{P_S}}[\Delta | M_{\sim P_S}])}{V(\Delta)} \text{ for climate process,} \quad (5.19)$$

$$PST_{P_F} = 1 - \frac{V_{M_{\sim P_F}}(E_{M_{P_F}}[\Delta | M_{\sim P_F}])}{V(\Delta)} \text{ for flow process,} \quad (5.20)$$

$$PST_{P_H} = 1 - \frac{V_{M_{\sim P_H}}(E_{M_{P_H}}[\Delta | M_{\sim P_H}])}{V(\Delta)} \text{ for heat process,} \quad (5.21)$$

$$PST_{P_R} = 1 - \frac{V_{M_{\sim P_R}}(E_{M_{P_R}}[\Delta | M_{\sim P_R}])}{V(\Delta)} \text{ for reaction process.} \quad (5.22)$$

Similar to the derivation of the first-order process sensitivity index, Equations (5.19) ~ (5.22) can be further expanded to parameter level to handle both random process models and random process model parameters for process sensitivity analysis. Taking PST_{P_S} as

an example, the $V_{M_{\sim P_S}}(E_{M_{P_S}}[\Delta | M_{\sim P_S}])$ term of Equation (5.19) can be rewritten as

$$\begin{aligned} & V_{M_{\sim P_S}}(E_{M_{P_S}}[\Delta | M_{\sim P_S}]) \\ &= E_{M_{\sim P_S}} \left(E_{M_{P_S}}[\Delta | M_{\sim P_S}] \right)^2 - \left(E_{M_{\sim P_S}}(E_{M_{P_S}}[\Delta | M_{\sim P_S}]) \right)^2 \end{aligned} \quad (5.23)$$

According to the law of total exception, Equation (5.23) can be expanded to the parameter level as

$$\begin{aligned}
 & V_{M_{\sim P_S}}(E_{M_{P_S}}[\Delta | M_{\sim P_S}]) \\
 &= E_{M_{\sim P_S}} E_{\theta_{\sim P_S} | M_{\sim P_S}} (E_{M_{P_S}} E_{\theta_{P_S} | M_{P_S}} [\Delta | \theta_{P_S}, M_{\sim P_S}, \theta_{P_S}, M_{P_S}])^2 \\
 &\quad - (E_{M_{\sim P_S}} E_{\theta_{\sim P_S} | M_{\sim P_S}} E_{M_{P_S}} E_{\theta_{P_S} | M_{P_S}} [\Delta | \theta_{P_S}, M_{\sim P_S}, \theta_{P_S}, M_{P_S}])^2 \\
 &= E_{M_{P_F, P_H, P_R}} E_{\theta_{P_F, P_H, P_R} | M_{P_F, P_H, P_R}} (E_{M_{P_S}} E_{\theta_{P_S} | M_{P_S}} [\Delta | \theta_{P_F, P_H, P_R}, M_{P_F, P_H, P_R}, \theta_{P_S}, M_{P_S}])^2 \\
 &\quad - (E_{M_{P_F, P_H, P_R}} E_{\theta_{P_F, P_H, P_R} | M_{P_F, P_H, P_R}} E_{M_{P_S}} E_{\theta_{P_S} | M_{P_S}} [\Delta | \theta_{P_F, P_H, P_R}, M_{P_F, P_H, P_R}, \theta_{P_S}, M_{P_S}])^2
 \end{aligned} \tag{5.24}$$

Under the assumptions that the selections of the process models are independent, and the parameters embedded in the process models are also independent, Equation (5.24) can be written as

$$\begin{aligned}
 & V_{M_{\sim P_S}}(E_{M_{P_S}}[\Delta | M_{\sim P_S}]) \\
 &= E_{M_{P_F}} E_{\theta_{P_F} | M_{P_F}} E_{M_{P_H}} E_{\theta_{P_H} | M_{P_H}} E_{M_{P_R}} E_{\theta_{P_R} | M_{P_R}} \left(\frac{E_{M_{P_S}} E_{\theta_{P_S} | M_{P_S}}}{[\Delta | \theta_{P_F}, M_{P_F}, \theta_{P_H}, M_{P_H}, \theta_{P_R}, M_{P_R}, \theta_{P_S}, M_{P_S}]} \right)^2 \\
 &\quad - \left(\frac{E_{M_{P_F}} E_{\theta_{P_F} | M_{P_F}} E_{M_{P_H}} E_{\theta_{P_H} | M_{P_H}} E_{M_{P_R}} E_{\theta_{P_R} | M_{P_R}} E_{M_{P_S}} E_{\theta_{P_S} | M_{P_S}}}{[\Delta | \theta_{P_F}, M_{P_F}, \theta_{P_H}, M_{P_H}, \theta_{P_R}, M_{P_R}, \theta_{P_S}, M_{P_S}]} \right)^2
 \end{aligned} \tag{5.25}$$

Since there is no parametric uncertainty in climate process and heat process, the two items $E_{\theta_{P_S} | M_{P_S}}$ and $E_{\theta_{P_H} | M_{P_H}}$ disappear; and there is no model uncertainty in reaction process, item $E_{M_{P_R}}$ disappear.

$$\begin{aligned}
 & V_{M_{\sim P_S}}(E_{M_{P_S}}[\Delta | M_{\sim P_S}]) \\
 &= E_{M_{P_F}} E_{\theta_{P_F} | M_{P_F}} E_{M_{P_H}} E_{\theta_{P_H} | M_{P_H}} (E_{M_{P_S}} [\Delta | \theta_{P_F}, M_{P_F}, M_{P_H}, \theta_{P_R}, M_{P_S}])^2 \\
 &\quad - (E_{M_{P_F}} E_{\theta_{P_F} | M_{P_F}} E_{M_{P_H}} E_{\theta_{P_H} | M_{P_H}} E_{M_{P_S}} [\Delta | \theta_{P_F}, M_{P_F}, M_{P_H}, \theta_{P_R}, M_{P_S}])^2
 \end{aligned} \tag{5.26}$$

Considering the groundwater flow process can be further decomposed by geological module (P_G) and permeability module (P_P), Equation (5.26) can be rewritten as:

$$\begin{aligned}
 & V_{M_{\sim P_S}}(E_{M_{P_S}}[\Delta | M_{\sim P_S}]) \\
 &= E_{M_{P_G}} E_{M_{P_P}} E_{\theta_{P_P} | M_{P_P}} E_{M_{P_H}} E_{\theta_{P_H} | M_{P_H}} (E_{M_{P_S}} [\Delta | \theta_{P_P}, M_{P_G}, M_{P_P}, M_{P_H}, \theta_{P_R}, M_{P_S}])^2 \\
 &\quad - (E_{M_{P_G}} E_{M_{P_P}} E_{\theta_{P_P} | M_{P_P}} E_{M_{P_H}} E_{\theta_{P_H} | M_{P_H}} E_{M_{P_S}} [\Delta | \theta_{P_P}, M_{P_G}, M_{P_P}, M_{P_H}, \theta_{P_R}, M_{P_S}])^2
 \end{aligned} \tag{5.27}$$

Given the reaction rate and permeability values are generated using LHS and paired with each other, Equation (5.27) can be re-arranged as

$$\begin{aligned}
& V_{M_{\sim P_S}}(E_{M_{P_S}}[\Delta | M_{\sim P_S}]) \\
& = E_{M_{P_G}} E_{M_{P_P}} E_{M_{P_H}} E_{\theta_{P_R}, \theta_{P_R}|M_{P_P}} (E_{M_{P_S}}[\Delta | \theta_{P_R, P_P}, M_{P_G}, M_{P_P}, M_{P_H}, M_{P_S}])^2 \\
& \quad - (E_{M_{P_G}} E_{M_{P_P}} E_{M_{P_H}} E_{\theta_{P_R}, \theta_{P_R}|M_{P_P}} E_{M_{P_S}}[\Delta | \theta_{P_R, P_P}, M_{P_G}, M_{P_P}, M_{P_H}, M_{P_S}])^2
\end{aligned} \quad (5.28)$$

Similarly, the $V_{M_{\sim P_F}}(E_{M_{P_F}}[\Delta | M_{\sim P_F}])$ of Equation (5-20), $V_{M_{\sim P_H}}(E_{M_{P_H}}[\Delta | M_{\sim P_H}])$ of Equation (5-21), and $V_{M_{\sim P_R}}(E_{M_{P_R}}[\Delta | M_{\sim P_R}])$ of Equation (5-22) can be derived as

$$\begin{aligned}
& V_{M_{\sim P_F}}(E_{M_{P_F}}[\Delta | M_{\sim P_F}]) \\
& = E_{M_{P_S}} E_{M_{P_H}} E_{\theta_{P_R}^{bin}} (E_{M_{P_G}} E_{M_{P_P}} E_{\theta_{P_P}|M_{P_P}} [\Delta | M_{P_S}, M_{P_H}, \theta_{P_R}^{bin}, \theta_{P_P}, M_{P_G}, M_{P_P}])^2 \\
& \quad - (E_{M_{P_S}} E_{M_{P_H}} E_{\theta_{P_R}^{bin}} E_{M_{P_G}} E_{M_{P_P}} E_{\theta_{P_P}|M_{P_P}} [\Delta | M_{P_S}, M_{P_H}, \theta_{P_R}^{bin}, \theta_{P_P}, M_{P_G}, M_{P_P}])^2
\end{aligned} \quad (5.29)$$

$$\begin{aligned}
& V_{M_{\sim P_H}}(E_{M_{P_H}}[\Delta | M_{\sim P_H}]) \\
& = E_{M_{P_S}} E_{M_{P_G}} E_{M_{P_P}} E_{\theta_{P_R}|M_{P_P}} (E_{M_{P_H}}[\Delta | M_{P_S}, \theta_{P_R, P_P}, M_{P_G}, M_{P_P}, M_{P_H}])^2 \\
& \quad - (E_{M_{P_S}} E_{M_{P_G}} E_{M_{P_P}} E_{\theta_{P_R}|M_{P_P}} E_{M_{P_H}}[\Delta | M_{P_S}, \theta_{P_R, P_P}, M_{P_G}, M_{P_P}, M_{P_H}])^2
\end{aligned} \quad (5.30)$$

$$\begin{aligned}
& V_{M_{\sim P_R}}(E_{M_{P_R}}[\Delta | M_{\sim P_R}]) \\
& = E_{M_{P_S}} E_{M_{P_G}} E_{M_{P_P}} E_{\theta_{P_P}^{bin}|M_{P_P}} E_{M_{P_H}} (E_{\theta_{P_R}}[\Delta | M_{P_S}, \theta_{P_P}^{bin}, M_{P_G}, M_{P_P}, M_{P_H}, \theta_{P_R}])^2 \\
& \quad - (E_{M_{P_S}} E_{M_{P_G}} E_{M_{P_P}} E_{\theta_{P_P}^{bin}|M_{P_P}} E_{M_{P_H}} E_{\theta_{P_R}}[\Delta | M_{P_S}, \theta_{P_P}^{bin}, M_{P_G}, M_{P_P}, M_{P_H}, \theta_{P_R}])^2
\end{aligned} \quad (5.31)$$

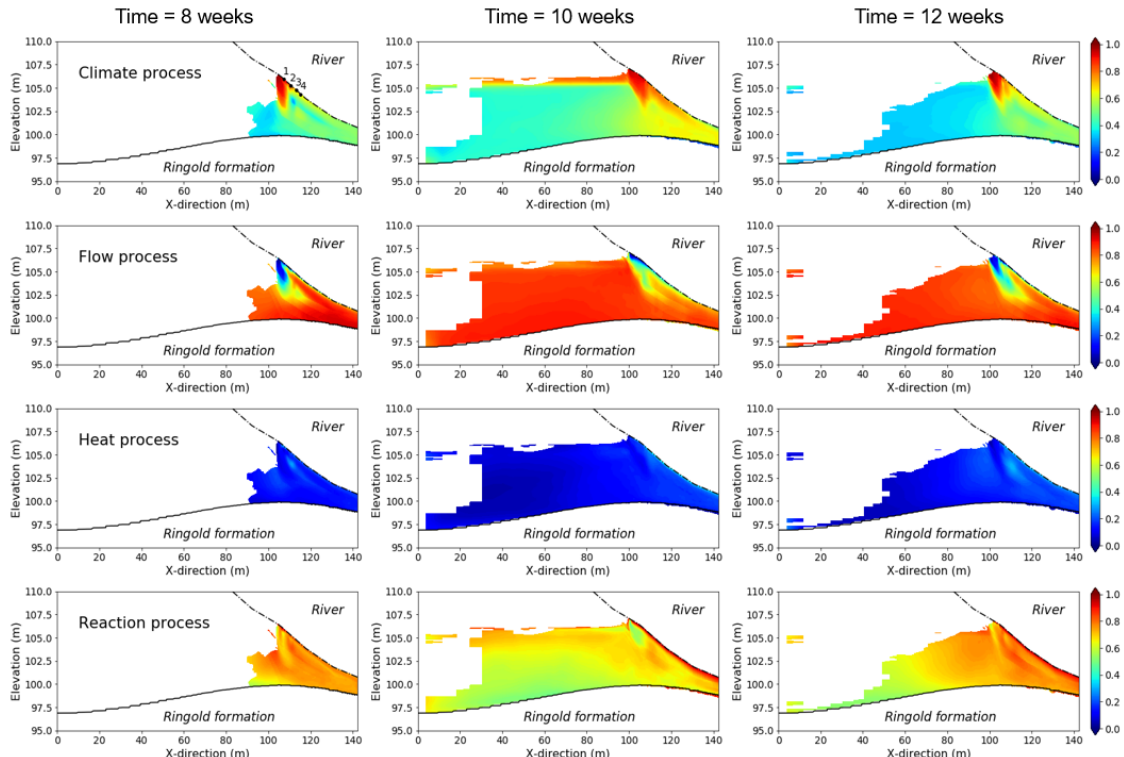


图 5-8 模拟时间为 8 周、10 周、12 周时，气候情景(P_S)、地下水流动(P_F)、热运移(P_H)和反应运移过程(P_R)的总效应过程敏感性分析指标的空间分布。

Figure 5-8 Spatial distribution of total-effect process sensitivity analysis indices for climate scenario, groundwater flow, heat transport, and reactive transport processes at the simulation times of 8, 10, and 12 weeks.

5.3.4 Second-order and Third-order Process Interactions

By virtue of the variance decomposition, Section 2.5.4 introduces the second-order process interaction is defined as:

$$PS_{K,V} = \frac{V_{K,V}(E_{\sim(K,V)}[\Delta | K, V])}{V(\Delta)} - PS_K - PS_V. \quad (5.32)$$

Since there are four processes in our case, a total of six (C_4^2) second-order process sensitivity indices can be defined. According to Equation (11), they are:

(1) the second-order process interaction between climate process and flow process:

$$PS_{P_S, P_F} = \frac{V_{P_S, P_F}(E_{\sim(P_S, P_F)}[\Delta | P_S, P_F])}{V(\Delta)} - PS_{P_S} - PS_{P_F}. \quad (5.33)$$

(2) the second-order process interaction between climate process and heat process:

$$PS_{P_S, P_H} = \frac{V_{P_S, P_H}(E_{\sim(P_S, P_H)}[\Delta | P_S, P_H])}{V(\Delta)} - PS_{P_S} - PS_{P_H}. \quad (5.34)$$

(3) the second-order process interaction between climate process and reaction process:

$$PS_{P_S, P_R} = \frac{V_{P_S, P_R}(E_{\sim(P_S, P_R)}[\Delta | P_S, P_R])}{V(\Delta)} - PS_{P_S} - PS_{P_R}. \quad (5.35)$$

(4) the second-order process interaction between flow process and heat process:

$$PS_{P_F, P_H} = \frac{V_{P_F, P_H}(E_{\sim(P_F, P_H)}[\Delta | P_F, P_H])}{V(\Delta)} - PS_{P_F} - PS_{P_H}. \quad (5.36)$$

(5) the second-order process interaction between flow process and reaction process:

$$PS_{P_F, P_R} = \frac{V_{P_F, P_R}(E_{\sim(P_F, P_R)}[\Delta | P_F, P_R])}{V(\Delta)} - PS_{P_F} - PS_{P_R}. \quad (5.37)$$

(6) the second-order process interaction between heat process and reaction process:

$$PS_{P_H, P_R} = \frac{V_{P_H, P_R}(E_{\sim(P_H, P_R)}[\Delta | P_H, P_R])}{V(\Delta)} - PS_{P_H} - PS_{P_R}. \quad (5.38)$$

Equations (5.32) ~ (5.38) enables us to consider the second-order process interaction effects between any two of the four processes. These equations can also be expanded to the parameter level. Taking the second-order process interaction between climate process and flow process as an example, the $V_{P_H, P_R}(E_{\sim(P_H, P_R)}[\Delta | P_H, P_R])$ term of Equation (5.33) can be rewritten as

$$\begin{aligned} & V_{P_S, P_F}(E_{\sim(P_S, P_F)}[\Delta | P_S, P_F]) \\ &= V_{M_{P_S, P_F}}(E_{M_{\sim(P_S, P_F)}}[\Delta | M_{P_S, P_F}]) \\ &= E_{M_{P_S, P_F}} \left(E_{M_{\sim(P_S, P_F)}}[\Delta | P_S, P_F] \right)^2 - \left(E_{M_{P_S, P_F}} E_{M_{\sim(P_S, P_F)}}[\Delta | P_S, P_F] \right)^2. \end{aligned} \quad (5.39)$$

According to the law of total exception, Equation (S18) can be expanded to the parameter level as

$$\begin{aligned} & V_{P_S, P_F}(E_{\sim(P_S, P_F)}[\Delta | P_S, P_F]) \\ &= E_{M_{P_S, P_F}} E_{\theta_{P_S, P_F} | M_{P_S, P_F}} (E_{M_{\sim(P_S, P_F)}} E_{\theta_{\sim(P_S, P_F)} | M_{\sim(P_S, P_F)}} [\Delta | \theta_{P_S, P_F}, M_{P_S, P_F}, \theta_{\sim(P_S, P_F)}, M_{\sim(P_S, P_F)}])^2 \\ &\quad - (E_{M_{P_S, P_F}} E_{\theta_{P_S, P_F} | M_{P_S, P_F}} E_{M_{\sim(P_S, P_F)}} E_{\theta_{\sim(P_S, P_F)} | M_{\sim(P_S, P_F)}} [\Delta | \theta_{P_S, P_F}, M_{P_S, P_F}, \theta_{\sim(P_S, P_F)}, M_{\sim(P_S, P_F)}])^2. \quad (5.40) \\ &= E_{M_{P_S, P_F}} E_{\theta_{P_S, P_F} | M_{P_S, P_F}} (E_{M_{P_H, P_R}} E_{\theta_{P_H, P_R} | M_{P_H, P_R}} [\Delta | \theta_{P_S, P_F}, M_{P_S, P_F}, \theta_{P_H, P_R}, M_{P_H, P_R}])^2 \\ &\quad - (E_{M_{P_S, P_F}} E_{\theta_{P_S, P_F} | M_{P_S, P_F}} E_{M_{P_H, P_R}} E_{\theta_{P_H, P_R} | M_{P_H, P_R}} [\Delta | \theta_{P_S, P_F}, M_{P_S, P_F}, \theta_{P_R, P_H}, M_{P_H, P_R}])^2 \end{aligned}$$

Under the assumptions that the selections of the process models are independent, and the parameters embedded in the process models are also independent, Equation (S19) can be written as

$$\begin{aligned} & V_{P_S, P_F}(E_{\sim(P_S, P_F)}[\Delta | P_S, P_F]) \\ &= E_{M_{P_S}} E_{M_{P_F}} E_{\theta_{P_S} | M_{P_S}} E_{\theta_{P_F} | M_{P_F}} \left(\frac{E_{M_{P_H}} E_{M_{P_R}} E_{\theta_{P_H} | M_{P_H}} E_{\theta_{P_R} | M_{P_R}}}{[\Delta | \theta_{P_S}, M_{P_S}, \theta_{P_F}, M_{P_F}, \theta_{P_H}, M_{P_H}, \theta_{P_R}, M_{P_R}]} \right)^2. \quad (5.41) \\ &\quad - \left(\frac{E_{M_{P_S}} E_{M_{P_F}} E_{\theta_{P_S} | M_{P_S}} E_{\theta_{P_F} | M_{P_F}} E_{M_{P_H}} E_{M_{P_R}} E_{\theta_{P_H} | M_{P_H}} E_{\theta_{P_R} | M_{P_R}}}{[\Delta | \theta_{P_S}, M_{P_S}, \theta_{P_F}, M_{P_F}, \theta_{P_H}, M_{P_H}, \theta_{P_R}, M_{P_R}]} \right)^2 \end{aligned}$$

Since there is no parametric uncertainty in climate process and heat process, the two items $E_{\theta_{P_S} | M_{P_S}}$, and $E_{\theta_{P_H} | M_{P_H}}$ disappear; and there is no model uncertainty in reaction process, item $E_{M_{P_R}}$ disappear:

$$\begin{aligned}
& V_{P_S, P_F} (E_{\sim(P_S, P_F)} [\Delta | P_S, P_F]) \\
& = E_{M_{P_S}} E_{M_{P_F}} E_{\theta_{P_F} | M_{P_F}} (E_{M_{P_H}} E_{\theta_{P_R}} [\Delta | M_{P_S}, \theta_{P_F}, M_{P_F}, M_{P_H}, \theta_{P_R}])^2 , \\
& - (E_{M_{P_S}} E_{M_{P_F}} E_{\theta_{P_F} | M_{P_F}} E_{M_{P_H}} E_{\theta_{P_R}} [\Delta | M_{P_S}, \theta_{P_F}, M_{P_F}, M_{P_H}, \theta_{P_R}])^2
\end{aligned} \quad (5.42)$$

Considering the groundwater flow process can be further decomposed by geological module (P_G) and permeability module (P_P), Equation (5.42) can be rewritten as:

$$\begin{aligned}
& V_{P_S, P_F} (E_{\sim(P_S, P_F)} [\Delta | P_S, P_F]) \\
& = E_{M_{P_S}} E_{M_{P_G}} E_{M_{P_P}} E_{\theta_{P_P} | M_{P_P}} (E_{M_{P_H}} E_{\theta_{P_R}} [\Delta | M_{P_S}, M_{P_G}, \theta_{P_P}, M_{P_P}, M_{P_H}, \theta_{P_R}])^2 , \\
& - (E_{M_{P_S}} E_{M_{P_G}} E_{M_{P_P}} E_{\theta_{P_P} | M_{P_P}} E_{M_{P_H}} E_{\theta_{P_R}} [\Delta | M_{P_S}, M_{P_G}, \theta_{P_P}, M_{P_P}, M_{P_H}, \theta_{P_R}])^2
\end{aligned} \quad (5.43)$$

Given the reaction rate and permeability values are generated using LHS and paired with each other, equation (S22) can be evaluated using the binning method:

$$\begin{aligned}
& V_{P_S, P_F} (E_{\sim(P_S, P_F)} [\Delta | P_S, P_F]) \\
& = E_{M_{P_S}} E_{M_{P_G}} E_{M_{P_P}} E_{\theta_{P_P}^{bin} | M_{P_P}} (E_{M_{P_H}} E_{\theta_{P_R}} [\Delta | M_{P_S}, M_{P_G}, \theta_{P_P}^{bin}, M_{P_P}, M_{P_H}, \theta_{P_R}])^2 , \\
& - (E_{M_{P_S}} E_{M_{P_G}} E_{M_{P_P}} E_{\theta_{P_P}^{bin} | M_{P_P}} E_{M_{P_H}} E_{\theta_{P_R}} [\Delta | M_{P_S}, M_{P_G}, \theta_{P_P}^{bin}, M_{P_P}, M_{P_H}, \theta_{P_R}])^2
\end{aligned} \quad (5.44)$$

Similarly, the $V_{P_S, P_H} (E_{\sim(P_S, P_H)} [\Delta | P_S, P_H])$ of Equation (13),

$V_{P_S, P_R} (E_{\sim(P_S, P_R)} [\Delta | P_S, P_R])$ of Equation (14), $V_{P_F, P_H} (E_{\sim(P_F, P_H)} [\Delta | P_F, P_H])$ of Equation (15),

$V_{P_F, P_R} (E_{\sim(P_F, P_R)} [\Delta | P_F, P_R])$ of Equation (16), and $V_{P_H, P_R} (E_{\sim(P_H, P_R)} [\Delta | P_H, P_R])$ of Equation

(17) can be derived as

$$\begin{aligned}
& V_{P_S, P_H} (E_{\sim(P_S, P_H)} [\Delta | P_S, P_H]) \\
& = E_{M_{P_S}} E_{M_{P_H}} (E_{M_{P_G}} E_{M_{P_P}} E_{\theta_{P_P} | M_{P_P}, \theta_{P_R}} [\Delta | M_{P_S}, M_{P_H}, M_{P_G}, \theta_{P_P}, M_{P_P}, \theta_{P_R}])^2 , \\
& - (E_{M_{P_S}} E_{M_{P_H}} E_{M_{P_G}} E_{M_{P_P}} E_{\theta_{P_P} | M_{P_P}, \theta_{P_R}} [\Delta | M_{P_S}, M_{P_H}, M_{P_G}, \theta_{P_P}, M_{P_P}, \theta_{P_R}])^2
\end{aligned} \quad (5.45)$$

$$\begin{aligned}
& V_{P_S, P_R} (E_{\sim(P_S, P_R)} [\Delta | P_S, P_R]) \\
& = E_{M_{P_S}} E_{\theta_{P_R}^{bin}} (E_{M_{P_H}} E_{M_{P_G}} E_{M_{P_P}} E_{\theta_{P_P} | M_{P_P}} [\Delta | M_{P_H}, M_{P_G}, \theta_{P_P}^{bin}, M_{P_P}, M_{P_S}, \theta_{P_R}])^2 , \\
& - (E_{M_{P_S}} E_{\theta_{P_R}^{bin}} E_{M_{P_H}} E_{M_{P_G}} E_{M_{P_P}} E_{\theta_{P_P} | M_{P_P}} [\Delta | M_{P_H}, M_{P_G}, \theta_{P_P}^{bin}, M_{P_P}, M_{P_S}, \theta_{P_R}])^2
\end{aligned} \quad (5.46)$$

$$\begin{aligned}
& V_{P_F, P_H} (E_{\sim(P_F, P_H)} [\Delta | P_F, P_H]) \\
& = E_{M_{P_G}} E_{M_{P_P}} E_{\theta_{P_P}^{bin} | M_{P_P}} (E_{M_{P_H}} E_{\theta_{P_R}} [\Delta | M_{P_G}, M_{P_P}, \theta_{P_P}^{bin}, M_{P_H}, M_{P_S}, \theta_{P_R}])^2 , \\
& - (E_{M_{P_G}} E_{M_{P_P}} E_{\theta_{P_P}^{bin} | M_{P_P}} E_{M_{P_H}} E_{\theta_{P_R}} [\Delta | M_{P_G}, M_{P_P}, \theta_{P_P}^{bin}, M_{P_H}, M_{P_S}, \theta_{P_R}])^2
\end{aligned} \quad (5.47)$$

$$\begin{aligned} & V_{P_R, P_F}(E_{\sim(P_R, P_F)}[\Delta | P_R, P_F]) \\ &= E_{M_{P_G}} E_{M_{P_P}} E_{\theta_{P_R}, \theta_{P_P} | M_{P_P}} (E_{M_{P_S}} E_{M_{P_H}} [\Delta | M_{P_G}, M_{P_P}, \theta_{P_R, P_P}, M_{P_S}, M_{P_H}])^2 , \quad (5.48) \\ & - (E_{M_{P_G}} E_{M_{P_P}} E_{\theta_{P_R}, \theta_{P_P} | M_{P_P}} E_{M_{P_S}} E_{M_{P_H}} [\Delta | M_{P_G}, M_{P_P}, \theta_{P_R, P_P}, M_{P_S}, M_{P_H}])^2 \end{aligned}$$

$$\begin{aligned} & V_{P_H, P_R}(E_{\sim(P_H, P_R)}[\Delta | P_H, P_R]) \\ &= E_{M_{P_H}} E_{\theta_{P_R}^{bin}} (E_{M_{P_S}} E_{M_{P_G}} E_{M_{P_P}} E_{\theta_{P_P} | M_{P_P}} [\Delta | M_{P_H}, \theta_{P_R}^{bin}, M_{P_S}, M_{P_G}, M_{P_P}, \theta_{P_R}])^2 . \quad (5.49) \\ & - (E_{M_{P_H}} E_{\theta_{P_R}^{bin}} E_{M_{P_S}} E_{M_{P_G}} E_{M_{P_P}} E_{\theta_{P_P} | M_{P_P}} [\Delta | M_{P_H}, \theta_{P_R}^{bin}, M_{P_S}, M_{P_G}, M_{P_P}, \theta_{P_R}])^2 \end{aligned}$$

According to Section 2.5.4, the third-order process interaction effect index can be derived straightforwardly:

$$PS_{K,V,W} = \frac{V_{K,V,W}(E_{\sim(K,V,W)}[\Delta | K, V, W])}{V(\Delta)} - PS_{K,V} - PS_{K,W} - PS_{V,W} - PS_K - PS_V - PS_W \quad (5.50)$$

The $V_{K,V,W}(E_{\sim(K,V,W)}[\Delta | K, V, W])$ term at the right hand side of Equation (5.50) considers the joint variance reduction by simultaneously fixing processes K , V and W ; $PS_{K,V}$, $PS_{K,W}$, and $PS_{V,W}$ denote the second-order process interaction effect indices between processes K and V , processes K and W , and processes V and W , respectively; PS_K , PS_V , and PS_W are the first-order process sensitivity indices for processes K , V , and W , respectively.

Specifically, a total of four third-order process sensitivity indices can be defined in our case, and they are:

(1) the third-order interaction among climate process, flow process and heat process:

$$PS_{P_S, P_F, P_H} = \frac{V_{(P_S, P_F, P_H)}(E_{\sim(P_S, P_F, P_H)}[\Delta | P_S, P_F, P_H])}{V(\Delta)} - PS_{P_S, P_F} - PS_{P_S, P_H} - PS_{P_F, P_H} - PS_{P_S} - PS_{P_F} - PS_{P_H} . \quad (5.51)$$

(2) the third-order interaction among climate process, heat process and reaction process:

$$PS_{P_S, P_F, P_H} = \frac{V_{(P_S, P_F, P_H)}(E_{\sim(P_S, P_F, P_H)}[\Delta | P_S, P_F, P_H])}{V(\Delta)} - PS_{P_S, P_F} - PS_{P_S, P_H} - PS_{P_F, P_H} - PS_{P_S} - PS_{P_F} - PS_{P_H} . \quad (5.52)$$

(3) the third-order interaction among climate process, heat process and reaction process:

$$PS_{P_S, P_H, P_R} = \frac{V_{(P_S, P_H, P_R)}(E_{\sim(P_S, P_H, P_R)}[\Delta | P_S, P_H, P_R])}{V(\Delta)} - PS_{P_S, P_H} - PS_{P_S, P_R} - PS_{P_H, P_R} - PS_{P_S} - PS_{P_H} - PS_{P_R}. \quad (5.53)$$

(4) the third-order interaction among climate process, flow process and reaction process:

$$PS_{P_S, P_F, P_R} = \frac{V_{(P_S, P_F, P_R)}(E_{\sim(P_S, P_F, P_R)}[\Delta | P_S, P_F, P_R])}{V(\Delta)} - PS_{P_S, P_F} - PS_{P_S, P_R} - PS_{P_F, P_R} - PS_{P_S} - PS_{P_F} - PS_{P_R}. \quad (5.54)$$

Equations (5.51) ~ (5.54) enables us to consider the third-order interaction effect among any three of the four processes. These equations can also be expanded to the parameter level. Taking the third-order interaction among climate process, flow process and heat process as an example, according to the definition of variance, the

$V_{(P_S, P_F, P_H)}(E_{\sim(P_S, P_F, P_H)}[\Delta | P_S, P_F, P_H])$ of Equation (5.51) can be rewritten as

$$\begin{aligned} & V_{(P_S, P_F, P_H)}(E_{\sim(P_S, P_F, P_H)}[\Delta | P_S, P_F, P_H]) \\ &= V_{M_{P_S, P_F, P_H}}(E_{M_{\sim(P_S, P_F, P_H)}}[\Delta | M_{P_S, P_F, P_H}]) \\ &= E_{M_{P_S, P_F, P_H}} \left(E_{M_{\sim(P_S, P_F, P_H)}}[\Delta | M_{P_S, P_F, P_H}] \right)^2 - \left(E_{M_{P_S, P_F, P_H}} E_{M_{\sim(P_S, P_F, P_H)}}[\Delta | M_{P_S, P_F, P_H}] \right)^2 \end{aligned} \quad (5.55)$$

According to the law of total exception, Equation (S29) can be expanded to the parameter level as

$$\begin{aligned} & V_{(P_S, P_F, P_H)}(E_{\sim(P_S, P_F, P_H)}[\Delta | P_S, P_F, P_H]) \\ &= E_{M_{P_S, P_F, P_H}} E_{\theta_{P_S, P_F, P_H} | M_{P_S, P_F, P_H}} \left(E_{M_{P_R}} E_{\theta_{P_R} | M_{P_R}} [\Delta | \theta_{P_S, P_F, P_H}, M_{P_S, P_F, P_H}, \theta_{P_R}, M_{P_R}] \right)^2 \\ &\quad - \left(E_{M_{P_S, P_F, P_H}} E_{\theta_{P_S, P_F, P_H} | M_{P_S, P_F, P_H}} E_{M_{P_R}} E_{\theta_{P_R} | M_{P_R}} [\Delta | \theta_{P_S, P_F, P_H}, M_{P_S, P_F, P_H}, \theta_{P_R}, M_{P_R}] \right)^2 \end{aligned} \quad (5.56)$$

Under the assumptions that the selections of the process models are independent, and the parameters embedded in the process models are also independent, Equation (S51) can be written as

$$\begin{aligned} & V_{(P_S, P_F, P_H)}(E_{\sim(P_S, P_F, P_H)}[\Delta | P_S, P_F, P_H]) \\ &= E_{M_{P_S}} E_{M_{P_F}} E_{M_{P_H}} E_{\theta_{P_S} | M_{P_S}} E_{\theta_{P_F} | M_{P_F}} E_{\theta_{P_H} | M_{P_H}} \left(E_{M_{P_R}} E_{\theta_{P_R} | M_{P_R}} [\bullet] \right)^2, \\ &\quad - \left(E_{M_{P_S}} E_{M_{P_F}} E_{M_{P_H}} E_{\theta_{P_S} | M_{P_S}} E_{\theta_{P_F} | M_{P_F}} E_{\theta_{P_H} | M_{P_H}} E_{M_{P_R}} E_{\theta_{P_R} | M_{P_R}} [\bullet] \right)^2 \end{aligned} \quad (5.57)$$

where $[\bullet] = [\Delta | \theta_{P_S}, M_{P_S}, \theta_{P_F}, M_{P_F}, \theta_{P_H}, M_{P_H}, \theta_{P_R}, M_{P_R}]$.

Since there is no parametric uncertainty in climate process and heat process, the two items $E_{\theta_{P_S}|M_{P_S}}$, and $E_{\theta_{P_H}|M_{P_H}}$ disappear; and there is no model uncertainty in reaction process, item $E_{M_{P_R}}$ disappear.

$$\begin{aligned} & V_{(P_S, P_F, P_H)}(E_{\sim(P_S, P_F, P_H)}[\Delta | P_S, P_F, P_H]) \\ &= E_{M_{P_S}} E_{M_{P_F}} E_{M_{P_H}} E_{\theta_{P_F}|M_{P_F}} \left(E_{\theta_{P_R}} [\Delta | M_{P_S}, \theta_{P_F}, M_{P_F}, M_{P_H}, \theta_{P_R}] \right)^2 \\ &\quad - \left(E_{M_{P_S}} E_{M_{P_F}} E_{M_{P_H}} E_{\theta_{P_F}|M_{P_F}} E_{\theta_{P_R}} [\Delta | M_{P_S}, \theta_{P_F}, M_{P_F}, M_{P_H}, \theta_{P_R}] \right)^2 \end{aligned} \quad (5.58)$$

Considering the groundwater flow process can be further decomposed by geological module (P_G) and permeability module (P_P), the above equation can be rewritten as:

$$\begin{aligned} & V_{(P_S, P_F, P_H)}(E_{\sim(P_S, P_F, P_H)}[\Delta | P_S, P_F, P_H]) \\ &= E_{M_{P_S}} E_{M_{P_G}} E_{M_{P_P}} E_{\theta_{P_P}|M_{P_P}} E_{M_{P_H}} \left(E_{\theta_{P_R}} [\Delta | M_{P_S}, \theta_{P_P}, M_{P_G}, M_{P_P}, M_{P_H}, \theta_{P_R}] \right)^2 \\ &\quad - \left(E_{M_{P_S}} E_{M_{P_G}} E_{M_{P_P}} E_{\theta_{P_P}|M_{P_P}} E_{M_{P_H}} E_{\theta_{P_R}} [\Delta | M_{P_S}, \theta_{P_P}, M_{P_G}, M_{P_P}, M_{P_H}, \theta_{P_R}] \right)^2 \end{aligned} \quad (5.59)$$

Given the reaction rate and permeability values are generated using LHS and paired with each other, Equation (5.59) can be evaluated using the binning method:

$$\begin{aligned} & V_{(P_S, P_F, P_H)}(E_{\sim(P_S, P_F, P_H)}[\Delta | P_S, P_F, P_H]) \\ &= E_{M_{P_S}} E_{M_{P_G}} E_{M_{P_P}} E_{\theta_{P_P}^{bin}|M_{P_P}} E_{M_{P_H}} \left(E_{\theta_{P_R}} [\Delta | M_{P_S}, M_{P_G}, \theta_{P_P}^{bin}, M_{P_P}, M_{P_H}, \theta_{P_R}] \right)^2 \\ &\quad - \left(E_{M_{P_S}} E_{M_{P_G}} E_{M_{P_P}} E_{\theta_{P_P}^{bin}|M_{P_P}} E_{M_{P_H}} E_{\theta_{P_R}} [\Delta | M_{P_S}, M_{P_G}, \theta_{P_P}^{bin}, M_{P_P}, M_{P_H}, \theta_{P_R}] \right)^2 \end{aligned} \quad (5.60)$$

Similarly, we can obtain

$$\begin{aligned} & V_{(P_F, P_H, P_R)}(E_{\sim(P_F, P_H, P_R)}[\Delta | P_F, P_H, P_R]) \\ &= E_{M_{P_G}} E_{M_{P_P}} E_{\theta_{P_P}|M_{P_P}} E_{M_{P_H}} \left(E_{M_{P_S}} [\Delta | \theta_{P_R, P_P}, M_{P_G}, M_{P_P}, M_{P_H}, M_{P_S}] \right)^2 \\ &\quad - \left(E_{M_{P_G}} E_{M_{P_P}} E_{\theta_{P_R}, \theta_{P_P}|M_{P_P}} E_{M_{P_H}} E_{M_{P_S}} [\Delta | \theta_{P_R, P_P}, M_{P_G}, M_{P_P}, M_{P_H}, M_{P_S}] \right)^2 \end{aligned} \quad (5.61)$$

$$\begin{aligned} & V_{(P_S, P_H, P_R)}(E_{\sim(P_S, P_H, P_R)}[\Delta | P_S, P_H, P_R]) \\ &= E_{M_{P_S}} E_{M_{P_H}} E_{\theta_{P_R}^{bin}|M_{P_P}} \left(E_{M_{P_G}} E_{M_{P_P}} E_{\theta_{P_P}|M_{P_P}} [\Delta | M_{P_S}, M_{P_H}, \theta_{P_R}^{bin}, M_{P_G}, M_{P_P}, \theta_{P_P}] \right)^2 \\ &\quad - \left(E_{M_{P_S}} E_{M_{P_H}} E_{\theta_{P_R}^{bin}|M_{P_P}} E_{M_{P_G}} E_{M_{P_P}} E_{\theta_{P_P}|M_{P_P}} [\Delta | M_{P_S}, M_{P_H}, \theta_{P_R}^{bin}, M_{P_G}, M_{P_P}, \theta_{P_P}] \right)^2 \end{aligned} \quad (5.62)$$

$$\begin{aligned} & V_{(P_S, P_F, P_R)}(E_{\sim(P_S, P_F, P_R)}[\Delta | P_S, P_F, P_R]) \\ &= E_{M_{P_S}} E_{M_{P_G}} E_{M_{P_P}} E_{\theta_{P_P}|M_{P_P}} \left(E_{M_{P_H}} [\Delta | M_{P_S}, \theta_{P_R, P_P}, M_{P_G}, M_{P_P}, M_{P_H}] \right)^2 \\ &\quad - \left(E_{M_{P_S}} E_{M_{P_G}} E_{M_{P_P}} E_{\theta_{P_R}, \theta_{P_P}|M_{P_P}} E_{M_{P_H}} [\Delta | M_{P_S}, \theta_{P_R, P_P}, M_{P_G}, M_{P_P}, M_{P_H}] \right)^2 \end{aligned} \quad (5.63)$$

Since there are four processes, we here consider the second-order and third-order

process interactions. Figure 5-9 illustrates the spatial distribution of second-order process sensitivity analysis indices at the simulation times of 8, 10, and 12 weeks according to Equations (5.33) ~ 5.38). The second-order process sensitivity indices between any of the two processes, except for the groundwater flow process and reactive transport process, are generally small across the model domain. It is reasonable since the groundwater flow process and reactive transport process are tightly coupled to solve the advection-dispersion equation. The results also indicate that the second-order process sensitivity indices contribute little to the total-effect process sensitivity indices. The larger difference between the first-order and total-effect process sensitivity indices indicates that the third-order process sensitivity indices cannot be ignored.

Figure 5-10 illustrates the spatial distribution of third-order process sensitivity analysis indices at the simulation times of 8, 10, and 12 weeks according to Equations (5.51) ~ (5.54). The third-order process sensitivity indices of climate scenario, groundwater flow, and reactive transport are obviously largest across the domain followed by the third-order process sensitivity indices of groundwater flow, heat transport, and reactive transport, which explains why the reactive transport process is unimportant (i.e., the low first-order process sensitivity indices) but influential (i.e., the high total-effect process sensitivity indices). As for the heat transport process, neither the first-order nor total-effect process sensitivity indices are high since the interaction effects between this process and the other three processes are all small. The results confirms that the heat transport process is the least important and influential uncertainty source for the carbon - consumption rate, indicating that the temperature - dependent reaction rates caused negligible difference in regulating the biogeochemical reactions in this carbon - limited system, compared to other processes.

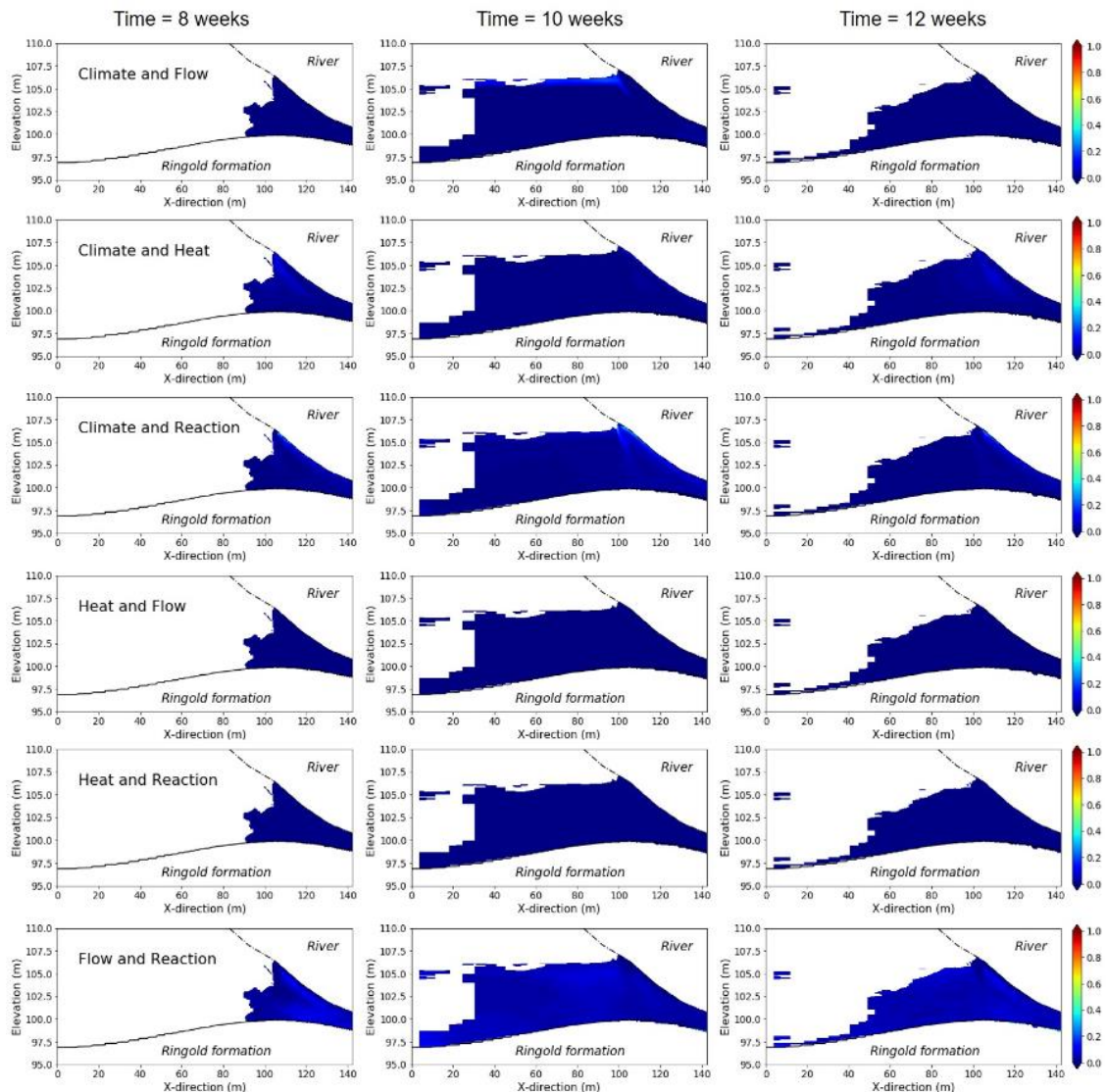


图 5-9 模拟时间为 8 周、10 周、12 周时，气候情景(P_S)、地下水水流(P_F)、热运移(P_H)和反应运移过程(P_R)的二阶过程敏感性分析指标的空间分布。

Figure 5-9 Spatial distribution of second-order process sensitivity analysis indices between climate scenario and groundwater flow, climate scenario and heat transport, climate scenario and reactive transport, heat transport and groundwater flow, and groundwater flow and reactive transport at the simulation times of 8, 10, and 12 weeks.

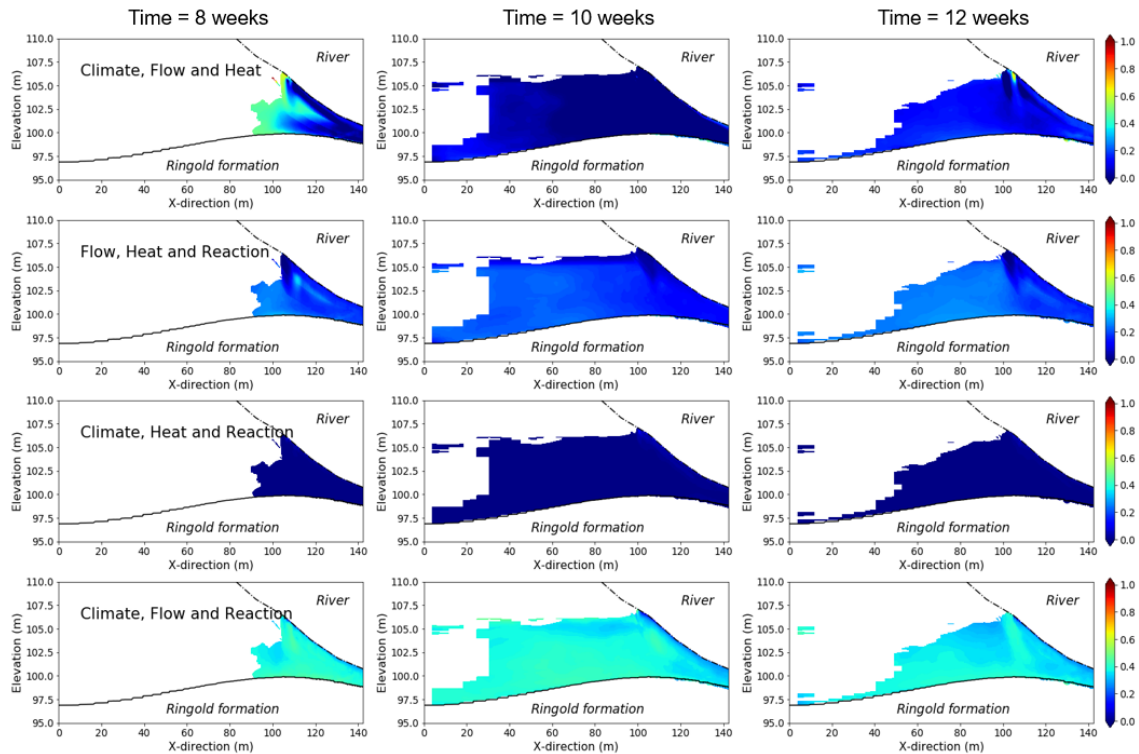


图 5-10 模拟时间为 8 周、10 周、12 周时，气候情景(P_S)、地下水水流(P_F)、热运移(P_H)和反应运移过程(P_R)的三阶过程敏感性分析指标的空间分布。

Figure 5-10 Spatial distribution of third-order process sensitivity analysis indices for climate scenario, groundwater flow, heat transport, and reactive transport processes at the simulation times of 8, 10, and 12 weeks.

5.3.5 MMADS Method for Identifying Non-Influential Processes

The multi-model difference-based process sensitivity analysis method uses the first two statistical moments, i.e., the mean and variance, of the model response difference (denoted as $d\Delta$) caused by the variation (uncertainty) of a process K when the other processes are fixed to measure the sensitivity of this process:

$$\begin{aligned} E(d\Delta | K) &= E_{\sim K} E_{T_K}(d\Delta | \sim K) \\ &= E_{M_{\sim K}} E_{T_{M_K}}(d\Delta | M_{\sim K}) \end{aligned} \quad (5.64)$$

$$\begin{aligned} V(d\Delta | K) &= E_{\sim K} V_{T_K}(d\Delta | \sim K) + V_{\sim K} E_{T_K}(d\Delta | \sim K) \\ &= E_{M_{\sim K}} V_{T_{M_K}}(d\Delta | M_{\sim K}) + V_{M_{\sim K}} E_{T_{M_K}}(d\Delta | M_{\sim K}) \end{aligned} \quad (5.65)$$

where T_{M_K} is the set of process model transitions within process K , i.e.,

$T_{M_K} = \{M_{K_i} \rightarrow M_{K_j}\}$ where $i, j = 1, 2, \dots, N_{M_K}$ and N_{M_K} is the number of process

models to simulate process K . $E(d\Delta | K)$ measures the average change of the model response due to the variation (uncertainty) of process K and $V(d\Delta | K)$ is used to detect how far the output difference is spread out. A process with both small mean and variance values is identified to be the non-influential process.

According to Equation (5.64), the mean values of the output difference of the four processes can be written as

$$\begin{aligned} E(d\Delta | P_S) &= E_{\sim P_S} E_{T_{P_S}}(d\Delta | \sim P_S) \\ &= E_{M_{\sim P_S}} E_{T_{M_{P_S}}}(d\Delta | M_{\sim P_S}) \end{aligned} \quad \text{for climate process,} \quad (5.66)$$

$$\begin{aligned} E(d\Delta | P_F) &= E_{\sim P_F} E_{T_{P_F}}(d\Delta | \sim P_F) \\ &= E_{M_{\sim P_F}} E_{T_{M_{P_F}}}(d\Delta | M_{\sim P_F}) \end{aligned} \quad \text{for flow process,} \quad (5.67)$$

$$\begin{aligned} E(d\Delta | P_H) &= E_{\sim P_H} E_{T_{P_H}}(d\Delta | \sim P_H) \\ &= E_{M_{\sim P_H}} E_{T_{M_{P_H}}}(d\Delta | M_{\sim P_H}) \end{aligned} \quad \text{for heat process,} \quad (5.68)$$

$$\begin{aligned} E(d\Delta | P_R) &= E_{\sim P_R} E_{T_{P_R}}(d\Delta | \sim P_R) \\ &= E_{M_{\sim P_R}} E_{T_{M_{P_R}}}(d\Delta | M_{\sim P_R}) \end{aligned} \quad \text{for reaction process.} \quad (5.69)$$

According to Equation (5.65), the variance values of the output difference for the four processes can be written as

$$\begin{aligned} V(d\Delta | P_S) &= E_{\sim P_S} V_{T_{P_S}}(d\Delta | \sim P_S) + V_{\sim P_S} E_{T_{P_S}}(d\Delta | \sim P_S) \\ &= E_{M_{\sim P_S}} V_{T_{M_{P_S}}}(d\Delta | M_{\sim P_S}) + V_{M_{\sim P_S}} E_{T_{M_{P_S}}}(d\Delta | M_{\sim P_S}) \end{aligned} \quad \text{for climate process,} \quad (5.70)$$

$$\begin{aligned} V(d\Delta | P_F) &= E_{\sim P_F} V_{T_{P_F}}(d\Delta | \sim P_F) + V_{\sim P_F} E_{T_{P_F}}(d\Delta | \sim P_F) \\ &= E_{M_{\sim P_F}} V_{T_{M_{P_F}}}(d\Delta | M_{\sim P_F}) + V_{M_{\sim P_F}} E_{T_{M_{P_F}}}(d\Delta | M_{\sim P_F}) \end{aligned} \quad \text{for flow process,} \quad (5.71)$$

$$\begin{aligned} V(d\Delta | P_H) &= E_{\sim P_H} V_{T_{P_H}}(d\Delta | \sim P_H) + V_{\sim P_H} E_{T_{P_H}}(d\Delta | \sim P_H) \\ &= E_{M_{\sim P_H}} V_{T_{M_{P_H}}}(d\Delta | M_{\sim P_H}) + V_{M_{\sim P_H}} E_{T_{M_{P_H}}}(d\Delta | M_{\sim P_H}) \end{aligned} \quad \text{for heat process,} \quad (5.72)$$

$$\begin{aligned} V(d\Delta | P_R) &= E_{\sim P_R} V_{T_{P_R}}(d\Delta | \sim P_R) + V_{\sim P_R} E_{T_{P_R}}(d\Delta | \sim P_R) \\ &= E_{M_{\sim P_R}} V_{T_{M_{P_R}}}(d\Delta | M_{\sim P_R}) + V_{M_{\sim P_R}} E_{T_{M_{P_R}}}(d\Delta | M_{\sim P_R}) \end{aligned} \quad \text{for reaction process,} \quad (5.73)$$

Extensions of Equations (5.66) ~ (5.73) to handle both parametric uncertainty and process model uncertainty are straightforward. Taking Equation (5.66) as an example, the

mean of the output difference for climate process can be written as

$$\begin{aligned} & E(d\Delta | P_S) \\ &= E_{M_{\sim P_S}} E_{\theta_{\sim P_S} | M_{\sim P_S}} E_{P_{M_{P_S}}} E_{P_{\theta_{P_S}} | P_{M_{P_S}}} (d\Delta | \theta_{\sim P_S}, M_{\sim P_S}, P_{\theta_{P_S}}, P_{M_{P_S}}) \\ &= E_{M_{P_F, P_H, P_R}} E_{\theta_{P_F, P_H, P_R} | M_{P_F, P_H, P_R}} E_{P_{M_{P_S}}} E_{P_{\theta_{P_S}} | P_{M_{P_S}}} (d\Delta | \theta_{P_F, P_H, P_R}, M_{P_F, P_H, P_R}, P_{\theta_{P_S}}, P_{M_{P_S}}) \end{aligned} \quad (5.74)$$

Under the assumption of independent process models and parameters, Equation (5.74) can be expanded using the law of total expectation:

$$\begin{aligned} & E(d\Delta | P_S) \\ &= E_{M_{P_F}} E_{\theta_{P_F} | M_{P_F}} E_{M_{P_H}} E_{\theta_{P_H} | M_{P_H}} E_{M_{P_R}} E_{\theta_{P_R} | M_{P_R}} E_{P_{M_{P_S}}} E_{P_{\theta_{P_S}} | P_{M_{P_S}}} \\ & \quad \left(d\Delta | \theta_{P_F}, M_{P_F}, \theta_{P_H}, M_{P_H}, \theta_{P_R}, M_{P_R}, P_{\theta_{P_S}}, P_{M_{P_S}} \right) \end{aligned} \quad (5.75)$$

Since there is no parametric uncertainty in climate process and heat process, the two items $E_{\theta_{P_S} | M_{P_S}}$ and $E_{\theta_{P_H} | M_{P_H}}$ disappear. Besides, there is no model uncertainty in reaction process, $E_{M_{P_R}}$ disappears. Equation (5.75) can be rewritten as

$$E(d\Delta | P_S) = E_{M_{P_F}} E_{\theta_{P_F} | M_{P_F}} E_{M_{P_H}} E_{\theta_{P_H}} E_{P_{M_{P_S}}} (d\Delta | \theta_{P_F}, M_{P_F}, M_{P_H}, \theta_{P_H}, P_{M_{P_S}}) \quad (5.76)$$

Considering the groundwater flow process can be further decomposed by geological module (P_G) and permeability module (P_P), the above equation can be rewritten as:

$$\begin{aligned} E(d\Delta | P_S) &= E_{M_{P_G}} E_{M_{P_P}} E_{\theta_{P_P} | M_{P_P}} E_{M_{P_H}} E_{\theta_{P_H}} E_{P_{M_{P_S}}} (d\Delta | \theta_{P_P}, M_{P_P}, M_{P_G}, M_{P_H}, \theta_{P_H}, P_{M_{P_S}}) \\ & \quad (5.77) \end{aligned}$$

Given the reaction rate and permeability values are paired with each other, equation (5.77) can be re-arranged as

$$E(d\Delta | P_S) = E_{M_{P_G}} E_{M_{P_P}} E_{M_{P_H}} E_{\theta_{P_P} | M_{P_P}} E_{P_{M_{P_S}}} (d\Delta | \theta_{P_R, P_P}, M_{P_P}, M_{P_G}, M_{P_H}, P_{M_{P_S}}) \quad (5.78)$$

Similarly, the mean of the output difference of flow, heat, and reaction processes can be written as

$$\begin{aligned} & E(d\Delta | P_H) \\ &= E_{M_{\sim P_H}} E_{\theta_{\sim P_H} | M_{\sim P_H}} E_{P_{M_{P_H}}} E_{P_{\theta_{P_H}} | P_{M_{P_H}}} (d\Delta | \theta_{\sim P_H}, M_{\sim P_H}, P_{\theta_{P_H}}, P_{M_{P_H}}) \\ &= E_{M_{P_S, P_F, P_R}} E_{\theta_{P_S, P_F, P_R} | M_{P_S, P_F, P_R}} E_{P_{M_{P_H}}} E_{P_{\theta_{P_H}} | P_{M_{P_H}}} (d\Delta | \theta_{P_S, P_F, P_R}, M_{P_S, P_F, P_R}, P_{\theta_{P_H}}, P_{M_{P_H}}) \end{aligned} \quad (5.79)$$

$$\begin{aligned} & E(d\Delta | P_F) \\ &= E_{M_{P_S}} E_{M_{P_H}} E_{\theta_{P_R}^{bin} | M_{P_G}} E_{P_{M_{P_G}}} E_{P_{\theta_{P_P}} | P_{M_{P_P}}} (d\Delta | M_{P_S}, M_{P_H}, \theta_{P_R}^{bin}, P_{\theta_{P_P}}, P_{M_{P_G}}, P_{M_{P_H}}) \end{aligned} \quad (5.80)$$

$$\begin{aligned} & E(d\Delta | P_H) \\ &= E_{M_{P_S}} E_{M_{P_P}} E_{M_{P_H}} E_{\theta_{P_R}, \theta_{P_P} | M_{P_P}} E_{P_{M_{P_H}}} (d\Delta | \theta_{P_R, P_P}, M_{P_P}, M_{P_G}, M_{P_S}, P_{M_{P_H}}) \end{aligned} \quad (5.81)$$

$$\begin{aligned} & E(d\Delta | P_R) \\ &= E_{M_{P_S}} E_{M_{P_G}} E_{M_{P_P}} E_{\theta^{bin}_{P_P} | M_{P_P}} E_{M_{P_H}} E_{P_{\theta_{P_R}}} (d\Delta | M_{P_S}, \theta^{bin}_{P_P}, M_{P_P}, M_{P_G}, M_{P_H}, P_{\theta_{P_R}}) \end{aligned} \quad (5.82)$$

Note that the binning method is used here again as the permeability and reaction rates are paired with each other.

As for the variance of the absolute difference of model output, taking Equation (5.70) as an example, the variance of the output difference for climate scenario can be written as

$$\begin{aligned} & V(d\Delta | P_S) \\ &= E_{M_{\sim P_S}} E_{T_{M_{P_S}}} (d\Delta | M_{\sim P_S}, T_{M_{P_S}})^2 \\ &\quad - \left(E_{M_{\sim P_S}} E_{T_{M_{P_S}}} (d\Delta | M_{\sim P_S}, T_{M_{P_S}}) \right)^2 \\ &= E_{M_{P_F, P_H, P_R}} E_{T_{M_{P_S}}} (d\Delta | M_{P_F, P_H, P_R}, T_{M_{P_S}})^2 \\ &\quad - \left(E_{M_{P_F, P_H, P_R}} E_{T_{M_{P_S}}} (d\Delta | M_{P_F, P_H, P_R}, T_{M_{P_S}}) \right)^2 \end{aligned} \quad (5.83)$$

According to the law of total expectation, Equation (5.83) can be expanded to the parameter level as

$$\begin{aligned} & V(d\Delta | P_S) \\ &= E_{M_{P_F, P_H, P_R}} E_{\theta_{P_F, P_H, P_R} | M_{P_F, P_H, P_R}} E_{P_{M_{P_S}}} E_{P_{\theta_{P_S}} | P_{M_{P_S}}} (d\Delta | \theta_{P_F, P_H, P_R}, M_{P_F, P_H, P_R}, P_{\theta_{P_S}}, P_{M_{P_S}})^2 \\ &\quad - \left(E_{M_{P_F, P_H, P_R}} E_{\theta_{P_F, P_H, P_R} | M_{P_F, P_H, P_R}} E_{P_{M_{P_S}}} E_{P_{\theta_{P_S}} | P_{M_{P_S}}} (d\Delta | \theta_{P_F, P_H, P_R}, M_{P_F, P_H, P_R}, P_{\theta_{P_S}}, P_{M_{P_S}}) \right)^2 \end{aligned} \quad (5.84)$$

Under the assumption of independent process models and parameters, Equation (5.84) can be expanded as:

$$\begin{aligned} & V(d\Delta | P_S) \\ &= E_{M_{P_F}} E_{\theta_{P_F} | M_{P_F}} E_{M_{P_H}} E_{\theta_{P_H} | M_{P_H}} E_{M_{P_R}} E_{\theta_{P_R} | M_{P_R}} E_{P_{M_{P_S}}} E_{P_{\theta_{P_S}} | P_{M_{P_S}}} (\bullet)^2 \\ &\quad - \left(E_{M_{P_F}} E_{\theta_{P_F} | M_{P_F}} E_{M_{P_H}} E_{\theta_{P_H} | M_{P_H}} E_{M_{P_R}} E_{\theta_{P_R} | M_{P_R}} E_{P_{M_{P_S}}} E_{P_{\theta_{P_S}} | P_{M_{P_S}}} (\bullet) \right)^2 \end{aligned} \quad (5.85)$$

where $(\bullet) = (d\Delta | \theta_{P_F}, M_{P_F}, \theta_{P_H}, M_{P_H}, \theta_{P_R}, M_{P_R}, P_{\theta_{P_S}}, P_{M_{P_S}})$.

Since there is no parametric uncertainty in climate process and heat process, the two items $E_{\theta_{P_S} | M_{P_S}}$ and $E_{\theta_{P_H} | M_{P_H}}$ disappear. Besides, there is no model uncertainty in

reaction process, $E_{M_{P_R}}$ disappears. Equation (5.85) can be rewritten as

$$\begin{aligned} & V(d\Delta | P_S) \\ &= E_{M_{P_G}} E_{M_{P_P}} E_{\theta_{P_P} | M_{P_P}} E_{M_{P_H}} E_{\theta_{P_R}} E_{P_{M_{P_S}}} (d\Delta | \theta_{P_R, P_P}, M_{P_P}, M_{P_G}, M_{P_H}, P_{M_{P_S}})^2 \\ &\quad - \left(E_{M_{P_G}} E_{M_{P_P}} E_{\theta_{P_P} | M_{P_P}} E_{M_{P_H}} E_{\theta_{P_R}} E_{P_{M_{P_S}}} (d\Delta | \theta_{P_R, P_P}, M_{P_P}, M_{P_G}, M_{P_H}, P_{M_{P_S}}) \right)^2 \end{aligned} \quad (5.86)$$

Given the reaction rate and permeability values are paired with each other, equation (S498) can be re-arranged as

$$\begin{aligned} & V(d\Delta | P_S) \\ &= E_{M_{P_G}} E_{M_{P_P}} E_{M_{P_H}} E_{\theta_{P_R} | M_{P_P}} E_{P_{M_{P_S}}} (d\Delta | \theta_{P_R, P_P}, M_{P_P}, M_{P_G}, M_{P_H}, P_{M_{P_S}})^2 \\ &\quad - \left(E_{M_{P_G}} E_{M_{P_P}} E_{M_{P_H}} E_{\theta_{P_R} | M_{P_P}} E_{P_{M_{P_S}}} (d\Delta | \theta_{P_R, P_P}, M_{P_P}, M_{P_G}, M_{P_H}, P_{M_{P_S}}) \right)^2 \end{aligned} \quad (5.87)$$

Similarly, the mean of the output difference of flow, heat, and reaction processes can be derived as

$$\begin{aligned} & V(d\Delta | P_F) \\ &= E_{M_{P_S}} E_{M_{P_H}} E_{\theta_{P_R}^{bin}} E_{P_{M_{P_G}}} E_{P_{M_{P_P}}} (d\Delta | M_{P_S}, \theta_{P_R}^{bin}, M_{P_H}, P_{\theta_{P_P}}, P_{M_{P_P}}, P_{M_{P_G}})^2 \\ &\quad - \left(E_{M_{P_S}} E_{M_{P_H}} E_{\theta_{P_R}^{bin}} E_{P_{M_{P_G}}} E_{P_{M_{P_P}}} E_{P_{\theta_{P_P}} | P_{M_{P_P}}} (d\Delta | M_{P_S}, \theta_{P_R}^{bin}, M_{P_H}, P_{\theta_{P_P}}, P_{M_{P_P}}, P_{M_{P_G}}) \right)^2 \end{aligned} \quad (5.88)$$

$$\begin{aligned} & V(d\Delta | P_H) \\ &= E_{M_{P_S}} E_{M_{P_G}} E_{M_{P_P}} E_{\theta_{P_R} | M_{P_P}} E_{P_{M_{P_H}}} (d\Delta | \theta_{P_R, P_P}, M_{P_P}, M_{P_G}, M_{P_S}, P_{M_{P_H}})^2 \\ &\quad - \left(E_{M_{P_S}} E_{M_{P_G}} E_{M_{P_P}} E_{\theta_{P_R} | M_{P_P}} E_{P_{M_{P_H}}} (d\Delta | \theta_{P_R, P_P}, M_{P_P}, M_{P_G}, M_{P_S}, P_{M_{P_H}}) \right)^2 \end{aligned} \quad (5.89)$$

$$\begin{aligned} & V(d\Delta | P_R) \\ &= E_{M_{P_S}} E_{M_{P_G}} E_{M_{P_P}} E_{\theta_{P_P} | M_{P_P}} E_{M_{P_H}} E_{P_{\theta_{P_R}}} (d\Delta | M_{P_S}, \theta_{P_P}^{bin}, M_{P_P}, M_{P_G}, M_{P_H}, P_{\theta_{P_R}})^2 \\ &\quad - \left(E_{M_{P_S}} E_{M_{P_G}} E_{M_{P_P}} E_{\theta_{P_P} | M_{P_P}} E_{M_{P_H}} E_{P_{\theta_{P_R}}} (d\Delta | M_{P_S}, \theta_{P_P}^{bin}, M_{P_P}, M_{P_G}, M_{P_H}, P_{\theta_{P_R}}) \right)^2 \end{aligned} \quad (5.90)$$

Note that the binning method is used here again as the permeability and reaction rates are paired with each other.

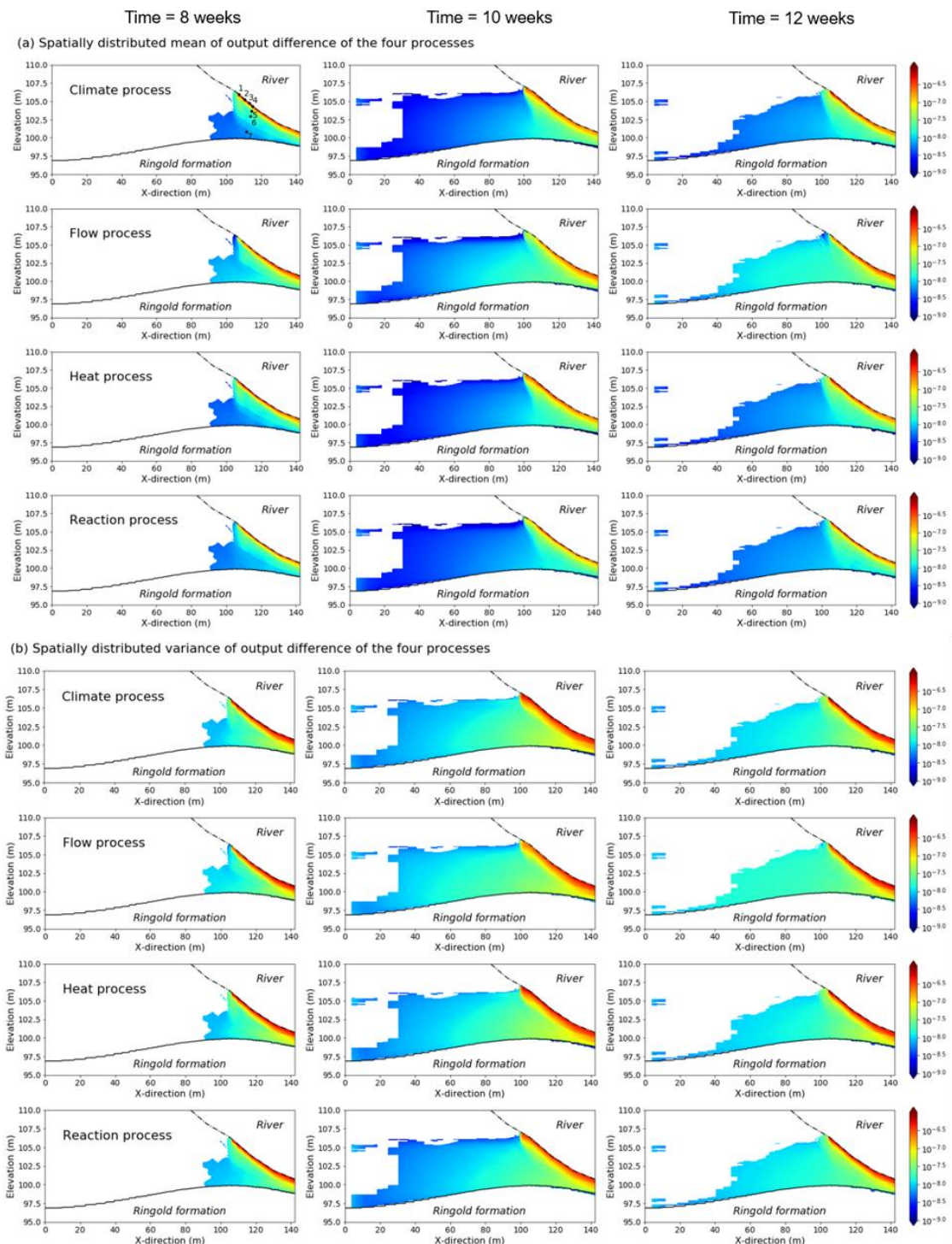


图 5-12 模拟时间为 8、10、12 周时，气候情景(P_S)、地下水水流(P_F)、热运移(P_H)和反应运移过程(P_R)的输出差值(a)均值和(b)方差对有机碳 OC 消耗速率的空间分布。黑色虚线为河流-沉积物界面，虚线为 Hanford 地层的上界。

Figure 5-11 Spatial distribution of the two sensitivity analysis measures of (a) mean and (b) variance of the output difference of climate scenario (P_S), groundwater flow (P_F), heat transport (P_H), and reactive transport processes (P_R) to the OC consumption rate at simulation times of 8, 10, 12 weeks. Black dotted line denotes the river-sediment interface and dashed line denotes the

upper bound of the Ringold formation.

Figures 5-11a and 5-11b illustrate the spatial distributions of the $E(\Delta)$ and $V(\Delta)$ values, respectively, for the four processes over the two-dimensional modeling domain for the three times of 8, 10, and 12 weeks. The figure shows that, for the OC consumption rate, the influence of the four processes decreases from the river-sediment interface toward the aquifer. This is physically reasonable because the river water is the primary source of organic carbon and oxygen and alteration to any of the four processes affects the organic carbon consumption rate. The influence of the four processes also changes with time, which is attributed to the fluctuation of the river stage in the six climate scenarios. More discussion on this is referred to Dai et al. (2019).

The process influence can be examined for any spatial points of interest by plotting the $E(\Delta)$ and $V(\Delta)$ values at the points in the manner of the Morris method. For the sake of demonstration, we selected seven points, whose locations in the two-dimensional modeling domain are shown in Figure 5-11a. Points 1 – 4 are located at the river-sediment interface, and their elevations are 105.97m, 105.23m, 104.76m, and 104.36m, which are the 90th, 50th, 10th, and 0th percentiles, respectively, of the river stages of the six climate scenarios. Points 5 – 7 are located beneath point 4 at the depth of 1m, 2m, and 5 m, respectively. Figure 5-12a plots the $E(\Delta)$ and $V(\Delta)$ values of the seven points at times of 8, 10, and 12 weeks. The four processes are plotted in four colors, and the seven points are denoted by Arabic numbers 1 – 7. The figure indicates that process influence varies in space. Across the three simulation times, at points 1 – 4, the least influential process is the flow process; at points 5 – 7, the least influential process is the heat process. These are physically reasonable. For points 1 – 4, since they are located at the river-sediment interface, the OC consumption rate is not controlled by groundwater flow but substantially by the river stage variation, which is also the reason that the climate process is the most influential one as shown in Figure 5-12a. At points 5 – 7, since they are located in the aquifer, their temperature variation has the smallest impacts on the organic carbon consumption rate. The spatial pattern revealed in at 8 weeks is also observed in the other two simulation times but with slight variation. Taking point 6 as an example, the influence of the climate, flow, and reaction processes is similar at 8 weeks, becomes different at 10 weeks, but is similar again at 12 weeks. The spatial and temporal patterns of process influence may be useful for model development and improvement by conducting laboratory experiments and/or designing field campaigns.

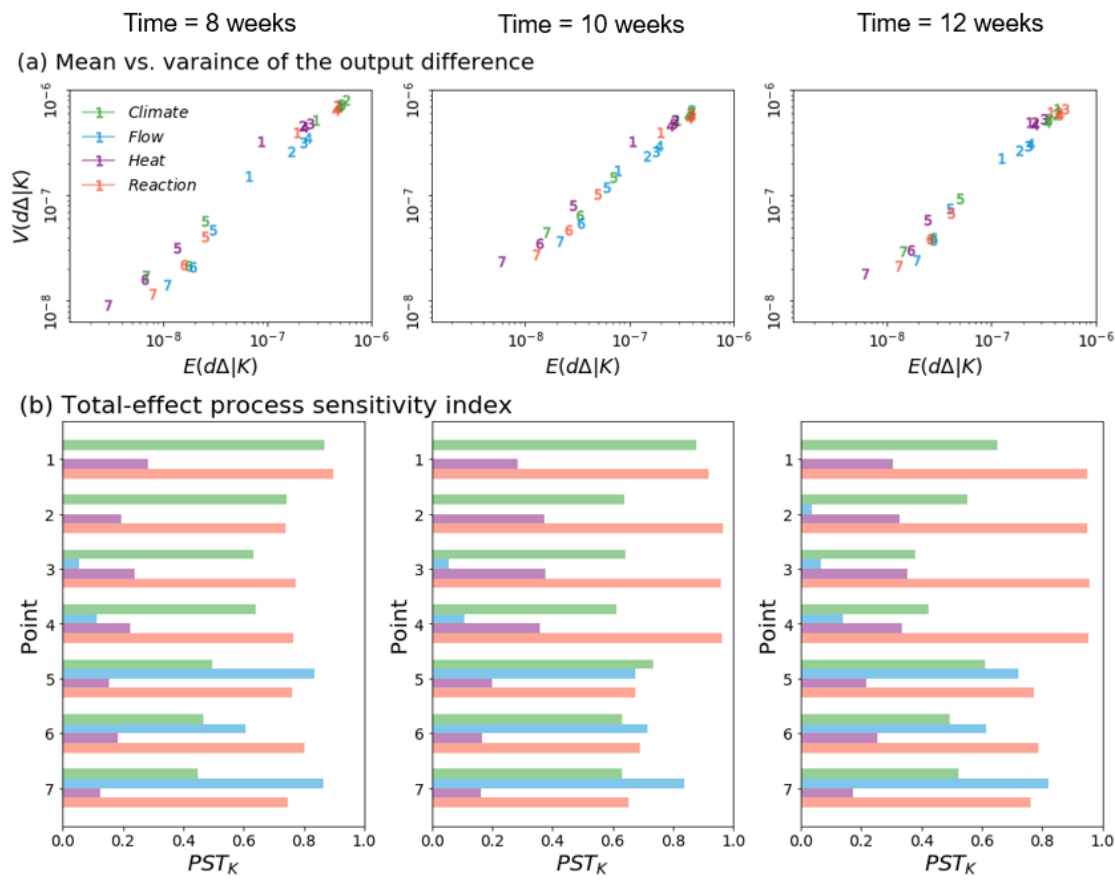


图 5-12 研究区 7 个特定点的总效应过程敏感性指标与 MMADS 结果比较

Figure 5-12 Comparison of the total-effect process sensitivity indices and the results of MMADS for the seven selected points

5.3.6 Comparison of the Two Methods and Implications

As the total-effect process sensitivity index and MMDS are both used for identifying the non-influential process, the seven points shown in Figure 5-11a are selected to compare the two process sensitivity analysis methods. Figure 5-12b illustrates the total-effect process sensitivity indices of the four processes of the seven points. For points 1~4, the total-effect process sensitivity indices shows that the groundwater flow process is the most non-influential process with lowest total-effect process sensitivity indices while for points 5~7, the heat transport process is the most non-influential process with the lowest total-effect process sensitivity indices. The results of MMDS are consistent with the above observations.

Table 5-2 presents a way of utilizing the sensitivity analysis results over the modeling domain as shown in Figures 5-7, 5-8 and 5-11. For each grid cell in the

modeling domain where the OC consumption rates are greater than $1 \times 10^{-7} \text{ mol} \cdot \text{m}^{-3} \cdot \text{s}^{-1}$ for all 12,000 simulation runs, we examine which process has the highest first-order process sensitivity index, which process has the lowest total-effect process sensitivity index, and which process has the smallest $E(\Delta)$ and $V(\Delta)$. The results are listed in Table 5-2. Taking the simulation time of 8 weeks as an example, there are 37,664 grid cells over the modeling domain of which the OC consumption rates are greater than $1 \times 10^{-7} \text{ mol} \cdot \text{m}^{-3} \cdot \text{s}^{-1}$ for all 12,000 simulation runs. We thus compute the sensitivity results for these grid cells for the four processes. For the first-order process sensitivity index, the climate process got highest first-order process sensitivity among the four processes at 11.24% of the 37,664 grid cells. For the total-effect process sensitivity index, the climate process got lowest total-effect process sensitivity among the four processes at 0.18% of the 37,664 grid cells. As for the multi-model difference-based process sensitivity analysis, climate process got the smallest $E(\Delta)$ and $V(\Delta)$ values at 0.15% of the 37,664 grid cells.

Considering all the three simulation times and the modeling domain, the flow process should be devoted more efforts to investigate for the purpose of reducing the uncertain of the OC consumption rate simulation. Both the variance-based process sensitivity analysis method and multi-model difference-based process sensitivity analysis method suggests the heat process is non-influential. Thus the biogeochemical model may be simplified without considering the heat process. In other words, the temperature-independent reaction rates may be sufficient to capture the OC consumption rate.

Both the two methods identified the heat process as the most non-influential process which contribute neglectable uncertainties to the OC consumption rate at all three simulation times in most of the biogeochemically active zones. This indicates that the temperature - dependent reaction rates caused negligible difference in regulating the biogeochemical reactions in this carbon limited system, compared to other processes. These sensitivity analysis results were supported by the simulated spatial and temporal dynamics of carbon consumption shown in Figure 5-6 that OC consumption was driven by the river water intrusion, which supplied organic carbon for the biogeochemical reactions. In practice, the complex biogeochemical model may be simplified by ignoring the heat process by using temperature - independent reaction rates. Thus, there may be no need to spend money on filed measurements of temperature in the river water or groundwater.

表 5-2 三个模拟期所有网格的过程敏感性分析点数百分比统计

Table 5-2 Statistical of the percentage of number of computed points over the entire domain for the three simulation times

Simulation time	8 weeks	10 weeks	12 weeks
Number of cells computed	37,664	55,157	52,008
Percentage of highest PS_K (%)			
Climate process	11.24	14.83	11.85
Flow process	88.31	84.88	87.74
Heat process	0.00	0.00	0.15
Reaction Process	0.45	0.29	0.26
Percentage of lowest PST_K (%)			
Climate process	0.18	0.11	0.20
Flow process	1.83	1.34	0.96
Heat process	97.99	98.55	98.84
Reaction Process	0.00	0.00	0.00
Percentage of lowest $E(d\Delta K)$ and $V(d\Delta K)$ (%)			
Climate process	0.15	0.10	0.09
Flow process	0.59	0.82	0.75
Heat process	96.29	97.76	96.55
Reaction Process	0.00	0.00	0.00

On the other hand, both the two methods identified the flow process as the most influential process which contribute significant uncertainties to the OC consumption rate at all three simulation times in most of the biogeochemically active zones. This indicates that the OC consumption was driven the flow process, specifically, by the river water intrusion, which supplied organic carbon for the biogeochemical reactions. A better predication of OC consumption rate at this area may require a better understanding of the geological formation structures and the permeability field within each formation, which may more extensive filed work on this aspect.

§5.4 Summary

This chapter used a complex groundwater biogeochemical model to compare the two sensitivity analysis methods: the variance-based process sensitivity analysis method and the MMADS analysis method. The first-order and total-effect process sensitivity

indices were interpreted for different purposes. This chapter demonstrated the total-effect process sensitivity index, and the multi-model difference-based sensitivity analysis method can both successfully identify the noninfluential process. This chapter also compared the variance-based process sensitivity analysis method and the hierarchical sensitivity analysis method proposed by Dai et al. (2019).

Applying the two sensitivity analysis methods to the complex biogeochemical model under model uncertainty provides better understanding of similarities and differences between the two methods. It is suggested that the first-order process sensitive index is used to for process prioritization. The most important process with highest first-order process sensitivity index should be devoted more efforts to reduce the uncertainty in the model simulation. The total-effect process sensitivity index is used for process fixing. The most non-influential process with lowest total-effect process sensitivity index may be ignored to simplify the model complexity. The multi-model difference-based process sensitivity method is an alternative computational cheap way to the total-effect process sensitivity index and could be used for process fixing.

Chapter 6 SAMMPy: An Open-source Python Package for Sensitivity Analysis under Multiple Models

This chapter presents SAMMPy, an open-source python package for performing process sensitivity analysis under multiple system models. Within the framework that an environmental system can be conceptualized by multiple processes, and each process is represented by one or more process models (i.e., the process-representation-based model structural uncertainty) with associated parameters. SAMMPy implements the two new sensitivity analysis methods discussed in Chapters 2 and 3 to enable simultaneous generation of a range of process sensitivity indices with considering both parametric uncertainty and process model uncertainty.

§6.1 Introduction

Either physically or empirically based, the environmental systems are typically first expressed mathematically and then implemented in the form of computer models for emulating and predicting the system behaviors under future earth resources. These models usually contain many uncertainty parameters and factors due to the natural heterogeneity and ever-on-going understanding of the underlying system processes. Sensitivity analysis has growing to be a ubiquitous tool to assist understanding and eventually improvement of environmental system models. The sensitivity analysis is purpose-driven, and different settings are proposed corresponding to the possible motivations according to Saltelli et al. (2004), such as: which are the most important parameters deserving of further investigation and measurements or can the model be simplified by ignoring some non-influential (or non-informative) parameters? The challenge of answering these scientifical questions has spawned development of a range of methods for sensitivity analysis, including the ones of Sobol's variance-based (Sobol' 2001), Morris's One-At-a-Time (Morris 1991), and PAWN's moment-independent approaches (Pianosi et al. 2015, Puy et al. 2020). A systematic review of the sensitivity analysis on recent advance can be found in (Borgonovo and Plischke 2016, Saltelli et al. 2019). Consequently, the community has

made great efforts to provide guidelines on application of sensitivity analysis with various freely available tools, such as: the MATLAB-based SAFE (Pianosi et al. 2015), UQLab (Marelli and Sudret 2014) and VARS-TOOL (Razavi et al. 2019), the C++ based PSUADE (<https://computing.llnl.gov/projects/psuade-uncertainty-quantification>), the sensitivity package in R (<https://cran.r-project.org/web/packages/sensitivity/index.html>), and the Python packages UQ-PyL (Wang et al. 2016), SALib (Herman and Usher 2017), pyEMU (White et al. 2016) and Uncertainpy (Tennoe et al. 2018).

Despite the thorough documents and good practices of above-mentioned tools for application of sensitivity analysis on earth and environmental system model, a common drawback of existing tools is they are rooted in the parametric uncertainty focusing on individual system model and fail to consider the process model uncertainty (or the model structural uncertainty) (Clark et al. 2008, Dai et al. 2017b, Walker et al. 2018). Generally, the earth system models are composed multiple interacting processes (Clark et al. 2015b). When performing sensitivity analysis on such complex process-based system models, parallelly to the parametric uncertainty, questions rise such as which are the most important process deserving of further investigation or can the model be simplified by ignoring some non-influential processes? Under individual system model configuration, i.e., there is no process model uncertainty, these questions can be answered by analyzing the sensitivity of parameters embedded in the processes. However, real-world processes comprised the system model may build on multiple plausible assumptions and the model behaviors depend on the particular choice of the process assumptions. When the available data and knowledge support using of multiple process models, a model developer is not only faced with the uncertainty parameters but also the uncertainty process models. Methods and tools to address process sensitivity considering both parametric and process model uncertainty are urgently needed.

To remedy the lack of available uncertainty analysis tools to include the process model uncertainty, this dissertation has developed a python package, SAMMPy, for performing process sensitivity analysis under multiple system models. The first release the SAMMPy includes the variance-based process sensitivity analysis (VBSA) and multi-model absolute difference-based sensitivity analysis (MMADS). VBSA provides both the first-order and total-effect process sensitivity indices for different purposes of sensitivity analysis. MMADS computes the mean and variance of the output difference for each process. A model object is designed as an interface to accept the information of

user defined system model, processes and corresponding processes models. The package also offers several visual tools including the histogram plots for parameter distributions, bar plots for comparing the first-order and total effect process sensitivity indices from VBSA and scatter plots of the mean and variance of the output difference from the MMADS. Example workflows of a mathematical test function and a one-dimensional groundwater flow model are documented in Jupyter notebooks that are also available in the SAMMPy repository. This chapter complements that documentation by providing an overview of the package.

§6.2 Structural of SAMMPy

Figure 6-1 shows how the SAMMPy package is organized into several folders. To better understand the file structure used in these folders and perform the process sensitivity analysis under multiple models, the following three steps must be followed:

- (1) Define the multiple system model configuration. The system model is conceptualized with multiple processes, each of which has its alternative process models to describe this process. The process models may have their own or shared parameters, which vary in their ranges and distributions.
- (2) Sample the random parameters within their variability space and execute the system model and obtain the model outputs using all process model and parameter combinations.
- (3) Perform the process sensitivity analysis and visualize the results.

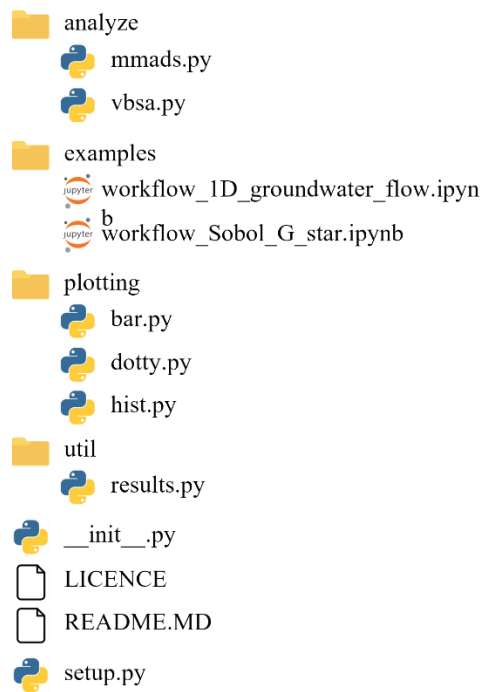


图 6-1 SAMMPy 软件包的组织架构

Figure 6-1 Organization of the SAMMPy package

The Python script “*init_.py*” defines a generic object which enables one to customize his/her own system model. The object aspects the information of the name of the system model, the names of processes involved in the system model, the available process models and the model weights used for each process, the global environmental variables, i.e., the constant parameter values during the simulation, and the random parameters with their range and distributions embedded in the process models. The folder “*examples*” provides workflows of a mathematical test function, the Sobol-G* function, and a one-dimensional groundwater flow model. For the example application of one-dimensional groundwater flow model, the system model is comprised by three processes and each of which has two alternative equally weighted process models with their associated parameters, the multiple system model configuration is defined by SAMMPy as:

```

>>>import sammpy as sm
>>>model = sm.model()
>>>model.name = 'gwmodel'
>>>model.frames = {'names' : ['rechrg', 'geol', 'snomlt'],
                  'options': [['rechrg_lin', 'rechrg_power'],
                             ['geol_single', 'geol_double'],
                             ['snomlt_degree', 'snomlt_restrcd']]],
  
```

```

'weights': [[0.5, 0.5],
            [0.5, 0.5],
            [0.5, 0.5]]}

>>> model.pars = {'names': ['a', 'b', 'K', 'K1', 'K2', 'f1', 'f2', 'r'],
                  'bounds': [[2.0, 0.4], [0.2, 0.5], [2.9, 0.5], [2.6, 0.3],
                             [3.2, 0.3], [3.5, 0.75], [2.5, 0.3], [0.3, 0.05]],
                  'dists': ['norm', 'unif', 'lognorm', 'lognorm', 'lognorm', 'norm', 'norm', 'norm']}

```

SAMMPy utilizes the SALib to generate the random parameters across their ranges and distributions. SALib is an open-source python library for sensitivity analysis and implements several widely used sampling techniques (Herman and Usher, 2017) supporting various distribution functions. The parameter values are generated as:

```
>>> param_values = model.sample(nobs=500, method='saltelli', seed=933090936)
```

In this case, 500 parameter values are generated with random seed 933090936 for each of the parameters defined in the *model.pars* using Saltelli's sampling scheme (for now it is the only supported one in SAMMPy). The distribution of the generated parameters can be displayed using histogram plots provided in the “plotting folder” as shown in Figure 6-2a.

```

>>> from sammpy.plotting import hist
>>> hist.plot(param_values)

```

The next step is to calculate the system model outputs under all possible process model and parameter combinations. An array, denoted as *Y*, is initialized to store the output values, of which the size is $2 \times 500 \times 2 \times 500 \times 2 \times 500$ in this case, corresponding to two recharge process models associated with 500 random parameters values, two geology process models associated with 500 random parameters values, and two snowmelt process models associated with 500 random parameters values.

After obtaining the output array, the process sensitivity analysis can be performed. SAMMPy provides two different process sensitivity analysis methods: variance-based process sensitivity analysis method (*vbsa.py*) and the MMADS analysis method (*mmads.py*) as shown in the folder “analyze”. The former computes both the first-order and total-effect process sensitivity indices and the later computes the mean and variance of the model output difference for each process, respectively. The results are reorganized into a directory by calling the *results.py* provided in the “util” folder.

```
>>> from sammpy.analyze import vbsa
```

```
>>>Ret_vbsa = vbsa.analyze(model, Y, print_to_console=True)
>>>from sammpy.analyze import mmds
>>>Ret_mmds = mmds.analyze(model, Y, print_to_console=True)
```

The “print_to_console” is used to control whether to display the computing results. The first-order and total effect process sensitivity indices can be compared using the bar plots and the mean vs. variance of the output difference are plotted in the dotty (scatter) plots as shown in Figure 6-2b and 6-2c, respectively.

```
>>>from sammpy.plotting import bar
>>>bar.plot(model, Ret_vbsa)
>>>from sammpy.plotting import dotty
>>>dotty.plot(model, Ret_mmds)
```

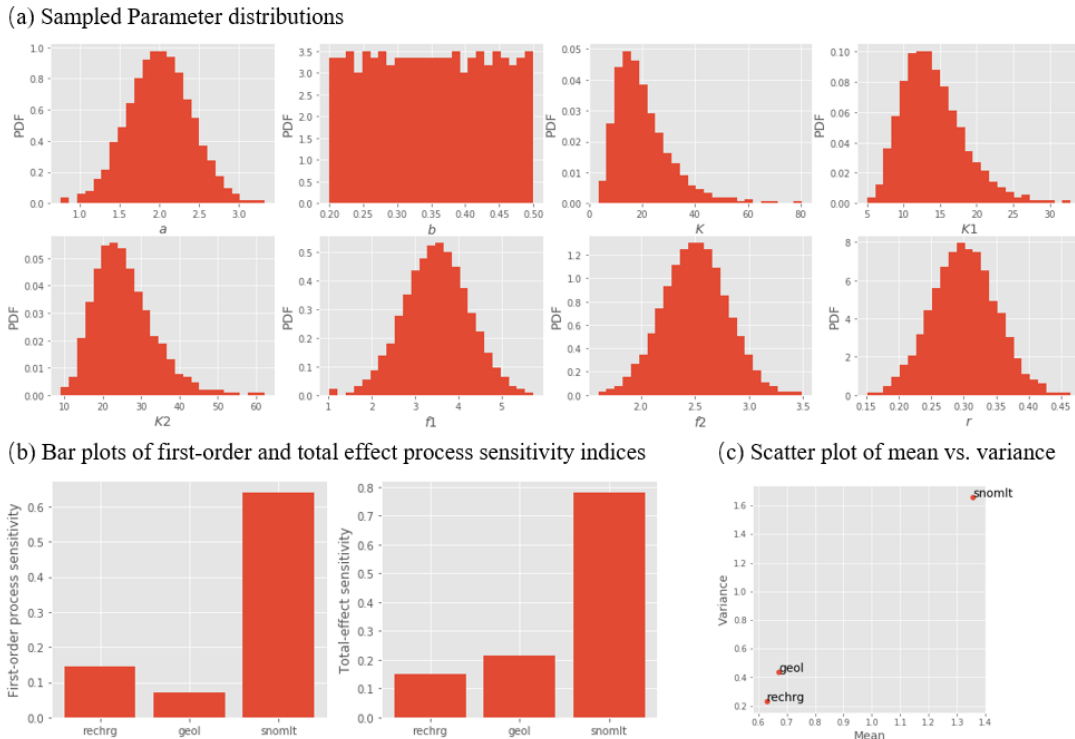


图 6-2 一维河间地块模型 SAMMPy 可视化示例：(a) 参数采样分布频率直方图；(b) 基于方差的过程敏感性分析方法的三个水文过程的一阶和总效应过程敏感性指标；(c) 基于绝对差值的过程敏感性分析方法的三个水文过程的系统模型输出差异的均值与方差散点图。

Figure 6-2 Examples of visualization tools implemented in the SAMMPy of the one-dimensional groundwater flow model: (a) histogram of sampled parameter distributions; (b) bar plots for the first-order and total-effect process sensitivity indices for the three process using variance-based sensitivity analysis; (c) scatter plots of the mean vs. variance of the output difference for the three processes using difference-based sensitivity analysis.

The modular structure of SAMMPy enables to plug-in new code easily. For instance,

new process sensitivity analysis methods can be included in the code by simply adding new functions to the “analyze” folder. Besides, it makes it easy to use portions of the code only. For example, the system models do not need to be coded in Python and external system model outputs can be loaded directly to apply the VBSA or MMDS sensitivity analysis.

§6.3 Software Available and Maintenance

6.3.1 Software Availability

Name of software: SAMMPy

Programming language: Python

Operating system: Windows, Linux and MacOS

Availability: <https://github.com/jyangfsu/SAMMPy>

Cost: Free for non-commercial academic research

SAMMPy is an open-source python package for performing process sensitivity analysis under multiple models. It is designed to facilitate the building and detailed analysis of system models when there are multiple process models to represent multiple processes. It provides both visualization tools and workflows to assist user in performing process sensitivity analysis under multiple system models. With a few lines of readable codes, the learning curve of SAMMPy is deep and short even for non-coding researchers.

6.3.2 Software Maintenance

SAMMPy is freely available for noncommercial research and educational purposes. The package is published to PyPI (The Python Package Index, which is a repository of software for the Python programming language, <https://pypi.org/>) and it can be easily installed. New version is being developed and will be progressively uploaded with new methods for parameter sampling, process sensitivity analysis, more flexible to run the multiple system model using a single command and reducing computational cost using surrogate models. Hopefully, SAMMPy could contribute towards improving the quantity of sensitivity analysis with multiple models and the understanding of the complex process-based environmental system models.

§6.4 Summary

SAMMPy is developed to facilitate the global sensitivity analysis with the presence of multiple models. SAMMPy is a modular modelling package that can vary model structure (process representation), allowing for the generation and running of a model ensemble that varies in process representations, parameter numbers, and parameter distributions. Example workflows of a mathematical test function and a one-dimensional groundwater flow model are documented in Jupyter Notebooks available in the GitHub repository. Ultimately, SAMMPy aims at contributing towards improving the quantity of sensitivity analysis with multiple models and the understanding of the complex process-based environmental system models.

Chapter 7 Summary, Contributions, and Future Work

The overarching goal of this dissertation is to develop two complementary new methods to identify controlling processes in subsurface hydrologic modeling under both process model and parameter uncertainty. This chapter summarizes the progress made toward achieving the goal, highlight key intellectual contributions, and suggest directions for future research.

§7 .1 Summary

This dissertation presents two complementary methods, namely, the variance-based process sensitivity analysis method and the MMADS analysis method, and their applications to identify controlling processes in subsurface hydrologic modeling under process model and parameter uncertainty. This dissertation also presents SAMMPy: an open-source Python package for Sensitivity Analysis under Multiple Models, to evaluate the sensitivity indices of the two new methods. The controlling processes are defined in the context of Factors Prioritization setting and Factors Fixing setting as discussed in Saltelli et al. (2004).

For Factors Prioritization, the purpose is to “make a rational bet on what is the factor that one should fix to achieve the greatest reduction in the uncertainty of the output” (Saltelli et al. 2004). The purpose of this sensitivity analysis is to spend resources to study the factors for achieving the greatest reduction in predictive uncertainty to improve model predictions. In line with this, controlling processes are those control reduction of predictive uncertainty. For Factors Fixing, the purpose is to “screen the input factors by identifying factors or sets of factors that are non-influential” (Saltelli et al. 2004). The purpose of this sensitivity analysis is to avoid spending resources to study the factors (i.e., exclude them from further investigation) that have non-influential contribution to predictive uncertainty. In this sense, controlling processes are those control how much uncertainty caused by themselves and their interactions with other processes.

With the Factors Prioritization setting, Dai et al. (2017b) defined the first-order process sensitivity index. With the Factor Fixing setting, this dissertation derives the total-

effect process sensitivity index to identify the most as well as the least influential processes. The total-effect process sensitivity index links Sobol's variance-based sensitivity analysis and model averaging method to consider both process model uncertainty and parametric uncertainty. The total-effect process sensitivity index differs from the first-order process sensitivity index, in that the former considers process interactions but the latter does not. The derivation and demonstration of total-effect sensitivity index are given in Chapter 2. The 1-D groundwater flow example indicates that the total-effect process sensitivity index considers process interactions and thus is different from the first-order process sensitivity index. Numerical evaluation of the two sensitivity indices is computational expensive because it relies on a brute force Monte Carlo scheme that requires tens of thousands even millions of model executions. To reduce computational cost, this dissertation develops a computationally efficient quasi-Monte Carlo method. This method is also presented in Chapter 2 with the 1-D groundwater flow example for demonstration.

To further reduce the computational cost for Factor Fixing setting, this dissertation develops a new MMADS analysis method to identify non-influential system processes with consideration of uncertainty in both process model structures and process model parameters. MMADS is an expansion of the Morris method from the parameter space to the parameter-process-model space. Differences of a model output are evaluated for: (1) within a process model, model parameters change from one set of values to another set of values, and (2) across two process models of the same system process, model parameters change from one set of values specific to one process model to another set of values specific to the other process models. The differences thus consider not only process model variation but also process model parameter variation. The variations are quantified by the mean and variance of the differences, which are evaluated using the model averaging approaches based on weights of process models. This method is presented in Chapter 3 and demonstrated by using the 1-D groundwater flow example. Besides, a binning method is also presented in Chapter 3 to reduce the computational cost for MMADS.

The developed methods were applied to two subsurface hydrologic models for identifying the controlling processes. The first one is a 2-D As sorption and reactive transport model based a laboratory experiment by Duan et al. (2020), which is presented in Chapter 4. Three processes, namely, the physical process, the chemical process, and

the sorption process were conceptualized. Utilizing the variance-based process sensitivity analysis method proposed in Chapter 2, this dissertation quantifies the relative importance and influence of three processes to arsenic concentrations at the pumping wells under individual system models as well as multiple system models. Results indicate that the most important and influential process on As concentration in the pumping well could change over time. At the very beginning of the simulation period after pumping started ($t < 16$ d), the chemical process significantly influences the As concentration in the pumping well. At the initial stage (16 d $< t < 32$ d), the physical process significantly influences the As concentration in the pumping well. At the middle stage (32 d $< t < 41$ d), the chemical aquifer heterogeneity significantly influences the arsenic concentration in groundwater. At the final stage ($t > 41$ d), the three different sorption models significantly influence the arsenic concentration in groundwater since they can enhance the sorption capacity the aquifer. The second one is a real-world biogeochemical model at the groundwater-surface water interface within the Hanford Site's 300 Area, which is presented in Chapter 5. Multiple uncertainty sources across four different processes, namely, the climate, flow, heat, and reaction processes were considered based on our understanding of the complex system. Variance-based process sensitivity analysis proposed in Chapter 2 as well as the multi-model absolute difference-based process sensitivity analysis methods developed in Chapter 3 were used to identify the controlling processes with respect to the spatio-temporal distribution of the OC consumption rate in the aquifer of the Hanford Site. The results revealed that both the groundwater flow and reactive transport processes contributed significantly to the predictive uncertainty in OC consumption rate, followed by the climate scenario that defines the driving forces of the system. The heat transport process was much less important compared to the other three processes.

All the sensitivity analysis methods are implemented by developing Python codes, and the codes are in a software called SAMMPy: a Python package for process Sensitivity Analysis under Multiple Models. The SAMMPy's design and structure are discussed in Chapter 6, and the package is released to the public for free download.

§7.2 Contributions

The main contributions of this dissertation are:

(1) The two new multi-model global sensitivity analysis methods which extend the traditional parameter sensitivity analysis methods for a single model and can be used to identify the controlling processes in subsurface hydrologic modeling with the presence of process model and parameter uncertainty. The derivation of the two methods is mathematically rigorous and general. Thus, it can be applied to a wide range of subsurface hydrologic and environmental modeling that improves our understanding of the Earth System Models.

(2) The applications of the two subsurface hydrologic models indicate that it is necessary to include model uncertainty and demonstrates how uncertainty estimates and sensitivity analysis can be combined to guide the identification of controlling processes, in hydrologic modeling to improve system robustness and reliability.

(3) The development of new open-source Python package SAMMPy facilities the sensitivity analysis under multiple models. It provides both visualization tools and workflows to assist user in performing process sensitivity analysis under multiple system models. With a few lines of readable codes, the learning curve of SAMMPy is deep and short even for non-coding researchers.

§7.3 Future Work

There are several possible extensions to the research presented in this dissertation. The first is to incorporate observation data \mathbf{D} to the current methods. In this dissertation, the uncertainty of the parameters is characterized by using the prior distributions and the model weights of the plausible process models are set to be equally weighted. With the presence of observation data \mathbf{D} , the distributions of the uncertainty parameters can be updated to posterior distributions and the posterior process model weights by adopting a Bayesian approach. For example, the posterior parameter distributions for a single system model combined by process models M_K and $M_{\sim K}$ can be evaluated as

$$p(\boldsymbol{\theta} | M_K, M_{\sim K}, \mathbf{D}) = \frac{p(\mathbf{D} | \boldsymbol{\theta}, M_K, M_{\sim K}) p(\boldsymbol{\theta} | M_K, M_{\sim K})}{\int p(\mathbf{D} | \boldsymbol{\theta}, M_K, M_{\sim K}) p(\boldsymbol{\theta} | M_K, M_{\sim K})} , \quad (7.1)$$

where $p(\boldsymbol{\theta} | M_K, M_{\sim K}, \mathbf{D})$ is the posterior parameter distribution for system model combined by process models M_K and $M_{\sim K}$ conditioned on data \mathbf{D} ; $p(\boldsymbol{\theta} | M_K, M_{\sim K})$ is the prior parameter distribution, and $p(\mathbf{D} | \boldsymbol{\theta}, M_K, M_{\sim K}, \mathbf{D})$ is the likelihood function. There are several Bayesian approaches tailored for hydrologic modeling that can be utilized to achieve this

goal, including the GLUE framework and DREAM(zs) algorithm as mentioned earlier.

A related issue is to link the data-worth analysis (or value-of-information) to the current methods. A major benefit of new data is its potential to help improve one's understanding of the system, in large part through a reduction in model predictive uncertainty and corresponding risk of failure (Neuman et al. 2012). The goal of the data-worth analysis is to determine the new data \mathbf{C} that can reduce the covariance of model outputs to the maximum extent conditioned on the augmented data set $[\mathbf{D}, \mathbf{C}]$. This is much related to the concept of factor prioritization setting used in this thesis. For example, impacts of the augmented data, \mathbf{C} , on the hydrologic processes can be evaluated by using the difference of partial variance values of the first-order process sensitivity index before and after they are collected.

Future research is needed to reduce computational cost of the multi-model global sensitivity analysis. Although this dissertation develops a computationally efficient estimator for variance-based process sensitivity analysis and the binning method for MMADS analysis method to reduce computational cost, the two methods are still computationally expensive due to their relying on Monte Carlo implementations. Long runtimes inhibit the use of the two methods especially for applications with greater conceptual model complexity and larger number of parameters. A possible solution is to use surrogate modeling to further break the computational barrier between models and model analysis needed by the multi-model sensitivity analysis. Surrogate modeling aims to provide an accurate but cheap-to-run model which emulates a specific output of a complex model in function of its inputs and parameters. It has the potential to reduce computational cost of executing complex models without sacrificing computational accuracy and a number of advanced surrogate modeling methods have been applied in the hydrologic modeling (Asher et al. 2015, 张将伟等, 2018, 闫雪嫚等, 2017).

Acknowledgements

The journey toward a PhD is one that cannot be undertaken alone. There have been so many people who encouraged me along the way that I have made it thus far, and I am eternally grateful for their support. First and foremost, I would like to thank my supervisor, Professor Zhonghua Tang in the School of Environmental Studies at the China University of Geosciences and my co-supervisor, Professor Ming Ye in the Department of Earth, Ocean, and Atmospheric Science and Department of Scientific Computing at the Florida State University. Professor Tang has introduced me to numerical modeling and taught me step by step how to be a good modeler. Professor Ye has always showed me how critical thinking can empower me to do more and succeed. It has truly been a privilege to be their student and I am most grateful for everything they have taught me about research, life, and making it all balance together. Their motivation, encouragement, guidance, and consistent support enabled me to develop an understanding of current research and to grow as an independent researcher. To the world they may be just supervisors, but to me they are HEROES.

I owe a great deal of thanks to Professor Quanrong Wang in the School of Environmental Studies at the China University of Geosciences, for lending his knowledge and support to every aspect of my research, and for providing invaluable feedback and guidance outside of research. I also wish to acknowledge the faculty members at the China University of Geosciences – Professors Dongjin Xiang, Yi-Ming Kuo, Chuanming Ma, Huirong Guo, Zhihua Chen, Junwei Wan, Hong Zhou, Zhang Wen, Peng Liu, Kun Huang, and Cong Jiang – thank you for devoting your time to discuss my research findings and provided valuable suggestions and insightful comments that have helped to improve this dissertation. The three anonymous reviewers are also greatly appreciated for their constructive feedbacks that substantially improved the dissertation.

To my lab-mates, past and present, in Office 310 of Wenhua Building and Office 215 of Research Building #4 of Wuhan Future City Campus, thank you so much for sharing this journey with me. It has been a pleasure to work with and learn from you. I would like to especially recognize Peng Yu, Haibo Li, Qingjun Deng, Tianyun Xiao, Qihai Luo, Lu

Zhou, Minzhi Chen, Changlong Zhao, Zhichao Zhang, Peixin He, Linyong Shao, Rui Chen, Huiyang Wang, Yaru Yang, Fengchun Shi, Jing Jing, Xinlin He, Lin Zuo, Feng Xiong, Xinying Geng, Yuanchuang Zhang, Liangzhe Ma, Qian Hu, Jialing Wu, Junxian Li, and Wenguang Shi for making my stay in CUG such a memorable experience. Special thanks need to give Dr. Xuehang Song and Dr. Pin Shuai at Pacific Northwest National Laboratory, Dr. Heng Dai at China University of Geosciences, Dr. Rong Li and Dr. Yanhua Duan at Southern University of Science and Technology for their generosity of sharing the PFLOTRAN models. This research would not have been possible without you all, and I am very grateful for all your help.

Outside of research, I have been extremely fortunate to have the support of a diverse group of friends who help me keep things in perspective. Pan Xu and Xin Yi are two of my closest friends who have accompanied me on this journey. We were in the same class as undergraduate students at Yangtze University and surely it was the destiny which brought us together again as graduate students at SES. We knew each other for more than ten years and they have done so much to lift my spirits, especially during the first two years living at CUG. To my roommates – Yang Li, Jiexiang Li, Tian Feng, and Weiqing Liu, thank you for sharing your kindness and talents and for letting me live vicariously through you. Another huge source of strength comes from the friends during my stay at Tallahassee, Florida. Xiaobing Kang, Sheng Luo, Juxiu Tong, Haiyan Zhao, Junfeng Lu, Hanqing Zhao, Jingze Zhang, Xueming Zheng, Jiawei Liu, Ningyuan Gu, Zhenhuan Lu, Zehao Chen, Pengfei Lv, Shuo Yan, Yuanjing Miao, Xiang Ma, Chang Liu, Congmin Liu, Nur Ahmed, Emily Lizotte, Greta Mikell, and many, many others – thank you for accompanying me, for the positive energy around me, and for bringing joy to my life in a country far away from home.

Finally, I would like to thank my parents for their steadfast love and support. Without them, I would not be where I am today. I credit them for instilling in me the importance of a good education, the determination to overcome whatever challenges may arise, and the confidence to forge my own path. Last but not least, I want to thank Tian Jiao for being my co-pilot on this incredible journey. Thank you for always believing in me, for teaching me to be patient with myself and others, and for giving me the strength to push through the tough times. No man succeeds without a good woman behind him. I look forward to starting the next chapter of our lives together.

References

- [1] AGUSA T, TRANG P T K, LAN, V M, et al. Human exposure to arsenic from drinking water in Vietnam[J]. *Science of The Total Environment*, 2014, 488-489, 562-569.
- [2] AJAMI N K, DUAN Q, SOROOSHIAN S. An integrated hydrologic Bayesian multimodel combination framework: Confronting input, parameter, and model structural uncertainty in hydrologic prediction[J]. *Water Resources Research*, 2007, 43(1), 19.
- [3] ASHER M J, CROKE B F W, JAKEMAN A J, et al. A review of surrogate models and their application to groundwater modeling[J]. *Water Resources Research*, 2015, 51(8), 5957-5973.
- [4] BÁRDOSSY A, DAS T. Influence of rainfall observation network on model calibration and application[J]. *Hydrology and Earth System Sciences*, 2018, 12(1), 77-89.
- [5] BARONI G., TARANTOLA S. A General Probabilistic Framework for uncertainty and global sensitivity analysis of deterministic models: A hydrological case study[J]. *Environmental Modelling & Software*, 2014, 51, 26-34.
- [6] BELL S A. A beginner's guide to uncertainty of measurement, 2011.
- [7] BEVEN K. Chapter 12 Uncertainty and the detection of structural change in models of environmental systems[M]. *Developments in Environmental Modelling*, 2002, 22, 227-250.
- [8] BEVEN K. Facets of uncertainty: epistemic uncertainty, non-stationarity, likelihood, hypothesis testing, and communication[J]. *Hydrological Sciences Journal*, 2016, 61(9), 1652-1665.
- [9] BEVEN K, BINLEY A. The future of distributed models: Model calibration and uncertainty prediction[J]. *Hydrological Processes*, 1992, 6(3), 279-298.
- [10] BHATTACHARYA P, WELCH A H, STOLLENWERK K G, et al. Arsenic in the environment: Biology and Chemistry[J]. *Science of The Total Environment*, 2007, 379(2-3), 109-120.

- [11] BIANCHI JANETTI E, GUADAGNINI L, RIVA M et al. Global sensitivity analyses of multiple conceptual models with uncertain parameters driving groundwater flow in a regional-scale sedimentary aquifer[J]. *Journal of Hydrology*, 2019, 574, 544-556.
- [12] BISSEN M, FRIMMEL F H. Arsenic — a Review. Part I: Occurrence, Toxicity, Speciation, Mobility[J]. *Acta hydrochimica et hydrobiological*, 2003a, 31(1), 9-18.
- [13] BISSEN M, FRIMMEL F H. Arsenic — a Review. Part II: Oxidation of Arsenic and its Removal in Water Treatment[J]. *Acta hydrochimica et hydrobiological*, 2003b, 31(2), 97-107.
- [14] BJORNSTAD B N, HORNER J A, VERMEUL V R, et al. Borehole Completion and Conceptual Hydrogeologic Model for the IFRC Well Field, 300 Area, Hanford Site[R], Pacific Northwest National Lab. (PNNL), Richland, 2009.
- [15] BONAN G B, LOMBARDONI D L, WIEDER W R, et al. Model Structure and Climate Data Uncertainty in Historical Simulations of the Terrestrial Carbon Cycle (1850-2014)[J]. *Global Biogeochemical Cycles*, 2019, 33(10), 1310-1326.
- [16] BORGONOVO E. A new uncertainty importance measure[J]. *Reliability Engineering & System Safety*, 2007, 92(6), 771-784.
- [17] BORGONOVO E, LU X, PLISCHKE E, et al. Making the most out of a hydrological model data set: Sensitivity analyses to open the model black-box[J]. *Water Resources Research*, 2017, 53(9), 7933-7950.
- [18] BORGONOVO E, PLISCHKE E. Sensitivity analysis: A review of recent advances[J]. *European Journal of Operational Research*, 2016, 248(3), 869-887.
- [19] BOX G E P, DRAPER N R. *Empirical model-building and response surfaces*[M]. John Wiley & Sons, Oxford, England, 1987.
- [20] BRADDOCK R D, SCHREIDER S Y. Application of the Morris algorithm for sensitivity analysis of the REALM model for the Goulburn irrigation system[J]. *Environmental Modeling & Assessment*, 2006, 11(4), 297-313.
- [21] BRENNER S, COXON G, HOWDEN N J K, et al. Process-based modelling to evaluate simulated groundwater levels and frequencies in a Chalk catchment in south-western England[J]. *Natural Hazards and Earth System Sciences*, 2018, 18(2), 445-461.
- [22] BURNHAM K P, ANDERSON D R. *Model Selection and Inference: A Practical Information-Theoretic Approach*[M], Springer-Verlag, New York, 2002.
- [23] CACUCI D G. *Sensitivity & Uncertainty Analysis*[M], Volume 1, New York, 2003

- [24] CALLAHAM J L, KOCH J V, BRUNTON B W, et al. Learning dominant physical processes with data-driven balance models[J]. *Nature Communications*, 2021, 12(1), 1016.
- [25] CAMPOLOGO F, CARIBONI J, SALTELLI A. An effective screening design for sensitivity analysis of large models[J]. *Environmental Modelling & Software*, 2007, 22(10), 1509-1518.
- [26] CHANG Y, WU J, JIANG G, et al. Identification of the dominant hydrological process and appropriate model structure of a karst catchment through stepwise simplification of a complex conceptual model[J]. *Journal of Hydrology*, 2017, 548, 75-87.
- [27] CHARLET L, CHAKRABORTY S, APPELO, C A J, et al. Chemodynamics of an arsenic “hotspot” in a West Bengal aquifer: A field and reactive transport modeling study[J]. *Applied Geochemistry*, 2007, 22(7), 1273-1292.
- [28] CHEN X, HAMMOND G E, MURRAY C J, et al. Application of ensemble-based data assimilation techniques for aquifer characterization using tracer data at Hanford 300 area[J]. *Water Resources Research*, 2013, 49(10), 7064-7076.
- [29] CHEN X, MURAKAMI H, HAHN M S, et al. Three-dimensional Bayesian geostatistical aquifer characterization at the Hanford 300 Area using tracer test data[J]. *Water Resources Research*, 2012, 48(6).
- [30] CIRIC C, CIFFROY P, CHARLES S. Use of sensitivity analysis to identify influential and non-influential parameters within an aquatic ecosystem model[J]. *Ecological Modelling*, 2012, 246, 119-130.
- [31] CLARK, M P, FAN Y, LAWRENCE D M, et al. Improving the representation of hydrologic processes in Earth System Models[J]. *Water Resources Research*, 2015a, 51(8), 5929-5956.
- [32] CLARK M P, KAVETSKI D, FENICIA F. Pursuing the method of multiple working hypotheses for hydrological modeling[J]. *Water Resources Research*, 2011, 47(9).
- [33] CLARK M P, NIJSSEN B, LUNDQUIST J D, et al. A unified approach for process-based hydrologic modeling: 1. Modeling concept[J]. *Water Resources Research*, 2015b, 51(4), 2498-2514.
- [34] CLARK M P, NIJSSEN B, LUNDQUIST J D, et al. A unified approach for process-based hydrologic modeling: 2. Model implementation and case studies[J]. *Water Resources Research*, 2015c, 51(4), 2515-2542.

- [35] CLARK M P, SLATER A G, RUPP D E, et al. Framework for Understanding Structural Errors (FUSE): A modular framework to diagnose differences between hydrological models[J]. Water Resources Research, 2008, 44(12).
- [36] CUSHING C E. Hanford Site National Environmental Policy Act (NEPA) Characterization[R], Pacific Northwest Lab. (PNNL), Richland, 1992.
- [37] DAI H, CHEN X, YE M, et al. Using Bayesian Networks for Sensitivity Analysis of Complex Biogeochemical Models[J]. Water Resources Research, 2019, 55, 3541–3555.
- [38] DAI H, CHEN X, YE M, et al. A geostatistics-informed hierarchical sensitivity analysis method for complex groundwater flow and transport modeling[J]. Water Resources Research, 2017a, 53(5):4327-4343.
- [39] DAI H, YE M. Variance-based global sensitivity analysis for multiple scenarios and models with implementation using sparse grid collocation[J]. Journal of Hydrology, 2015, 528:286-300.
- [40] DAI H, YE M, WALKER A P, et al. A new process sensitivity index to identify important system processes under process model and parametric uncertainty[J]. Water Resources Research, 2017b, 53(4):3476-3490.
- [41] DELL'OCA A, RIVA M, GUADAGNINI A. Global sensitivity analysis for multiple interpretive models with uncertain parameters[J]. Water Resources Research, 2020, 56(2): e2019WR025754.
- [42] DELL'OCA A, RIVA M, GUADAGNINI A. Moment-based metrics for global sensitivity analysis of hydrological systems[J]. Hydrology and Earth System Sciences, 2017, 21(12):6219-6234.
- [43] DETTINGER M D, WILSON J L. First order analysis of uncertainty in numerical models of groundwater flow part: 1. Mathematical development[J]. Water Resources Research, 1981, 17(1):149-161.
- [44] DOHERTY J E, R.J. H, TONKIN M J. Approaches to highly parameterized inversion: a guide to using PEST for model-parameter and predictive-uncertainty analysis[R]. Reston, Virginia, 2010.
- [45] DRAPER D. Assessment and propagation of model uncertainty[J]. Journal of the Royal Statistical Society: Series B (Methodological), 1995, 57(1):45-70.

- [46] DUAN Y, GAN Y, WANG Y, et al. Temporal variation of groundwater level and arsenic concentration at Jianghan Plain, central China[J]. *Journal of Geochemical Exploration*, 2015, 149:106-119.
- [47] DUAN Y, GAN Y, WANG Y, et al. Arsenic speciation in aquifer sediment under varying groundwater regime and redox conditions at Jianghan Plain of Central China[J]. *Sci Total Environ*, 2017, 607-608:992-1000.
- [48] DUAN Y, LI R, GAN Y, et al. Impact of Physico-Chemical Heterogeneity on Arsenic Sorption and Reactive Transport under Water Extraction[J]. *Environmental Science & Technology*, 2020, 54(23):14974-14983.
- [49] DUBUS I G, BROWN C D, BEULKE S. Sensitivity analyses for four pesticide leaching models[J]. *Pest Management Science*, 2003, 59(9):962-982.
- [50] DUBUS I G, BROWN C D, BEULKE S. Sources of uncertainty in pesticide fate modelling[J]. *Science of The Total Environment*, 2003, 317(1-3):53-72.
- [51] FATICHI S, VIVONI E R, OGDEN F L, et al. An overview of current applications, challenges, and future trends in distributed process-based models in hydrology[J]. *Journal of Hydrology*, 2016, 537:45-60.
- [52] FENDORF S, MICHAEL H A, VAN GEEN A. Spatial and Temporal Variations of Groundwater Arsenic in South and Southeast Asia[J]. *Science*, 2010, 328(5982):1123-1127.
- [53] FENDORF S, NICO P S, KOCAR B D, et al. Chapter 12 - Arsenic Chemistry in Soils and Sediments [M]. *Developments in Soil Science*. Elsevier. 2010: 357-378.
- [54] FENICIA F, KAVETSKI D, SAVENIJE H H G. Elements of a flexible approach for conceptual hydrological modeling: 1. Motivation and theoretical development[J]. *Water Resources Research*, 2011, 47(11).
- [55] FRANCKE T, BARONI G, BROSINSKY A, et al. What Did Really Improve Our Mesoscale Hydrological Model? A Multidimensional Analysis Based on Real Observations[J]. *Water Resources Research*, 2018, 54(11):8594-8612.
- [56] FRITZ B G. Investigation of the Hyporheic Zone at 300 Area Hanford Site[R]. 2007.
- [57] GAN Y, DUAN Q, GONG W, et al. A comprehensive evaluation of various sensitivity analysis methods: A case study with a hydrological model[J]. *Environmental Modelling & Software*, 2014, 51:269-285.

- [58] GAN Y, WANG Y, DUAN Y, et al. Hydrogeochemistry and arsenic contamination of groundwater in the Jianghan Plain, central China[J]. Journal of Geochemical Exploration, 2014, 138:81-93.
- [59] GAN Y J, DUAN Q Y, GONG W, et al. A comprehensive evaluation of various sensitivity analysis methods: A case study with a hydrological model[J]. Environmental Modelling & Software, 2014, 51:269-285.
- [60] GEE G W, OOSTROM M, FRESHLEY M D, et al. Hanford site vadose zone studies: An overview[J]. Vadose Zone Journal, 2007, 6(4):899-905.
- [61] GEPHART R E. Hanford: A Conversation About Nuclear Waste and Cleanup[M]. Columbus: Battelle Press, 2003.
- [62] GLASGOW H S, FORTNEY M D, LEE J, et al. MODFLOW 2000 head uncertainty, a first-order second moment method[J]. Ground Water, 2003, 41(3):342-50.
- [63] GORELICK S M, ZHENG C. Global change and the groundwater management challenge[J]. Water Resources Research, 2015, 51(5):3031-3051.
- [64] GRAYSON R B, BLOSCHL G. Spatial Patterns in Catchment Hydrology: Observations and Modeling[M]. Cambridge, U. K: Cambridge Univ. Press, 2000.
- [65] GÜNTHER D, MARKE T, ESSERY R, et al. Uncertainties in Snowpack Simulations—Assessing the Impact of Model Structure, Parameter Choice, and Forcing Data Error on Point-Scale Energy Balance Snow Model Performance[J]. Water Resources Research, 2019, 55(4):2779-2800.
- [66] GUPTA H V, CLARK M P, VRUGT J A, et al. Towards a comprehensive assessment of model structural adequacy[J]. Water Resources Research, 2012, 48(8).
- [67] HAMMOND G E, LICHTNER P C, MILLS R T. Evaluating the performance of parallel subsurface simulators: An illustrative example with PFLOTRAN[J]. Water Resources Research, 2014, 50(1):208-228.
- [68] HARVEY J, GOOSEFF M. River corridor science: Hydrologic exchange and ecological consequences from bedforms to basins[J]. Water Resources Research, 2015, 51(9):6893-6922.
- [69] HERMAN J, USHER W. SALib: An open-source Python library for Sensitivity Analysis[J]. The Journal of Open Source Software, 2017, 2(9):771-784.
- [70] HERMAN J D, REED P M, WAGENER T. Time-varying sensitivity analysis clarifies the effects of watershed model formulation on model behavior[J]. Water Resources Research, 2013, 49(3):1400-1414.

- [71] HOCK R. Temperature index melt modelling in mountain areas[J]. *Journal of Hydrology*, 2003, 282(1-4):104-115.
- [72] HOETING J A, MADIGAN D, RAFTERY A E, et al. Bayesian Model Averaging: A Tutorial[J]. *Statistical Science*, 1999, 14(4):382-401.
- [73] HÖGE M, GUTHKE A, NOWAK W. The hydrologist's guide to Bayesian model selection, averaging and combination[J]. *Journal of Hydrology*, 2019, 572:96-107.
- [74] HØJBERG A L, REFGAARD J C. Model uncertainty – parameter uncertainty versus conceptual models[J]. *Water Science and Technology*, 2005.
- [75] HOMMA T, SALTELLI A. Importance measures in global sensitivity analysis of nonlinear models[J]. *Reliability Engineering & System Safety*, 1996, 52(1):1-17.
- [76] HUANG K, LIU Y Y, YANG C, et al. Identification of Hydrobiogeochemical Processes Controlling Seasonal Variations in Arsenic Concentrations Within a Riverbank Aquifer at Jianghan Plain, China[J]. *Water Resources Research*, 2018, 54(7):4294-4308.
- [77] HUQ M E, FAHAD S, SHAO Z, et al. Arsenic in a groundwater environment in Bangladesh: Occurrence and mobilization[J]. *Journal of Environmental Management*, 2020, 262:110318.
- [78] ILLMAN W A, ZHU J, CRAIG A J, et al. Comparison of aquifer characterization approaches through steady state groundwater model validation: A controlled laboratory sandbox study[J]. *Water Resources Research*, 2010, 46(4).
- [79] IOOSS B, LEMAÎTRE P. A Review on Global Sensitivity Analysis Methods [M]. Uncertainty Management in Simulation-Optimization of Complex Systems: Algorithms and Applications. Boston, MA; Springer US. 2015: 101-122.
- [80] JANETTI E B, GUADAGNINI L, RIVA M, et al. Global sensitivity analyses of multiple conceptual models with uncertain parameters driving groundwater flow in a regional-scale sedimentary aquifer[J]. *Journal of Hydrology*, 2019, 574:544-556.
- [81] JANG E, HE W, SAVOY H, et al. Identifying the influential aquifer heterogeneity factor on nitrate reduction processes by numerical simulation[J]. *Advances in Water Resources*, 2017, 99:38-52.
- [82] JOHANNESSEN K H, YANG N, TRAHAN A S, et al. Biogeochemical and reactive transport modeling of arsenic in groundwaters from the Mississippi River delta plain: An analog for the As-affected aquifers of South and Southeast Asia[J]. *Geochimica et Cosmochimica Acta*, 2019, 264:245-272.

- [83] JUNG H B, CHARETTE M A, ZHENG Y. Field, Laboratory, and Modeling Study of Reactive Transport of Groundwater Arsenic in a Coastal Aquifer[J]. *Environmental Science & Technology*, 2009, 43(14):5333-5338.
- [84] KAVETSKI D, FENICIA F. Elements of a flexible approach for conceptual hydrological modeling: 2. Application and experimental insights[J]. *Water Resources Research*, 2011, 47(11).
- [85] KAVETSKI D, KUCZERA G, FRANKS S W. Bayesian analysis of input uncertainty in hydrological modeling: 1. Theory[J]. *Water Resources Research*, 2006, 42(3).
- [86] KAVETSKI D, KUCZERA G, FRANKS S W. Bayesian analysis of input uncertainty in hydrological modeling: 2. Application[J]. *Water Resources Research*, 2006, 42(3).
- [87] KETEMA A A, LANGERGRABER G. Sensitivity analysis of the CLARA Simplified Planning Tool using the Morris screening method[J]. *Water Science and Technology*, 2015, 71(2):234-244.
- [88] KING D M, PERERA B J C. Morris method of sensitivity analysis applied to assess the importance of input variables on urban water supply yield - A case study[J]. *Journal of Hydrology*, 2013, 477:17-32.
- [89] KLEIJNEN J P C. Sensitivity Analysis Versus Uncertainty Analysis: When to Use What? [M]. Predictability and Nonlinear Modelling in Natural Sciences and Economics. Dordrecht; Springer Netherlands. 1994: 322-333.
- [90] KNOBEN W J M, FREER J E, PEEL M C, et al. A Brief Analysis of Conceptual Model Structure Uncertainty Using 36 Models and 559 Catchments[J]. *Water Resources Research*, 2020, 56(9).
- [91] KOBOLD M, BRILLY M. The use of HBV model for flash flood forecasting[J]. *Natural Hazards and Earth System Sciences*, 2006, 6(3):407-417.
- [92] KUSTAS W P, RANGO A, UIJLENHOET R. A simple energy budget algorithm for the snowmelt runoff model[J]. *Water Resources Research*, 1994, 30(5):1515-1527.
- [93] LATIEF F D E, FAUZI U. Kozeny-Carman and empirical formula for the permeability of computer rock models[J]. *International Journal of Rock Mechanics and Mining Sciences*, 2012, 50:117-123.
- [94] LI L, MAHER K, NAVARRE-SITCHLER A, et al. Expanding the role of reactive transport models in critical zone processes[J]. *Earth-Science Reviews*, 2017, 165:280-301.

- [95] LI M, QIAN W-J, GAO Y, et al. Functional Enzyme-Based Approach for Linking Microbial Community Functions with Biogeochemical Process Kinetics[J]. *Environmental Science & Technology*, 2017, 51(20):11848-11857.
- [96] LICHTNER P, HAMMOND G, LU C, et al. PFLOTRAN User Manual: A Massively Parallel Reactive Flow and Transport Model for Describing Surface and Subsurface Processes[R]. 2015.
- [97] LIU H F, DAI H, NIU J, et al. Hierarchical sensitivity analysis for a large-scale process-based hydrological model applied to an Amazonian watershed[J]. *Hydrology and Earth System Sciences*, 2020, 24(10):4971-4996.
- [98] LU D, YE M, CURTIS G P. Maximum likelihood Bayesian model averaging and its predictive analysis for groundwater reactive transport models[J]. *Journal of Hydrology*, 2015, 529:1859-1873.
- [99] MA R, ZHENG C, LIU C, et al. Assessment of controlling processes for field-scale uranium reactive transport under highly transient flow conditions[J]. *Water Resources Research*, 2014, 50(2):1006-1024.
- [100] MA R, ZHENG C, ZACHARA J M, et al. Utility of bromide and heat tracers for aquifer characterization affected by highly transient flow conditions[J]. *Water Resources Research*, 2012, 48(8).
- [101] MAI J, CRAIG J R, TOLSON B A. Simultaneously determining global sensitivities of model parameters and model structure[J]. *Hydrology and Earth System Sciences*, 2020, 24(12):5835-5858.
- [102] MALE F, JENSEN J L, LAKE L W. Comparison of permeability predictions on cemented sandstones with physics-based and machine learning approaches[J]. *Journal of Natural Gas Science and Engineering*, 2020, 77.
- [103] MARELLI S, SUDRET B. UQLab: A Framework for Uncertainty Quantification in Matlab [M]. *Vulnerability, Uncertainty, and Risk*. 2014: 2554-2563.
- [104] MARKSTROM S L, HAY L E, CLARK M P. Towards simplification of hydrologic modeling: identification of dominant processes[J]. *Hydrology and Earth System Sciences*, 2016, 20(11):4655-4671.
- [105] MARTINEC J, RANGO A, ROBERTS R. Snowmelt runoff model (SRM) user's manual[R]. Berne, 1998.

- [106] MENDOZA P A, CLARK M P, BARLAGE M, et al. Are we unnecessarily constraining the agility of complex process-based models[J]. Water Resources Research, 2015, 51(1):716-728.
- [107] MONTANARI A, KOUTSOYANNIS D. A blueprint for process - based modeling of uncertain hydrological systems[J]. Water Resources Research, 2012, 48(9).
- [108] MORRIS M D. Factorial Sampling Plans for Preliminary Computational Experiments[J]. Technometrics, 1991, 33(2):161-174.
- [109] MOULIN L, GAUME E, OBLED C. Uncertainties on mean areal precipitation: assessment and impact on streamflow simulations[J]. Hydrology and Earth System Sciences, 2009, 13(2):99-114.
- [110] MUTAVDZIC PAVLOVIC D, CURKOVIC L, BLAZEK D, et al. The sorption of sulfamethazine on soil samples: isotherms and error analysis[J]. Science of the Total Environment, 2014, 497-498:543-552.
- [111] NEITSCH S L, ARNOLD J G, KINIRY J R, et al. Soil and Water Assessment Tool Theoretical Documentation Version 2009[R]. Texas Water Resources Institute. Available electronically from <https://hdl.handle.net/1969.1/128050>, 2011.
- [112] NEUMAN S P. Maximum likelihood Bayesian averaging of uncertain model predictions[J]. Stochastic Environmental Research and Risk Assessment (SERRA), 2003, 17(5):291-305.
- [113] NEUMAN S P, WIERENGA P J. A comprehensive strategy of hydrogeologic modeling and uncertainty analysis for nuclear facilities and sites[R]. 2003.
- [114] NEUMAN S P, XUE L, YE M, et al. Bayesian analysis of data-worth considering model and parameter uncertainties[J]. Advances in Water Resources, 2012, 36:75-85.
- [115] NIKOLAIDIS N P, DOBBS G M, LACKOVIC J A. Arsenic removal by zero-valent iron: field, laboratory and modeling studies[J]. Water Research, 2003, 37(6):1417-1425.
- [116] PEBESMA E J. Multivariable geostatistics in S: the gstat package[J]. Computers & Geosciences, 2004, 30(7):683-691.
- [117] PI K, WANG Y, XIE X, et al. Remediation of arsenic-contaminated groundwater by in-situ stimulating biogenic precipitation of iron sulfides[J]. Water Res, 2017, 109:337-346.

- [118] PIANOSI F, SARRAZIN F, WAGENER T. A Matlab toolbox for Global Sensitivity Analysis[J]. *Environmental Modelling & Software*, 2015, 70:80-85.
- [119] PIANOSI F, WAGENER T. A simple and efficient method for global sensitivity analysis based on cumulative distribution functions[J]. *Environmental Modelling & Software*, 2015, 67:1-11.
- [120] PODGORSKI J, BERG M. Global threat of arsenic in groundwater[J]. *Science*, 2020, 368(6493):845-850.
- [121] POETER E, ANDERSON D. Multimodel Ranking and Inference in Ground Water Modeling[J]. *Groundwater*, 2005, 43(4):597-605.
- [122] POETER E P, HILL M C. MMA, A Computer Code for Multi-Model Analysis[R]. 2007.
- [123] POSTMA D, LARSEN F, THAI N T, et al. Groundwater arsenic concentrations in Vietnam controlled by sediment age[J]. *Nature Geoscience*, 2012, 5(9):656-661.
- [124] POULIN A, BRISSETTE F, LECONTE R, et al. Uncertainty of hydrological modelling in climate change impact studies in a Canadian, snow-dominated river basin[J]. *Journal of Hydrology*, 2011, 409(3-4):626-636.
- [125] PUY A, LO PIANO S, SALTELLI A. A sensitivity analysis of the PAWN sensitivity index[J]. *Environmental Modelling & Software*, 2020, 127.
- [126] RALEIGH M S, LUNDQUIST J D, CLARK M P. Exploring the impact of forcing error characteristics on physically based snow simulations within a global sensitivity analysis framework[J]. *Hydrology and Earth System Sciences*, 2015, 19(7):3153-3179.
- [127] RAZAVI S, SHEIKHOLESLAMI R, GUPTA H V, et al. VARS-TOOL: A toolbox for comprehensive, efficient, and robust sensitivity and uncertainty analysis[J]. *Environmental Modelling & Software*, 2019, 112:95-107.
- [128] RAZAVI S, TOLSON B A, BURN D H. Review of surrogate modeling in water resources[J]. *Water Resources Research*, 2012, 48(7).
- [129] REFSGAARD J C, VAN DER SLUIJS J P, HØJBERG A L, et al. Uncertainty in the environmental modelling process – A framework and guidance[J]. *Environmental Modelling & Software*, 2007, 22(11):1543-1556.
- [130] RENARD B, KAVETSKI D, KUCZERA G, et al. Understanding predictive uncertainty in hydrologic modeling: The challenge of identifying input and structural errors[J]. *Water Resources Research*, 2010, 46(5).

- [131] ROJAS R, FEYEN L, DASSARGUES A. Conceptual model uncertainty in groundwater modeling: Combining generalized likelihood uncertainty estimation and Bayesian model averaging[J]. Water Resources Research, 2008, 44(12).
- [132] ROSOLEM R, GUPTA H V, SHUTTLEWORTH W J, et al. A fully multiple-criteria implementation of the Sobol' method for parameter sensitivity analysis[J]. Journal of Geophysical Research: Atmospheres, 2012, 117(D7).
- [133] SALTELLI A. Making best use of model evaluations to compute sensitivity indices[J]. Computer Physics Communications, 2002, 145(2):280-297.
- [134] SALTELLI A, ALEKSANKINA K, BECKER W, et al. Why so many published sensitivity analyses are false: A systematic review of sensitivity analysis practices[J]. Environmental Modelling & Software, 2019, 114:29-39.
- [135] SALTELLI A, ANNONI P, AZZINI I, et al. Variance based sensitivity analysis of model output. Design and estimator for the total sensitivity index[J]. Computer Physics Communications, 2010, 181(2):259-270.
- [136] SALTELLI A, RATTO M, ANDRES T, et al. Global Sensitivity Analysis. The Primer[M]. 2007.
- [137] SALTELLI A, TARANTOLA S, CAMPOLONGO F, et al. Sensitivity Analysis in Practice: A Guide to Assessing Scientific Models[M]. 2004.
- [138] SATHE S S, MAHANTA C. Groundwater flow and arsenic contamination transport modeling for a multi aquifer terrain: Assessment and mitigation strategies[J]. J Environ Manage, 2019, 231:166-181.
- [139] SHAJI E, SANTOSH M, SARATH K V, et al. Arsenic contamination of groundwater: A global synopsis with focus on the Indian Peninsula[J]. Geoscience Frontiers, 2021, 12(3).
- [140] SHEN Z Y, CHEN L, CHEN T. Analysis of parameter uncertainty in hydrological and sediment modeling using GLUE method: a case study of SWAT model applied to Three Gorges Reservoir Region, China[J]. Hydrology and Earth System Sciences, 2012, 16(1):121-132.
- [141] SHI X Q, YE M, CURTIS G P, et al. Assessment of parametric uncertainty for groundwater reactive transport modeling[J]. Water Resources Research, 2014, 50(5):4416-4439.

- [142] SHUAI P, CHEN X, SONG X, et al. Dam Operations and Subsurface Hydrogeology Control Dynamics of Hydrologic Exchange Flows in a Regulated River Reach[J]. *Water Resources Research*, 2019.
- [143] SINGH V P. Hydrologic modeling: progress and future directions[J]. *Geoscience Letters*, 2018, 5(1).
- [144] SIVAKUMAR B. Dominant processes concept in hydrology: moving forward[J]. *Hydrological Processes*, 2004, 18(12):2349-2353.
- [145] SIVAKUMAR B. Dominant processes concept in hydrology: moving forward[J]. *Hydrological Processes*, 2004, 18:2349-2353.
- [146] SIVAKUMAR B. Dominant processes concept, model simplification and classification framework in catchment hydrology[J]. *Stochastic Environmental Research and Risk Assessment*, 2007, 22(6):737-748.
- [147] SIVAPALAN M. Process complexity at hillslope scale, process simplicity at the watershed scale: is there a connection?[J]. *Hydrological Processes*, 2003, 17(5):1037-1041.
- [148] SMEDLEY P L, KINNIBURGH D G. A review of the source, behaviour and distribution of arsenic in natural waters[J]. *Applied Geochemistry*, 2002, 17(5):517-568.
- [149] SOBOL' I M. Global sensitivity indices for nonlinear mathematical models and their Monte Carlo estimates[J]. *Mathematics and Computers in Simulation*, 2001, 55(1-3):271-280.
- [150] SONG H S, THOMAS D G, STEGEN J C, et al. Regulation-Structured Dynamic Metabolic Model Provides a Potential Mechanism for Delayed Enzyme Response in Denitrification Process[J]. *Front Microbiol*, 2017, 8:1866.
- [151] SONG X, BRYAN B A, PAUL K I, et al. Variance-based sensitivity analysis of a forest growth model[J]. *Ecological Modelling*, 2012, 247:135-143.
- [152] SONG X, CHEN X, STEGEN J, et al. Drought Conditions Maximize the Impact of High - Frequency Flow Variations on Thermal Regimes and Biogeochemical Function in the Hyporheic Zone[J]. *Water Resources Research*, 2018, 54(10):7361-7382.
- [153] SONG X M, ZHANG J Y, ZHAN C S, et al. Global sensitivity analysis in hydrological modeling: Review of concepts, methods, theoretical framework, and applications[J]. *Journal of Hydrology*, 2015, 523:739-757.

- [154] SPIELER D, MAI J, CRAIG J R, et al. Automatic Model Structure Identification for Conceptual Hydrologic Models[J]. *Water Resources Research*, 2020, 56(9): e2019WR027009.
- [155] STEEFEL C I, APPELO C A J, ARORA B, et al. Reactive transport codes for subsurface environmental simulation[J]. *Computational Geosciences*, 2014, 19(3):445-478.
- [156] STEINBOCK J, WEISSENBRUNNER A, JULING M, et al. Uncertainty evaluation for velocity-area methods[J]. *Flow Measurement and Instrumentation*, 2016, 48:51-56.
- [157] STOLLENWERK K G. Geochemical Processes Controlling Transport of Arsenic in Groundwater: A Review of Adsorption [M]. *Arsenic in Ground Water: Geochemistry and Occurrence*. Boston, MA; Springer US. 2003: 67-100.
- [158] STOLZE L, ZHANG D, GUO H, et al. Model-Based Interpretation of Groundwater Arsenic Mobility during in Situ Reductive Transformation of Ferrihydrite[J]. *Environmental Science & Technology*, 2019, 53(12):6845-6854.
- [159] SUN X, MEIN R G, KEENAN T D, et al. Flood estimation using radar and raingauge data[J]. *Journal of Hydrology*, 2000, 239(1-4):4-18.
- [160] TENNOE S, HALNES G, EINEVOLL G T. Uncertainpy: A Python Toolbox for Uncertainty Quantification and Sensitivity Analysis in Computational Neuroscience[J]. *Front Neuroinform*, 2018, 12:49.
- [161] THIEMANN M, TROSSET M, GUPTA H, et al. Bayesian recursive parameter estimation for hydrologic models[J]. *Water Resources Research*, 2001, 37(10):2521-2535.
- [162] TIAN W. A review of sensitivity analysis methods in building energy analysis[J]. *Renewable and Sustainable Energy Reviews*, 2013, 20:411-419.
- [163] VAN ESSE W R, PERRIN C, BOOIJ M J, et al. The influence of conceptual model structure on model performance: a comparative study for 237 French catchments[J]. *Hydrology and Earth System Sciences*, 2013, 17(10):4227-4239.
- [164] VAN GRIENSVEN A, MEIXNER T, GRUNWALD S, et al. A global sensitivity analysis tool for the parameters of multi-variable catchment models[J]. *Journal of Hydrology*, 2006, 324(1-4):10-23.

- [165] VAN HOEY S, SEUNTJENS P, VAN DER KWAST J, et al. A qualitative model structure sensitivity analysis method to support model selection[J]. *Journal of Hydrology*, 2014, 519:3426-3435.
- [166] VAN WERKHOVEN K, WAGENER T, REED P, et al. Rainfall characteristics define the value of streamflow observations for distributed watershed model identification[J]. *Geophysical Research Letters*, 2008, 35(11).
- [167] VOEGELIN A, HUG S J. Catalyzed oxidation of arsenic(III) by hydrogen peroxide on the surface of ferrihydrite: an in situ ATR FTIR study[J]. *Environmental Science & Technology*, 2003, 37(5):972-8.
- [168] VRUGT J A. Markov chain Monte Carlo simulation using the DREAM software package: Theory, concepts, and MATLAB implementation[J]. *Environmental Modelling & Software*, 2016, 75:273-316.
- [169] VRUGT J A, DIKS C G H, GUPTA H V, et al. Improved treatment of uncertainty in hydrologic modeling: Combining the strengths of global optimization and data assimilation[J]. *Water Resources Research*, 2005, 41(1).
- [170] VRUGT J A, GUPTA H V, BOUTEN W, et al. et al. A shuffled complex evolution metropolis algorithm for optimization and uncertainty assessment of hydrologic model parameters[J]. *Water Resources Research*, 2003, 39(8): 1201.
- [171] WALKER A P, JOHNSON A L, ROGERS A, et al. Multi-hypothesis comparison of Farquhar and Collatz photosynthesis models reveals the unexpected influence of empirical assumptions at leaf and global scales[J]. *Global Change Biology*, 2021, 27(4):804-822.
- [172] WALKER A P, YE M, LU D, et al. The multi-assumption architecture and testbed (MAAT v1.0): R code for generating ensembles with dynamic model structure and analysis of epistemic uncertainty from multiple sources[J]. *Geoscientific Model Development*, 2018, 11(8):3159-3185.
- [173] WALKER W E, HARREMOËS P, ROTMANS J, et al. Defining Uncertainty: A Conceptual Basis for Uncertainty Management in Model-Based Decision Support[J]. *Integrated Assessment*, 2003, 4(1):5-17.
- [174] WALLIS I, PROMMER H, SIMMONS C T, et al. Evaluation of conceptual and numerical models for arsenic mobilization and attenuation during managed aquifer recharge[J]. *Environmental Science & Technology*, 2010, 44(13):5035-41.

- [175] WANG C, DUAN Q, TONG C H, et al. A GUI platform for uncertainty quantification of complex dynamical models[J]. Environmental Modelling & Software, 2016, 76:1-12.
- [176] WHITE J T, FIENEN M N, DOHERTY J E. A python framework for environmental model uncertainty analysis[J]. Environmental Modelling & Software, 2016, 85:217-228.
- [177] WHO. Guidelines for Drinking-Water Quality, fourth ed[M]. Geneva, Switzerland: 2011.
- [178] WILLIAMS M D, THORNE P D, ROCKHOLD M L, et al. Three - dimensional groundwater models of the 300 Area at the Hanford Site[R]. Richland, WA, 2008.
- [179] YE M, MEYER P D, LIN Y-F, et al. Quantification of model uncertainty in environmental modeling[J]. Stochastic Environmental Research and Risk Assessment, 2010, 24(6):807-808.
- [180] YE M, MEYER P D, NEUMAN S P. On model selection criteria in multimodel analysis[J]. Water Resources Research, 2008, 44(3).
- [181] YE M, NEUMAN S P, MEYER P D. Maximum likelihood Bayesian averaging of spatial variability models in unsaturated fractured tuff[J]. Water Resources Research, 2004, 40(5).
- [182] YE M, POHLMANN K F, CHAPMAN J B. Expert elicitation of recharge model probabilities for the Death Valley regional flow system[J]. Journal of Hydrology, 2008, 354(1-4):102-115.
- [183] YE M, POHLMANN K F, CHAPMAN J B, et al. A model-averaging method for assessing groundwater conceptual model uncertainty[J]. Ground Water, 2010, 48(5):716-28.
- [184] YEN H, WANG X, FONTANE D G, et al. A framework for propagation of uncertainty contributed by parameterization, input data, model structure, and calibration/validation data in watershed modeling[J]. Environmental Modelling & Software, 2014, 54:211-221.
- [185] YU Q, WANG Y, XIE X, et al. Reactive transport model for predicting arsenic transport in groundwater system in Datong Basin[J]. Journal of Geochemical Exploration, 2018, 190:245-252.

- [186] ZACHARA J M, CHEN X, MURRAY C, et al. River stage influences on uranium transport in a hydrologically dynamic groundwater-surface water transition zone[J]. Water Resources Research, 2016, 52(3):1568-1590.
- [187] ZACHARA J M, LONG P E, BARGAR J, et al. Persistence of uranium groundwater plumes: Contrasting mechanisms at two DOE sites in the groundwater-river interaction zone[J]. Journal of Contaminant Hydrology, 2013, 147:45-72.
- [188] ZENG X, DONG J, WANG D, et al. Identifying key factors of the seawater intrusion model of Dagu river basin, Jiaozhou Bay[J]. Environmental Research, 2018, 165:425-430.
- [189] ZENG X K, WU J C, WANG D, et al. Assessing Bayesian model averaging uncertainty of groundwater modeling based on information entropy method[J]. Journal of Hydrology, 2016, 538:689-704.
- [190] ZHENG C, WANG P P. MT3DMS: A Modular Three-Dimensional Multispecies Model for Simulation of Advection, Dispersion and Chemical Reactions of Contaminants in Groundwater Systems; Documentation and User's Guide. [R]. Vicksburg, Mississippi, 1999.
- [191] ZINKE L. Groundwater arsenic[J]. Nature Reviews Earth & Environment, 2020, 1(11):558-558.
- [192] 张将伟, 卢文喜, 曲延光, 等. 基于 Monte Carlo 方法的地表水地下水耦合模拟模型不确定分析[J]. 水利学报, 2018, 49(10): 1254-1263.
- [193] 董磊华, 熊立华, 万民. 基于贝叶斯模型加权平均方法的水文模型不确定性分析[J]. 水利学报, 2011, 18(1): 140-144.
- [194] 黄国如, 解河海. 基于 GLUE 方法的流域水文模型的不确定性分析[J]. 华南理工大学学报(自然科学版), 2007, 35(3): 137-149.
- [195] 刘培贵, 束龙仓. 傍河水源地地下水水流数值模拟的不确定性[J]. 吉林大学学报(地球科学版), 2008, 38(4):639-643.
- [196] 陆乐, 吴吉春, 陈景雅. 基于贝叶斯方法的水文地质参数识别[J]. 水文地质工程地质, 2008, (5): 58-63.
- [197] 束龙仓, 朱元生. 地下水资源评价中国的不确定性因素分析[J]. 水文地质工程地质, 2000, (6):6-8.
- [198] 宋晓猛, 张建云, 占车生, 等. 水文模型参数敏感性分析方法评述[J]. 水利水电科技进展, 2015, 35(6):105-112.

-
- [199] 夏强.地下水不确定性问题的多模型分析方法及应用[D].中国地质大学（北京）, 2011.
 - [200] 薛亮, 夏强.贝叶斯多模型分析方法的对比研究[J].水利发电, 2016, 42(4): 31-40.
 - [201] 杨运, 吴吉春, 骆乾坤, 等. DREAM 算法分析地下水数值模拟不确定性的影响因素[J].地质评论, 2016, 62(2):353-361.
 - [202] 闫雪漫, 卢文喜, 欧阳琦. 基于替代模型的非点源污染模拟不确定性分析[J]. 中国环境科学, 2017, 37(8): 3011-3018.
 - [203] 王慧亮, 李叙勇, 解莹. 多模型方法在非点源污染负荷中的应用展望[J]. 水科学进展, 2011, 22(5): 727-732.
 - [204] 吴吉春, 陆乐. 地下水模拟不确定性分析 [J]. 南京大学学报（自然科学）, 2011, 47(3): 227-234.